Development and Application of Electrospray Ionization Mass Spectrometry (ESI-MS) Methods for Measuring Carbohydrate-Active-Enzyme (CAZyme) Kinetics

by

Zhixiong Li

A thesis submitted in partial fulfillment of the requirements for the degree of

Doctor of Philosophy

Department of Chemistry
University of Alberta

Abstract

This thesis focuses on the development of electrospray ionization mass spectrometry (ESI-MS)-based methods for measuring carbohydrate-active enzyme (CAZyme) kinetics and their applications for profiling CAZyme specificity, glycoprotein remodeling and disease diagnosis.

Chapter 2 introduces CUPRA-ZYME, a versatile and quantitative ESI-MS assay for measuring the kinetic parameters of CAZyme reactions, monitoring pathways and profiling substrate specificities. The method employs the recently developed competitive universal proxy receptor assay (CUPRA), which is implemented in a time-resolved manner. Measurements of the hydrolysis kinetics of CUPRA substrates containing ganglioside oligosaccharides by the glycosyl hydrolase human neuraminidase 3 serve to validate the reliability of CUPRA-ZYME for quantifying kinetic parameters and highlight its use in establishing catalytic pathways. Application to libraries of substrates demonstrate the potential of CUPRA-ZYME for quantitative profiling of the substrate specificities of glycosidases and glycosyltransferases.

Measuring CAZyme kinetics for glycoprotein substrates is challenging due to their heterogeneity. Chapter 3 introduces a simple but quantitative ESI-MS method suitable for glycoprotein substrates. The assay, referred to as Center-of-Mass (CoM) Monitoring (CoMMon), relies on continuous monitoring of the CoM of an ensemble of glycoprotein substrates and their corresponding CAZyme products. Notably, there is no requirement for calibration curves, internal standards, labelling, or mass spectrum deconvolution. The reliability of the CoMMon method was demonstrated by neuraminidase-catalyzed cleavage of *N*-acetylneuraminic acid (Neu5Ac) residues from a series of glycoproteins of varying molecular weights and degrees of glycosylation. Reaction progress curves and initial rates determined by CoMMon are in good agreement with results obtained, simultaneously, using an isotopically-labeled Neu5Ac internal standard, which enabled

the time-dependent concentration of released Neu5Ac to be precisely measured. To illustrate the applicability of CoMMon to glycosyltransferase reactions, the assay is used to measure the kinetics of sialylating a series of asialoglycoproteins by the human sialyltransferase ST6Gal1. The kinetic data show no correlation between initial rate and the number of acceptor sites. Moreover, the apparent kinetics are well described by double exponential functions. This finding, combined with the results of high-performance liquid chromatography (HPLC) analysis of the *N*-glycans released from the substrates during the sialylation reaction, suggest that ST6Gal1 has a preference for the α1-3 branch.

Drawing on the methodological advances made in Chapter 2 and 3, a top down MS method for quantifying the α2-3- and α2-6-linked Neu5Ac content of prostate specific antigen (PSA) is introduced in Chapter 4. The assay employs CoMMon and a combination of specific (for α2-3-linked Neu5Ac) and nonspecific neuraminidases. Moreover, it is free of errors associated with lectin-based quantification of *N*-glycans containing both α2-3- and α2-6-linked Neu5Ac and avoids the sample handling steps required for HPLC analysis. The assay is validated using PSA from a commercial source and PSA standards containing all α2-3- or α2-6-linked Neu5Ac. The α2-3 Neu5Ac content of a PSA standard measured with the assay agrees with values obtained by HPLC analysis of released *N*-glycans. To illustrate the potential of the assay for clinical diagnosis of prostate cacer (PCa) and disease staging, the relative α2-3 Neu5Ac content on PSA extracted from serum of low, intermediate and high risk PCa individuals are determined. The results indicate a high sensitivity and specificity for discrimination of both low risk PCa and high risk PCa or low and intermediate risk PCa.

Preface

The research work presented in Chapter 2 of this thesis has been published as: Li, Z.; Kitov, P. I.; Kitova, E. N.; Mozenah, F.; Rodrigues, E.; Chapla, D. G.; Moremen, K. W.; Macauley, M. S.; Klassen, J. S. CUPRA-ZYME: an assay for measuring carbohydrate-active enzyme activities, pathways, and substrate specificities. *Anal. Chem*. **2020**, *92*, 3228–3236. I was responsible for data collection, analysis and manuscript preparation. Dr. Pavel Kitov was responsible for the synthesis of CUPRA substrate and Dr. Elena Kitova assisted with the manuscript edits. Fahima Mozenah and Emily Rodrigues contributed to the synthesis of one CUPRA substrate. Prof. Kelly Moreman and Prof. Matthew Macauley helped with editing of the manuscript. Prof. John Klassen was the supervisory author.

The experiments about substrates specificity of human nuerminidase detailed in Section 2.3.4 has been published as: Kitov, P. I.; Kitova, E. N.; Han, L.; Li, Z.; Jung, J.; Rodrigues, E.; Hunter, C. D.; Cairo, C. W.; Macauley, M. S.; Klassen, J. S. A quantitative, high-throughput method identifies protein–glycan interactions via mass spectrometry. *Commun. Biol*. **2019**, 2, 268-274. I was responsible for data collection in Section 2.3.4. Human NEU2 and NEU3 were expressed and purified by Dr. Carmanah Hunter. Data was processed by a SWARM software developed by Dr. Kitov, P. I.

The research work presented in Chapter 3 of this thesis has been published as: Li, Z.; Kitov, P. I.; Kitova, E. N.; Bui, D. T.; Moremen, K. W.; Wakarchuk, W. W.; Mahal, L. K.; Macauley, M. S.; Klassen, J. S. Quantifying CAZyme Activity with Glycoprotein Substrates using ESI-MS and Center-of-Mass Monitoring (CoMMon). *Anal. Chem.* **2021**, *93*, 15262–15270. I was responsible for data collection, analysis and manuscript preparation. Dr. Elena Kitova assisted with the manuscript edits and Dr. Pavel Kitov was responsible for the developing of software. Duong Bui

contributed to the UPLC-MS experiment. Prof. Warren Wakarchuk, Prof. Lara Mahal, Prof. Kelly Moremen and Prof. Matthew Macauley helped with editing of the manuscript. Prof. John Klassen was the supervisory author.

The research work presented in Chapter 4 of this thesis has been adapted to a manuscript in preparation. I was responsible for sample preparation, data collection, analysis and manuscript preparation. Duong Bui contributed to the UPLC-MS experiment. Blood serum samples were from Prof. Hon Leong at Sunnybrook hospital. Serum PSA level was quantified by Yanxiang Shao and Stephanie White. Prof. Hon Leong, Prof. Stanley Liu and Prof. Lara Mahal helped with editing of the manuscript. The human blood samples used in Chapter 4 were collected in Sunnybrook Research Institute with the approval of the Research Ethics Board committee at Sunnybrook Health Sciences Centre (Toronto, ON). The mass spectrometry analysis of purified proteins from patient serum samples was approved by the Health Research Ethics Board at the University of Alberta (Pro00122665).

Acknowledgement

The wonderful journey of my graduate study is close to the end, and here, I really appreciate my supervisor Prof. John S. Klassen for giving me the opportunity to join this excellent group. Moreover, his patience and guidance for the student, his rugosity and passion for the research inspired me in my daily research work. I am also grateful to my defense committee members, Prof. Ran Zhao, Prof. Liang Li, Prof. Lara Mahal, Prof. Todd L. Lowary and Prof. Lars Konermann, for their support and insightful comments into my research.

I would like to extend my gratitude to Dr. Elena N. Kitova, Dr. Pavel I. Kitov, Dr. Ling Han and Dr. Amr El-Hawiet for their constructive advice, extensive knowledge and technical support. I would also like to thank Prof. Christopher Cairo for providing us with the human neuraminidase, Prof. Kelley W. Moremen for providing us with the human sialyltransferase, Prof. Matthew Macauley for providing us with the neuraminidase and Blake Zheng for his training in human neuraminidase expression and purification.

It is also a great pleasure to work with all my excellent group members, Han Ling, Yilin Wang, Jianing Li, Dr. Heajin Prak, Duong Bui and James Favell. I wish you all the best in your careers. I would also like to thank my dear friend Erick Baez, Linh Nguyen, Yuki Kamijo and Morgan Bianca for the wonderful time we spent together and those happy memories we made.

Finally, I would like to give special thanks to my parents and Meng Wang for their encouragement and spiritual support.

Table of Contents

List of Tables

List of Figures

List of Abbreviations

Ab	Abundance of gas-phase ions
AC	Alternating current
ADC	Analogue-to-digital converter
AGP	α-1-acid glycoprotein
BF	Bovine fetuin
BPH	Benign prostatic hyperplasia
CaR	*Catch-and-release*
CAZyme	Carbohydrate-active enzyme
CE	Capillary electrophoresis
CEM	Chain injection model
CID	Collision-induced dissociation
CIEF	Capillary isoelectrofocusing
CMP	Cytidine 5'-monophosphate
CoM	Center of mass
CoMMon	Center of mass monitoring
CP	CUPRA product
CRM	Charged residue model
CS	CUPRA substrate
CUPRA	Competitive Universal Proxy Receptor Assay
CZE	Capillary zone electrophoresis
DC	Direct current
DMSO	Dimethyl sulfoxide
DTT	Dithiothreitol
Du	Duty cycle
ECD	Electron-capture dissociation

ECM	Extracellular matrix
EDTA	Ethylenediaminetetraacetic acid
EOF	Electroosmotic flow
ER	Endoplasmic reticulum
ESI	Electrospray ionization
ETD	Electron-transfer dissociation
FAC-FD	Frontal affinity chromatography using fluorescence detection
fPSA	Free prostate specific antigen
Fuc	Fucose
Gal	Galactose
GalNAc	*N*-acetylgalactosamine
GBP	Glycan binding protein
Glc	Glucose
GlcNAc	*N*-acetylglucosamine
GHs	Glycosyl hydrolases
GP	Glycoprotein
GPI	Glycosylphosphatidylinositol
GTs	Glycosyltransferases
hCA	Human carbonic anhydrase
HCD	Higher energy collisional dissociation
Hex	Hexose
HexNAc	*N*-acetylhexosamine
hGal-3C	C terminal domain of human galectin-3
HILIC	Hydrophilic interaction chromatography
hK3	Human kallikrein 3
Hp	Human haptoglobin
Hp1-1	haptoglobin phenotype 1-1

HPAEC-PAD	High-performance anion-exchange chromatography with pulsed amperometric detection
HPLC	High-performance liquid chromatography
IAA	Iodoacetamide
IEM	Ion evaporation model
IgG	Immunoglobulin G
IMS	Ion mobility separation
IRMPD	Infrared multiphoton dissociation
IS	Internal standard
ITC	Isothermal titration calorimetry
K_a	Association constant
$K_{a,app}$	Apparent association constant
K_d	Dissociation constant
K_M	Michaelis constant
L	Ligand
Lac	Lactose
LacNAc	*N*-acetyllactosamine
LC	Liquid Chromatography
LIF	Laser-induced fluorescence
LNnO	Lacto-N-neooctaose
L_{proxy}	Proxy ligand
Lyz	Lysozyme
m/z	Mass-to-charge ratio
MAA	*Maackia amurensis* agglutinin
mAb	Monoclonal antibody
Man	Mannose
MD	Molecular dynamics

MEKC	Micellar electrokinetic capillary chromatography
M-LAC	Multi-lectin affinity chromatography
MS	Mass spectrometry
mSA	Mono-streptavidin
MW	Molecular weight
ND	Not detected
NEU2	Human neuraminidase 2
NEU3	Human neuraminidase 3
Neu5Ac	*N*-acetylneuraminic acid
NEUA	Neuraminidase from *Arthrobacter ureafaciens* (Isoenzyme S)
NEUC	Neuraminidase from *Clostridium perfringens* (NanI subtype)
NEUS	Neuraminidase from *Streptococcus pneumoniae* (NanB subtype)
NHS	N-hydroxysuccinimide
P	Protein
PCa	Prostate cancer
PGC	Porous graphitized carbon chromatography
PHI	Prostate Health Index
P_{ref}	Reference protein
PSA	Prostate specific antigen
PTMs	Post-translation modifications
R	Abundance ratio
R_{eq}	Sensor response at saturation
Res	Resolution
RF	Radio frequency
RF	Response factor
RFU	Relative fluorescence units
RP	Reversed phase

R_{sat}	Sensor response at saturation
SEC	Size exclusion chromatography
Sia	Sialic acid
SNA	*Sambucus nigra* agglutinin
SPR	Surface plasmon resonance
SRIG	Stacked ring ion guides
ST	Sialyltransferase
ST3Gal4	Human beta-galactoside alpha-2,3-sialyltransferase 4
ST6Gal1	Human beta-galactoside alpha-2,6-sialyltransferase 1
TEAA	Triethylammonium acetate
TFA	Trifluoroacetic acid
TOF	Time-of-flight
tPSA	Total prostate specific antigen
T-wave	Travelling-wave
UHMR	Ultra-high mass range
$^{Uni}P_{proxy}$	Universal proxy protein
v_0	Initial rate
v_{max}	Maximum rate
v_{rel}	Relative initial rate
α1AT	alpha-1-antitrypsin
α2M	alpha-2-macroglobulin

Chapter 1

Stuyding Carbohydrate-Active Enzyme Kinetics by Electrospray Ionization Mass Spectrometry

1.1 Carbohydrates and Carbohydrate-Active enzymes (CAZymes)

1.1.1 Carbohydrates

Carbohydrates, one of the major classes of biomolecules, are widely distributed in nature and living organisms. Carbohydrates usually follow a general empirical formula $C_x(H_2O)_n$ and, based on the degree of polymerization, they are divided into three groups: monosaccharides, oligosaccharides and polysaccharides.[1] Monosaccharides (e.g., galactose and glucose) are the simplest carbohydrate forms and cannot be hydrolyzed into any simpler units. They are the building blocks of oligosaccharides and polysaccharides, which are linked via glycosidic bonds - acetal or ketal bonds that connect anomeric carbon of one monosaccharide to a hydroxyl group provided by another monosaccharide. Oligosaccharides are short-chain carbohydrates composed of 3 to 10 monosaccharide units (e.g., maltotriose and cyclodextrin). Polysaccharides are large carbohydrates composed of more than 10 monosaccharide units (e.g., starch and cellulose).[1]

Monosaccharides, oligosaccharides and polysaccharides, which are generally referred to as glycans, can exist as free molecules (e.g., milk oligosaccharides) or be covalently attached to other types of biomolecules (e.g., lipids, proteins, peptides and RNA) to form glycoconjugates. Glycoconjugates are classified based on the type of chemical species (referred to as the aglycone) that is connected to the glycans and include glycoproteins, glycolipids, glycopeptides and recently

discovered glycoRNA.[2] The reactions to form glycoconjugates by enzyme-catalyzed covalent attachment of a carbohydrate to aglycone, is referred to as glycosylation. Glycoconjugates represent the most structurally and functionally diverse molecules in nature because many glycosylation features can be varied, including the site of glycan attachment, glycan size, composition and structure.[3] Primarily, the structural complexity of glycoconjugates is the result of an enormous number of possible structural glycan isomers due to chirality of the glycosidic bond and the high degree of branching of glycan structures. Such diversity is illustrated by two major classes of glycoconjugates, glycolipids and glycoproteins, briefly described below.

Glycolipids are a class of glycoconjugates in which a lipid is covalently linked to glycans through a glucose or galactose residue and is further extended by other monosaccharides such as glucose, galactose, fucose, sialic acid and *N*-acetylgalactosamine residues. Glycolipids are generally classified into two groups: glycosphingolipids (GSLs), in which the glycans are linked to a sphingolipid group; and glycoglycerolipids, in which the glycans are linked to a glycerol group. Glycolipids are found on the surface of all eukaryotic cell membranes (in the outer leaflet of the plasma membrane, with their carbohydrate portions exposed on the cell surface) where they play important roles including maintaining membrane stability, facilitating cellular interactions and modulating of signal transduction.[4-6]

Glycoproteins are a class of glycoconjugates in which a protein is covalently linked to one or more glycans on its polypeptide backbone through a variety of linkages, either an *N*-and *O*-linkage (other uncommon linkages such as phospho-linkage will not be discussed here). Glycans linked to proteins via attachment to oxygen on serine or theronine are called *O*-glycans. *O*-glycans are covalently linked to a serine or threonine residue, mainly via an *N*-acetylgalactosamine (other types of *O*-glycans also exist such as *O*-linked mannose, glucose, galactose, fucose). Following

the *N*-acetylgalactosamine, *O*-glycans are extended with other types of monosaccharides including *N*-acetylglucosamine, galactose, fucose or sialic acid, forming a linear or branching structure.[7,8] So far, eight types of core structures are found for *O*-glycans with core structures 1 to 4 being predominant. They present in either linear or branching structure and can be further extended with other monosaccharides leading to a huge diversity of *O*-glycans (Figure 1.1a).[7-10] Glycans linked to protein via attachment to nitrogen on asparagine are called *N*-glycans. These glycans are covalently linked to an asparagine residue on the protein within a consensus peptide sequence: Asn-X-Ser/Thr (X can be any amino acid except proline).[11] All eukaryotic *N*-glycans share a common penta-saccharide core structure (Manα1-3(Manα1-6)Manβ1-4GlcNAcβ1–4GlcNAcβ1–Asn-X-Ser/Thr) and can be generally classified into three types: (1) high mannose type *N*-glycans, in which only mannose residues are found on the core structure; (2) complex type *N*-glycans, which have added GlcNAc residues at both the α1-3 and α1-6 mannose arms and do not contain mannose residues apart from the core structure; and (3) hybrid type *N*-glycans, in which only mannose residues are attached to Manα1-6 branch and other types of monosaccharides can be present on Manα1-3 branch (Figure 1.1b).[12] *N*- and *O*-glycans on proteins play important roles in protein solubility, structural stabilization and interactions with other molecules.[13] Moreover, glycoproteins embedded in the membrane bilayer have numerous biological roles in cell-cell communications, signaling, bacterial and viral infection, adhesion, inflammation as well as normal and pathological cellular developments.[4-6,14]

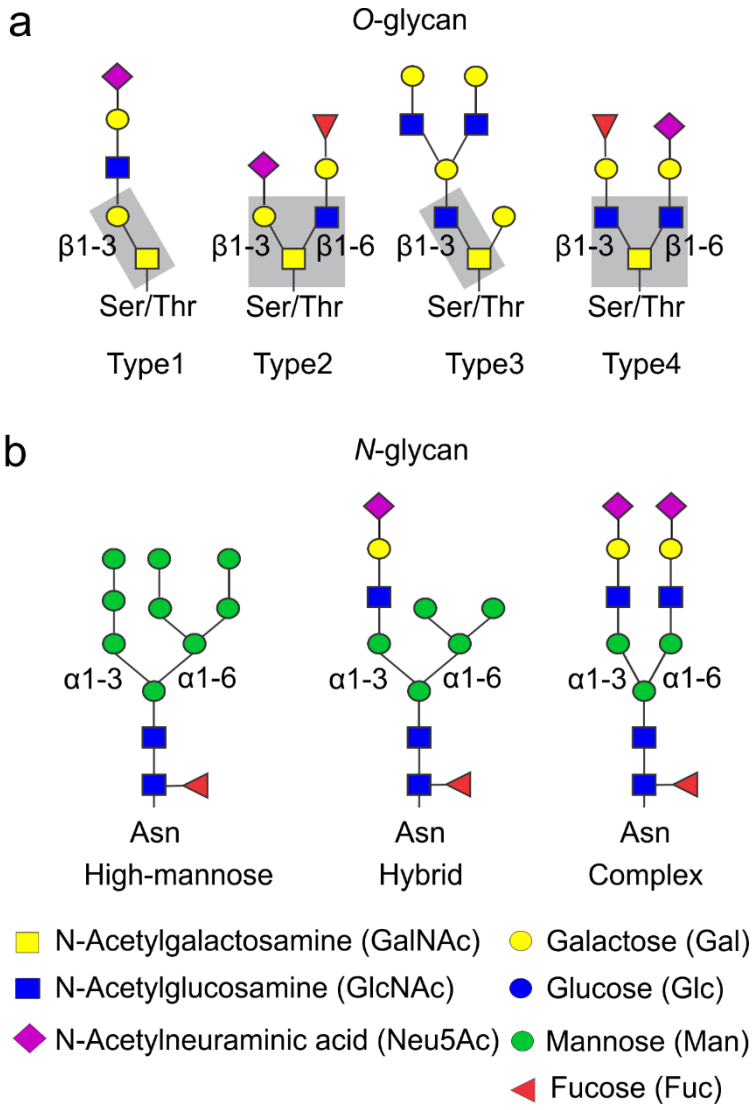

Figure 1.1 (a) Schematic of *O*-glycan core structures type 1 to 4 (shown in grey box) extended with other monosaccharides. (b) Schematic of three types of *N*-glycans: high-mannose, hybrid and complex. Common monosaccharides exist in human represented by symbols based on accepted nomenclature are shown in the legend.

1.1.2 Carbohydrate-Active enzymes (CAZymes)

Glycans and glycoconjugates are implicated in diverse biological functions in living organisms, including energy storage, cell-cell recognition and signal transduction,[15,16] The

diversity of glycan and glycoconjuate structures is controlled by a group of enzymes called Carbohydrate-Active enzymes (CAZymes), which are involved in the biosynthesis, modification, binding and catabolism of carbohydrates. CAZymes are widely distributed in all living organisms.[17] The functional diversity (specificity) of these enzymes is enormous and reflects the wide diversity of glycan structures found in nature. CAZymes account for ~1-3% of the proteins encoded by the genomes of most organisms, they are organized into several families defined by amino acid sequences that cluster around at least one biochemically characterized member (CAZy-database, http://www.cazy.org). [18,19] Based on the sequence similarity, CAZymes are divided into six functionally distinct families: glycosyl hydrolases (GHs), glycosyltransferases (GTs), polysaccharide lyases, carbohydrate esterases, carbohydrate-binding modules (CBMs) and auxiliary activity families (e.g., ligninolytic and lytic polysaccharide mono-oxygenases).[17] The two most abundant CAZyme families, GHs and GTs, which synthesize or break-down the glycosidic bond, respectively, are mainly responsible for the diversity of glycans and glyconconjugates. A brief introduction of GHs and GTs, which are the main CAZymes studied in this thesis, is given below.

Glycosyl hydrolases (GHs), also referred to as glycosidases or glycoside hydrolases, represent the most abundant family accounting for ~47% of all CAZymes.[17,20] They are responsible for the hydrolysis of glycosidic bonds within carbohydrates and glycoconjugates, which leads to the formation of a free glycan and the corresponding aglycone. The GHs are named based on the free glycan produced in the reaction. For example, glucosidases catalyze the reaction to produce free glucose and neuraminidases catalyze the reaction to produce free neuraminic acid. Based on the sequence similarity classification system (there are also other ways to classified GHs, such as

catalytic mechanism), there are currently 173 different GHs families listed in CAZyme database with over 30000 entries.[20]

Glycosyltransferases (GTs) represent the second most abundant family accounting for ~41% of all known CAZymes.[20] They are responsible for the synthesis of glycosidic bonds, which involves the transfer of a glycan from an activated nucleotide-sugar donor to an acceptor to form a larger glycan or a glycoconjugate. A sugar donor is a glycan linked with a nucleotide such as uridine diphosphate (UDP) or cytidine monophosphate (CMP).[21] Nine different sugar nucleotide donors are employed by GTs in mammals, including UDP-glucose, UDP-galactose, UDP-*N*-acetylgalactosamine (GalNAc), UDP-*N*-acetylglucosamine (GlcNAc), UDP-xylose, UDP-glucuronic acid, GDP-mannose, GDP-fucose and CMP-sialic acid (CMP-*N*-acetylneuraminic acid for humans).[14] An acceptor can be another glycan, or protein, lipid, nucleic acid, antibiotic or small molecule. GTs are named based on the glycans transferred from the nucleotide-sugar donor. For example, glucosyltransferases transfer glucose from UDP-glucose to an acceptor and sialyltransferases transfer sialic acid from CMP-sialic acid to an acceptor. Different GTs can be further classified by the acceptor structures and linkages formed with acceptor, for example β-galactoside α-2,6-sialyltransferase 1 (ST6Gal1) is one of the sialyltransferases that transfer sialic acid to a terminal galactose (attached to internal structure with β linkage) with an α-2,6 linkage.[22] There are currently 115 different GTs families listed in the CAZyme database with over 12000 entries.[20]

The large diversity of natural glycans and their complexity has motivated numerous studies aimed at uncovering novel CAZymes and exploiting them for biotechnology applications. For example, in protein glycoengineering CAZymes can be used to control the glycosylation of biotherapeutics, develop vaccines, and for diseases diagnostics (including cancer).[23-25] Insights

into the activity and substrate specificity of novel CAZymes are needed to support these efforts. Originally, assignments of the functions of CAZymes were based on their sequences. However, such predictions were later found to be unreliable because the sequence-based CAZyme families often group together enzymes with differing substrate specificity.[18] Therefore, it was recognised that activity and specificity of novel CAZymes have to be established experimentally. However, while the number of entries in CAZy database is increasing exponentially every year, the number of biochemically characterized enzymes is growing far more slowly.[26] The main reason for this discrepancy is the lack of reliable and robust methods for CAZymes activity quantification (as described in detail below), therefore new analytical methods are needed.

This thesis mainly focuses on the development of electrospray ionization mass spectrometry (ESI-MS)-based methods for the characterization of GT and GH kinetics. Validation of these methods was performed using both GHs and GTs: the neuraminidases from GH33 family (NEU, EC 3.2.1.18, also referred to as sialidases), including human NEU3, neuraminidase from *Clostridium perfringens* (denoted as NEUC, NanI subtype) and neuraminidase from *Streptococcus pneumoniae* (denoted as NEUS, NanB subtype); and human sialyltransferases from GT29 family (ST, EC 2.4.99.X) including human β-galactoside α-2,3 sialyltransferase 4 (ST3Gal4) and human β-galactoside α-2,6 sialyltransferase 1 (ST6Gal1) served as model systems.

Human NEU3, one of the four neuraminidases found in humans (NEU1-NEU4), is a plasma membrane-associated neuraminidase. It exhibits broad substrate specificity and catalyzes the cleavage of terminal Neu5Ac from oligosaccharides, gangliosides and glycoproteins. In addition, a recent study indicates that NEU3 has a preference for α2-3 over α2-6 and α2-8 linkages.[27] NEUC (NanI subtype) is one of the three neuraminidases (NanH, NanI and NanJ) produced by *Clostridium perfringens*, a gram-positive bacterium. Similar to NEU3, NEUC

exhibits broad activity to substrates including oligosaccharides, gangliosides and glycoproteins with a preference for α2-3-linked Neu5Ac.[28] NEUS (NanB subtype) is one of the three neuraminidases (NanA, NanB and NanC) produced by *Streptococcus pneumoniae*. Unlike NEU3 and NEUC, which have broad substrate specificity, NEUS has a strict specificity for α2-3 linked Neu5Ac.[29] This makes it an ideal enzyme for the identification of Neu5Ac linkage in natural glycans and glycoconjugates.

Human ST6Gal1, one of the two galactoside α-2,6 sialyltransferases found in humans, catalyzes the transfer of Neu5Ac residue with an α2-6 linkage to a terminal galactose. It shows strict specificity for terminal galactose linked to an internal *N*-acetylglucosamine with a β1-4 linkage (Galβ1-4GlcNAc).[30] Human ST3Gal4, one of the six galactoside α-2,3 sialyltransferases found in humans, catalyzes the transfer of Neu5Ac residue with an α2-3 linkage to a terminal galactose. Unlike ST6Gal1, which shows strict specificity for Galβ1-4GlcNAc, ST3Gal4 has activity for both Galβ1-4GlcNAc and Galβ1-3GlcNAc acceptors.[31]

Development of the quantitative, robust and internal standard-free ESI-MS methods to measure CAZyme kinetics using NEU3, NEUC, NEUS, ST3Gal4 and ST6Gal1 as model CAZymes and different substrates including oligosaccharides and glycoproteins, is described in the following chapters. In the following sections, a brief introduction of CAZyme kinetics and assays is given, along with a brief review of principles of ESI-MS analysis, including direct ESI-MS binding measurements and ESI-MS-based enyme kinetic assays.

1.2 CAZyme kinetics and CAZyme assays

1.2.1 CAZyme kinetics

Neuraminidases (e.g. NEU3, NEUC and NEUS) are a group of GHs that catalyze the cleavage of terminal sialic acid (Neu5Ac for humans) from any sialylated glycoconjugates (Figure 1.2). These are single substrate reactions and they generally follow Michaelis-Menten kinetics.[27-29, 32] A brief description of the Michaelis-Menten mechanism and the determination of kinetic parameters of single-substrate reactions is provided below.

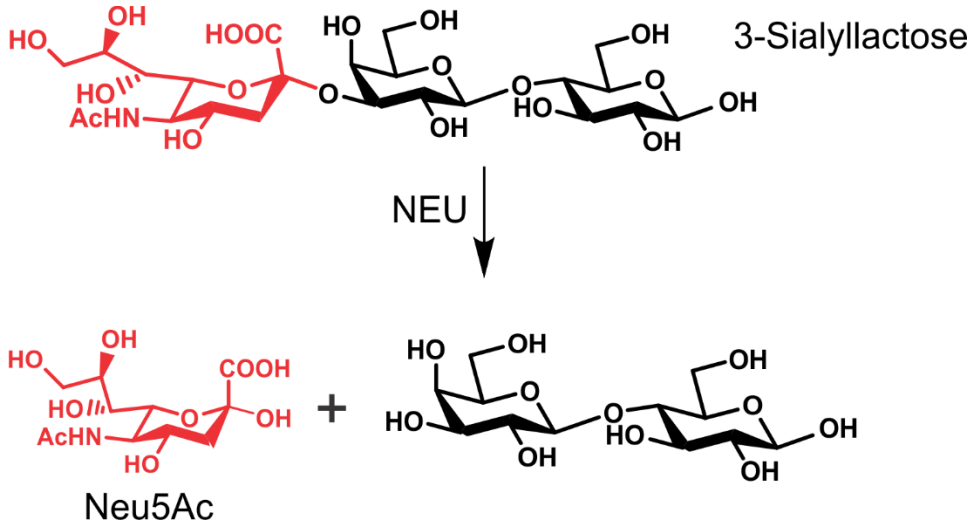

Figure 1.2 A representative reaction of NEU catalyzed cleavage of Neu5Ac (shown in red) from 3'-sialyllactose.

The simplest kinetic scheme for a single-substrate enzyme reaction is shown in Eq1.1:

$$E + S \underset{k_{-1}}{\overset{k_1}{\rightleftharpoons}} ES \xrightarrow{k_2} E + P \qquad (1.1)$$

where the E, S, ES and P represent enzyme, substrate, enzyme-substrate complex and product, respectively. According to this mechanism, the substrate binds reversibly (with forward (association) and reverse (dissociation) rate constants k_1 and k_{-1}, respectively) to the CAZyme

active site to form the enzyme-substrate complex (ES). In the consecutive step, with rate constant k_2, the enzymatic product is formed and simultaneously released to regenerate the free enzyme. The rate of product formation (v) is controlled by the consecutive step, which depends on the concentration of ES, as shown in Eq1.2:

$$v = \frac{d[\mathrm{P}]}{d\mathrm{t}} = k_2[\mathrm{ES}] \qquad (1.2)$$

The Michaelis-Menten mechanism can be analyzed by applying the steady-state approximation to the ES intermediate.[33] Based on the steady-state approximation, the concentration change of ES complex is taken to be constant with time and can be expressed by Eq1.3:

$$\frac{d[\mathrm{ES}]}{d\mathrm{t}} = k_1[\mathrm{E}][\mathrm{S}] - k_{-1}[\mathrm{ES}] - k_2[\mathrm{ES}] = 0 \qquad (1.3)$$

This equation can be rearranged to give an expression of [ES] in terms of [E] and [S], Eq1.4:

$$[\mathrm{ES}] = \frac{k_1[\mathrm{E}][\mathrm{S}]}{k_{-1} + k_2} \qquad (1.4)$$

This expression can be further simplified by introducting the Michaelis constant (K_M), Eq 1.5:

$$K_\mathrm{M} = \frac{k_2 + k_{-1}}{k_1} \qquad (1.5)$$

to give Eq 1.6:

$$[\mathrm{ES}] = \frac{[\mathrm{E}][\mathrm{S}]}{K_\mathrm{M}} \qquad (1.6)$$

Based on mass balance considerations, the intial enzyme concentration ($[\mathrm{E}]_0$) can be written as Eq1.7:

$$[\mathrm{E}]_0 = [\mathrm{E}] + [\mathrm{ES}] \qquad (1.7)$$

Rearraning the equation gives an expression for [E], Eq1.8:

$$[\mathrm{E}] = [\mathrm{E}]_0 - [\mathrm{ES}] \qquad (1.8)$$

which when introduced to Eq 1.6 gives Eq1.9:

$$[\mathrm{ES}] = \frac{([\mathrm{E}]_0 - [\mathrm{ES}])[\mathrm{S}]}{K_\mathrm{M}} \quad (1.9)$$

Because the substrate concentration is typically in large excess relative to the enzyme concentration, [S] is approximately equal to $[S]_0$. As a result, Eq1.9 can be written as Eq1.10:

$$[\mathrm{ES}] = \frac{([\mathrm{E}]_0 - [\mathrm{ES}])[\mathrm{S}]_0}{K_\mathrm{M}} \quad (1.10)$$

Rearranging gives Eq1.11:

$$[\mathrm{ES}] = \frac{[\mathrm{E}]_0[\mathrm{S}]_0}{K_\mathrm{M} + [\mathrm{S}]_0} \quad (1.11)$$

Substitution of the expression for [ES] into Eq1.2 gives the Michaelis-Menten equation, Eq1.12:

$$v = \frac{k_2[\mathrm{E}]_0[\mathrm{S}]_0}{K_\mathrm{M} + [\mathrm{S}]_0} \quad (1.12)$$

According to this expression, when $[S]_0$ is $\gg K_M$, the rate of reaction reaches a limiting value (maximum rate, v_{max}), which depends on is k_2 and $[E]_0$ but is independent of $[S]_0$, Eq1.13:

$$v_{\max} = k_2[\mathrm{E}]_0 \quad (1.13)$$

Substitution into Eq1.12 gives a more general form of Michaelis-Menten equation:

$$v = \frac{v_{max}[\mathrm{S}]_0}{K_\mathrm{M} + [\mathrm{S}]_0} \quad (1.14)$$

The kinetic parameters v_{max} and K_M are useful for describing a giving enzyme-substrate system. The K_M reflects the affinity of the enzyme to a specific substrate (e.g., smaller K_M indicate a higher affinity of substrate to the enzyme and the rate will reach v_{max} with a lower concentration of substrate). The K_M constant is independent of enzyme concentration but related to conditions such as temperature and pH.[33] The v_{max} indicates the maximum reaction rate and is often used to determine k_2, which is generally referred to as k_{cat} and represents the number of substrate converted to product per unit time. It can be determined from v_{max} and $[E]_0$ using Eq1.15:

$$k_{\mathrm{cat}} = \frac{v_{max}}{[\mathrm{E}]_0} \quad (1.15)$$

The initial rate (v_0), which is the instantaneous rate at the start of the reaction, is experimentally used to determine the enzyme kinetic parameters. To quantify v_0, an enzyme progress curve is constructed based on the concentration changes of product or substrate as a function of time. Linear fitting of the progress curve at early reaction time (usually before ~20% of the substrate is consumed) gives v_0 (Figure 1.3a). Different initial substrate concentrations (usually range from 0 to 5xK_M) are titrated with the same concentration of enzyme to get the initial rate at different $[S]_0$. Non-linear regression analysis (using the Michaelis-Menten equation) of the dependence of v_0 on $[S]_0$ gives K_M and v_{max}. Notably, K_M corresponds to the concentration of substrate with a rate equal to one-half v_{max} (Figure 1.3b).

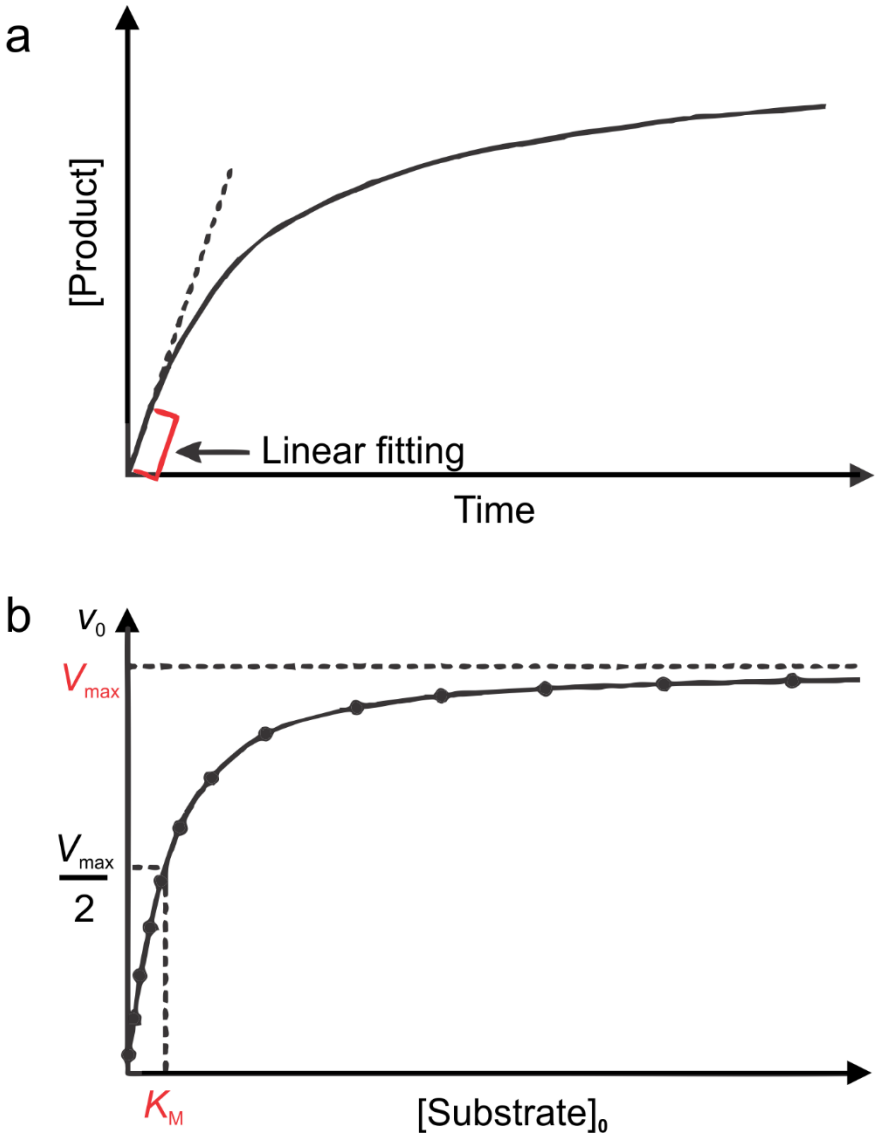

Figure 1.3 Schematic diagrams of (a) a representative progress curve of enzymatic reaction, data points in early reaction time is linear fitted and initial rate will be the slope. (b) A representative Michaelis-Menten plot, K_M equals to the initial concentration of substrate with half v_{max}.

In contrast to GHs, GTs utilize two substrates, a donor and an acceptor. For example, ST6Gal1 and ST3Gal4, which are used in this work, transfer Neu5Ac from a cytidine monophosohate-Neu5Ac (CMP-Neu5Ac) donor to a terminal galactose acceptor (Figure 1.4). Experimental measurement of kinetic parameters (v_{max} and K_M) of two substrate enzyme reactions is usually accomplished by keeping one of the substrates at a fixed concentration and measuring kinetics at different concentrations of the other substrate.[34] Under these conditions, the enzyme kinetics can be approximated as the single-substrate reaction and can be analyzed using the Michaelis-Menten equation (Eq1.14).

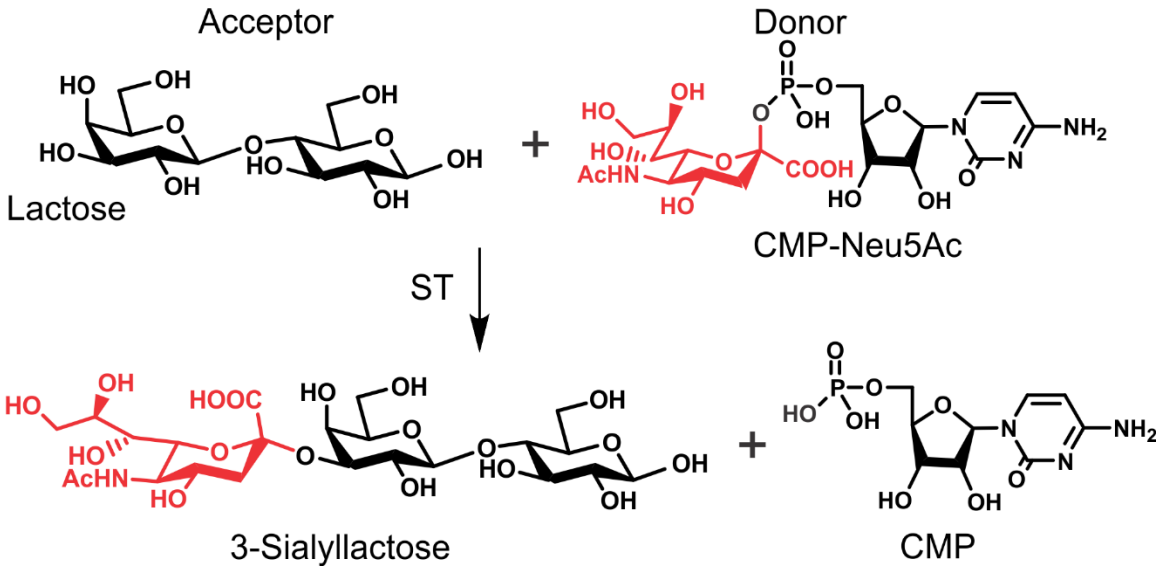

Figure 1.4 A representative reaction ST catalyzed transferring of Neu5Ac (shown in red) from CMP-Neu5Ac as a donor to lactose as acceptor.

1.2.2 CAZyme assays

Measurements of CAZyme kinetics provide insight into enzyme activity and substrate specificity. Such information is of fundamental interest and supports diverse applications. However, versatile and robust kinetic assays suitable for natural CAZyme substrates, in particular glycoproteins and glycolipids, are limited. Consequently, the structure-activity relationships of many CAZymes are poorly understood. Kinetic studies rely on measuring the concentrations of substrates or products at different time points during the reaction. Optical methods are the most widely used approaches (e.g. fluorescence based measurements) for CAZyme kinetics measrements.[35-42] Optical density can be converted into concentration based on Beer's Law and, as such, can be used to measure initial rate (v_0), maximum rate (v_{max}) and K_M. However, most naturally occurring glycans do not exhibit optical properties and, therefore, enzymatic processing of glycan substrates typically cannot be directly monitored using spectrophotometry-based kinetic assays. Application of optical methods generally requires the introduction of a chromophore (e.g. fluorophore) into the substrate.[35-38] For GH catalyzed hydrolysis reaction, the kinetics can be measured by using fluorophore labelled substrate such as 9H-(1,3-dichloro-9,9-dimethylacridin-2-one-7-yl) β-d-galactopyranoside (DDAOG, Figure 1.5a) used by Wen and co-works.[39] GH kinetics can be also measured by labelling the free product removed from the substrate. For example, Cairo and co-workers quantified the activity of human neuraminidases with different substrates by labelling the free sialic acid with 1,2-phenylenediamine (Figure 1.5b).[40] However, labelling the product requires extra steps to quench the reaction at different reaction times. Compared with GH, enzymatic reactions catalyzed by GT are more complicated as a donor (e.g. CMP-Sia) and an acceptor (e.g. Lactose) are involved in the reaction and different strategies were developed to measure the kinetics of GT. For example, Withers and co-workers developed a high-throughput screening

method, based on labelling diffrent acceptor with a BODIPY fluorophore (Figure 1.5c), that enabled screening of $>10^6$ GTs mutants for a directed-evolution study.[41] Walker and co-workers also developed a high-throughput screening method for identification of active-site inhibitors of GT.[42] Unlike the method developed by Withers, the donor for GT was labelled with fluorescein (Figure 1.5d).[42]

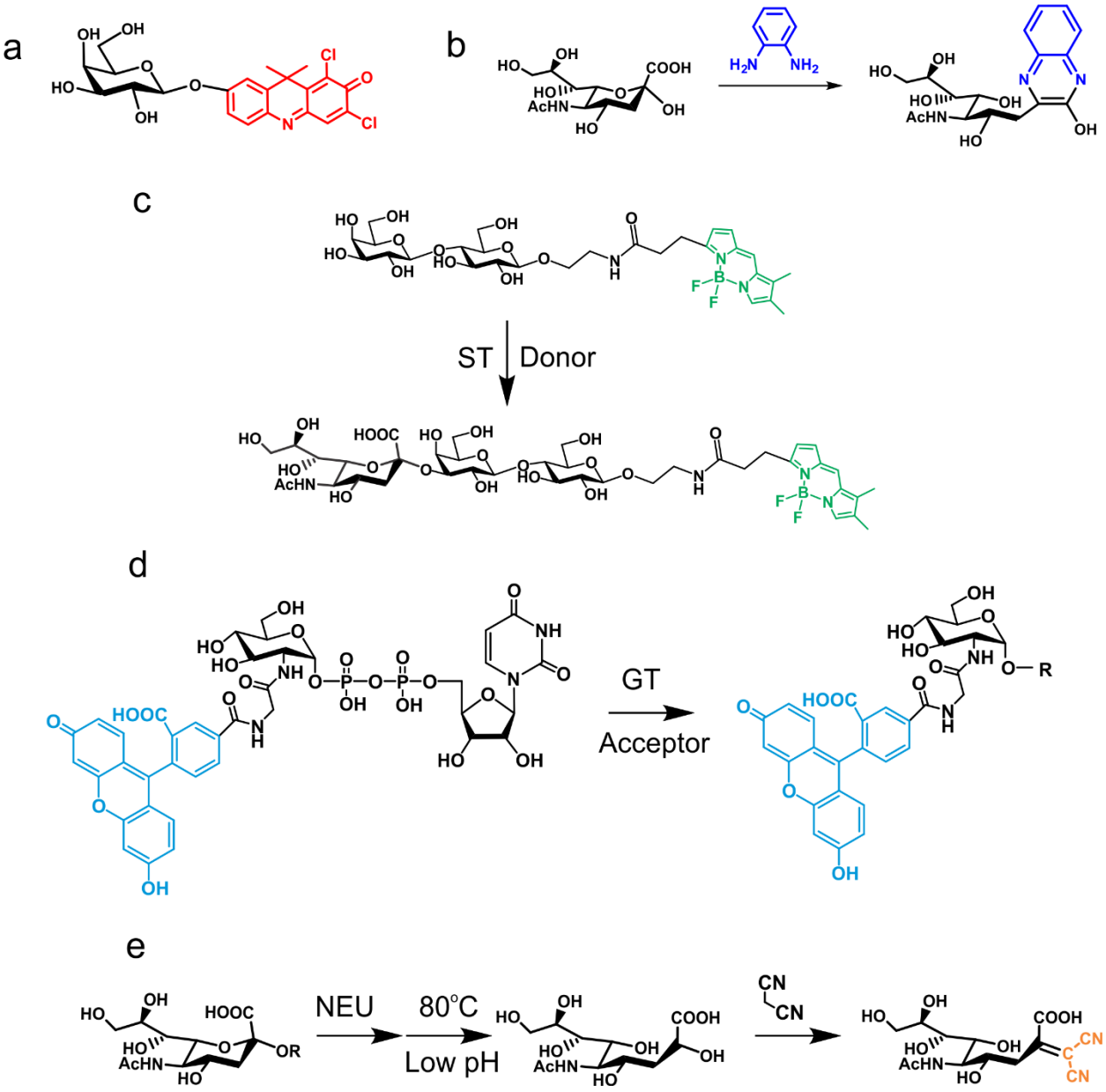

Figure 1.5 Representative schematic diagrams for monitoring reaction of (a) Glucosidase by using a fluorophore labelled substrate, (b) NEU by labelling the product with 1,2-phenylenediamine, (c) ST by labelling acceptor with BODIPY, (d) GT by labelling donor with fluorescein and (e) NEU by a second reaction to label sialic acid with malononitrile.

Despite the numerous methods developed based on the introduction of fluorophores, such modifications, depending on their nature and location, may influence CAZyme activity. Moreover, optical methods are susceptible to fluorescence quenching at high concentrations and not readily amenable to analyzing multiple substrates simultaneously. Alternatively, CAZyme kinetics can be monitored using an optical method coupled with a secondary chemical or enzymatic reaction, which generates an optically detectable signal from the CAZyme product. For example, the release of sialic acid from glycans by a sialidase can be monitored by reacting the monosaccharide with malononitrile to produce a fluorescent product (Figure 1.5e).[35] Multi-enzyme schemes, wherein a second enzyme acts rapidly on the CAZyme product to produce a coloured/fluorescent secondary product, are frequently used for GHs. However, developing coupled assays for GTs is more challenging.[36] Some of the reported methods rely on the detection of the donor leaving group (e.g., the nucleotide diphosphate, UDP) by displacing a corresponding fluorophore-labeled donor product from an immobilized antibody or through some other fluorescence-based readout achieved using coupled chemical/enzymatic reactions.[37,38]

The radiometric method is another widely used technique for CAZyme kinetics study.[43] Two major requirements in this method are substrate labelled with a radioactive isotope (e.g. ^{14}C and ^{3}H) and a rapid method of quantitatively separating product from unreacted substrate. After quenching the enzyme reaction at a certain time, the product is separated (by various techniques such as TLC or scintillation proximity assay (SPA)) and then the radioactivity of labeled substrate is measured and used for calculation of initial rate (v_0), maximum rate (v_{max}) and K_M. However, an extraction (or chromatography) step is required in order to separate radiolabeled substrate from the product in this method, which limits its application for high-throughput screening. To address this issue, a scintillation proximity based assay was developed recently and was employed in a kinetics

study for glycosyltransferases.[44-47] In this method, the acceptors are immobilized on scintillation-coated microshperes, the transfer of the radiolabelled sugar onto the acceptor brings the radioemitter in close proximity to the microsphere bead and results in the emission of a light signal. This assay overcome the requirement of extraction step and moreover, signal can be directly detected in-situ. For example, Von Ahsen and co-workers developed a miniaturized high-throughput screening scintillation proximity assay and screened 800,000 compounds as potential inhibitor for a human fucoyltransferase.[47] Despite the efforts to overcome the limitation of extraction step, the availability of radioactive-labelled glycan substrates is a significant limitation. Moreover, synthesis and use of the radioactive-labelled carbohydrate substrate are restricted to labs with special safety certificate.

In addition to optical and radiometric assays, there are other assays available to study CAZyme kinetics. For example, nuclear magnetic resonance (NMR) has been used for the quantification of the kinetics of GHs and GTs, their specificity and mechanism.[48,49] However, NMR is limited by the large sample requirement and low sensitivity. DNA-linked enzyme-coupled assays have also been demonstrated for some GTs and throughput is highly improved.[50,51] For example, Anderson and co-workers developed a DNA-Linked Enzyme-Coupled assay based on a competition between two enzymatic reactions for the same cofactor, which the depletion of the cofactor in the first reaction results in no modification in the second reaction (Figure 1.6).[50] The assay is initiated by the addition of a linear DNA encoding a promoter and a GT of interest to a translation system. After an initial incubation period, UDP-Glc is added to the reaction. If the CAZyme of interest is able to glucosylate the substrate, UPD-Glc concentrations will decrease. Later T4-β-glucosyltransferase (TbGT) and a DNA probe are added to the reaction. T4-β-glucosyltransferase could catalyze the transfer of glucose (Glc) from uridine diphosphoglucose

(UDP-Glc) to 5-hydroxymethylcytosine (5-HMC) in double-stranded DNA. The probe is a linear DNA fragment where all cytosines have been modified to 5-HMC (qPCR readouts) or a hairpin DNA oligonucleotide modified to contain two 5-HMC within an MfeI (a restriction enzyme found from *Mycoplasma fermentans*) recognition site, a 5-fluorophore, and a 3-quencher (fluorescence readouts). These methods, however, require multiple and typically expensive reagents (i.e., antibodies or enzymes) to implement, may be susceptible to background interferences and may not be readily applied to mixtures of substrates.

There are also different ESI-MS based methods to measure CAZyme kinetics that will be described in the following section. Before the introduction of ESI-MS CAZyme assays, a brief description of ESI and the mass spectrometers used in the present work will be given.

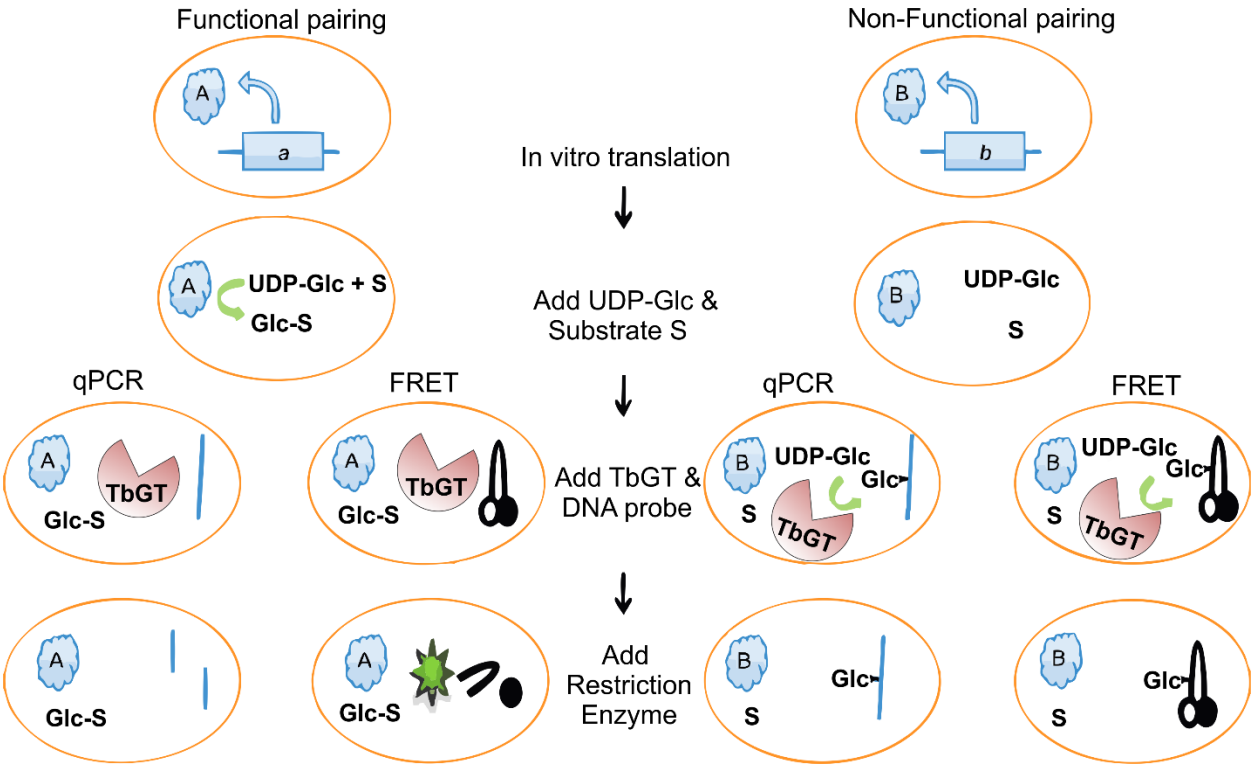

Figure 1.6 DNA-linked enzyme-coupled assay (DLEnCA). An overview of DLEnCA where the end readout is either qPCR or fluorescence using FRET. (i) A functional pairing of enzyme A and substrate S, leading to depletion of UDP-Glc and no modification of either qPCR or FRET probe by TbGT. The end result is the digestion of probes upon restriction enzyme addition. (ii) A nonfunctional pairing of enzyme B and chemical S, leading to no depletion of UDP-Glc and no modification of probes by TbGT. The end result is the protection of the probes from restriction enzyme digestion. Key: TbGT = T4-β-glucosyltransferase; Glc = glucose. Adapted from Ref 50.

1.3 Electrospray Ionization (ESI) Mass Spectrometry

A mass spectrometer separates and measures the mass-to-charge ratio (*m/z*) of gaseous ions produced from an analyte. A mass spectrometer usually can be divided into three parts: (1) ion source, which is used to generate gaseous ions; (2) mass analyzer, which is used to sort the gaseous

ions by their *m/z*; (3) detector, which measures and records the data and then converts into mass spectrum. With the emergence of so-called soft ionization techniques (e.g. ESI and matrix-assisted laser desorption ionization (MALDI)), mass spectrometry has become one of the most widely used analytical tools in biomolecular sciences. Among the applications are protein structure analysis and measrements of protein-ligand interactions and enzyme kinetics.

1.3.1 Electrospray ionization

In ESI, analytes are transferred (as ions) from solution to the gas phase at atmospheric pressure. Importantly, it enables the detection of non-volatile biomolecules (such as peptides, proteins and nucleotides), intact, as well as their non-covalent interactions and extends the mass range by the formation of multiply charged ions, which also enhances the dissociation efficiency in tandem MS. In conventional ESI, an analyte solution is loaded into an electrically conducting capillary held at a high electric potential around ± 2 to ± 6 kV.[52] The mechanism of the ESI process, as described by Kebarle and co-workers,[53] involves the production of charged droplets from electrolytes present in solution; the shrinkage of the droplets by solvent evaporation, accompanied with droplet fissions and the formation of very small, highly charged offspring droplets from which gas phase ions are produced (Figure 1.7). For the purpose of this chapter, the principle of ESI will be explained in terms of its operation in positive ion mode. Under an electric field of ~10^6 V/m, charges are separated in the analyte solution that results in the formation of a cone (Taylor cone, shown in Figure 1.8) extended from the capillary tip, carrying excess positively charged analytes.[54] When electrostatic repuslion exceeds the surface tension of the solution, a fine jet is ejected from the distal end of the Taylor cone and disintegrates into charged droplets, forming an electrospray plume. Shrinkage of the droplets, initially with diameters in the micrometer (μm) range occurs as a result of solvent evaporation. As the surface area/volume ratio of the droplets increases, the Rayleigh

limit z_R (shown in Eq.1.15), where electrostatic repulsion is balanced by the surface tension, is approached.[55] At or around 10-20% below the Rayleigh limit, surface tension is overcome by Coulombic repulsion, and these droplets (parent droplets) eject numerous smaller droplets (offspring droplets) carrying off 2-5% of their mass and 5-20% of their charge during each cycle of this process (termed droplet jet fission), until radii are decreased to a few nanometers.[52]

$$z_R = \frac{8\pi}{e}\sqrt{\varepsilon_0 \gamma R_d^3} \qquad (1.15)$$

where e is the elementary charge, ε_0 is the vacuum permittivity, γ is the surface tension of solvent, and R_d is the droplet radius.

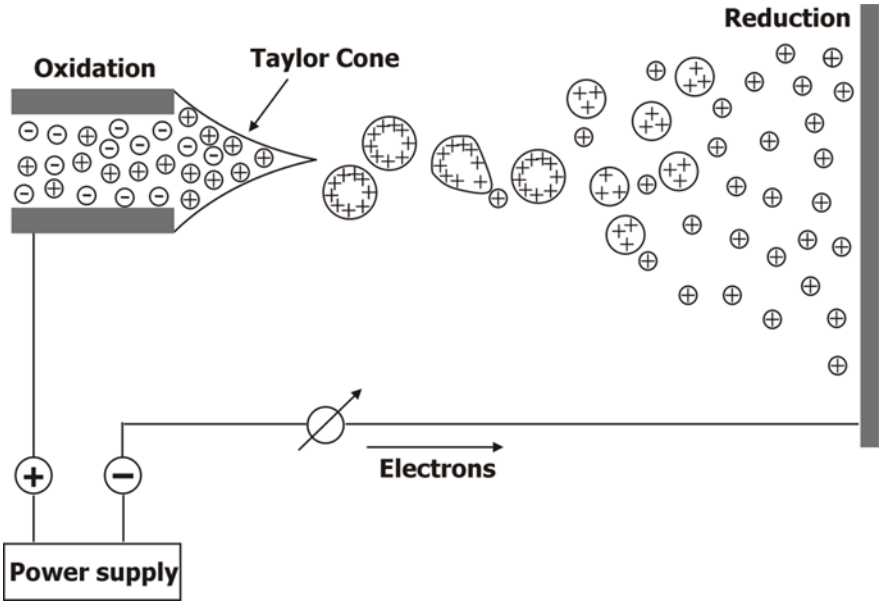

Figure 1.7 Schematic representation of ESI carried out in positive ion mode and the processes that lead to the formation of gas phase ions, adapted from Ref 53.

Nanoflow ESI (nanoESI) refers to ESI performed using solution flow rates in the range of nL min^{-1}. It is commonly performed using 1-5 μL of analyte solution loaded into a borosilicate

glass capillary with an orifice of 1-5 μm diameter (or ~100 nm for submicron emitter).[54] Voltages of around 0.5 – 1 kV (for positive mode) are applied to the capillary through either a coated conductive material (e.g. gold) or an inserted metal wire. The size of initial droplets produced from nanoESI is around 10 times smaller compare to conventional ESI, which leading to higher tolerance to buffer salts.[54] Non-surface active analytes such as oligosaccharides and glycoconjugates benefit from increased surface/volume ratio of parent droplets in nanoESI (i.e.the access to such analytes located in the bulk of a droplet is facilitated), resulting in higher sensitivity.[56] Furthermore, high spray stability is realized for analytes containing solvents with high surface tensions (e.g. water, aqueous salt solution) at lower capillary voltages, which could be a problem for conventional ESI due to low spray stability and a higher voltage is often required.[56]

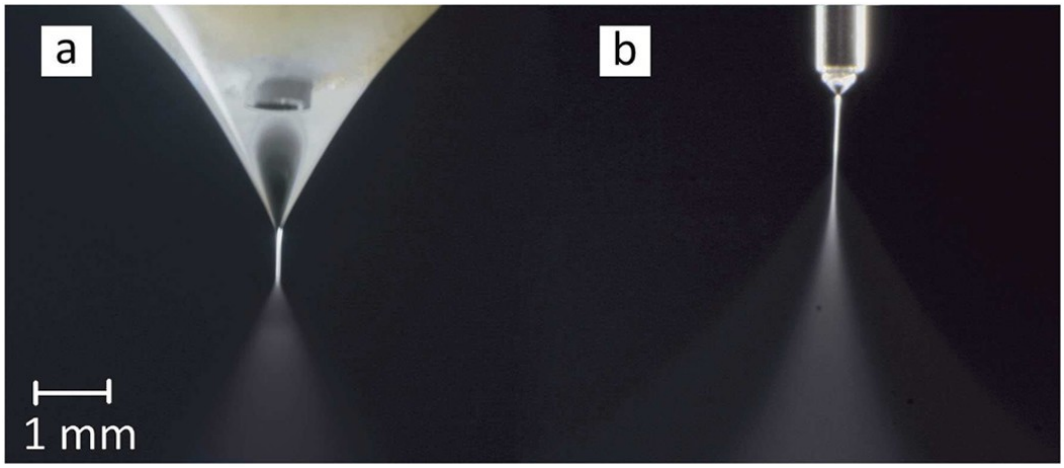

Figure 1.8 Example of a stationary Taylor cone at different capillary voltage of 7.3kV (a) and 4.3 kV (b), adapted from Ref 57.

To date, three different mechanisms have been proposed to explain the formation of gaseous ions by ESI (Figure 1.9). In the ion evaporation model (IEM), as droplets shrink to around

10 nm in diameter by solvent evaporation and fission due to electrostatic repulsion, a strong electric field compensates for the ionic solvation energies and solvated ions are ejected directly from the surface of the droplets.[58] This model explains well the ionization of species with low MW (<~3000 Da), but not suited for large analytes with globular shape (such as folded proteins).[52] In the charged residue model (CRM), the highly charged nanodroplets undergo successive fissions until the last hydration shell evaporates, and the surface charges are transferred to the analyte forming a multiply charged gaseous ion.[59] According to this mechanism, the charge states of the analyte ions are governed by the Rayleigh stability limit of droplets, which is related to their surface area and the nature of the solvent. The charge states will also depend on the gas phase basicity of the analyte and solvent. Comparison of charge states calculated using the Rayleigh equation and determined experimentally for globular proteins observed in ESI further supports the CRM theory.[60,61] However, unfolded proteins, resulting from denaturation (e.g. elevated temperature, pH changes, disulfide disruption), mutation or absence of cofactor (e.g. metal ions and organic moieties), typically exhibit higher charge states than natively folded proteins.[62] The chain ejection model (CEM) has been proposed to account for this behavior, which was also supported by the results of molecular dynamics (MD) simulations.[59,62] In this model, the interior hydrophobic residues of proteins, exposed to the hydrophilic solvent due to protein unfolding, are gradually expelled and experience proton equilibration with the highly charged droplets, and are finally ejected as highly charged unfolded gas phase ions.[59,62]

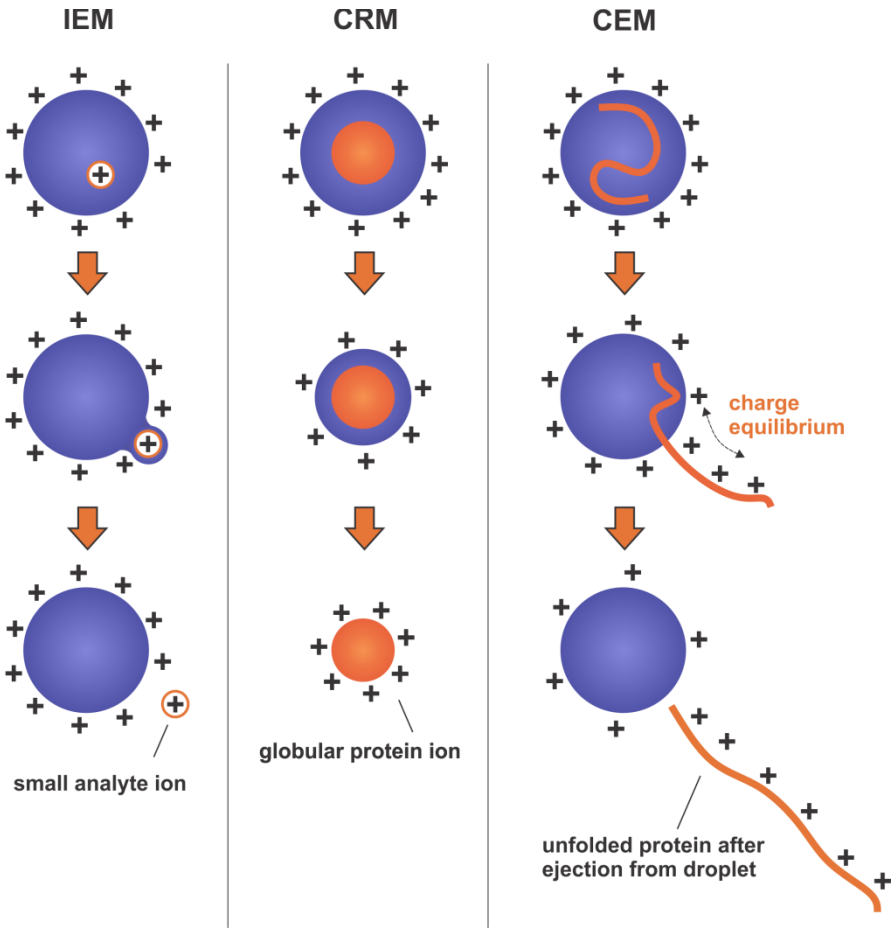

Figure 1.9 Three proposed mechanisms of ion formation in ESI, adapted from Ref 59.

1.3.2 MS instrumentation

In the present work, a Synapt G2 Q-IMS-TOF mass spectrometer (Waters UK Ltd., Manchester, UK), a Q Exactive Orbitrap mass spectrometer and an Ultra-high mass range (UHMR) Q Exactive orbitrap mass spectrometer (Thermo Fisher Scientific, Bremen, Germany) were used. A brief description of these mass spectrometers is given in the following sections.

1.3.2.1 Hybrid Quadrupole Time of Flight mass spectrometer

A Synapt G2-S quadrupole ion-mobility separation time-of-flight (Q-IMS-TOF) mass spectrometer (Waters UK Ltd., Manchester, UK), equipped with a nanoESI source was used in

Chapter 2. A schematic illustration of the instrument is shown in Figure 1.10. The instrument principally consists of several sections: z-spray source section (IntelliStart), ion guide (StepWave), quadrupole, a travelling wave section consisting of Trap, ion mobility separation (IMS) and Transfer (TriWave), and quantitative TOF-reflectron *m/z* analyzer (QuanTof). By applying an electric potential to the platinum wire inserted in a borosilicate glass capillary, analytes in buffered solutions are ionized by nanoESI at atmospheric pressure and enter the ionization source through a Z spray^{TM}. The ion beam expands and is captured by the entrance of a two-stage ion funnel, StepWave^{TM}. Ions are efficiently radially confined and guided by radio frequency (RF) voltages with the same amplitude but opposite phase applied to a stack of ring electrodes with decreasing radii of the central aperture. Ions in the first stage are directed to the non-coaxial second stage while neutral molecules are extracted into an exhaust pipe. The focused ions then transmitted through the quadrupole mass filter, Trap collision cell, IMS cell, Transfer collision cell, and finally reach the TOF mass analyzer for detection. In addition, ions can be also transmitted to ion mobility separation cell for separation of isobaric/isomeric ions based on their ion mobility difference. A more detailed description of quadrupole, ion mobility separation and TOF parts are given below.

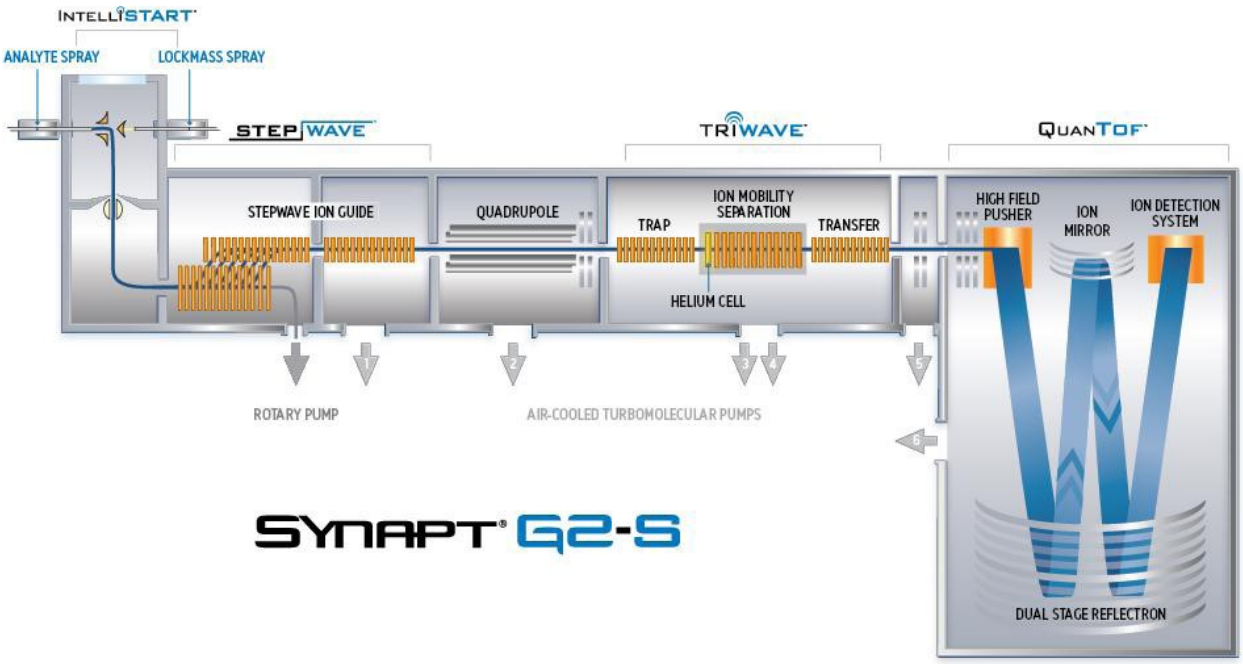

Figure 1.10 A schematic diagram of the Synapt G2-S Q-IMS-TOF mass spectrometer, adapted from Waters user's manual.

1.3.2.1.1 Quadrupole Mass filter

A quadrupole mass analyzer comprises four parallel rod electrodes with hyperbolic or circular cross-sections extending in the z direction. A voltage of (U+Vcos(ωt)) with same polarity is applied to the opposite rods and same voltage with different polarity is applied to adjacent rods, where U is the direct current (DC) and Vcos(ωt) is the radio frequency (RF) voltage with RF amplitude V and RF frequency ω (Figure 1.11). The electric potential distribution of a hyperbolic quadrupole at time *t* can be described as:

$$\phi(x,y)=[U+V\cos(\omega t)]\frac{x^2-y^2}{2r_0} \qquad (1.16)$$

where ϕ is the potential distribution, *x* and y are coordinates along the x and y axis, *U* and *V* are the magnitudes of a DC and a RF, ω is the angular frequency, and r_o is the distance from the center

(z axis) to the inner surface of an electrode. Electrodes along the X axis are held at potentials of the same amplitude but opposite in sign as the electrodes along the Y axis.

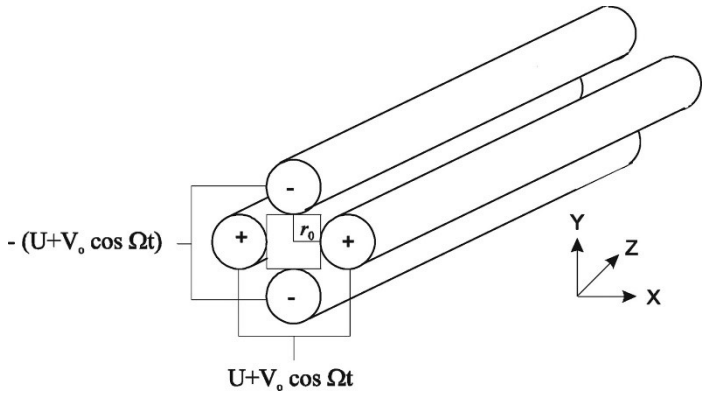

Figure 1.11 Schematic diagram of cross-sections of a cylindrical quadrupole, adapted from Ref55.

According to Newton's law of $F = m\,a$, trajectory of any ions can be described as:

$$F_x = -\frac{ex}{r_0^2}[U + Vcos(\omega t)] \tag{1.17}$$

$$F_y = \frac{ey}{r_0^2}[U + Vcos(\omega t)] \tag{1.18}$$

$$F_z = 0 \tag{1.19}$$

where e is the electron charge, z is the charge number, m is the mass of the ion in kg. Mathieu's equation can be derived as

$$\frac{d^2u}{d\xi^2} + \left[a_u + 2q_u\cos(2\xi)\right]u = 0 \tag{1.20}$$

$$a_u = \frac{8ezU}{mr_0^2\omega^2} \tag{1.21}$$

$$q_u = \frac{4ezV}{mr_0^2\omega^2} \qquad (1.22)$$

where $\xi = \omega t/2$, u is either x or y. Solutions to Eq. 1.20 can be obtained by plotting a and q, also known as the stability diagram (as shown in Figure 1.12), which can be used to determine the stability of ions in a quadrupole at different m/z. Practically, the ratio of a to q, or $2U/V$, is always kept at constant so that only certain ions with restricted m/z can traverse the quadrupole, while the others hit the rods, being neutralized and pumped away.[64] By decreasing the slope ($2U/V$) of a straight line with an intercept at zero (also known as the mass scan line), the band pass region (represented by the width, Δq) become wider, allowing an increasing m/z range pass through (increased sensitivity), while the resolution is reduced. Therefore, the quadrupole acts as a mass filter by variation of the magnitude of U and V while keeping $2U/V$ at constant.

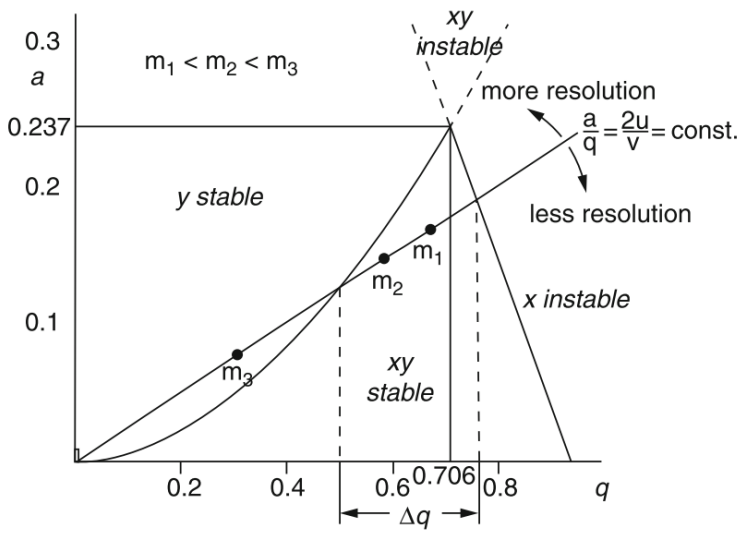

Figure 1.12 Stability diagram of a quadrupole analyzer, adapted from Ref 54.

The RF-only operation mode of the quadrupole can be achieved by setting U to zero (corresponding to the scan line equivalent to the q axis), and in this case, ions at a wide range of m/z are transmitted. The lowest m/z of ions with stable trajectories is determined by the right-hand q-intercept.[65]

1.3.2.1.2 Traveling-wave device

The Traveling-wave (T-wave) device in Synapt G2-S transfers ions from the quadrupole to the ToF with optimum efficiency, and it consists of three consecutive T-wave stacked ring ion guides (SRIG): Trap, IMS and transfer T-wave. The ion guide is composed of an even number of stacked ring-shaped electrodes arranged orthogonally to the ion transmission axis (Figure 1.13).[66,67] An opposite phased RF voltage is applied to the adjacent electrodes for radial confinement and high transmission of the ions along the axial direction within the device. To propel the ions along the device, a DC voltage is applied to the electrode pairs, causing a potential barrier that ions within the region cannot cross. As the DC voltage is stepped to the adjacent pair and sequentially along the rings of the device at regular time intervals, the ion barrier moves forward and creates a "traveling wave" that drives the ions through the device. Using a T-wave, ions can transfer with a high speed, which allows high data acquisition rates with the high sensitivity maintained. Such T-wave technology is employed in Synapt G2-S mass spectrometer for the StepWave ion guide, Trap, IMS and Transfer region.

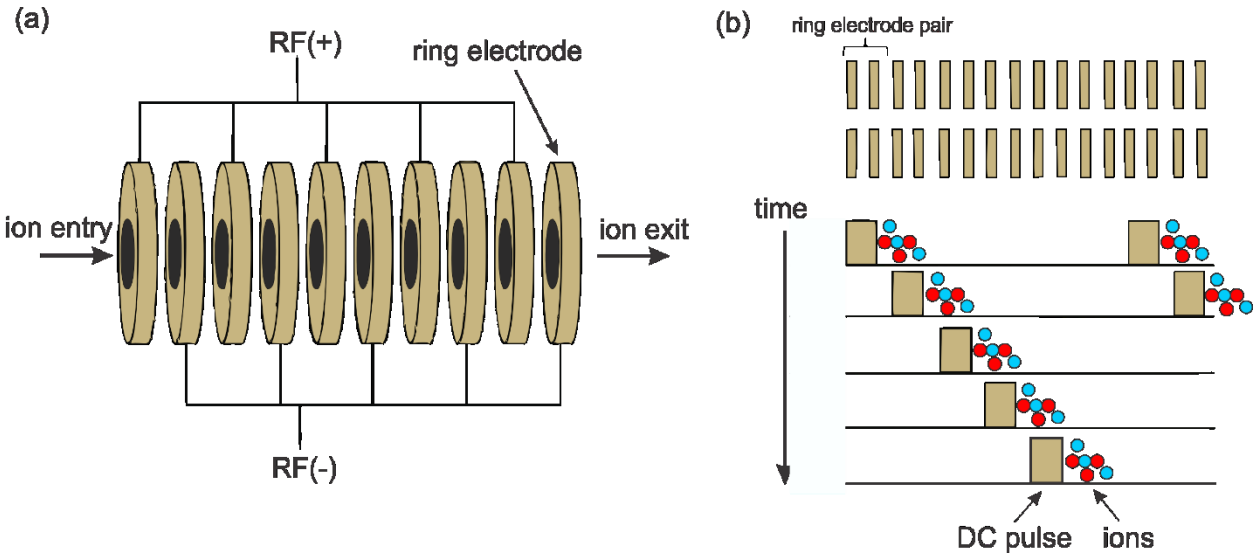

Figure 1.13 Diagrams of (a) stacked rings of a travelling wave device and (b) its operational principle (adapted from reference 66).

The IMS section in T-wave device can be further used to separate and identify ions in gas phase according to their mobility difference, which are based on their charge, size and shape, through an electric filed filled with buffer gas (N_2 or He).[68-70] In IMS, the motion of ion is driven by the electrostatic force through the chamber and opposed by collisions of ions with the buffer gas at the same time. Larger ions with greater collision cross section undergo more collisions than smaller ions and thereby resulting a longer drift time to migrate through the drift cell. There are several types of ion mobility instrumentation that have been successfully coupled with MS such as drift tube IMS (DTIMS),[71] field asymmetric waveform IMS (FAIMS),[72] and T-wave IMS (TWIMS).[66,67,73-75]

The Synapt G2-S mass spectrometer implements a TWIMS technique. Comparing to a uniform static electric field used for classic IMS, a non-uniform, moving electric fields/voltage pulsed (T-Wave technology) are performed in TWIMS. Ions are pushed and separated based on their mobility in a reverse buffer gas (N_2) flow. Ions with lower mobility experience more friction

and eventually slip behind the wave and travel more slowly.[67] Since the ions are given an additional axial velocity by the T-wave, their transit time is reduced (typically in ms). A high-pressure helium-filled cell is placed at the entrance of the IMS T-Wave cell to minimize the scatter and/or fragmentation of ions by collisionally cooling transferred ions.

Ions separated in the IMS cell are then transmitted to the gas-filled transfer T-wave, which is typically operated at 10^{-2} mbar gas pressure, 1-2 V and 300 m/s of travelling wave to maintain the mobility separation. After that, ions are transported to TOF mass analyzer for detection.

1.3.2.1.3 TOF mass analyzer

TOF mass analyzers, in which ions of different *m/z* are detected according to their flight time in a field-free drift tube, provide high sensitivity (high ion transmission), a high acquisition rate (up to 30 scans per second in Synapt G2-S), and a wide mass range (up to 100,000 *m/z*) in the Synapt G2-S). Ions transmitted from transfer T-wave are focused into an ion beam by transfer lens and are accelerated orthogonally into a flight tube by a high-field pusher (typically at 5-10 kV). The velocity of an ion in a field-free region after acceleration can be calculated as:

$$v = \sqrt{\frac{2ezU}{m}} \tag{1.23}$$

where m is the mass of an ion, U is the acceleration voltage, e is the electron charge, z is the charge number. If the ion travels a distance s, the travelling time t is:

$$t = \frac{s}{\sqrt{2eU}} \sqrt{\frac{m}{z}} \tag{1.24}$$

Ions of different kinetic energies then enter a dual-stage reflectron (shown in Figure 1.14), which consists of multiple ring electrodes at a two-stage increasing negative electric potentials. Ions are decelerated by the retarding electric field (typically set to around 5–10% higher than U) until their

velocities reach 0 and are reflected back to the detector.[54] More energetic ions penetrate deeper and thus stay longer in the reflectron than the ions with less kinetic energy. Reflectrons result in significant correction of spatial and velocity spreads of ions of same *m/z* and the resolving power is also improved due to the extended flight paths.[77] Arrival times of ions with different *m/z* and the intensity of the signal are accurately recorded and converted to mass spectra by an analogue-to-digital converter (ADC).

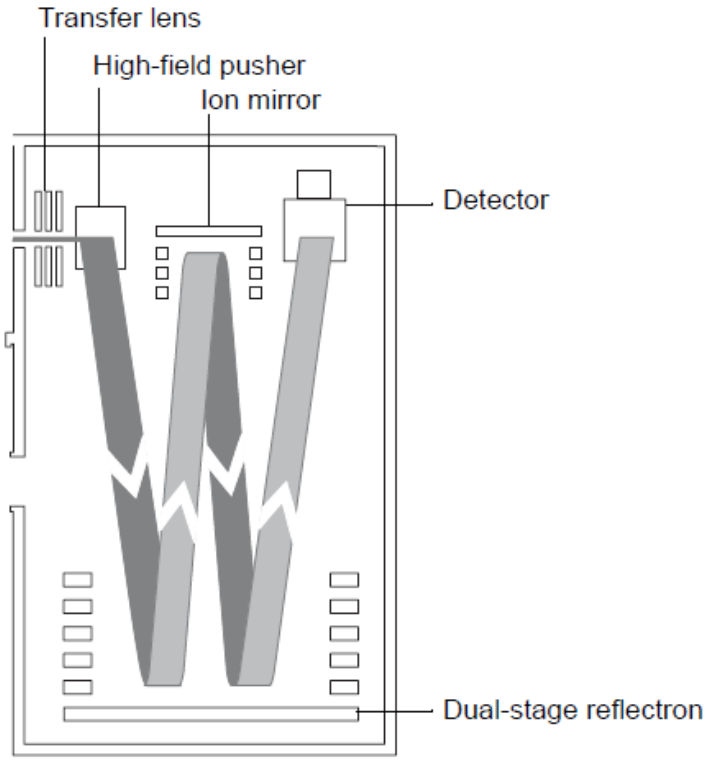

Figure 1.14 TOF analyzer of Synapt G2-S in high resolution (double-pass) mode, adapted from Waters user's manual.

1.3.2.2 Orbitrap mass spectrometer

A Q Exactive Orbitrap and an Ultra-high mass range (UHMR) Q Exactive Orbitrap mass spectrometer (Thermo Fisher Scientific, Bremen, Germany), each equipped with a nanoESI source were used in Chapter 2, 3 and 4.

The Orbitrap mass analyzer is composed of two electrodes (a spindle-like central electrode at high voltage and a grounded outer barrel-like electrode separated into a half by a dielectric ceramic ring) as shown in Figure 1.15 and 1.16. When the voltage is applied between the outer and the central electrodes, the resulting electric field is strictly linear along the axis of the central electrode (z) and thus oscillations along this direction will be purely harmonic. At the same time, the radial component of the field strongly attracts ions to the central electrode.[78]

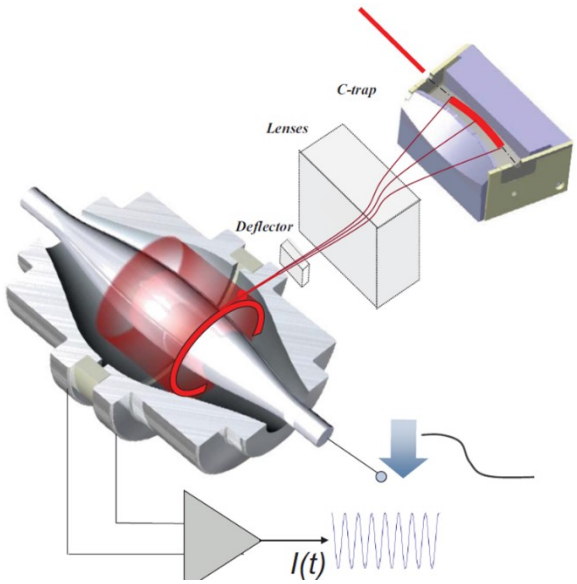

Figure 1.15 Schematic diagram of an Orbitrap mass analyzer, frequency of current image for different ions are analyzed and then converted into spectrum by FT. Figure adapted from Thermo Fisher user's manual.

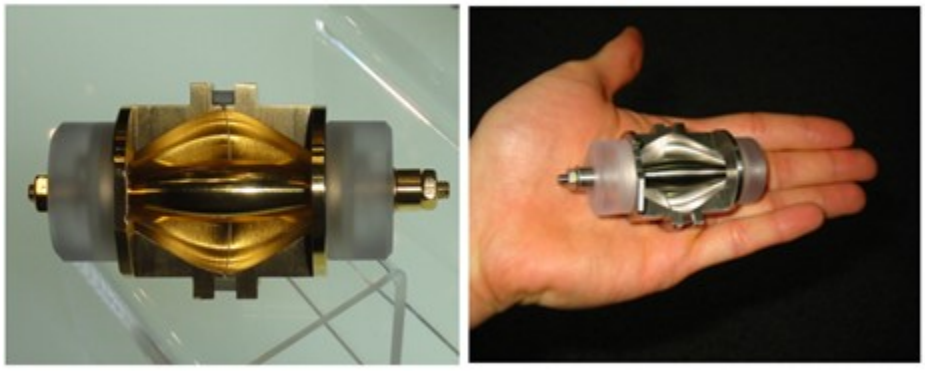

Figure 1.16 Orbitrap mass analyzer in the Thermo Fisher Q Exactive mass spectrometer used in the present work. Figure adapted from Thermo Fisher user's manual.

An ion package is injected as a focused beam tangentially into the Orbitrap analyzer off the equatorial plane of symmetry (z =0) from an RF-only nitrogen filled multipole termed the C-trap and starts to rotate around the central electrode with decreasing radius under increasing electrode potential (termed "electrodynamic squeezing").[79] With a voltage applied between the central and outer electrodes, a radial electric field bends the ion trajectory toward the central electrode while tangential velocity creates an opposing centrifugal force. Ions are directed simultaneously by the axial electric field E_z oscillate along the z axis at frequency ω_z (Eq. 1.25), while rotation frequency ω_φ corresponding to angular motion (Eq. 1.26) and radial oscillation ω_r corresponding to radial motion (Eq. 1.27) under the radial field E_r can be derived.[80]

$$\omega_z = \sqrt{k \cdot \frac{ze}{m_i}} \qquad (1.25)$$

$$\omega_{\varphi}=\frac{\omega_z}{\sqrt{2}}\sqrt{\left(\frac{R_m}{R_c}\right)^2-1} \tag{1.26}$$

$$\omega_r=\omega_z\sqrt{\left(\frac{R_m}{R_c}\right)^2-2} \tag{1.27}$$

where R_c is circular radius of ions, R_m is the characteristic radius, k is the field curvature and e is the elementary charge. Only the harmonic axial oscillations frequency ω_z is independent of initial positions and kinetic energies of ions, which can be detected in time domain by the image current. After amplification, the digitized image current in the time domain is Fourier-transformed into the frequency domain in the same way as Fourier Transformed and then converted to mass to charge spectrum. The mass resolving power *Res* can be calculated as Eq. 1.28:

$$Res=\frac{m_i}{\Delta m_i}=\frac{1}{2\Delta\omega_z}\sqrt{k\cdot\frac{ze}{m_i}} \tag{1.28}$$

However, the actual resolution of Orbitrap is limited by the time of the detectable signal. Therefore, ultra-high vacuum (typically ~2×10^{-10} mbar) is required to reduce the collisions with residual gas, which can result in loss of the coherence of ion packages and potential ion fragmentation. Besides, another prerequisite for the successful image current detection is the proper ion injection. A curved RF-only gas filled (typically operated with ~1 mTorr of nitrogen) multipole, C trap, serves as an external ion storage device prior to the injection, where ions are collected and thermalized through collisions with nitrogen gas. Ions are ejected from the C-trap through the gap between the inner electrodes by applying fast high-voltage electric pulses (~ 100 nanoseconds), and subsequently converge on the entrance of the Orbitrap.[54]

Shown in Figure 1.17 is a schematic diagram of the Thermo Fisher Q Exactive UHMR mass spectrometer used in the present work. Gaseous ions generated from nanoESI at atmospheric pressure are drawn into the ion transfer capillary by decreasing pressure and transported to the RF-lens where they are captured and focused into an ion beam. Ions are then transmitted to the low pressure ion optics regions and enter the injection flatapole, where they are trapped, focused and desolvated by maintaining a negative potential on the injection flatapole lens and a positive potential on inter-flatapole lens. Subsequently, ejected ions are focused and guided through the bent flatapole by an axial DC field and a focusing RF field. Neutral particles and solvent droplets are removed due to the 90^{o} arc. A hyperbolic segmented quadrupole (HyperQuad^{TM}) mass filter is employed to selectively transfer ions with improved ion transmission and optimized isolation window. Exiting from the gas-free multipole, ions release their kinetic energy through collisions with gas and pass through the C trap in an ion beam and detected in the Orbitrap mass analyzer. Ion fragmentation can be induced by employing the HCD (Higher energy collisional dissociation) cell, a straight multipole connected to the C trap.

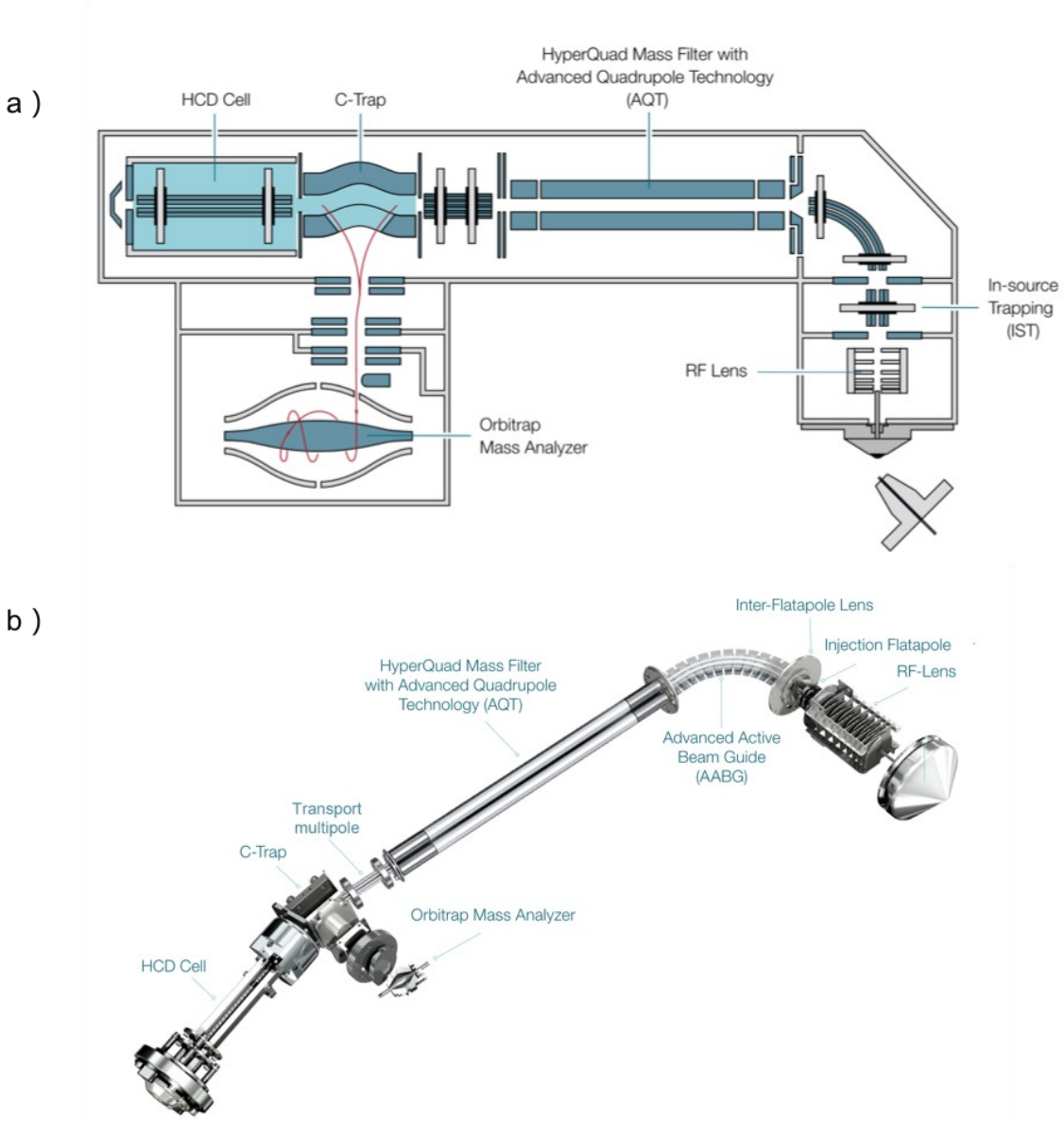

Figure 1.17 a) Cartoon schematic diagram of the Thermo Fisher Q Exactive UHMR mass spectrometer. b) Detailed components of the Thermo Fisher Q Exactive UHMR mass spectrometer, adapted from Thermo Fisher user's manual.

1.4 Response factor in ESI-MS based CAZyme assays

Electrospray ionization mass spectrometry has emerged as a versatile, label-free method for monitoring enzyme reactions. Measurements can be performed in off-line or on-line.[81-91] In off-line ESI-MS assays, the enzymatic reaction is typically quenched by addition of organic solvent (e.g. acetonitrile) or high temperature (to denature the enzyme) at different reaction times. While straightforward to implement, accurate quantification of the kinetic parameters requires a large number data points, which will lead to a large consumption of sample and time. On-line ESI-MS assay is more widely used due to lower sample consumption requirements. In this approach, the enzymatic reaction is continuously monitored, which enables a more accurate quantification of kinetic parameters. Another unique advantage of ESI-MS is that it allows for the monitoring of multiple substrates provided they have distinct molecular weights (MWs), thus allowing libraries of substrates to be screened simultaneously and is ideal for profiling substrate specificity.

Although numerous ESI-MS based assays have been developed for studying enzyme kinetics, a major limitation of these assays is the mass spectrum cannot be used directly for quantification of product or substrate. This is due to the non-uniform ESI-MS response factors of the substrate and corresponding product, which lead to nonlinear dependences of ESI-MS intensities (abundances) on solution concentrations.[92] The response factor in ESI-MS depends on various factors including: (1) the ionization efficiency during the electrospray process, which is related to the chemical properties of an analyte ion (e.g. strcture, hydrophobicity); (2) the transmission of the analyte ion in the mass spectrometer; and (3) the differences in the detection efficiency.

Many research groups have made efforts to correct response factor issue by quantifying the ionization efficiency. And several models were set up to connect analyte concentration and signal

based on the evaporation rate, log*P*, hydrophobicity an surface area.[53,93-95] However, there are only very limited comparable data from different papers and cannot give accurate prediction for any analytes.[96] An alternative way to correct response factor issue is to use internal standard (IS) with known concentration, which is commonly used for the quantification of an analyte.[89-91,97,98] An IS should be structurally similar with analyte to show the same response factor. Therefore, stable isotopically labelled analogue of analyte (e.g. containing ^{13}C, ^{15}N, ^{2}H) with the same chemical properties will be the ideal IS. Moreover, it is important that the mass difference between IS and analyte is at least 3 Da in order to avoid the interference with the signal of isotopic peaks of the analytes. In addition, the IS should be pure enough to prevent any contributions to the analyte signal.

By introducing an IS with identical or nearly-so response factor as the substrate or product and at known concentration, the solution concentration of the substrate or product can be directly determined from the mass spectrum. As an example, the concentration of the enzymatic product can be calculated using Eq 1.29:

$$[\text{Product}] = \frac{[\text{IS}_{\text{product}}]Ab(\text{Product})}{Ab(\text{IS}_{\text{product}})} \qquad (1.29)$$

where $[\text{IS}_{\text{product}}]$ is the concentration of internal standard of the product, and *Ab*(Product) and *Ab*(IS $\text{IS}_{\text{product}}$) are the measured abundances (or intensity) of product and IS, respectively.

However, isotopic labelled standard material are frequently not available commercially, prohibitively expensive or difficult to synthesize which will limit the development of ESI-MS based kinetics assays.[85-91] Addressing such standard material limitation is one major goal in the present work and is discussed in the following Chapters.

1.5 Direct ESI-MS based assay to quantify protein-ligand interactions

ESI-MS has been widely used to quantify interactions between proteins and ligands (including proteins, carbohydrates, lipids, nucleic acids, and small molecules).[99] Protein-ligand interactions are also employed in the ESI-MS method development for CAZyme kinetic study in the present work described in Charpter 2, therefore a brief description of direct ESI-MS assay to quantify protein-ligand interactions by Synapt G2-S are provided here.

For a reversible interaction (eq 1.30) of a monovalent protein (P) with a monovalent ligand (L) in solution, a complex (PL) is formed, equilibrium can be described as:

$$P + L \rightleftharpoons PL \qquad (1.30)$$

The abundance (*Ab*) ratio (*R*) of the ligand-bound protein (PL) to free protein (P) ions measured by ESI-MS is taken to be equal to the equilibrium concentration ratio in a solution, Eq 1.31:

$$R = \frac{Ab(\mathrm{PL})}{Ab(\mathrm{P})} = \frac{[\mathrm{PL}]}{[\mathrm{P}]} \qquad (1.31)$$

The [P] and [PL] are equilibrium concentrations of the protein and protein–ligand complex in a solution, respectively. With known initial concentrations of protein ($[P]_0$) and ligand ($[L]_0$), the apparent association constant (K_a) and dissociation constant (K_d) can be calculated by eqs 1.33a and 1.33b:

$$K_a = \frac{[\mathrm{PL}]}{[\mathrm{P}][\mathrm{L}]} = \frac{R}{[\mathrm{L}]_0 - \frac{R}{1+R}[\mathrm{P}]_0} \qquad (1.33a)$$

$$K_d = \frac{[\mathrm{P}][\mathrm{L}]}{[\mathrm{PL}]} = \frac{[\mathrm{L}]_0 - \frac{R}{1+R}[\mathrm{P}]_0}{R} = \frac{[\mathrm{L}]_0}{R} + \frac{[\mathrm{P}]_0}{1+R} \qquad (1.33b)$$

Here [L] is the equilibrium concentration of the ligand.

Normally, the affinity K_a is determined by a titration experiment performed at a fixed protein concentration and varied concentrations of the ligand. Nonlinear regression analysis of the

experimentally determined concentration- dependence of the fraction of ligand-bound protein ($R/(R+1)$) is employed to extract the K_a by eq 1.34:[99]

$$\frac{R}{R+1} = \frac{1+K_a[L]_0+K_a[P]_0-\sqrt{(1-K_a[L]_0+K_a[P]_0)^2+4K_a[L]_0}}{2K_a[P]_0} \qquad (1.34)$$

Experimentally, the values of Ka can be measured accurately with the direct ESI-MS range from ~10^2 to ~10^7 M^{-1}, which fits to most protein-carbohydrate interactions.

Protein–ligand interactions in solution are probed in the ESI-MS binding assays by transferring the free and ligand-bound proteins to gas phase by ESI and detecting the maintained equilibrium abundance of these species. Therefore, any physical or chemical process during ESI and in the gas phase that affects those distributions will lead to incorrect K_a values and, potentially, obscure the true binding stoichiometry. There are four common sources of error associated with ESI-MS assays: (1) in-source dissociation, (2) nonspecific protein–ligand binding, (3) non-uniform response factors and (4) ESI-induced changes in solution pH and temperature.[99] Non-specific protein-ligand binding, which is the main source of error in the present work and ESI-induced pH changes, are described below as well as the strategies for its correction.

1.6 Nonspecific ligand binding during ESI-MS assay

As ions transferred from solution to gas phase during the ESI process, one fundamental assumption for quantification by ESI-MS is that the equilibrium abundances of species in solution are maintained equally to those of corresponding ions in gas phase. However, ionization can be affected by physical and chemical processes, which can ultimately lead to inaccurate results. One common source of errors in ESI-MS measurements is nonspecific binding, its formation and available strategies to tackle the problem are discussed below.[99]

Nonspecific binding of the free ligand in solution to protein or protein-ligand complex during the ESI process[100-103] will lead to false positives in the binding data. Such nonspecific binding can be explained according to the CRM model discussed in Section 1.3. Briefly, during an evaporation process of a droplet until it reaches the Rayleigh limit, it will further undergo fission and release smaller droplets. However, if one or more free ligand beside the P and PL present in the offspring droplet, nonspecific ionic or neutral intermolecular interactions occur upon solvent evaporation gaseous ions with nonspecifically interacting protein and ligands are produced (Figure 1.18). The observation of multiple ligand-bound protein ions exhibiting a Poisson-like distribution can be a sign of non-specific binding due to the statistical nature of the phenomenon. Non-specific binding is more significant at high free ligand concentration, therefore, one common method to minimize the non-specific binding is to reduce the concentration of ligand used in the experiment.[103] However, this strategy cannot be applied to relatively low affinity interactions (K_a $<10^4$ M^{-1}) as detectable complexes ions are typically obtained at high ligand concentrations (>0.05 mM).[99]

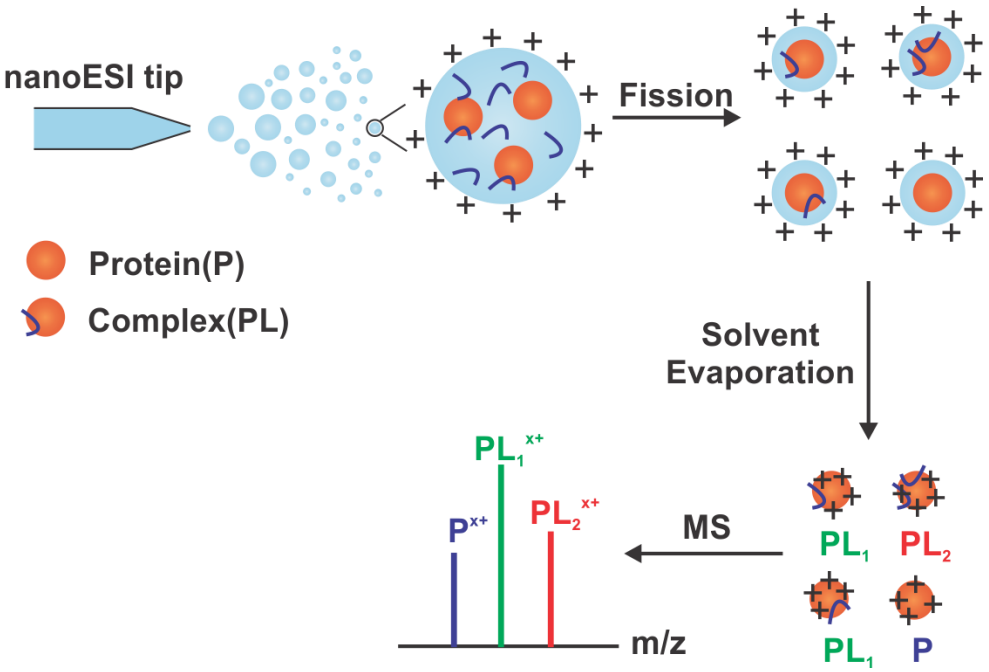

Figure 1.18 Schematic diagram of occurrence of nonspecific binding during the ESI process under the positive ion mode, adapted from Ref 92.

A number of methods have been developed to correct ESI mass spectra for the occurrence of nonspecific ligand binding.[104-110] The reference protein method, involving the introduction of a non-interacting reference protein (P_{ref}) into the solution, is the most straightforward approach to quantitatively correct for the contribution of nonspecific binding with the underlying assumption that in-source dissociation is absent and that the distribution of nonspecific protein-ligand complexes is not influenced by the nature of proteins.[105,106] The measured (apparent) abundance (Ab_{app}) of complexes in the presence of nonspecific binding can be described as:

$$Ab_0(\mathrm{PL_N}) = \left[Ab_{app}(\mathrm{PL_N}) - f_{1,\mathrm{P_{ref}}} Ab(\mathrm{PL_{N-1}}) - \ldots f_{\mathrm{N,P_{ref}}} Ab(\mathrm{P}) \right] / f_{0,\mathrm{P_{ref}}} \qquad (1.35)$$

where $f_{\mathrm{N,Pref}}$ is the fraction of P_{ref} that undergoes nonspecific binding of N molecules to L.[98] Notably, this method for correcting nonspecific binding has been successfully applied to protein interactions with proteins, carbohydrates, divalent metal ions, amino acids and peptides.[104-106,111]

1.7 ESI induced pH change in solution

The CAZyme activities and protein-ligand interactions are sensitive to pH in solution phase. However, the solution pH is changing due to the electrochemical reactions at the electrode during the ESI process.[101,112] An inert platinum is used during ESI process for instrument used in this work, therefore the major electrochemical reaction at the electrode will be the oxidation of H_2O in positive mode and negative mode, as shown in eqs 1.36a and 1.36b, respectively:

$$3H_2O \rightarrow \frac{1}{2}O_2 + 2H_3O^+ + 2e^- \quad (1.36a)$$

$$2H_2O + 2e^- \rightarrow H_2 + 2OH^- \quad (1.36b)$$

The produced H_3O^+ and OH^- will lead to a change of pH (>1 pH unit after spraying for 30 min) when a low flow rate is used for nanoESI.

An appropriate buffer could minimize the change of pH during ESI, such as "physiological" buffer phosphate buffered saline (PBS). However, PBS buffer contains large amount of phosphate, sodium and potassium ions that are not compatible with ESI-MS. Recently, submicron emitters (inner diameters around 50 nm) were shown to be able to desalt protein and protein complex ion formed by ESI directly from a biologically relevant buffer, but these emitters were not be able to perform a long-time enzymatic reaction due to damage of spray to the fragile tip, which will lead to the loss of signal.[113]

In this work, the initial rate, which is the key parameter to determine K_M and v_{max}, is experimentally determined by the linear fitting of the enzyme progress curve at early reaction time as described in previous section. Therefore, the pH change is considered unchanged during the early reaction time.

1.8 Present work

ESI-MS has become an important tool for measuring enzyme kinetics due to its versatility and one unique advantange is that it allows for the simultaneous detection of substrate(s) and product(s). However, the requirement for internal standards to quantify concentration of product or substrate during the enzymatic reaction is a significant limitation to its application to CAZymes. One of the main goals of the present work is to develop IS-free ESI-MS based methods to study CAZyme kinetics. A detailed description is given below. Chapter 2 describes an ESI-MS assay for measuring CAZyme kinetics for oligosaccharide substrates. Chapter 3 describes an ESI-MS method for CAZyme kinetics involving with glycoprotein substrates. Building on these advances, Chapter 4 describes an enzyme-assisted ESI-MS assay to quantify α2-3 Neu5Ac on prostate specific antigen (PSA) for clinical prostate cancer diagnosis.

Chapter 2 focuses on the development a versatile and quantitative ESI-MS based approach, CUPRA-ZYME, to quantify CAZyme kinetics involving oligosaccharide substrates, monitoring their reaction pathways and profiling substrate specificities. The method is based on a recently developed competitive universal proxy receptor assay (CUPRA), implemented in a time-resolved manner. In this approach, oligosaccharide substrates are labelled at their reducing end with an affinity tag (CUPRA substrate, CS), which binds with known affinity to a universal proxy protein ($^{Uni}P_{proxy}$). During the enzymatic reaction, CS is converted into CUPRA product (CP), which also interacts with $^{Uni}P_{proxy}$. The relative abundances of the ($^{Uni}P_{proxy}$+CP) and ($^{Uni}P_{proxy}$+CS) ions measured by ESI-MS are used to construct the enzyme progress curve. Measurements of the hydrolysis kinetics of CS containing ganglioside oligosaccharides by a human neuraminidase served to validate the reliability of kinetic parameters measured by CUPRA-ZYME and highlight its use in establishing catalytic pathways. Profiling substrate specificities is demonstrated by

screening the library of oligosaccharide substrates with human sialyltransferases ST6Gal1 and ST3Gal4. Finally, we show how the comparison of the reactivity of CUPRA substrates and glycan substrates present on glycoproteins, measured simultaneously, affords a unique opportunity to quantitatively study how the structure and protein environment of natural glycoconjugate substrates influences CAZyme activity.

Glycoproteins belong to another large group of natural substrates for CAZymes. However, measuring CAZyme kinetics for glycoprotein substrates is challenging due to their heterogeneity. Chapter 3 introduces a simple quantitative ESI-MS method for measuring the kinetics of CAZyme reactions involving glycoprotein substrates. The assay, referred to as Center-of-Mass (CoM) Monitoring (CoMMon), relies on continuous monitoring of the CoM of an ensemble of glycoprotein substrates and their corresponding CAZyme products. To demonstrate the reliability of CoMMon, we applied the method to the neuraminidase-catalyzed cleavage of Neu5Ac residues from a series of glycoproteins of varying molecular weights and degree of glycosylation. To illustrate the applicability of CoMMon to glycosyltransferase reactions, the assay was used to measure the kinetics of sialylation of a series of asialoglycoproteins by a human sialyltransferase. Finally, the application of of CoMMon to measure CAZyme kinetics for large glycoprotein substrates, for which individual species (glycan compositions) cannot be resolved by ESI-MS, was demonstrated.

Chapter 4 introduces an enzyme-assisted top-down ESI-MS method for quantification of the fractional content of α2-3- linked Neu5Ac on prostate specific antigen (PSA) for prostate cancer (PCa) diagnosis. The assay employs CoMMon method and a combination of specific (to remove α2-3-linked Neu5Ac) and nonspecific neuraminidases. The method was validated through comparison of the α2-3 Neu5Ac content of PSA from a commercial source with results obtained

using an IS approach and from hydrophilic interaction ultrahigh performance liquid chromatography (HILIC-UPLC) analysis of the released PSA glycans. To illustrate the potential of the assay for clinical diagnosis of PCa and disease staging, the relative α2-3 Neu5Ac content was quantified for PSA extracted from blood serum of low, intermediate and high-risk prostate cancer patients. The results indicate a high sensitivity and specificity for discrimination of both low risk PCa and high risk PCa or low and intermediate risk PCa.

1.9 References

(1) Cummings, J. H.; Stephen, A. M. Carbohydrate terminology and classification. *Eur. J. Clin. Nutr.* **2007**, *61*, S5–S18.

(2) Flynn, R. A.; Pedram, K.; Malaker, S. A.; Batista, P. J.; Smith, B. A. H.; Johnson, A. G.; George, B. M.; Majzoub, K.; Villalta, P. W.; Carette, J. E.; Bertozzi, C. R. Small RNAs are modified with *N*-glycans and displayed on the surface of living cells. *Cell* **2021**, *184*, 3109-3124.

(3) Hart, G. W. Structural and functional diversity of glycoconjugates. *Capill. Electrophor. Carbohydrates* **2003**, 3–24.

(4) Yu, R. K.; Suzuki, Y.; Yanagisawa, M. Membrane glycolipids in stem cells. *FEBS Lett.* **2010**, *584*, 1694–1699.

(5) Simons, K.; Ikonen, E. Functional Rafts in Cell Membranes. *Nature* **1997**, *387*, 569−572.

(6) Dennis, J. W.; Granovsky, M.; Warren, C. E. Protein Glycosylation in Development and Disease. *Bioessays* **1999**, *21*, 412−421.

(7) Hounsell, E. F.; Davies, M. J.; Renouf, D. V. *O*-linked protein glycosylation structure and function. *Glycoconj. J.* **1996**, *13*, 19–26.

(8) Van den Steen, P.; Rudd, P. M.; Dwek, R. A.; Opdenakker, G. Concepts and principles of *O*-linked glycosylation. *Crit. Rev. Biochem. Mol. Biol.* **1998**, *33*, 151–208.

(9) Brockhausen, I. Pathways of *O*-glycan biosynthesis in cancer cells. *Biochim. Biophys. Acta* **1999**, *1473*, 67–95.

(10) Wopereis, S.; Lefeber, D. J.; Morava, E.; Wevers, R. A. Mechanisms in protein *O*-glycan biosynthesis and clinical and molecular aspects of protein *O*-glycan biosynthesis defects: a review. *Clin. Chem.* **2006**, *52*, 574–600.

(11) Mellquist, J. L.; Kasturi, L.; Spitalnik, S. L.; Shakin-Eshleman, S. H. The amino acid following an Asn-X-Ser/Thr sequon is an important determinant of *N*-linked core glycosylation efficiency. *Biochemistry* **1998**, *37*, 6833–6837.

(12) Imperiali, B.; O'Connor, S. E. Effect of *N*-linked glycosylation on glycopeptide and glycoprotein structure. *Curr. Opin. Chem. Biol.* **1999**, *3*, 643–649.

(13) Ardejani, M. S.; Noodleman, L.; Powers, E. T.; Kelly, J. W. Stereoelectronic effects in stabilizing protein-*N*-glycan interactions revealed by experiment and machine learning. *Nat. Chem.* **2021**, *13*, 480–487.

(14) Varki A. *Essentials of glycobiology*. 3rd edition. Cold Spring Harbor, New York: Cold Spring Harbor Laboratory Press. 2015

(15) Nelson, D. L.; Cox, M. M. *Lehninger Principles of Biochemistry* 5th Ed. **2008**, New York: W.H. Freeman.

(16) Dwek, R. A. Glycobiology: Toward Understanding the Function of Sugars. *Chem. Rev.* **1996**, *96*, 683–720.

(17) Cantarel, B. L.; Coutinho, P. M.; Rancurel, C.; Bernard, T.; Lombard, V.; Henrissat, B. The carbohydrate-active enzymes database (CAZy): an expert resource for glycogenomics. *Nucleic Acids Res.* **2008**, *37*, D233–D238.

(18) Henrissat, B. A classification of glycosyl hydrolases based on amino acid sequence similarities. *Biochem. J.* **1991**, *280*, 309–316.

(19) Davies, G. J.; Gloster, T. M.; Henrissat, B. Recent structural insights into the expanding world of Carbohydrate-Active enzymes. *Curr. Opin. Struct. Biol.* **2005**, *15*, 637–645.

(20) Drula, E.; Garron, M.-L.; Dogan, S.; Lombard, V.; Henrissat, B.; Terrapon, N. The

Carbohydrate-Active enzyme database: functions and literature. *Nucleic Acids Res.* **2022**, *50*, D571–D577.

(21) Chang, A.; Singh, S.; Phillips Jr, G. N.; Thorson, J. S. Glycosyltransferase structural biology and its role in the design of catalysts for glycosylation. *Curr. Opin. Biotechnol.* **2011**, *22*, 800–808.

(22) Taniguchi N, Honke K, Fukuda M, Narimatsu H, Yamaguchi Y, Angata T, Eds. Handbook of glycosyltransferases and related genes. Springer, Japan, Tokyo. **2014**

(23) Zhang, Z.; Wuhrer, M.; Holst, S. Serum sialylation changes in cancer. *Glycoconj. J.* **2018**, *35*, 139–160.

(24) Hou, G.; Liu, G.; Yang, Y.; Li, Y.; Yuan, S.; Zhao, L.; Wu, M.; Liu, L.; Zhou, W. Neuraminidase 1 (NEU1) promotes proliferation and migration as a diagnostic and prognostic biomarker of hepatocellular carcinoma. *Oncotarget* **2016**, *7*, 64957–64966.

(25) Pinho, S. S.; Reis, C. A. Glycosylation in cancer: mechanisms and clinical implications. *Nat. Rev. Cancer* **2015**, *15*, 540.

(26) Helbert, W.; Poulet, L.; Drouillard, S.; Mathieu, S.; Loiodice, M.; Couturier, M.; Lombard, V.; Terrapon, N.; Turchetto, J.; Vincentelli, R.; Henrissat, B. Discovery of novel carbohydrate-active enzymes through the rational exploration of the protein sequences space. *Proc. Natl. Acad. Sci.* **2019**, *116*, 6063 LP – 6068.

(27) Albohy, A.; Li, M. D.; Zheng, R. B.; Zou, C.; Cairo, C. W. Insight into substrate recognition and catalysis by the human neuraminidase 3 (NEU3) through molecular modeling and site-directed mutagenesis. *Glycobiology.* **2010**, *20*, 1127–1138.

(28) Li, J.; McClane, B. A. The sialidases of Clostridium perfringens type D strain CN3718 differ in their properties and sensitivities to inhibitors. *Appl. Environ. Microbiol.* **2014**, *80*, 1701–

1709.

(29) Xu, G.; Potter, J. A.; Russell, R. J. M.; Oggioni, M. R.; Andrew, P. W.; Taylor, G. L. Crystal structure of the NanB sialidase from *Streptococcus Pneumoniae*. *J. Mol. Biol.* **2008**, *384*, 436–449.

(30) Weinstein, J.; de Souza-e-Silva, U.; Paulson, J. C. Sialylation of glycoprotein oligosaccharides N-linked to asparagine. Enzymatic characterization of a Gal beta 1 to 3(4)GlcNAc alpha 2 to 3 sialyltransferase and a Gal beta 1 to 4GlcNAc alpha 2 to 6 sialyltransferase From Rat Liver. *J. Biol. Chem.* **1982**, *257*, 13845–13853.

(31) Kitagawa, H.; Paulson, J. C. Cloning of a novel alpha 2,3-sialyltransferase that sialylates glycoprotein and glycolipid carbohydrate groups. *J. Biol. Chem.* **1994**, *269*, 1394–1401.

(32) Achyuthan, K. E.; Achyuthan, A. M. Comparative enzymology, biochemistry and pathophysiology of human exo-α-sialidases (Neuraminidases). *Comp. Biochem. Physiol. Part B Biochem. Mol. Biol.* **2001**, *129*, 29–64.

(33) Srinivasan B. A guide to the Michaelis–Menten equation: steady state and beyond. *FEBS J.* **2021**.

(34) Wagner, G. K.; Pesnot, T. Glycosyltransferases and Their Assays. *ChemBioChem* **2010**, *11*, 1939–1949.

(35) Li, K. Determination of sialic acids in human serum by reversed-phase liquid chromatography with fluorimetric detection. *J. Chromatogr. B Biomed. Sci. Appl.* **1992**, *579*, 209–213.

(36) Dennis, W.; Gal, U. A Coupled assay for UDP-GlcNAc: Galβl-3GalNAc-R β1,6-N-acetylglucosaminyltransferase(GlcNAc to GalNAc). *Anal. Biochem.* **1992**, *266*, 262–266.

(37) Lowery, R.; Kleman-Leyer, K.; Staeben, M.; Westermeyer, T. Detecting the activity of an

screening acceptor substrates, inhibitors, or activators of enzymes catalyzing group transfer reactions to facilitate the development of more selective and therapeutic drugs. US patent No. 20080233592 (2008).

(38) Kumagai, K., Kojima, H., Okabe, T., and Nagano, T. Development of a highly sensitive, high-throughput assay for glycosyltransferases using enzyme-coupled fluorescence detection. *Anal. Biochem.* **2014**, *447*, 146−155.

(39) Gong, H.; Zhang, B.; Little, G.; Kovar, J.; Chen, H.; Xie, W.; Schutz-Geschwender, A.; Olive, D. M. β-Galactosidase Activity Assay Using Far-Red-Shifted Fluorescent Substrate DDAOG. *Anal. Biochem.* **2009**, *386*, 59–64.

(40) Hunter, C. D.; Porter, E. M.; Cairo, C. W. Human Neuraminidases Have Reduced Activity towards Modified Sialic Acids on Glycoproteins. *Carbohydr. Res.* **2020**, *497*, 108139.

(41) Aharoni, A.; Thieme, K.; Chiu, C. P. C.; Buchini, S.; Lairson, L. L.; Chen, H.; Strynadka, N. C. J.; Wakarchuk, W. W.; Withers, S. G. High-Throughput Screening Methodology for the Directed Evolution of Glycosyltransferases. *Nat. Methods* **2006**, *3*, 609–614.

(42) Helm, J. S.; Hu, Y.; Chen, L.; Gross, B.; Walker, S. Identification of Active-Site Inhibitors of MurG Using a Generalizable, High-Throughput Glycosyltransferase Screen. *J. Am. Chem. Soc.* **2003**, *125*, 11168–11169.

(43) Pavelka, S. Radiometric enzyme assays: development of methods for extremely sensitive determination of types 1, 2 and 3 iodothyronine deiodinase enzyme activities. *J. Radioanal. Nucl. Chem.* **2010**, *286*, 861–865.

(44) Hood, C. M.; Kelly, V. A.; Bird, M. I.; Britten, C. J. Measurement of α(1-3) fucosyltransferase activity using scintillation proximity. *Anal. Biochem.* **1998**, *255*, 8–12.

(45) Miyashiro, M.; Furuya, S.; Sugita, T. A high-throughput screening system for α1–3

fucosyltransferase-VII inhibitor utilizing scintillation proximity assay. *Anal. Biochem.* **2005**, *338*, 168–170.

(46) Ahsen, O. von; Voigtmann, U.; Klotz, M.; Nifantiev, N.; Schottelius, A.; Ernst, A.; Müller-Tiemann, B.; Parczyk, K. A miniaturized high-throughput screening assay for fucosyltransferase VII. *Anal. Biochem.* **2008**, *372*, 96–105.

(47) von Ahsen, O.; Voigtmann, U.; Klotz, M.; Nifantiev, N.; Schottelius, A.; Ernst, A.; Müller-Tiemann, B.; Parczyk, K. A miniaturized high-throughput screening assay for fucosyltransferase VII. *Anal. Biochem.* **2008**, *372*, 96–105.

(48) Brokx, R. D.; Revers, L.; Zhang, Q.; Yang, S.; Mal, T. K.; Ikura, M.; Gariépy, J. Nuclear magnetic resonance-based dissection of a glycosyltransferase specificity for the mucin MUC1 tandem repeat. Biochemistry **2003**, *42*, 13817–13825.

(49) Exnowitz, F.; Meyer, B.; Hackl, T. NMR for direct determination of Km and Vmax of enzyme reactions based on the lambert W function-analysis of progress curves. *Biochim. Biophys. Acta (BBA)-Proteins Proteomics* **2012**, *1824*, 443–449.

(50) Sukovich, D. J., Modavi, C., de Raad, M., Prince, R. N., and Anderson, J. C. DNA-linked enzyme-coupled assay for probing glucosyltransferase specificity. *ACS Synth. Biol.* **2015**, *4*, 833-841.

(51) Sun, H.; Ma, S.; Li, Y.; Qi, H.; Ning, X.; Zheng, J. Electrogenerated chemiluminescence biosensing method for the discrimination of DNA hydroxymethylation and assay of the β-glucosyltransferase activity. *Biosens. Bioelectron.* **2016**, *79*, 92−97.

(52) Liuni, P.; Wilson, D. J. Understanding and optimizing electrospray ionization techniques for proteomic analysis. *Expert Rev. Proteomics* **2011**, *8*, 197–209.

(53) Tang, L.; Kebarle, P. From ions in solution to ions in the gas phase - the mechanism of

electrospray mass spectrometry. *Anal. Chem*. **1993**, *65*, 972A-986A.

(54) Gross, J. H. *Mass Spectrometry*; Springer International Publishing: Cham, **2017**; Vol. 56.

(55) Rayleigh, Lord. XX. On the equilibrium of liquid conducting masses charged with electricity. *London, Edinburgh, Dublin Philos. Mag. J. Sci.* **1882**, *14*, 184–186.

(56) Karas, M.; Bahr, U.; Dülcks, T. Nano-Electrospray ionization mass spectrometry: addressing analytical problems beyond routine. *Fresenius. J. Anal. Chem.* **2000**, *366*, 669–676.

(57) Morad, M. R.; Rajabi, A.; Razavi, M.; Sereshkeh, S. R. P. A very stable high throughput taylor cone-jet in electrohydrodynamics. *Sci. Rep.* **2016**, *6*, 38509.

(58) Iribarne, J. V. On the evaporation of small ions from charged droplets. *J. Chem. Phys.* **1976**, *64*, 2287-2294.

(59) Konermann, L.; Ahadi, E.; Rodriguez, A. D.; Vahidi, S. Unraveling the mechanism of electrospray ionization. *Anal. Chem.* **2013**, *85*, 2–9.

(60) Kaltashov, I. A.; Mohimen, A. Estimates of protein surface areas in solution by electrospray ionization mass spectrometry. *Anal. Chem.* **2005**, *77*, 5370

(61) McAllister, R. G.; Metwally, H.; Sun, Y.; Konermann, L. Release of native-like gaseous proteins from electrospray droplets via the charged residue mechanism: insights from molecular dynamics simulations. *J. Am. Chem. Soc.* **2015**, *137*, 12667–12676.

(62) Metwally, H.; Duez, Q.; Konermann, L. Chain ejection model for electrospray ionization of unfolded proteins: evidence from atomistic simulations and ion mobility spectrometry. *Anal. Chem.* **2018**, *90*, 10069–10077.

(63) March, R. E.; Todd, J. F. J. Radio frequency quadrupole technology: evolution and contributions to mass spectrometry. *Int. J. Mass Spectrom.* **2015**, *377*, 316–328.

(64) Miller, P. E.; Denton, M. B. The quadrupole mass filter: basic operating concepts. *J. Chem. Educ.* **1986**, *63*, 617.

(65) Kero, F. A.; Pedder, R. E.; Yost, R. A. Quadrupole mass analyzers: theoretical and practical considerations. In *Encyclopedia of Genetics, Genomics, Proteomics and Bioinformatics*; **2009**.

(66) Pringle, S. D.; Giles, K.; Wildgoose, J. L.; Williams, J. P.; Slade, S. E.; Thalassinos, K.; Bateman, R. H.; Bowers, M. T.; Scrivens, J. H. An investigation of the mobility separation of some peptide and protein ions using a new hybrid quadrupole/travelling wave IMS/oa-ToF instrument. *Int. J. Mass Spectrom.* **2007***, 261*, 1.

(67) Giles, K.; Pringle, S. D.; Worthington, K. R.; Little, D.; Wildgoose, J. L.; Bateman, R. H. Applications of a travelling wave-based radio-frequency-only stacked ring ion guide. *Rapid Commun. Mass Spectrom.* **2004***, 18*, 2401–2414.

(68) Karasek, F. W. Plasma chromatography. *Anal. Chem.* **1974***, 46*, 710A.

(69) McCullough, B. J.; Kalapothakis, J.; Eastwood, H.; Kemper, P.; MacMillan, D.; Taylor, K.; Dorin, J.; Barran, P. E. *Anal. Chem.* **2008**, *80*, 6336.

(70) Sergio, A.; Manel, A.; Marcelo, B. Development of an ion mobility quadrupole time of flight mass spectrometer. *Anal. Chim. Acta.* **2011***, 703*, 114.

(71) Cohen, M. J.; Karasek, F. W. Plasma chromatography™-a new dimension for gas chromatography and mass spectrometry. *J. Chromatogr. Sci.* **1970***, 8*, 330.

(72) Buryakov, I. A.; Krylov, E. V.; Nazarov, E. G.; Rasulev, U. K. A new method of separation of multi-atomic ions by mobility at atmospheric pressure using a high-frequency amplitude-asymmetric strong electric field. *Int. J. Mass Spectrom. Ion Processes.* **1993***, 128*, 143.

(73) Shvartsburg, A. A.; Smith, R. D. Fundamentals of traveling wave ion mobility spectrometry.

Anal. Chem. **2008**, *80*, 9689.

(74) Wildgoose, J.; McKenna, T.; Hughes, C.; Giles, K.; Pringle, S.; Campuzano, I.; Langridge, J.; Bateman, R. H. Using a novel travelling wave ion mobility device coupled with a time-of-flight mass spectrometer for the analysis of intact proteins. *Mol. Cell. Proteomics.* **2006**, *5*, S14.

(75) Ruotolo, B. T.; Benesch, J. L. P.; Sandercock, A. M.; Hyung, S.-J.; Robinson, C. V. Ion mobility–mass spectrometry analysis of large protein complexes. *Nat. Protocols.* **2008**, *3*, 1139.

(76) Giles, K.; Williams, J. P.; Campuzano, I. Enhancements in travelling wave ion mobility resolution. *Rapid Commun. Mass Spectrom.* **2011**, *25*, 1559.

(77) Guilhaus, M. Special feature: Tutorial. Principles and instrumentation in time-of-flight mass spectrometry. Physical and instrumental concepts. *J. Mass Spectrom.* **1995**, *30*, 1519–1532.

(78) Zubarev, R. A.; Makarov, A. Orbitrap mass spectrometry. *Anal. Chem.* **2013**, *85*, 5288–5296.

(79) Perry, R. H.; Cooks, R. G.; Noll, R. J. Orbitrap mass spectrometry: instrumentation, ion motion and applications. *Mass Spectrom. Rev.* **2008**, *27*, 661–699.

(80) Makarov, A. Electrostatic Axially Harmonic Orbital Trapping: A high-performance technique of mass analysis. *Anal. Chem.* **2000**, *72*, 1156–1162.

(81) Liesener, A.; Karst, U. Monitoring enzymatic conversions by mass spectrometry: a critical review. *Anal. Bioanal. Chem.* **2005**, *382*, 1451–1464.

(82) Pi, N.; Armstrong, J. I.; Bertozzi, C. R.; Leary, J. A. Kinetic analysis of NodST sulfotransferase using an electrospray ionization mass spectrometry assay. *Biochemistry* **2002**, *41*, 13283–13288.

(83) Norris, A. J.; Whitelegge, J. P.; Faull, K. F.; Toyokuni, T. Analysis of enzyme kinetics using

electrospray ionization mass spectrometry and multiple reaction monitoring: fucosyltransferase V. *Biochemistry* **2001**, *40*, 3774–3779.

(84) Danan, L. M.; Yu, Z.; Hoffhines, A. J.; Moore, K. L.; Leary, J. A. Mass spectrometric kinetic analysis of human tyrosylprotein sulfotransferase-1 and -2. *J. Am. Soc. Mass Spectrom.* **2008**, *19*, 1459–1466.

(85) Fabris, D. Steady-state kinetics of ricin a-chain reaction with the sarcin−ricin loop and with HIV-1 Ψ-RNA hairpins evaluated by direct infusion electrospray ionization mass spectrometry. *J. Am. Chem. Soc.* **2000**, *122*, 8779–8780.

(86) Cheng, S.; Wu, Q.; Xiao, H.; Chen, H. Online monitoring of enzymatic reactions using time-resolved desorption electrospray ionization mass rpectrometry. *Anal. Chem.* **2017**, *89*, 2338–2344.

(87) Sandbhor, M. S.; Soya, N.; Albohy, A.; Zheng, R. B.; Cartmell, J.; Bundle, D. R.; Klassen, J. S.; Cairo, C. W. Substrate recognition of the membrane-associated sialidase NEU3 requires a hydrophobic aglycone. *Biochemistry* **2011**, *50*, 6753–6762.

(88) Hines, H. B.; Brueggemann, E. E.; Hale, M. L. High-performance liquid chromatography–mass selective detection assay for adenine released from a synthetic RNA substrate by ricin A chain. *Anal. Biochem.* **2004**, *330*, 119–122.

(89) Gerber, S. A.; Scott, C. R.; Turecek, F.; Gelb, M. H. Analysis of rates of multiple enzymes in cell lysates by electrospray ionization mass spectrometry. *J. Am. Chem. Soc.* **1999**, *121*, 1102–1103.

(90) Deng, G.; Gu, R.-F.; Marmor, S.; Fisher, S. L.; Jahic, H.; Sanyal, G. Development of an LC–MS based enzyme activity assay for MurC: application to evaluation of inhibitors and kinetic analysis. *J. Pharm. Biomed. Anal.* **2004**, *35*, 817–828.

(91) Ge, X.; Sirich, T. L.; Beyer, M. K.; Desaire, H.; Leary, J. A. A Strategy for the determination of enzyme kinetics using electrospray ionization with an ion trap mass spectrometer. *Anal. Chem.* **2001**, *73*, 5078–5082.

(92) Gabelica, V.; Galic, N.; Rosu, F.; Houssier, C.; De Pauw, E. Influence of response factors on determining equilibrium association constants of non-covalent complexes by electrospray ionization mass spectrometry. *J. Mass Spectrom.* **2003**, *38*, 491–501.

(93) Golubović, J.; Birkemeyer, C.; Protić, A.; Otašević, B.; Zečević, M. Structure–Response Relationship in Electrospray Ionization-Mass Spectrometry of Sartans by Artificial Neural Networks. *J. Chromatogr. A* **2016**, *1438*, 123–132.

(94) Huffman, B. A.; Poltash, M. L.; Hughey, C. A. Effect of Polar Protic and Polar Aprotic Solvents on Negative-Ion Electrospray Ionization and Chromatographic Separation of Small Acidic Molecules. *Anal. Chem.* **2012**, *84*, 9942–9950.

(95) Henriksen, T.; Juhler, R. K.; Svensmark, B.; Cech, N. B. The Relative Influences of Acidity and Polarity on Responsiveness of Small Organic Molecules to Analysis with Negative Ion Electrospray Ionization Mass Spectrometry (ESI-MS). *J. Am. Soc. Mass Spectrom.* **2005**, *16*, 446–455.

(96) Liigand, P.; Liigand, J.; Kaupmees, K.; Kruve, A. 30 Years of Research on ESI/MS Response: Trends, Contradictions and Applications. *Anal. Chim. Acta* **2021**, *1152*, 238117.

(97) Stokvis, E.; Rosing, H.; Beijnen, J. H. Stable Isotopically Labeled Internal Standards in Quantitative Bioanalysis Using Liquid Chromatography/Mass Spectrometry: Necessity or Not? *Rapid Commun. Mass Spectrom.* **2005**, *19*, 401–407.

(98) Wang, S.; Cyronak, M.; Yang, E. Does a Stable Isotopically Labeled Internal Standard Always Correct Analyte Response?: A Matrix Effect Study on a LC/MS/MS Method for the

Determination of Carvedilol Enantiomers in Human Plasma. *J. Pharm. Biomed. Anal.* **2007**, *43*, 701–707.

(99) Kitova, E. N.; El-Hawiet, A.; Schnier, P. D.; Klassen, J. S. Reliable determinations of protein–ligand interactions by direct ESI-MS measurements. Are we there yet? *J. Am. Soc. Mass Spectrom.* **2012**, *23*, 431–441.

(100) Marshall, A. G.; Hendrickson, C. L.; Jackson, G. S. Fourier transform ion cyclotron resonance mass spectrometry: a primer. *Mass Spectrom. Rev.* **1998**, *17*, 1–35.

(101) Wang, W.; Kitova, E. N.; Klassen, J. S. Influence of solution and gas phase processes on protein-carbohydrate binding affinities determined by nanoelectrospray fourier transform ion cyclotron resonance mass spectrometry. *Anal. Chem.* **2003**, *75*, 4945–4955.

(102) Hossain, B. M.; Konermann, L. Pulsed hydrogen/deuterium exchange MS/MS for studying the relationship between noncovalent protein complexes in solution and in the gas phase after electrospray ionization. *Anal. Chem.* **2006**, *78*, 1613–1619.

(103) Wang, W.; Kitova, E. N.; Klassen, J. S. Nonspecific protein-carbohydrate complexes produced by nanoelectrospray ionization. Factors influencing their formation and stability. *Anal. Chem.* **2005**, *77*, 3060–3071.

(104) Sun, J.; Kitova, E. N.; Wang, W.; Klassen, J. S. Method for distinguishing specific from nonspecific protein-ligand complexes in nanoelectrospray ionization mass spectrometry. *Anal. Chem.* **2006**, *78*, 3010–3018.

(105) Sun, N.; Soya, N.; Kitova, E. N.; Klassen, J. S. Nonspecific interactions between proteins and charged biomolecules in electrospray ionization mass spectrometry. *J. Am. Soc. Mass Spectrom.* **2010**, *21*, 472–481.

(106) Sun, J.; Kitova, E. N.; Sun, N.; Klassen, J. S. Method for identifying nonspecific protein-

protein interactions in nanoelectrospray ionization mass spectrometry. *Anal. Chem.* **2007**, *79*, 9301–9311.

(107) Daubenfeld, T.; Bouin, A. P.; van der Rest, G. A Deconvolution method for the separation of specific versus nonspecific interactions in noncovalent protein-ligand complexes analyzed by ESI-FT-ICR mass spectrometry. *J. Am. Soc. Mass Spectrom.* **2006**, *17*, 1239–1248.

(108) Shimon, L.; Sharon, M.; Horovitz, A. A method for removing effects of nonspecific binding on the distribution of binding stoichiometries: application to mass spectroscopy data. *Biophys. J.* **2010**, *99*, 1645–1649.

(109) Sun, N.; Sun, J.; Kitova, E. N.; Klassen, J. S. Identifying nonspecific ligand binding in electrospray ionization mass spectrometry using the reporter molecule method. *J. Am. Soc. Mass Spectrom.* **2009**, *20*, 1242–1250.

(110 Kitova, E. N.; Soya, N.; Klassen, J. S. Identifying specific small-molecule interactions using electrospray ionization mass spectrometry. *Anal. Chem.* **2011**, *83*, 5160–5167.

(111) Deng, L.; Sun, N.; Kitova, E. N.; Klassen, J. S. Direct quantification of protein-metal ion affinities by electrospray ionization mass spectrometry. *Anal. Chem.* **2010**, *82*, 2170–2174.

(112) Van Berkel, G. J.; Asano, K. G.; Schnier, P. D. Electrochemical Processes in a Wire-in-a-Capillary Bulk-Loaded, Nano-Electrospray Emitter. *J. Am. Soc. Mass Spectrom*. **2001**, *12*, 853–862.

(113) Báez Bolivar, E. G.; Bui, D. T.; Kitova, E. N.; Han, L.; Zheng, R. B.; Luber, E. J.; Sayed, S. Y.; Mahal, L. K.; Klassen, J. S. Submicron Emitters Enable Reliable Quantification of Weak Protein–Glycan Interactions by ESI-MS. *Anal. Chem*. **2021**, *93*, 4231–4239.

Chapter 2

CUPRA-ZYME: An assay for measuring carbohydrate-active enzyme activities, pathways and substrate specificities †

2.1 Introduction

Carbohydrate-Active enZymes (CAZymes) are a large group of enzymes involved in the synthesis, degradation and modification of carbohydrates. The CAZyme database, (CAZy; www.cazy.org) contains sequence information for >340,000 enzymes, which are organized into families defined by sequence similarity, structure and function.[1] The four principal families are glycosyl hydrolases (glycosidases), glycosyltransferases, polysaccharide lyases and carbohydrate esterases.[2] Carbohydrate binding modules and auxiliary activity families (e.g., ligninolytic and lytic polysaccharide mono-oxygenases) are also part of this enzyme classification system. However, substrate specificity can't be predicted entirely from sequence, so for the majority of CAZymes their substrate is not known. The most direct route to ascribing a function to a putative CAZyme involves demonstrating enzymatic activity on carbohydrate-based substrates.[3]

The CAZymes, which exist as both intra- and extracellular enzymes,[4,5] play critical roles in diverse physiological processes in humans. For example, endogenous CAZymes control the glycosylation of proteins and lipids, while exogenous enzymes associated with bacteria are

† Part of this chapter has been published as:

1. Li, Z.; Kitov, P. I.; Kitova, E. N.; Mozenah, F.; Rodrigues, E.; Chapla, D. G.; Moremen, K. W.; Macauley, M. S.; Klassen, J. S. *Anal. Chem.* **2020**, *92*, 3228–3236.
2. Kitov, P. I.; Kitova, E. N.; Han, L.; Li, Z.; Jung, J.; Rodrigues, E.; Hunter, C. D.; Cairo, C. W.; Macauley, M. S.; Klassen, J. S. *Commun. Biol.* **2019**, *2*, 268-274.

responsible for the digestion of complex carbohydrates in the gut.[6] CAZymes also have important industrial and biotechnological applications, are important drug targets and represent promisingbiomarkers for the diagnosis of a variety of diseases, including certain cancers.[7–9] Measurements of the activities, pathways and substrate specificities are fundamental to a comprehensive understanding of the biological functions of CAZymes and exploiting these enzymes for industrial and biomedical applications.[10–13] Despite their importance, deficiencies in the available analytical tools hinder kinetic studies of CAZymes and, as a result, knowledge of the substrate specificities of most of these enzymes is incomplete. In fact, it is estimated that fewer than 1% of the putative CAZymes predicted from DNA sequence data within the CAZy database are associated with any experimental data.[14]

Most naturally occurring glycans do not exhibit optical properties and, therefore, enzymatic processing of glycan substrates typically can't be directly monitored using spectrophotometry-based kinetic assays. Application of optical methods generally requires the introduction of a suitable chromophore (e.g. fluorophore) into the substrate. However, such modifications, depending on their nature and location, may influence CAZyme activity. Moreover, optical methods are susceptible to fluorescence quenching at high concentrations and not readily amenable to analyzing multiple substrates simultaneously. Alternatively, glycan processing kinetics may be monitored using a secondary chemical or enzymatic reaction, which generates an optically detectable signal from the CAZyme product. For example, the release of sialic acid from glycans by a sialidase can be monitored by reacting the monosaccharide with malononitrile to produce a fluorescent product.[15] Multi-enzyme schemes, wherein a second enzyme acts rapidly on the CAZyme product to produce a coloured/fluorescent secondary product, are frequently used for glycosyl hydrolases. However, developing coupled assays for glycosyltransferases is more

challenging.[16] Some of the reported methods rely on the detection of the donor leaving group (e.g., the nucleotide diphosphate, UDP) by displacing a corresponding fluorophore-labeled donor product from an immobilized antibody or through some other fluorescence-based readout achieved using coupled chemical/enzymatic reactions.[17,18] DNA-linked enzyme-coupled assays have also been demonstrated for some glycosyltransferases.[19,20] These methods, however, require multiple and typically expensive reagents (i.e., antibodies or enzymes) to implement, may be susceptible to background interferences and may not be readily applied to mixtures of substrates. Radiometric methods, which employ substrates containing a radioactive isotope, have been widely used to study CAZyme-catalyzed reactions in the past.[21] In such assays, the change in radiation intensity is the evaluated signal. Radio-labeling is attractive in that it does not change the kinetic property of the natural substrate (provided the label does not lead to a significant kinetic isotope effect).[22] However, an extraction (or chromatography) step is required in order to separate radiolabeled substrate from the product. Additionally, the availability of radioactive-labelled glycan substrates compounds is often limited and use of the assay is restricted to safety certified labs. Therefore, the demand for more versatile and, in particular, label-free assays for measuring CAZyme activities is high, particularly for enzymes involved in building up glycans, namely the glycosyltransferases.[23]

Electrospray ionization mass spectrometry (ESI-MS) has emerged as a versatile, label-free method for monitoring enzyme reactions.[23–33] A unique advantage of ESI-MS is that it allows for the simultaneous detection of substrate and product and, if present at observable concentrations, intermediates. Also, it can be readily implemented on multiple substrates provided they have distinct molecular weights (MWs), thus allowing libraries of substrates to be screened simultaneously. Such an approach is ideal for profiling substrate specificity. However, because of differences in ESI-MS response factors, correlating the measured substrate and product ion

abundances to solution concentrations represents a challenge and quantitative monitoring of the enzyme-catalyzed reaction progress generally requires the use of internal standards, which can be expensive or difficult to synthesize, or calibration curves.[28–33]

Here, we introduce a versatile and quantitative assay for measuring the kinetic parameters of CAZyme reactions, establishing their catalytic pathways and profiling their substrate specificities. The method, referred to as CUPRA-ZYME (Figure 2.1a), is based on the recently developed Competitive Universal Proxy Receptor Assay (CUPRA) and time-resolved ESI-MS measurements.[34] CUPRA employs oligosaccharides labeled at the reducing end with an affinity tag. Examples of three different CUPRA linker (CL)-affinity tag combinations, which were used in the present work, are given in Figure 2.1b. The affinity tag are recognized by a protein receptor (referred to as the universal proxy receptor, $^{Uni}P_{proxy}$), and direct ESI-MS analysis of the non-covalent complexes of the heterobifunctional glycan ligands (called CUPRA ligands) and $^{Uni}P_{proxy}$. Changes in relative abundances (as measured by ESI-MS) of specific $^{Uni}P_{proxy}$-CUPRA ligand complexes upon introduction of a glycan-binding protein (GBP) to identify ligand binding and allow affinities to be quantified. When performed in a time-resolved fashion and in the presence of a CAZyme, CUPRA allows for time-dependent changes in the concentrations of CUPRA ligands that are substrates (i.e., CUPRA substrates, CS (Figure 2.1c)) to be measured. Because of the ESI-MS response factor-independent manner in which substrate concentration is measured, CUPRA-ZYME eliminates the need for calibration curves or internal standards, which are generally required with ESI-MS-based enzyme kinetics.[28–33] Moreover, the concentrations of products and any intermediates that retain the affinity tag can also be quantified, independent of the nature of the chemical modification catalyzed by the CAZyme.

Kinetic measurements of the hydrolysis of CS prepared from ganglioside oligosaccharides by the glycosyl hydrolase human neuraminidase 3 (NEU3) were used to establish the reliability of CUPRA-ZYME for measuring kinetic parameters and highlight its use for studying multistep enzyme reactions. Measurements performed on human neuraminidase (NEU2 and NEU3), human sialytransferases (ST6Gal1 and ST3Gal4) with libraries of CS demonstrate the potential of the assay to profile the substrate specificities of glycohydrolases and glycosyltransferases rapidly and quantitatively. Finally, we illustrate how kinetic measurements performed simultaneously on CS and glycans present on glycoproteins offers unprecedented insight into influence of the substrate environment in natural glycoconjugates on CAZyme activity.

2.2 Experimental

2.2.1 Materials

2.2.1.1 Proteins &CAZymes

Human carbonic anhydrase (hCA, type 1, MW 28,848 Da), lysozyme (Lyz, from chicken egg white, MW 14,310 Da), neuraminidase (NEU, from *Clostridium perfringens*) and SAvPhire monomeric streptavidin (mSA, MW 15,650 Da) were purchased from Sigma-Aldrich Canada (Oakville, Canada). Human neuraminidase 2 and 3 (NEU2 and NEU3) were a gift from Prof. C. Cairo (University of Alberta). Expression of recombinant human sialyltransferases ST6Gal1 (UniProt P15907, amino acid residues 75-406) and ST3Gal4 (UniProt Q11206, amino acid residues 41-333) were performed in Freestyle 293F cells (ThermoFisher Scientific) as GFP fusions in the pGEn2 vector as previously described.[35] Purification by Ni-NTA chromatography, cleavage of the GFP fusion tag with recombinant TEV protease, and further purification by Ni-NTA chromatography and gel filtration was also performed as previously described.[35] Human prostate

specific antigen (PSA, from seminal plasma) was purchased from Lee BioSolutions (Maryland Heights, MO, USA). All proteins and enzymes were dialyzed against an aqueous solution of 200 mM ammonium acetate (pH 7) using an Amicon 0.5 mL microconcentrator (EMD Millipore, Billerica, MA) with a MW cutoff of 3 kDa and stored at -20℃ before using.

2.2.1.2 Carbohydrates and other materials

N-acetyl-D-neuraminic acid (Neu5Ac), cytidine-5′-monophospho-N-acetylneuraminic acid (CMP-Neu5Ac) and manganese dichloride ($MnCl_2$) were purchased from Sigma-Aldrich Canada (Oakville, Canada). Biotin-PEG4-amine was purchased from BroadPharm (San Diego, USA). N-acetyl-D-neuraminic acid-1,2,3-$^{13}C_3$ (Neu5Ac-$^{13}C_3$) was purchased from Omicron Biochemicals, Inc. (South Bend, IN, USA). With the exception of Lac (Galβ1-4Glc, Sigma-Aldrich Canada, Oakville), 6SL (Neu5Acα2-6Galβ1-4Glc, Carbosynth, San Diego, USA), LNAc2 (Galβ1-3GlcNAc, Dextra Laboratories Ltd, Reading, UK), LNAc-ethylamine (Galβ1-4GlcNAc-ethylamine, Figure 2.2) and 3SLNAc-ethylamine (Neu5Acα2-3Galβ1-4GlcNAc-ethylamine, the Figure 2.2), the oligosaccharides used to prepare the CUPRA substrates shown in Table 2.1 were purchased from Elicityl SA (Crolles, France). The free N-glycans Galβ1-4GlcNAcβ1-2Manα1-3(Galβ1-4GlcNAcβ1-2Manα1-6)Manβ1-4GlcNAcβ1-4GlcNAc and Neu5Acα2-6Galβ1-4GlcNAcβ1-2Manα1-3(Galβ1-4GlcNAcβ1-2Manα1-6)Manβ1-4GlcNAcβ1-4GlcNAc were purchased from Chemily Glycoscience (Peachtree Corners, USA). Biotin-PEG4-amine was purchased from BroadPharm (San Diego, USA).

2.2.1.3 CUPRA substrates

CUPRA substrates (CS) employing three different CUPRA linker (CL)-affinity tag combinations were used in this chapter; representative structures are shown in Figure 2.1b. The majority of the CS, which were originally used as CUPRA ligands for library screening,[34] possess a CUPRA linker

(CL) containing sulfonamide affinity tag, which was attached through a short PEG linker followed by Phe-Phe dipeptide and terminated with phenylsulfonamide (CL^{S1}, Figure 2.1c). This linker was attached to the free reducing end of the oligosaccharide via *N*-glycosidic linkage (CS^{S1}). The detailed synthesis procedures used for the production of CL^{S1} and the CS^{S1} are given elsewhere and only a brief synthesis scheme is shown in Figure 2.3.[34] In the case of LNAc and 3SLNAc (to improve the yield and solubility), CL^{S1} was modified (CL^{S2}, Figure 2.1b) and coupled (Figure 2.4) via squaric acid amide to the amine-terminated aglycone to give CS^{S2} structures (Figure 2.1c). The biotin containing CUPRA linker (biotin-PEG4-amine, CL^{B}, Figure 2.1b) was conjugated directly to the free oligosaccharide (3′-sialyllactose, 3SL) according to the brief synthesis scheme in Figure 2.4b to give CS^{B} (Figure 2.1c). Human carbonic anhydrase type 1(hCA), which binds with relatively high affinity to sulfonamide-containing compounds at neutral pH, served as $^{Uni}P_{proxy}$ for CS^{S1} and CS^{S2}.[34] The monomeric streptavidin protein SAvPhire, which exhibits a high affinity for biotin analogs, served as $^{Uni}P_{proxy}$ for CS^{B}.[36]

2.2.2 Mass spectrometry and data analysis

ESI-MS measurements were carried out in positive ion mode using three instruments, a Synapt G2S ESI quadrupole-ion mobility separation-time-of-flight (Q-IMS-TOF) mass spectrometer (Waters, Manchester, UK) and Q-Exactive Ultra High Mass Range (UHMR) Hybrid Quadrupole-Orbitrap and Q Exactive Classic Hybrid Quadrupole-Orbitrap mass spectrometers (Thermo Fisher Scientific, U.K.), each equipped with a nanoflow ESI (nanoESI) source. The nanoESI tips were produced from borosilicate capillaries using a P-1000 micropipette puller (Sutter Instruments, Novato, CA). To carry out nanoESI, a platinum wire was inserted into the back end of the tip, making contact with the sample solution, and a voltage of 0.8-0.9 kV was applied. The capillary temperature was set to 60 ºC on the G2S and 120 °C on the Q-Exactive Orbitrap instruments. For

the UHMR instrument, the *m/z* range was set from 350 to 6050, the S-lens RF level was set at 35, the maximum inject time was set at 200 and each 10 microscans were combined to a single scan. For the Q Exactive Classic Orbitrap instrument, the *m/z* range was set from 200 to 3000, the S-lens RF level was set at 10, the maximum inject time was set at 200 and each 10 microscans were combined to a single scan. Kinetic data were acquired continuously and mass spectra were averaged for 1 min time periods. The resulting average mass spectra were used to quantify kinetics. Raw data were processed using the Thermo Xcalibur 2.2 software. For the Synapt G2S instrument, the Cone voltage was set to 25 V, both Trap and Transfer voltages were 0 V. Argon was used in the Trap and Transfer ion guides at pressures of 3.37×10^{-4} mbar and 5.01×10^{-4} mbar, respectively. Mass spectra were collected with a speed of 2 s per scan and average spectra of each 30 scans (1 min) were obtained for each time point. Data were acquired and pre-processed using MassLynx software (version 4.1); ion intensities were extracted using in-house software.

In some measurements, a ^{13}C-labeled Neu5Ac (Neu5Ac-$^{13}C_3$) was used as an internal standard (IS). At a given reaction time, the concentration of free Neu5Ac in solution was calculated from the ratio of the total ion abundance of Neu5Ac and Neu5Ac-$^{13}C_3$ and the concentration of Neu5Ac-$^{13}C_3$, eq 2.1:

$$[\text{Neu5Ac}] = \frac{[\text{Neu5Ac-}^{13}\text{C}_3]Ab(\text{Neu5Ac})}{Ab(\text{Neu5Ac-}^{13}\text{C}_3)} \tag{2.1}$$

where *Ab*(Neu5Ac) and *Ab*(Neu5Ac-$^{13}C_3$) are the gas-phase abundances of Neu5Ac and Neu5Ac-$^{13}C_3$ ions.

To compare the reactivity of CS and *N*-glycan substrates present in PSA, their time-dependent fractional abundances were analyzed using a single or double exponential decay function, eqs 2.2a and 2.2b, respectively:

$$F_{CS} = e^{-kt} \tag{2.2a}$$

$$F_{N\text{-}glycan} = f_1 e^{-k_1 t} + f_2 e^{-k_2 t} \quad (2.2b)$$

The fractional abundance of CS (F_{CS}) was calculated from eq 2.3a:

$$F_{CS} = \frac{Ab(^{Uni}P_{proxy}+CS)}{Ab(^{Uni}P_{proxy}+CS) + Ab(^{Uni}P_{proxy}+CP)} \quad (2.3a)$$

The bi-antennary *N*-glycan of the PSA sample used in this chapter contains two Neu5Ac, which are either α2,3- and α2,6-linked. Treatment of PSA with NEU3 results first in the formation of mono-sialylated PSA (monosialo-PSA) and then desialylated PSA (asialo-PSA). Therefore, the fractional abundance of PSA *N*-glycan substrates ($F_{N\text{-}glycan}$), which corresponds to the fractional abundance of Neu5Ac, was calculated using eq 2.3b:

$$F_{N\text{-}glycan} = \frac{2Ab(\text{PSA}) + Ab(\text{monosialo-PSA})}{2[Ab(\text{asialo-PSA})+Ab(\text{monosialo-PSA})+Ab(\text{PSA})]} \quad (2.3b)$$

where *Ab*(PSA), *Ab*(monosialo-PSA) and *Ab*(asialo-PSA) are the gas-phase ion abundances of PSA, monosialo-PSA and asialo-PSA, respectively. Asialo-PSA, which can accept two Neu5Ac, served as acceptor substrate for the reactions with the sialyltransferase ST6Gal1 and ST3Gal4 and the fractional abundance of available acceptor substrate was calculated using eq 2.3c:

$$F_{N\text{-}glycan} = \frac{2Ab(\text{asialo-PSA})+Ab(\text{monosialo-PSA})}{2[Ab(\text{asialo-PSA})+Ab(\text{monosialo-PSA})+Ab(\text{PSA})]} \quad (2.3c)$$

In eq 2.2a, *k* is the apparent rate constant for conversion of CS. For the PSA substrate, k_1 and k_2 in eq 2.2b are the apparent rate constants for cleavage of α2,3- and α2,6-linked Neu5Ac and f_1 and f_2 represent the fractional abundances of Neu5Ac with α2,3- and α2,6-linkages, respectively. For the asialo-PSA substrate, k_1 and k_2 in eq 2.2b are the apparent rate constants for addition of the first and second Neu5Ac and f_1 and f_2 are both set to 0.5.

2.2.3 CUPRA-ZYME

To implement the CUPRA-ZYME assay (Figure 2.1a) aliquots of stock solutions of CAZyme, $^{Uni}P_{proxy}$, CS and Lyz (Lysozyme, P_{ref}), all in 200 mM aqueous ammonium acetate, were manually mixed in an eppendorf tube and then transferred to the nanoESI tip. Unless otherwise noted, measurements were carried out at pH 7 and 25 °C. ESI mass spectra were collected continuously starting 3 min after mixing. Where required, the mass spectrum was corrected for the occurrence of nonspecific CS-$^{Uni}P_{proxy}$ binding formed during the ESI process using the reference protein method, which has been described in detail elsewhere.[37-39] Lyz served as P_{ref} in all kinetic experiments.

Progress curves (plots of concentrations of CS and CUPRA product(s) (CP) versus time) were constructed from the time-resolved ESI mass spectra. The concentrations of CS and CP were calculated according to the total abundances (*Ab*) of the gas-phase ions (considering all detected charge states) of the corresponding $^{Uni}P_{proxy}$ complexes (($^{Uni}P_{proxy}$+CS) and ($^{Uni}P_{proxy}$+CP)) and the known initial CS concentration ($[CS]_0$), eqs 2.4a and 2.4b:

$$[CP] = \frac{[CS]_0 \, Ab(^{Uni}P_{proxy} + CP)}{Ab(^{Uni}P_{proxy} + CP) + Ab(^{Uni}P_{proxy} + CS)} \tag{2.4a}$$

$$[CS] = \frac{[CS]_0 \, Ab(^{Uni}P_{proxy} + CS)}{Ab(^{Uni}P_{proxy} + CP) + Ab(^{Uni}P_{proxy} + CS)} \tag{2.4b}$$

Kinetic parameters (K_M and v_{max}) were established by fitting the Michaelis-Menten equation to the initial rates measured over a series of initial CS concentrations, eq 2.5:

$$v_0 = \frac{v_{max}[CS]_0}{K_M + [CS]_0} \tag{2.5}$$

where v_0 is initial velocity, v_{max} is maximum velocity and K_M is substrate concentration at half v_{max}. The initial rates were determined from linear best fits of the [CP] versus reaction time plots; unless otherwise noted, data acquired from 3 min to 10 min were used.

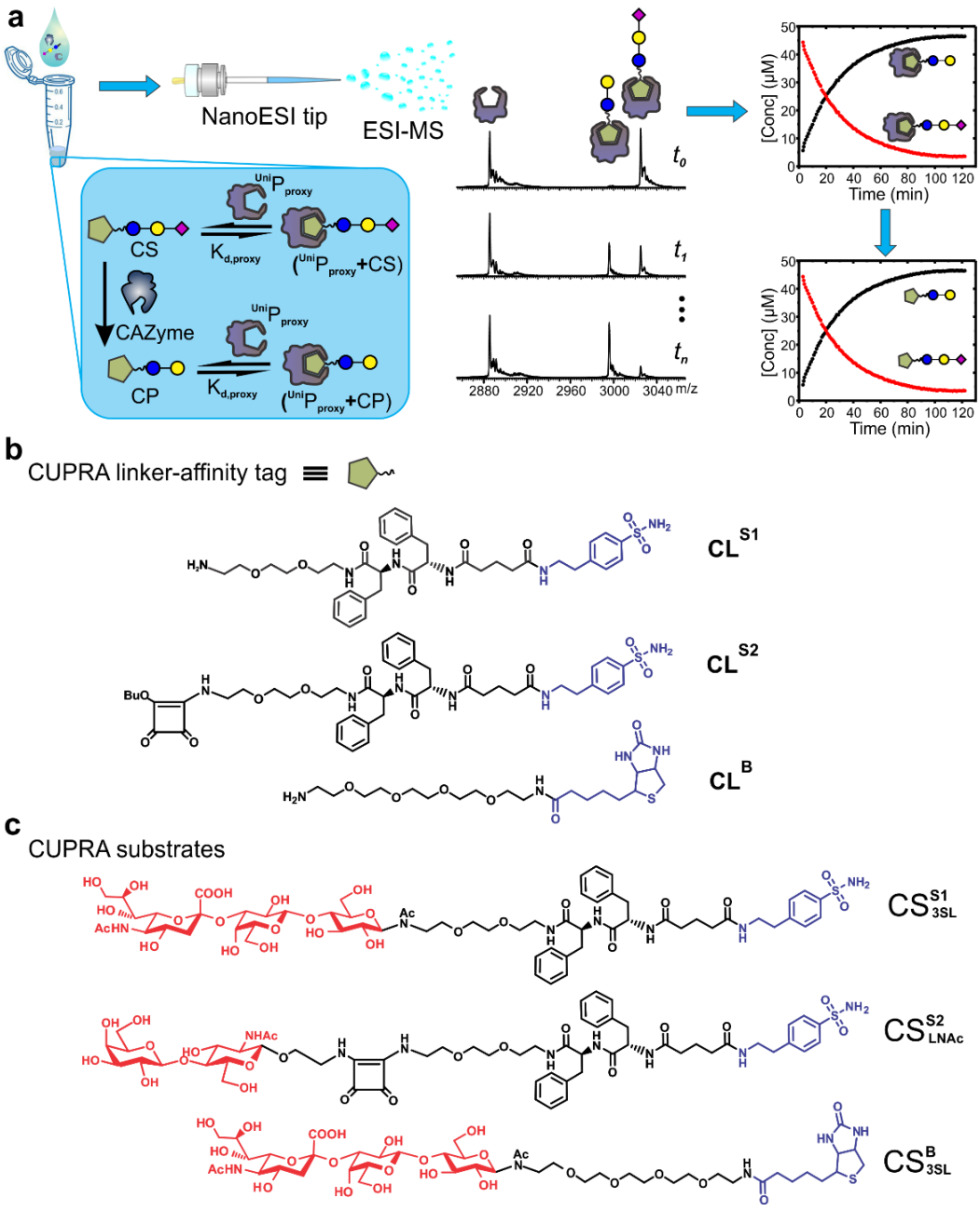

Figure 2.1. CUPRA-ZYME kinetic assay. (a) Workflow of CUPRA-ZYME method, wherein the time-dependent CUPRA substrate (CS) and product (CP) concentrations are determined from the relative abundances of CS and CP bound to a universal proxy protein ($^{Uni}P_{proxy}$) measured by ESI-MS. (b) Structures of the three CUPRA linker-affinity tags (CL) used in this work. (c) Structures of three CS used in this work; the glycan moiety is shown in red, the affinity tag in blue and the linker in black.

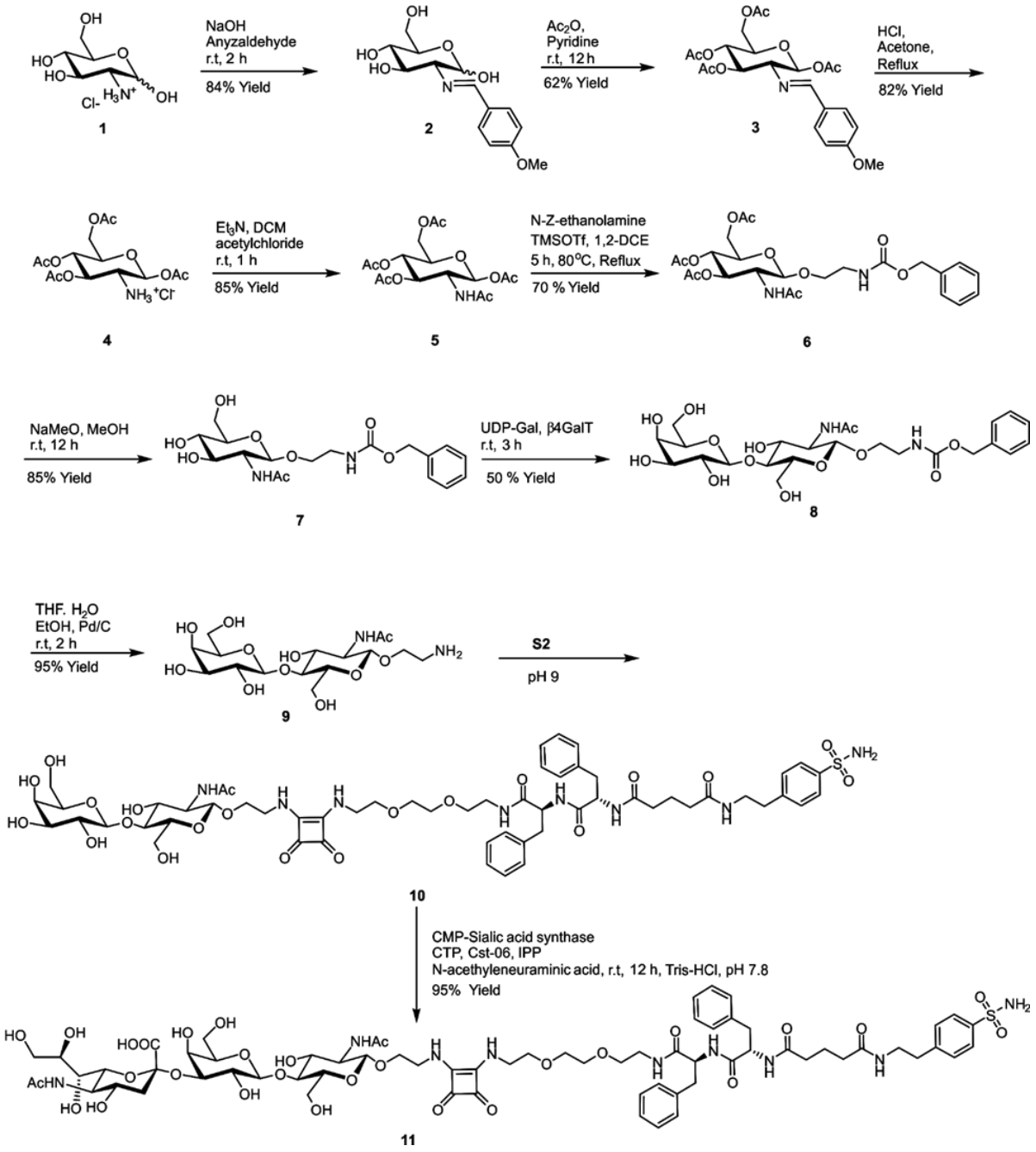

Figure 2.2. Synthetic scheme for the preparation of $\mathbf{CS^{S2}_{LNAc}}$ and $\mathbf{CS^{S2}_{3SLNAc}}$.

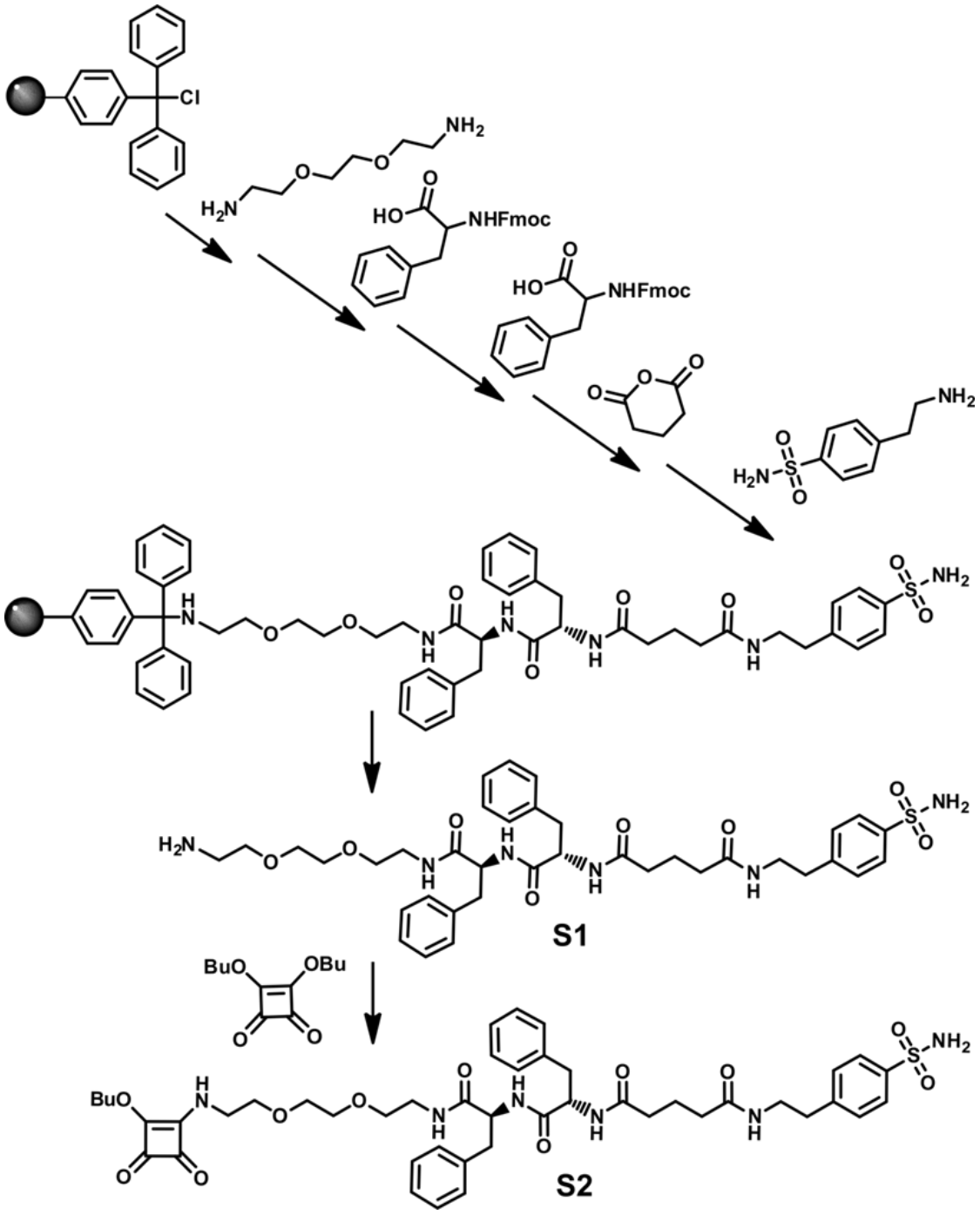

Figure 2.3. Simplified scheme of solid-phase assisted synthesis of phenyl sulfonamide-containing CUPRA linkers **S1** and **S2**. CUPRA substrates modified by this linker via N-glycosidic linkage to the free reducing end are denoted as $\mathbf{CS}^{\mathbf{S1}}$ and $\mathbf{CS}^{\mathbf{S2}}$ correspondingly.

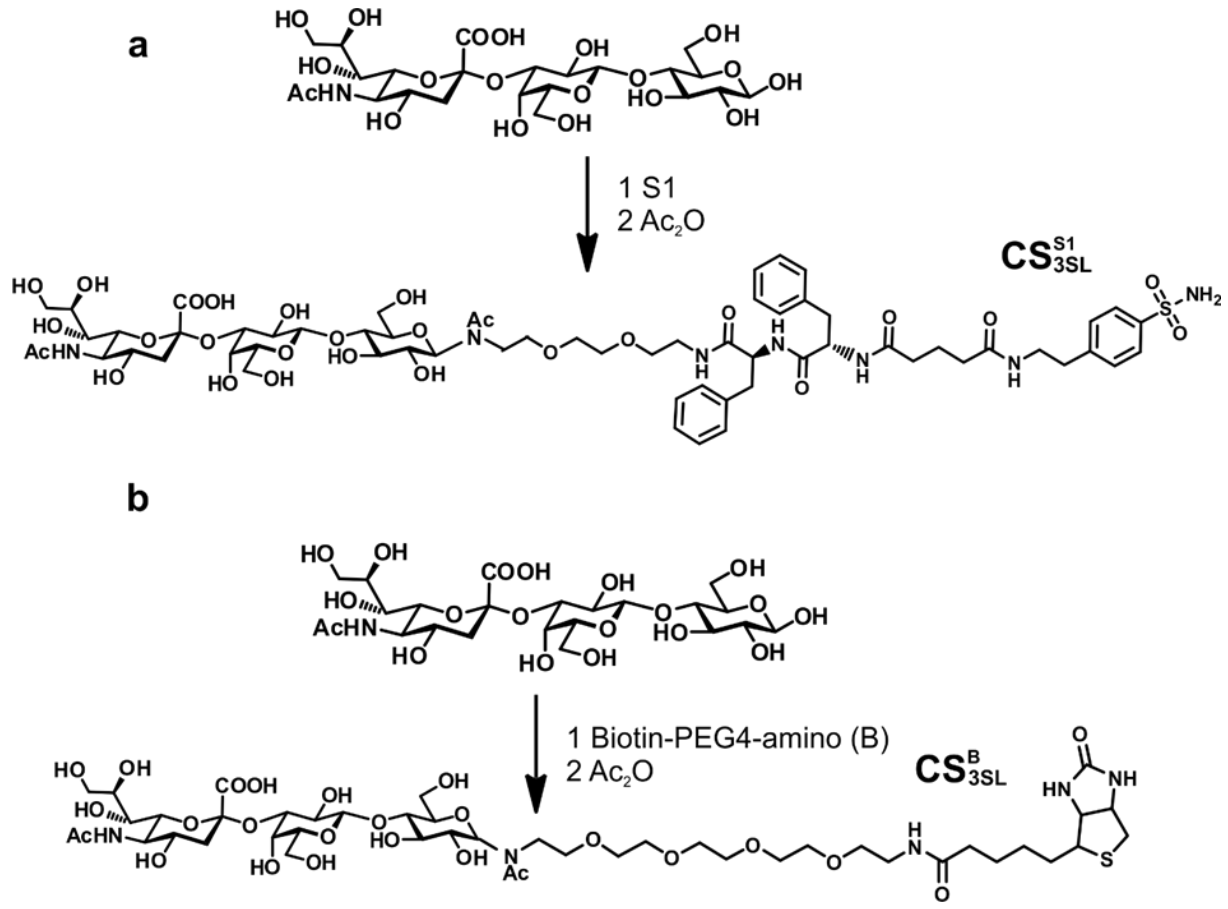

Figure 2.4. Simplified scheme for the introduction of (a) S1, (b) biotin-PEG4-amino to 3SL to give CS^{S1}_{3SL}, and CS^{B}_{3SL}, respectively.

2.3 Results and Discussion

2.3.1 Hydrolysis of 3'-sialyllactose by NEU3

To demonstrate the reliability of CUPRA-ZYME for quantitatively monitoring CAZyme reactions, we studied the human glycosyl hydrolase NEU3. Within cells, NEU3 is a plasma membrane-associated neuraminidase, which preferentially cleaves terminal α2-3-linked Neu5Ac residues on both glycoproteins and glycolipids.[40-42] The ganglioside GM3, which contains α2-3-linked Neu5Ac, is believed to be the natural substrate of NEU3.[4] Accordingly, we monitored the catalytic activity of human NEU3 towards CS^{S1}_{3SL}, which contains the trisaccharide Neu5Acα2-3Glcβ1-

4GlcNAc (3'-sialyllactose; 3SL).

With the goal of determining K_M, CUPRA-ZYME measurements were performed using CS_{3SL}^{S1} and human NEU3 at seven different initial concentrations, ranging from 10 μM to 500 μM. Shown in Figure 2.5a are representative ESI mass spectra measured for aqueous ammonium acetate solutions (200 mM, pH 7 and 25 ºC) of NEU3, CS_{3SL}^{S1} , $^{Uni}P_{proxy}$ (hCA) and P_{ref} measured at reaction times (t) of 20 min and 40 min. Also shown is the corresponding mass spectrum measured for the same solution but with no NEU3 present (i.e., t = 0 min). Protonated ions corresponding to free $^{Uni}P_{proxy}$ and the ($^{Uni}P_{proxy}$ + CS_{3SL}^{S1}) complex, at charge states +9 and +10, are evident in the mass spectra. Also, ions of the $^{Uni}P_{proxy}$ bound to the lactose-containing CUPRA reaction product, ($^{Uni}P_{proxy}$ + CP_{Lac}^{S1}) were also detected at 20 min and 40 min reaction times, as were ions (protonated and sodiated) corresponding to the other reaction product, Neu5Ac. As expected, the relative abundances of the ($^{Uni}P_{proxy}$ + CS_{3SL}^{S1}) ions decrease with reaction time, while those of the ($^{Uni}P_{proxy}$ + CP_{Lac}^{S1}) and Neu5Ac ions increase. Qualitatively similar results were obtained from mass spectra acquired at higher initial substrate concentrations. However, at concentrations above 100 μM, signal corresponding to nonspecific interactions between $^{Uni}P_{proxy}$ and CP_{Lac}^{S1} and CS_{3SL}^{S1} was evident. For example, as illustrated in Figure 2.6a, at an initial CS_{3SL}^{S1} concentration of 200 μM, signal corresponding to $^{Uni}P_{proxy}$ bound to two CS_{3SL}^{S1} was observed at early reaction times, while later in the reaction $^{Uni}P_{proxy}$ bound to two CP_{Lac}^{S1} were detected. At intermediate reaction times, $^{Uni}P_{proxy}$ ions bound simultaneously to CS_{3SL}^{S1} and CP_{Lac}^{S1} were detected. To minimize error in the time-dependent CS_{3SL}^{S1} and CP_{Lac}^{S1} concentration measurements resulting from nonspecific binding, the measured distributions of P_{ref} bound to CS_{3SL}^{S1} and CP_{Lac}^{S1} (Figure 2.6b) were used to correct the mass spectra.[37-39]

Shown in Figure 2.5b are the progress curves (time-dependent concentration of CP^{S1}_{Lac}, calculated from the abundances of the ($^{Uni}P_{proxy}$ + CS^{S1}_{3SL}) and ($^{Uni}P_{proxy}$ + CP^{S1}_{Lac}) ions using eq 2.4a and 2.4b) measured at reaction times ranging from 3 min to 85 min for the seven different initial concentrations (from 10 µM to 500 µM) of CS^{S1}_{3SL}. Because of ion suppression effects and extensive nonspecific binding, measurements at higher concentrations were not performed. The portions of the progress curves (3 min to 10 min) used to determine v_0 are shown in Figure 2.5c. Non-linear fitting of the Michaelis-Menten equation (eq 2.5) to plots of initial rates versus initial substrate concentrations was used to establish the kinetic parameters (Figure 2.5d). This analysis gave a Michaelis constant (K_M) of 210 ± 62 µM and v_{max} of 9.8 ± 1.3 µM min^{-1}. In principle, the catalytic constant (k_{cat}) can be calculated from the nominal molar concentration of NEU3 used for these measurements. However, because the concentration of active enzyme is most certainly lower than the nominal concentration, this approach is likely to underestimate k_{cat} significantly.

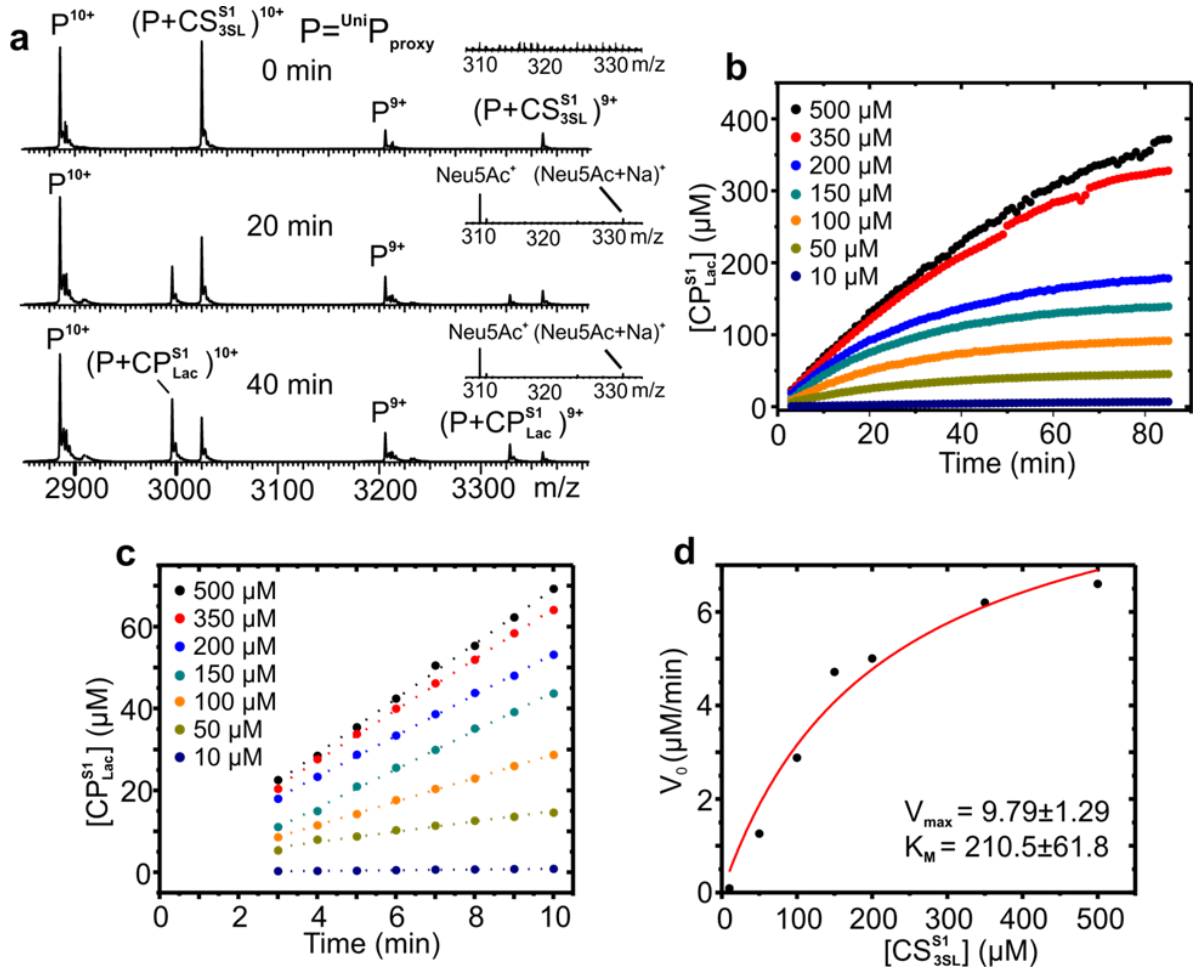

Figure 2.5. Human neuraminidase enzyme kinetics measured by CUPRA-ZYME. (a) Representative ESI mass spectra acquired for aqueous ammonium acetate solutions (200 mM, pH 7 and 25 ºC) of NEU3 (6.25 µg mL^{-1}), CS^{S1}_{3SL} (10 µM) and $^{Uni}P_{proxy}$ (20 µM). (b) Progress curves ($[CP^{S1}_{Lac}]$ versus reaction time) measured using seven different initial concentration of CS^{S1}_{3SL} (10 µM, 50 µM, 100 µM, 150 µM, 200 µM, 350 µM and 500 µM). (c) Initial rates determined by linear fitting of progress curves shown in (b) from 3 min to 10 min. (d) Plot of initial rates versus initial CS^{S1}_{3SL} concentrations. Red curve corresponds to best fit of eq 2.2 to the experimental data.

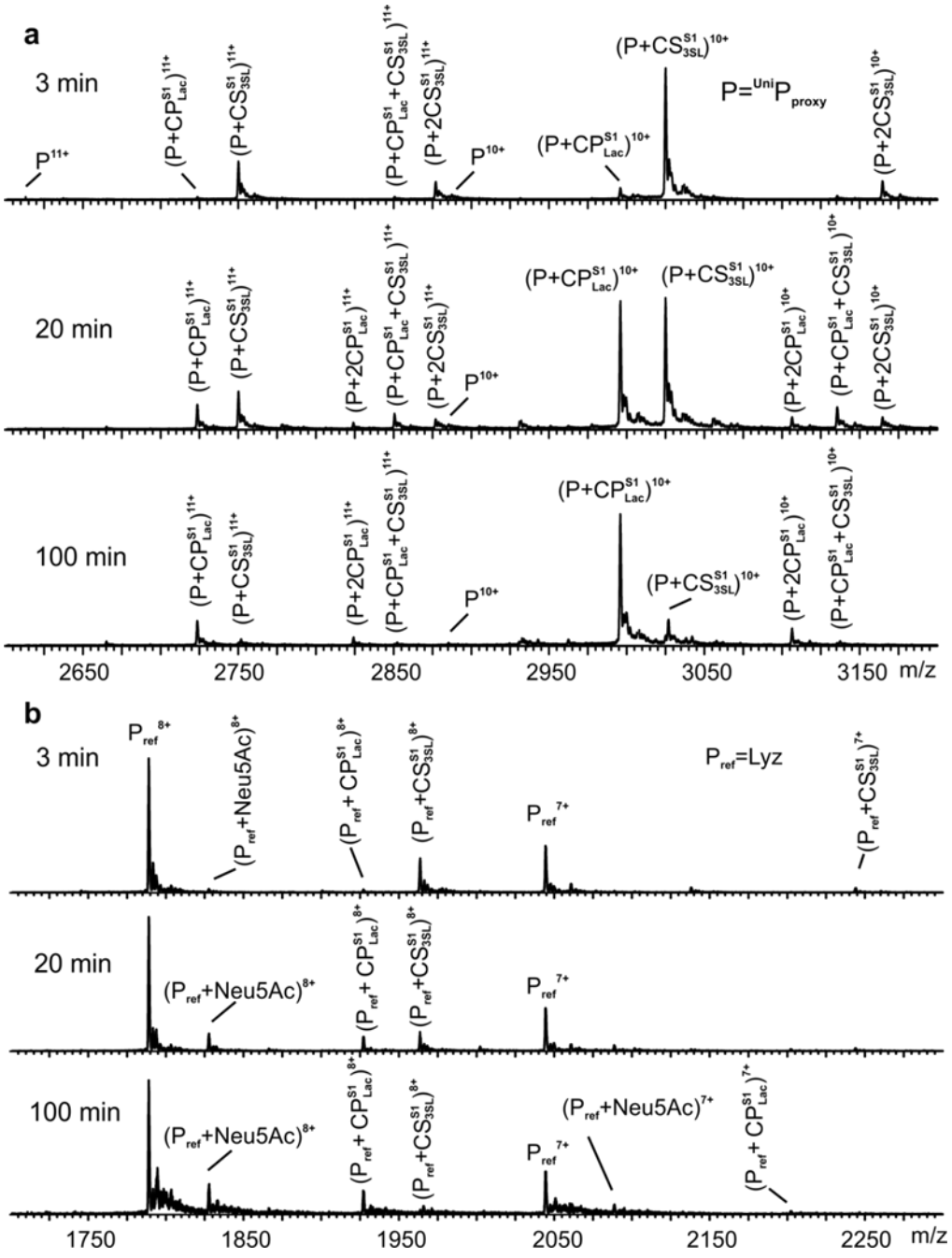

Figure 2.6. Representative ESI mass spectra acquired for an aqueous ammonium acetate solution (200 mM, pH 7 and 25 ºC) of NEU3 (6.25 μg mL^{-1}), $^{Uni}P_{proxy}$ (hCA, 20 μM), CS^{S1}_{3SL} (200 μM) and P_{ref} (Lyz, 4.8 μM) measured at 3 min, 20 min and 100 min reaction times. Shown in (a) is the portion of the mass spectrum that contains the $^{Uni}P_{proxy}$ ions and in (b) is the portion of the mass spectrum that contains the P_{ref} ions.

The K_M measured by CUPRA-ZYME agrees, within combined error, with a value (140 ± 30 μM) reported for 3SL functionalized, at the reducing end, with boron-dipyrromethene (BODIPY),[43] and also a value (166 μM) measured for the GM3 ganglioside using a radiometric assay.[42] It is important to note, however, that reported values were determined at acidic pH, 4.5 and 3.8, respectively, and it is known that the activity of NEU3 is sensitive to pH.[42,44] Therefore, to more conclusively establish that CUPRA-ZYME correctly reports on the time-dependent CS and CP concentrations, the aforementioned measurements were repeated in the presence of known concentration of *N*-acetyl-D-neuraminic acid-1,2,3-$^{13}C_3$ (Neu5Ac-$^{13}C_3$), which served as an internal standard for the Neu5Ac product. As can be seen from the mass spectra data acquired using an initial CS^{S1}_{3SL} concentration of 50 μM (Figure 2.7a), the total abundance of Neu5Ac ions increases, relative to that of the Neu5Ac-$^{13}C_3$ ions, with reaction time. Based on the reasonable assumption that Neu5Ac and Neu5Ac-$^{13}C_3$ have identical ESI-MS response factors, the time-dependent concentration of Neu5Ac was calculated from the abundance ratio of Neu5Ac and Neu5Ac-$^{13}C_3$ ions and the initial concentration of Neu5Ac-$^{13}C_3$ (eq 2.1). Shown in Figure 2.7b is a plot of Neu5Ac concentration versus reaction time. Also shown is the time-dependent concentration of CP^{S1}_{Lac} measured independently using CUPRA-ZYME. Notably, the two progress curves are essentially indistinguishable. Similar agreement (between product concentrations measured by CUPRA-ZYME and the internal standard) was obtained using higher initial concentrations of CS^{S1}_{3SL} (data not shown). Together, these results establish that CUPRA-ZYME provides an accurate measure of the time-dependent CS and CP concentrations in solution.

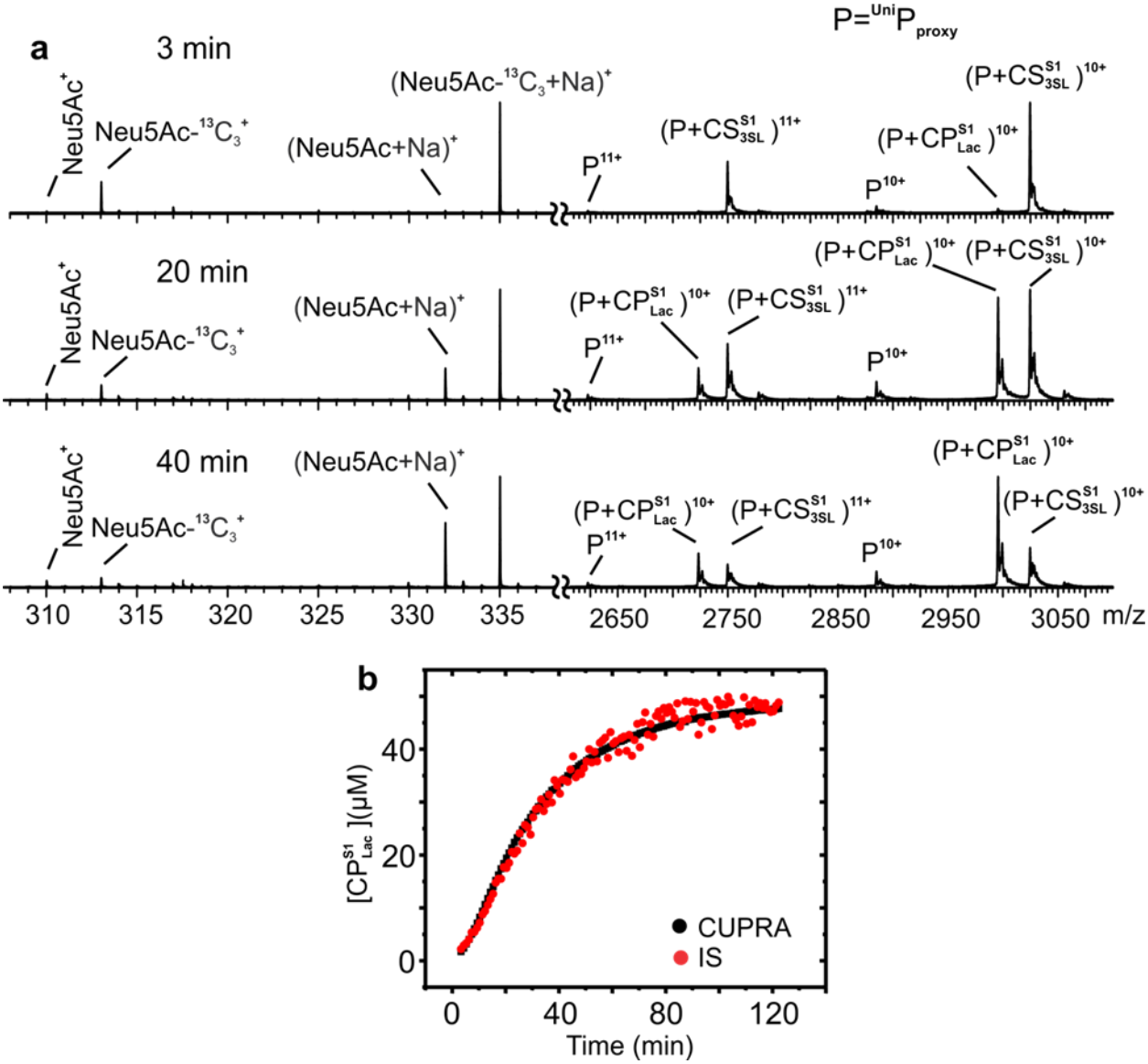

Figure 2.7. (a) Representative ESI mass spectra acquired for an aqueous ammonium acetate solution (200 mM, pH 7 and 25 ºC) of NEU3 (6.25 μg mL^{-1}), $^{Uni}P_{proxy}$ (hCA, 20 μM), CS^{S1}_{3SL}(50 μM) and the internal standard (IS) Neu5Ac-$^{13}C_3$ (50 μM) measured at 3 min, 20 min and 40 min reaction times. Shown are the portions of the mass spectrum that contains the $^{Uni}P_{proxy}$ and Neu5Ac ions. (b) Time-dependent concentrations of the CP^{S1}_{Lac} and Neu5Ac products measured by CUPRA-ZYME and IS, respectively.

Because the affinity of CS^{S1}_{3SL} for the $^{Uni}P_{proxy}$ hCA is quite high (13 ± 4 μM in 200 mM aqueous ammonium acetate at pH 7 and 25 ºC),[34] a substantial fraction of CS^{S1}_{3SL} will be bound to the $^{Uni}P_{proxy}$, particularly at low initial concentrations. For example, at 10 μM CS^{S1}_{3SL}, 98% of the substrate will be bound to $^{Uni}P_{proxy}$ at the start of the reaction. To establish that CS^{S1}_{3SL} binding to $^{Uni}P_{proxy}$ (hCA) does not influence the NEU3 kinetics, measurements were carried out in the absence of $^{Uni}P_{proxy}$ but in the presence of Neu5Ac-$^{13}C_3$. The reaction progress curves measured for initial CS^{S1}_{3SL} concentrations ranging from 10 μM to 500 μM and the corresponding regions from which the initial rates were determined are shown in Figures 2.8a and 2.9b, respectively. Fitting of the Michaelis-Menten equation to these data gives a K_M of 274 ± 76 μM and v_{max} of 9.7 ± 1.3 μM min^{-1}. Importantly, the K_M value agrees, within combined error, with the value measured by CUPRA-ZYME under the same solution conditions, indicating that binding of CS^{S1}_{3SL} to $^{Uni}P_{proxy}$ has little or no effect on the NEU3 activity. This finding may reflect the fast (relative to hydrolysis) on-off kinetics of CS^{S1}_{3SL} binding to $^{Uni}P_{proxy}$, wherein only free CS^{S1}_{3SL} is processed, or suggest that NEU3 is indifferent to $^{Uni}P_{proxy}$ binding the substrate. As discussed in more detail below, the latter view is supported by the kinetic data acquired for CS^{B}_{3SL}.

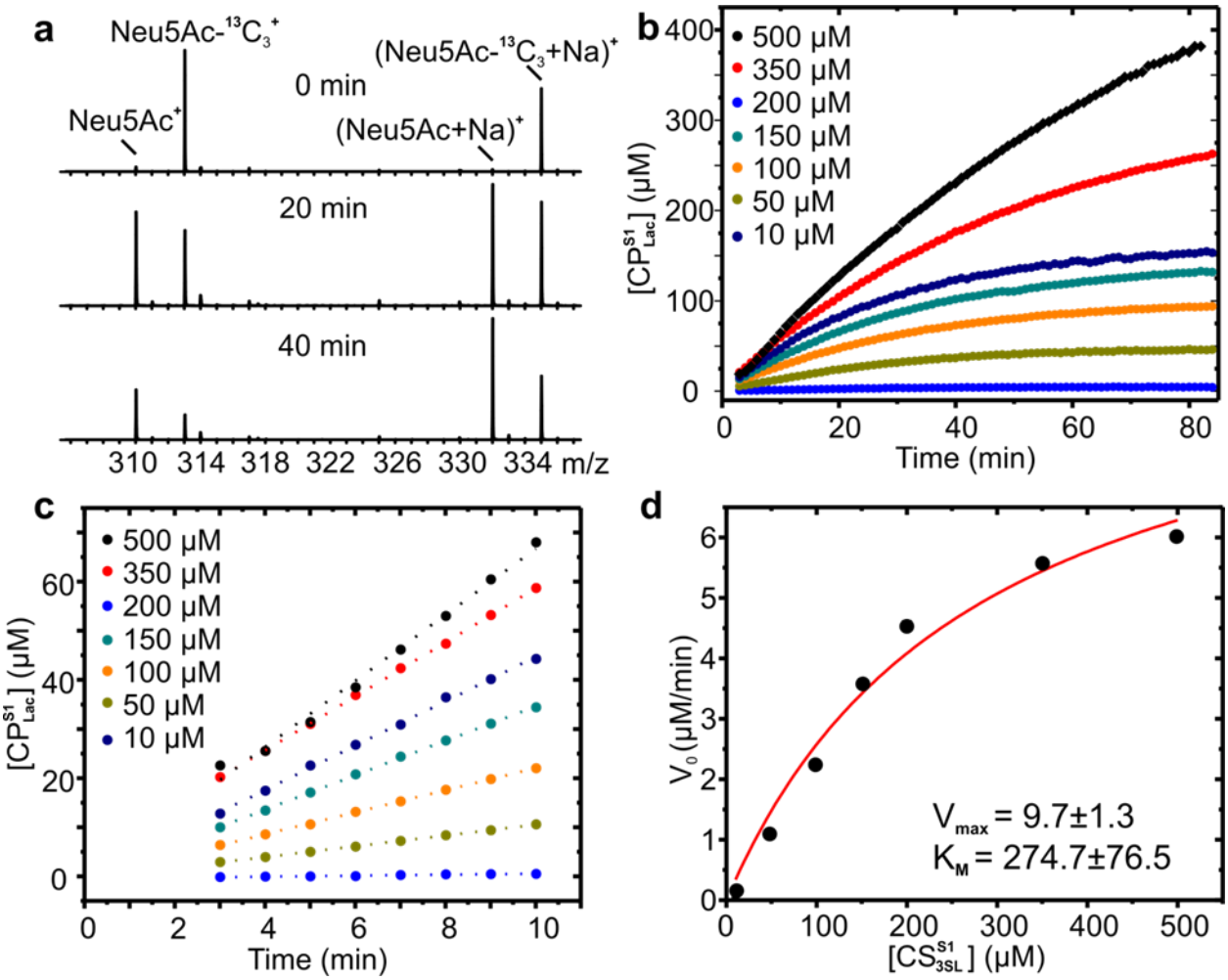

Figure 2.8. (a) Representative ESI mass spectra acquired for an aqueous ammonium acetate solution (200 mM, pH 7 and 25 ºC) of NEU3 (6.25 µg mL^{-1}), CS^{S1}_{3SL}(50 µM) and internal standard (IS) Neu5Ac-$^{13}C_3$ (25 µM) measured at 3 min, 20 min and 40 min reaction times. The region shown (m/z 316 – m/z 336) contains the Neu5Ac ions. (b) Progress curves (time-dependent concentration of Neu5Ac product) measured using seven different initial concentration of CS^{S1}_{3SL} (10 µM, 50 µM, 100 µM, 150 µM, 200 µM, 350 µM and 500 µM). (c) Initial rates determined by linear fitting of the progress curves shown in (b) from 3 min to 10 min. (d) Plot of initial rates versus initial CS^{S1}_{3SL} concentrations. Red curve corresponds to best fit of eq 2.2 to the experimental data.

2.3.2 pH profile of NEU3

Because the affinity of CS^{S1}_{3SL} (and the resulting CP^{S1}_{Lac}) for hCA decreases substantially with decreasing pH, CUPRA-ZYME measurements are not easily performed near the optimal pH (approximately 4.8) of NEU3 or other neuraminidases using CS^{S1} and hCA as $^{Uni}P_{proxy}$.[45,46] This pH restriction was overcome using a CS^{B} substrate (CS^{B}_{3SL}), which contains a biotin affinity tag (Figure 2.1b) and mSA as the $^{Uni}P_{proxy}$. Although the affinity of CS^{B}_{3SL} for mSA wasn't measured in the present work, the reported affinity of biotin is 7.7 nM and is expected to remain high over a wide range of pH.[38] Prior to applying CUPRA-ZYME with CS^{B}_{3SL} and mSA to assess the activity pH profile of NEU3, we first sought to compare the NEU3 hydrolysis kinetics of CS^{S1}_{3SL} and CS^{B}_{3SL} at neutral pH. To do this, the assay was performed on a solution containing both CS^{S1}_{3SL} and CS^{B}_{3SL}, along with their corresponding $^{Uni}P_{proxy}$ (mSA and hCA). The results, which are summarized in Figure 2.9, show that the progress curves measured with both substrate-$^{Uni}P_{proxy}$ pairs are very similar. This finding suggests that, at least in the case of NEU3, the structural differences between CS^{S1}_{3SL} and CS^{B}_{3SL} and the interaction with $^{Uni}P_{proxy}$ do not significantly influence enzyme activity.

To establish a NEU3 activity pH profile, CUPRA-ZYME was performed on aqueous ammonium acetate solutions (25 °C) of NEU3, $^{Uni}P_{proxy}$ (mSA) and CS^{B}_{3SL} at pH of 4.0, 4.5, 5.0, 6.0 and 7.0. Shown in Figure 2.10a are representative mass spectra measured under the most acidic condition, at 3 min, 20 min and 40 min reaction times. Because of the high affinity of mSA for the substrate and resulting CP (CP^{B}_{Lac}), only bound $^{Uni}P_{proxy}$ was observed in the mass spectra. The progress curve measured at each solution pH is shown in Figure 2.10b. Using the initial rates determined from these curves, the influence of pH on the relative activity of NEU3 was assessed (Figure 2.10c). It can be seen that NEU3 activity is highest at pH 5.0, which is consistent with previous reports of the optimal pH of this enzyme being in the 4.5 to 5.0 range.[40,42,44] While there

is only a modest decrease in activity from pH 5.0 to pH 4.5, the enzyme loses almost all activity at pH 4.0. It can also be seen that NEU3 remains quite active at higher pH, with relative activities (compared to pH 5.0) of approximately 70% and 60% at pH 6.0 and 7.0, respectively.

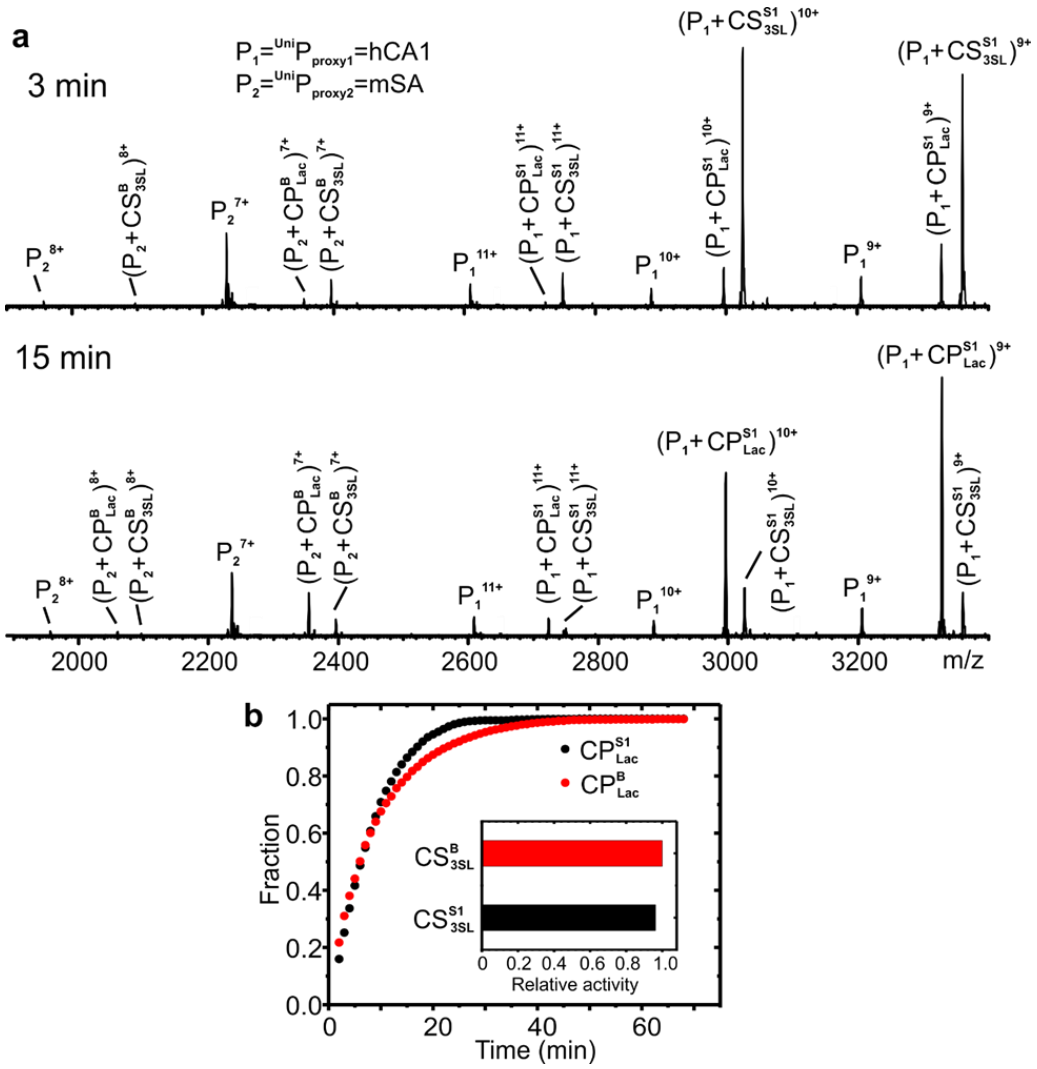

Figure 2.9. (a) Representative ESI mass spectra acquired for an aqueous ammonium acetate solution (200 mM, pH 7 and 25 ºC) of NEU3 (12.5 μg mL^{-1}), $^{Uni}P_{proxy}$ (hCA for CS^{S1}_{3SL}, 2 μM; mSA for CS^{B}_{3SL}, 3 μM), CS^{S1}_{3SL} and CS^{B}_{3SL}(both 5 μM) measured at 3 min and 15 min reaction times. (b) Time-dependent fractional concentration of CS^{S1}_{3SL}(black) and CS^{B}_{3SL}(red). The relative reactivity was established from the measured initial rates and normalized to that of CS^{B}_{3SL}.

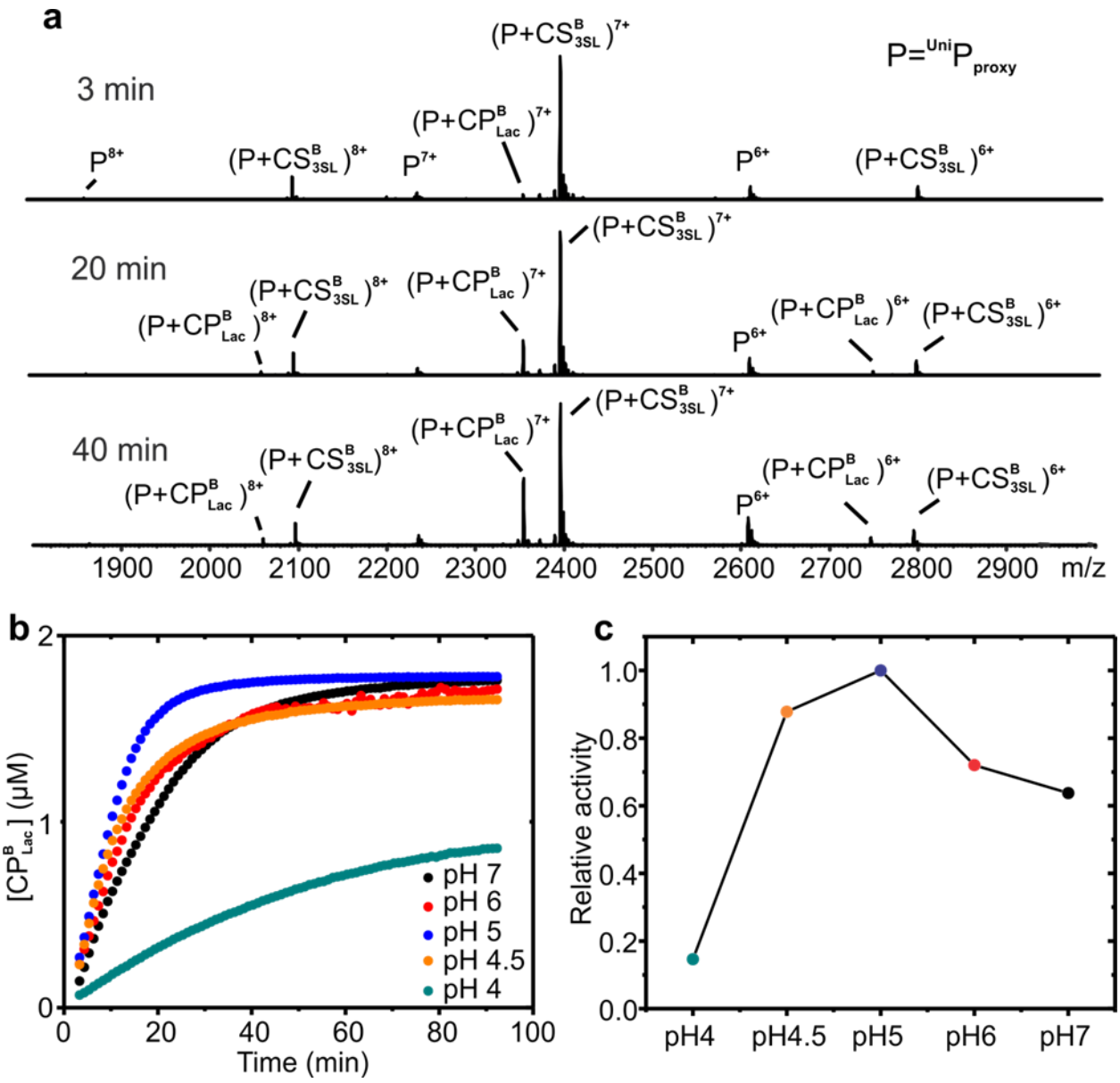

Figure 2.10. (a) Representative ESI mass spectra acquired for an aqueous ammonium acetate solution (200 mM, pH 4.0 and 25 ºC) of NEU3 (6.25 μg mL^{-1}), $^{Uni}P_{proxy}$ (mSA, 1.8 μM) and CS^{B}_{3SL}(1.8 μM) measured at 3 min, 20 min and 40 min. (b) Time-resolved concentration of CP^{B}_{Lac} measured at pH 4.0, pH 4.5, pH 5.0, pH 6.0 and pH 7.0. (c) Relative activity of NEU3 at different pH determined from initial rates at different pH and normalized to the value at pH 5.

2.3.3 Hydrolysis of GD3 tetrasaccharide by NEU3: evidence of endoneuraminidase activity

A unique feature of CUPRA-ZYME is the ability to simultaneously quantify not only the substrate(s) and product(s) of a given CAZyme but also reaction intermediates (i.e., enzymatic products that are also substrates of the CAZyme) that are produced. Moreover, the assay can be used to study CAZyme pathways that involve multiple enzymes and enzymatic steps. To illustrate the ability of CUPRA-ZYME to monitor a multistep CAZyme reaction, we applied the assay to the hydrolysis of the CS^{S1} substrate containing the GD3 ganglioside tetrasaccharide Neu5Acα2-8Neu5Acα2-3Galβ1-4Glcβ-OH (CS^{S1}_{GD3}). This tetrasaccharide contains both an external α2-8- and an internal α2-3-linked Neu5Ac. NEU3 is generally considered to be an exoneuraminidase and is expected to first cleave the terminal Neu5Ac of CS^{S1}_{GD3} to give CP^{S1}_{3SL}, which itself is a substrate (i.e., $CP^{S1}_{3SL} \equiv CS^{S1}_{3SL}$) and will be converted to CP^{S1}_{Lac}.[2]

Shown in Figure 2.11a are representative mass spectra measured for aqueous ammonium acetate solutions (200 mM, pH 7 and 25 ºC) of NEU3 (6.25 μg mL^{-1}), CS^{S1}_{GD3} (90 μM) and $^{Uni}P_{proxy}$ (hCA, 20 μM) measured at 3 min, 40 min and 80 min. Analysis of the mass spectra show that consumption of CS^{S1}_{GD3} is accompanied by the formation of CP^{S1}_{Lac}, as well as CP^{S1}_{3SL}. Inspection of the corresponding plots of concentration versus reaction time (Figure 2.11c) reveals that the concentration of CP^{S1}_{3SL} initially increases and then decays at longer times. This is accompanied by a slight delay (induction period) in the appearance of CP^{S1}_{Lac}. These findings are consistent with the stepwise loss of Neu5Ac from CS^{S1}_{GD3}. However, inspection of the low m/z region of the mass spectra reveals the presence of ions (protonated and sodiated and protonated with loss of water) corresponding to dineuraminic acid (Neu5Acα2-8Neu5Ac) (Figure 2.11b). Dineuraminic acid can only be formed by cleavage of the internal α2-3-linkage. The concentration of dineuraminic acid could not be reliably determined from the mass spectra because a suitable (and stable) internal

standard was not available. Nevertheless, it can be seen that the relative abundance of dineuraminic acid ions initially increase and then decrease with time. This behavior is consistent with dineuraminic acid being a substrate of NEU3 and converted to Neu5Ac. To the best of our knowledge, this represents the first report of a human neuraminidase exhibiting endoneuraminidase activity.

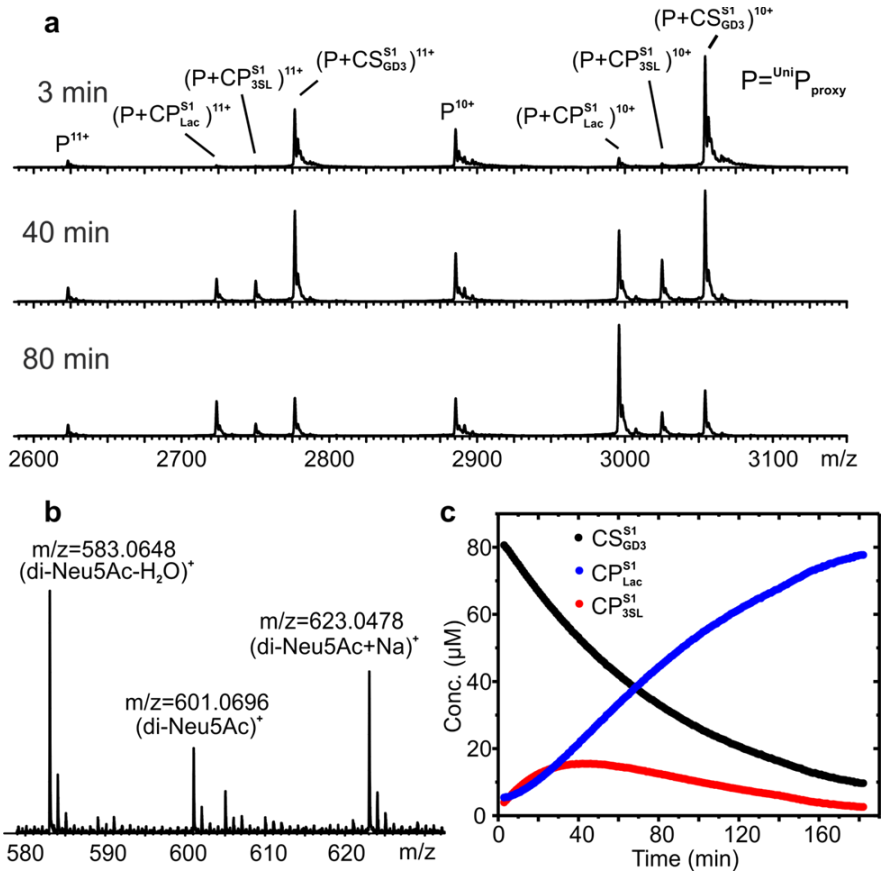

Figure 2.11. Endoneuraminidase activity of NEU3 revealed by CUPRA-ZYME. (a) Representative mass spectra acquired for aqueous ammonium acetate solutions (200 mM, pH 7 and 25 °C) of NEU3 (6.25 μg mL^{-1}), $^{Uni}P_{proxy}$ (hCA, 20 μM) and CS^{S1}_{GD3} (90 μM) measured at 3 min, 20 min and 40 min reaction time. (b) The region shown (m/z 580 – m/z 630) contains the dineuraminic acid ions. (c) Time-dependent concentrations of CS^{S1}_{GD3} (shown in black), CP^{S1}_{3SL} (blue) and CP^{S1}_{Lac} (red).

2.3.4 Substrate specificities of human sialyltransferases and human neuraminidases

Because CUPRA-ZYME allows multiple substrates to be monitored simultaneously, provided they have different MWs, the assay is ideally suited to quantitatively profile the substrate specificities of CAZymes. This approach is illustrated here for two human neuraminidases (NEU2 and NEU3) and two human sialyltransferases (ST6Gal1 and ST3Gal4). NEU2 and NEU3 both can remove Neu5Ac from substrates such as oligosaccharides and glycoproteins, but with different specificities for different Neu5Ac linkages.[40-42] ST6Gal1 transfers Neu5Ac in an α2-6-linkage from a CMP-Neu5Ac donor to a Galβ1-4GlcNAc acceptor,[47] and ST3Gal4 transfers Neu5Ac in an α2-3-linkage from CMP-Neu5Ac to Galβ1-4GlcNAc, Galβ1-3GlcNAc or Galβ1-3GalNAc acceptors.[48,49] A library of 13 CS (5 μM for each, structures shown in Table 2.1) was incubated with $^{Uni}P_{proxy}$ (hCA, 5 μM), CS^{S1}_{3SL} (5 μM, which served as the reference substrate) and NEU2 or NEU3 at pH 7 and 25 °C. The relative (to CS^{S1}_{3SL}) reactivities of all tested CUPRA substrates, determined from the first 5 min of the reaction, are listed in Table 2.2. A library of 20 CS (5 μM for each, structures shown in Table 2.1) was split into 5 smaller libraries according to their MWs and each was incubated with $^{Uni}P_{proxy}$ (hCA, 20 μM), CS^{S2}_{LNAc} (5 μM, which served as the reference substrate) and ST6Gal1 or ST3Gal4 at pH 7 and 25 °C. The relative (to CS^{S2}_{LNAc}) reactivities of all tested CUPRA substrates, determined from the first 5 min of the reaction, are listed in Table 2.3.

CS	Structure	MW
CS^{S1}_{3SL}	Neu5Acα2-3Galβ1-4Glc-**S1**	1395.55
CS^{S1}_{6SL}	Neu5Acα2-6Galβ1-4Glc-**S1**	1395.55
CS^{S1}_{GD3}	Neu5Aca2-8Neu5Aca2-3Galb1-4Glc-**S1**	1686.65
CS^{B}_{3SL}	Neu5Acα2-3Galβ1-4Glc-**B**	1120.18
CS^{S2}_{3SLNAc}	Neu5Acα2-3Galβ1-4GlcNAc-**S2**	1534.59
CS^{S2}_{LNAc}	Galβ1-4GlcNAc-**S2**	1243.34
CS^{S1}_{LNAc2}	Galβ1-3GlcNAc-**S1**	1145.48
CS^{S1}_{BTriT2}	Galα1-3Galβ1-4GlcNAc-**S1**	1307.54
$CS^{S1}_{HPentaT2}$	Fucα1-2Galβ1-4GlcNAcβ1-3Galβ1-4Glc-**S1**	1615.65
$CS^{S1}_{AHexaT1}$	GalNAcα1-3(Fucα1-2)Galβ1-3GlcNAcβ1-3Galβ1-4Glc-**S1**	1818.73
$CS^{S1}_{AHexaT2}$	GalNAcα1-3(Fucα1-2)Galβ1-4GlcNAcβ1-3Galβ1-4Glc-**S1**	1818.73
CS^{S1}_{AsGM2}	GalNAcβ1-4Galβ1-4Glc-**S1**	1307.54
CS^{S1}_{Gb3T2}	Galα1-4Galβ1-4GlcNAc-**S1**	1307.54
CS^{S1}_{Gb5}	Galβ1-3GalNAcβ1-3Galα1-4Galβ1-4Glc-**S1**	1631.64
CS^{S1}_{GbF}	GalNAcα1-3GalNAcβ1-3Galα1-4Galβ1-4Glc-**S1**	1672.67
CS^{S1}_{GbA}	GalNAcα1-3(Fucα1-2)Galβ1-3GalNAcβ1-3Galα1-4Galβ1-4Glc-**S1**	1980.78
CS^{S1}_{GbB}	Galα1-3(Fucα1-2)Galβ1-3GalNAcβ1-3Galα1-4Galβ1-4Glc-**S1**	1939.75
CS^{S1}_{Lac}	Galβ1-4Glc-**S1**	1104.46
CS^{S1}_{LNT}	Galβ1-3GlcNAcβ1-3Galβ1-4Glc-**S1**	1469.59
CS^{S1}_{LNnT}	Galβ1-4GlcNAcβ1-3Galβ1-4Glc-**S1**	1469.59
CS^{S1}_{GLNT}	GlcAβ1-3Galβ1-3GlcNAcβ1-3Galβ1-4Glc-**S1**	1645.62
CS^{S1}_{LaTria}	Galβ1-3(Fucα1-4)GlcNAc-**S1**	1291.54
CS^{S1}_{LaHexa}	Galβ1-3(Fucα1-4)GlcNAcβ1-3Galβ1-4(Fucα1-3)Glc-**S1**	1761.71
CS^{S1}_{LxTria}	Galβ1-4(Fucα1-3)GlcNAc-**S1**	1291.54
$CS^{S1}_{LxTetra}$	Galβ1-4(Fucα1-3)GlcNAcβ1-3Gal-**S1**	1453.59
CS^{S1}_{LxHexa}	Galβ1-4(Fucα1-3)GlcNAcβ1-3Galβ1-4(Fucα1-3)Glc-**S1**	1761.71
CS^{S1}_{GA01}	Galβ1-3GalNAcβ1-4(Neu5Acα2-3)Galβ1-4Glc-**S1**	1760.68
CS^{S1}_{GA02}	Fucα1-2Galβ1-3GalNAcβ1-4(Neu5Acα2-3)Galβ1-4Glc-**S1**	1906.74

CS^{S1}_{GA03}	Neu5Acα2-3Galβ1-3GalNAcβ1-4Galβ1-4Glc-**S1**	1760.68
CS^{S1}_{GA07}	GalNAcβ1-4(Neu5Acα2-3)Galβ1-4Glc-**S1**	1598.63
CS^{S1}_{GA08}	Galβ1-4(Neu5Acα2-3)Galβ1-4Glc-**S1**	1557.60
CS^{S1}_{GA09}	Galβ1-3GalNAcβ1-4(Neu5Acα2-8Neu5Acα2-3)Galβ1-4Glc-**S1**	2051.78
CS^{S1}_{GA10}	GalNAcβ1-4(Neu5Acα2-8 Neu5Acα2-3)Galβ1-4Glc-**S1**	1889.72
CS^{S1}_{GL07}	Neu5Acα2-3Galα-4Galβ-4Glc-**S1**	1557.60
CS^{S1}_{GL08}	Neu5Acα2-3Galβ1-3GalNAcβ1-3Galα1-4Galβ1-4Glc-**S1**	1922.73
CS^{S1}_{LE08}	Neu5Acα2-3Galβ1-4(Fucα1-3)GlcNAcβ1-3Gal-**S1**	1744.71

Table 2.1. List of CUPRA substrates (CS) used in this study, their structures and molecular weights (MW).

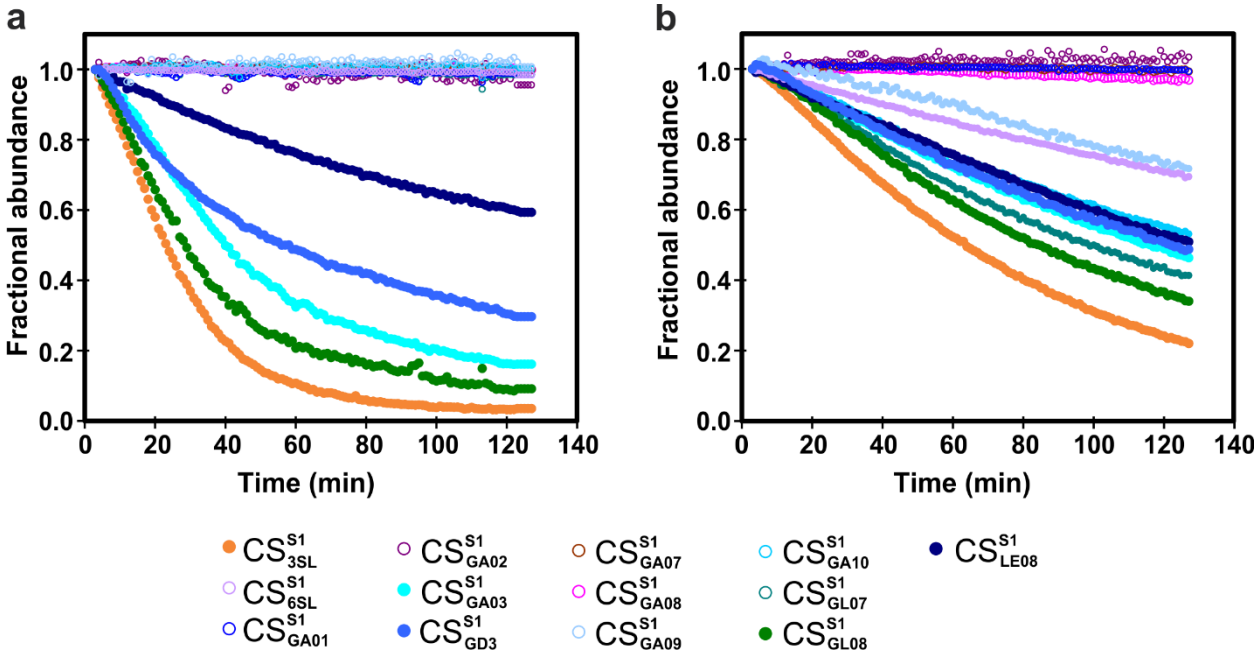

Figure 2.12. Substrate specificities of human neuraminidases NEU2 and NEU3 measured by CUPRA-ZYME. Time-dependent fractional concentrations of 13 CS (Table 2.1) in aqueous ammonium acetate solutions (200 mM, pH 7 and 25 °C) of CS (each 5 µM), $^{Uni}P_{proxy}$ (hCA, 5 µM) and (a) NEU2 (0.2 µM) or (b) NEU3 (0.2 µM).

Under these conditions, the time-resolved CUPRA-ZYME data (Figure 2.12) clearly show that both NEU2 and NEU3 exhibit a preference for CS^{S1}_{3SL} (Table 2.2). All CS containing terminal α2-3-linked Neu5Ac were substrates of NEU3, with initial rates that are 10–50% that of CS^{S1}_{3SL}. Those with α2-6-linked Neu5Ac were worse substrates for both enzymes (e.g. CS^{S1}_{6SL}), consistent with previous reports.[43] Interestingly, all α2-8-linked Neu5Ac residues were substrates for NEU3 (CS^{S1}_{GD3}, CS^{S1}_{GA09} and CS^{S1}_{GA10}), but only CS^{S1}_{GD3} was a substrate for NEU2. Substrates containing branching after the α2-3-linkage were poor substrates for both enzymes. NEU2 did not tolerate Neu5Acα2-3 linked to Galα1-4Gal in CS^{S1}_{GL07}. Substrates with internal Fuc residues (e.g. CS^{S1}_{LE08}) were better tolerated by NEU3, compared to NEU2, in contrast to reported results for a structurally-similar substrate (Neu5Acα2-3Galβ1-4GlcNAc(Fucα2-3)).[43] We note, however, that previous reports have examined NEU2 and NEU3 activity under more acidic solution conditions. Furthermore, the nature of the substrate aglycone may influence the activity of human neuraminidases.[29]

CS	NEU2	NEU3
$\mathbf{CS^{S1}_{GA01}}$	0.000	0.008
$\mathbf{CS^{S1}_{GA02}}$	0.000	0.000
$\mathbf{CS^{S1}_{GA03}}$	0.524	0.551
$\mathbf{CS^{S1}_{GD3}}$	0.443	0.298
$\mathbf{CS^{S1}_{GA07}}$	0.000	0.009
$\mathbf{CS^{S1}_{GA08}}$	0.000	0.034
$\mathbf{CS^{S1}_{GA09}}$	0.000	0.247
$\mathbf{CS^{S1}_{GA10}}$	0.000	0.292
$\mathbf{CS^{S1}_{GL07}}$	0.000	0.462
$\mathbf{CS^{S1}_{GL08}}$	0.918	0.523
$\mathbf{CS^{S1}_{3SL}}$	1.000	1.000
$\mathbf{CS^{S1}_{6SL}}$	0.004	0.275
$\mathbf{CS^{S1}_{LE08}}$	0.188	0.494

Table 2.2. Relative reactivities (related to CS^{S1}_{3SL}) of sialylated CS measured by time-resolved CUPRA-ZYME method for NEU2 and NEU3 in 200 mM aqueous ammonium acetate (pH 7, 25 ºC).

For ST6Gal1 and ST3Gal4, the time-resolved CUPRA-ZYME data (Figure 2.13) show that, of the CS tested, only CS^{S2}_{LNAc} and CS^{S1}_{LNnT} (reactivity of 60% compared to CS^{S2}_{LNAc}) serve as acceptors for ST6Gal1. These results are consistent with the reported finding that ST6Gal1 is highly specific for substrates possessing a terminal Galβ1-4GlcNAc disaccharide.[47] Moreover, the lack of reactivity observed for CS^{S1}_{LxTria}, $CS^{S1}_{LxTetra}$ and CS^{S1}_{LxHexa} indicate that fucosylation of the GlcNAc residue introduces steric effects not tolerated by ST6Gal1. ST3Gal4 requires the participation of divalent cations for optimal activity (data not shown),[50-52] thus $MnCl_2$ (125 μM) was added to the solutions to test this enzyme. ST3Gal4 was found to exhibit somewhat more relaxed substrate specificities. But, like ST6Gal1, CS^{S2}_{LNAc} is preferred and CS^{S1}_{LNnT} is a reasonably good substrate (relative reactivity 60%). However, unlike ST6Gal1, ST3Gal4 is able to transfer Neu5Ac with reasonably high efficiency to substrates containing terminal Galβ1-4Glc (CS^{S1}_{Lac}, 69%; CS^{S1}_{LNT}, 9%) and Galβ1-3GlcNAc (CS^{S1}_{LNAc2}, 12%; CS^{S1}_{Gb5}, 4%) motifs.

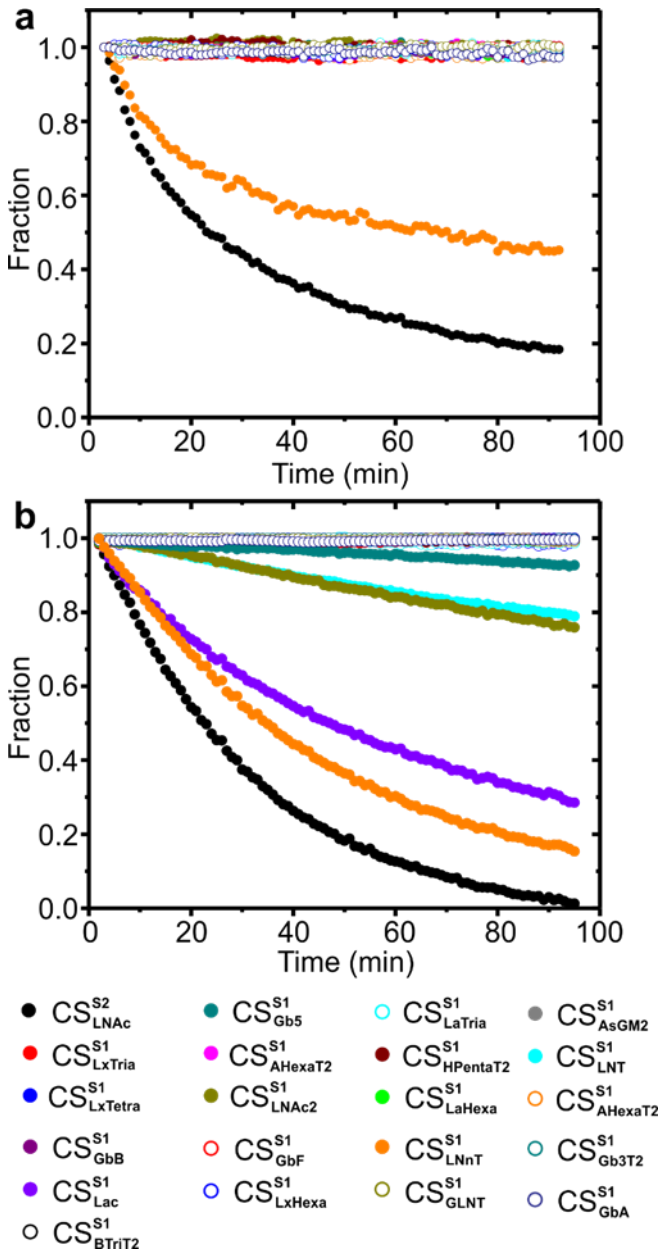

Figure 2.13. Substrate specificities of human sialyltransferases ST6Gal1 and ST3Gal4 measured by CUPRA-ZYME. Time-dependent fractional concentrations of 21 CS (Table 2.1) in aqueous ammonium acetate solutions (200 mM, pH 7 and 25 °C) of CS (each 5 μM), $^{Uni}P_{proxy}$ (hCA, 20 μM) and (a) ST6Gal1 (42 μg mL^{-1}) or (b) ST3Gal4 (200 μg mL^{-1}) and $MnCl_2$ (125 μM).

Library	CS	ST6Gal1	ST3Gal4 [a]
Reference	$\mathbf{CS^{S2}_{LNAc}}$	1.00	1.00
1	$\mathbf{CS^{S1}_{Lac}}$	0.00	0.70
1	$\mathbf{CS^{S1}_{BTriT2}}$	0.00	0.00
1	$\mathbf{CS^{S1}_{GbF}}$	0.00	0.00
1	$\mathbf{CS^{S1}_{LxHexa}}$	0.00	0.00
2	$\mathbf{CS^{S1}_{LNAc2}}$	0.00	0.12
2	$\mathbf{CS^{S1}_{LaTria}}$	0.00	0.00
2	$\mathbf{CS^{S1}_{HPentaT2}}$	0.00	0.00
2	$\mathbf{CS^{S1}_{LaHexa}}$	0.00	0.00
3	$\mathbf{CS^{S1}_{LxTria}}$	0.00	0.00
3	$\mathbf{CS^{S1}_{LxTetra}}$	0.00	0.00
3	$\mathbf{CS^{S1}_{Gb5}}$	0.00	0.04
3	$\mathbf{CS^{S1}_{AHexaT1}}$	0.00	0.00
4	$\mathbf{CS^{S1}_{Gb3T2}}$	0.00	0.00
4	$\mathbf{CS^{S1}_{LNnT}}$	0.60	0.64
4	$\mathbf{CS^{S1}_{GLNT}}$	0.00	0.00
4	$\mathbf{CS^{S1}_{GbA}}$	0.00	0.00
5	$\mathbf{CS^{S1}_{AsGM2}}$	0.00	0.00
5	$\mathbf{CS^{S1}_{LNT}}$	0.00	0.09
5	$\mathbf{CS^{S1}_{AHexaT2}}$	0.00	0.00
5	$\mathbf{CS^{S1}_{GbB}}$	0.00	0.00

Table 2.3. Relative (to CS^{S2}_{LNAc}) reactivity of CS measured by CUPRA-ZYME for ST6Gal1 and ST3Gal4 in 200 mM aqueous ammonium acetate solutions (pH 7, 25 ºC). Initial reaction rates for each CS were determined by linear fitting of the progress curves from 3 min to 7 min. The 20 CS (5 μM for each) were split into five libraries according to their MWs; CS^{S2}_{LNAc} (5 μM) was added to each library as a reference substrate.

2.3.5 Comparison of CUPRA and glycoprotein substrates

The functional characterization of CAZymes is usually performed using model substrates, which typically comprise the minimal glycan structure recognized by the enzyme. However, there have been few attempts to correlate the kinetics measured for these model substrates and those of the natural glycans, particularly in the case of *N*- and *O*-linked glycans associated with proteins. Because of the amenability of CUPRA-ZYME to be performed simultaneously with non-CUPRA substrates (e.g. glycoproteins), it is ideally suited to quantitatively assess the relative reactivities of model substrates and natural glycan substrates.

To illustrate how CUPRA-ZYME, combined with high resolution ESI-MS, can be leveraged to gain insight into the influence of substrate environment in natural glycoconjugates on CAZyme activity, we first compared the hydrolysis kinetics of human prostate specific antigen (PSA) by NEU3 with those of CS possessing α2-3- and α2-6-linked Neu5Ac. PSA, a 28.4 kDa glycoprotein (237 amino acids) produced by the prostate epithelial cells, is a widely used biomarker for prostate cancer screening.[53,54] The protein possesses a single glycosylation site at Asn 45 occupied by bi-antennary complex *N*-linked glycan.[55,56] The commercial sample of PSA consists of two major species with MWs of 28400.50 Da and 28283.93 Da, which correspond to bi-antennary fucosylated ($Hex_5HexNAc_4Fuc_1$α-$Neu5Ac_2$) and non-fucosylated ($Hex_5HexNAc_4$α-$Neu5Ac_2$) PSA (Figure 2.14). The Neu5Ac residues in PSA are known to be both α2-3- and α2-6-linked.

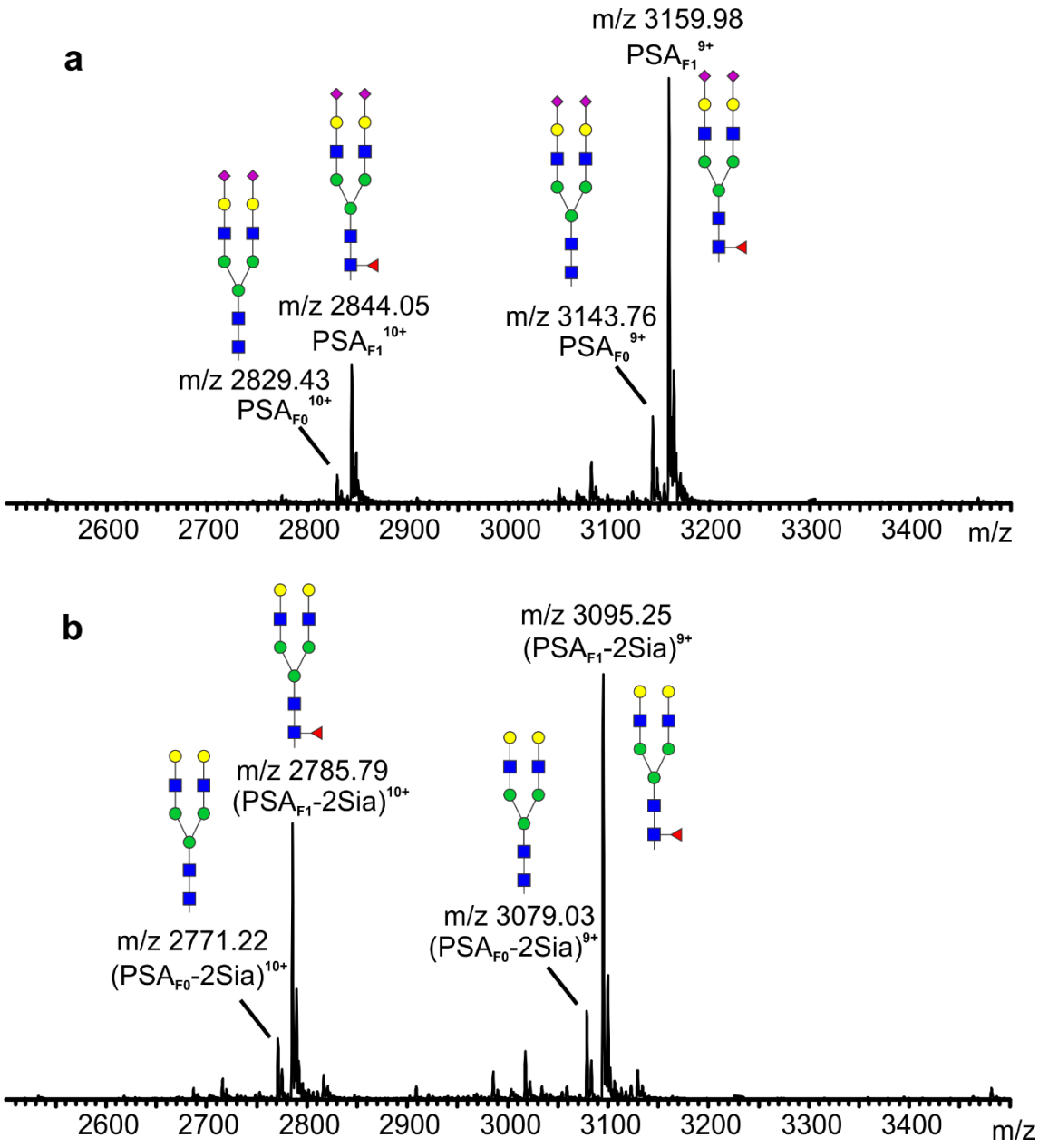

Figure 2.14. Representative ESI mass spectra acquired for an aqueous ammonium acetate solution (200 mM, pH 7 and 25 °C) of human prostate specific antigen (PSA) and asialo-PSA. (a) Spectrum of PSA (5 μM). (b) Spectrum of asialo-PSA (5 μM, treated overnight with neuraminidase from *Clostridium perfringens*). The glycan composition corresponding to the two most abundant glycoforms of PSA, denoted as PSA_{F0} and PSA_{F1}, are shown.

To assess the reactivity of the Neu5Ac-containing *N*-glycan substrates in PSA at neutral pH, NEU3 kinetic measurements were performed on a solution containing PSA, CS^{S1}_{6SL} and CS^{S2}_{3SLNAc}, together with hCA (Figure 2.15). As expected, the hydrolysis of CS^{S2}_{3SLNAc} is faster, approximately 3.5 times, than of CS^{S1}_{6SL} (Figure 2.18a).[34] The progress curve measured for PSA exhibits behavior that is consistent with the presence of both the more reactive α-2-3-linked Neu5Ac and the less reactive α2-6-linked Neu5Ac. Analysis of the kinetic data indicates that α2-3-linked Neu5Ac in the bi-antennary *N*-glycans of PSA, which represents 51% of the Neu5Ac in the glycoprotein, is 5.2 times more reactive than CS^{S2}_{3SLNAc}, while the α2,6-linked Neu5Ac is 2.7 times less reactive than CS^{S1}_{6SL} (Table 2.4). These results show that the relative hydrolysis kinetics of α2-3- and α2-6-linked Neu5Ac within glycoproteins may differ substantially. In the case of PSA, there is a 50-fold difference between the reactivity of α2-3- and α2-6-linked Neu5Ac. In contrast, for the CS investigated, there is only a 3.6-fold difference.

To demonstrate how this same approach is applicable to glycosyltransferases, we compared the rates of Neu5Ac transfer from CMP-Neu5Ac to asialo-PSA and CS^{S2}_{LNAc} by ST6Gal1 and ST3Gal4 at neutral pH. The asialo-PSA was prepared by incubating PSA with the bacterial NEU overnight, followed by mild heating to deactivate the enzyme. Analysis of the kinetic data in Figure 2.18b reveals that asialo-PSA and CS^{S2}_{LNAc} exhibit similar reactivity (i.e., $k = 1.4k_1$, where k is the rate constant for transfer of α2,3-linked Neu5Ac to CS^{S2}_{LNAc} and k_1 is the apparent rate constant for transfer of α2,3-linked Neu5Ac to asialo-PSA with ST3Gal4 (Table 2.4). However, it can also be seen that conversion of monoasialo-PSA to di-sialylated PSA proceeds with very poor efficiency ($k_2 = 0.017k_1$, where k_2 is the apparent rate constant for transfer of α2,3-linked Neu5Ac to monoasialo-PSA). The corresponding mass spectra show that mono-sialylated PSA is the only product detected at long reaction times (Figure 2.16). Moreover, the progress curve for the

formation of CP^{S2}_{3SLNAc} (Figure 2.18b) confirms that the absence of PSA product is not due to a loss in ST3Gal4 activity. Rather, the results indicate that the remaining branch of mono-sialylated PSA is a very poor substrate for ST3Gal4. Because this behavior was not observed (data not shown) for free bi-antennary *N*-glycan substrates (Galβ1-4GlcNAcβ1-2Manα1-3(Galβ1-4GlcNAcβ1-2Manα1-6)Manβ1-4GlcNAcβ1-4GlcNAc and Neu5Acα2-6Galβ1-4GlcNAcβ1-2Manα1-3(Galβ1-4GlcNAcβ1-2Manα1-6)Manβ1-4GlcNAcβ1-4GlcNAc), the present results suggest that PSA is responsible for blocking the transfer of the second Neu5Ac, presumably through steric effects.

Inspection of the mass spectra shown in Figure 2.17, which reveals both mono-sialylated and di-sialylated PSA ions at long reaction times, suggests that ST6Gal1 is significantly more efficient than ST3Gal4 at transferring two molecules of Neu5Ac to the *N*-glycan substrates of asialo-PSA. However, analysis of the time-resolved data (Figure 2.18c) shows that the apparent rate constant for the addition of the second Neu5Ac (i.e., k_2) is only 3-fold larger than that for ST3Gal4 (Table 2.4). The greater efficiency by which ST6Gal1 produces di-sialylated PSA originates primarily from the much faster transfer of the first Neu5Ac ($k_1 = 75k_2$). This strong preference of ST6Gal1 for the asialo-PSA substrate is also reflected in the much slower conversion kinetics measured for CS^{S2}_{LNAc} ($k = 0.16k_1$, Table 2.4).

Taken together, the results obtained for the CS and monoasialo-PSA and PSA demonstrate that the reactivity of simple model substrates may differ significantly from that of natural glycoconjugates. The current work also highlights how CUPRA-ZYME, combined with high resolution ESI-MS, provides a straightforward approach to quantifying the influence of *N*-glycan structure and local (protein) environment on CAZyme activity.

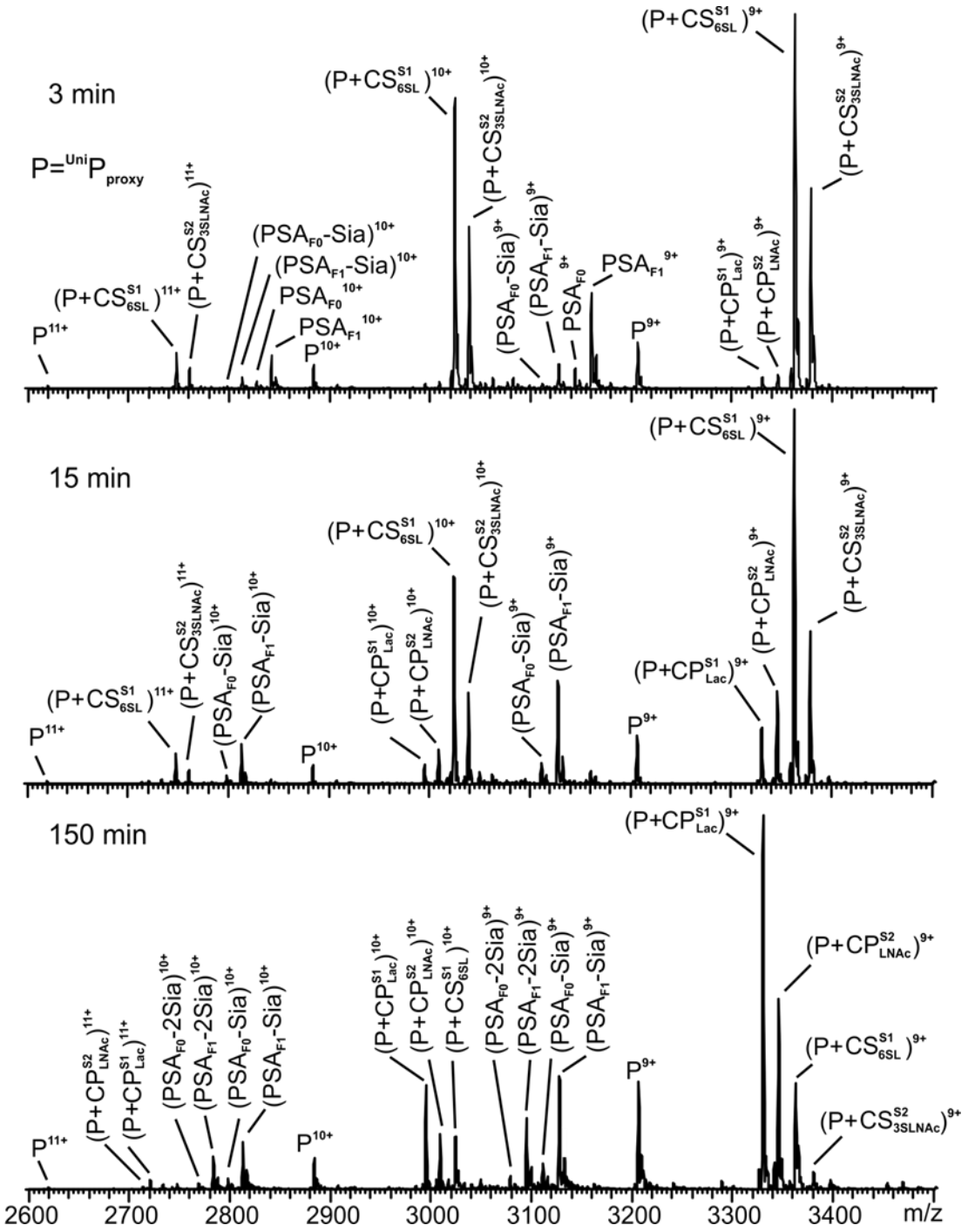

Figure 2.15. Representative ESI mass spectra acquired for an aqueous ammonium acetate solution (200 mM, pH 7 and 25 °C) of PSA (10μM), $^{Uni}P_{proxy}$ (hCA, 10 μM), CS^{S1}_{6SL} (20 μM) and CS^{S2}_{3SLNAc} (20 μM) treated with NEU3 at 3 min, 15 min and 150 min.

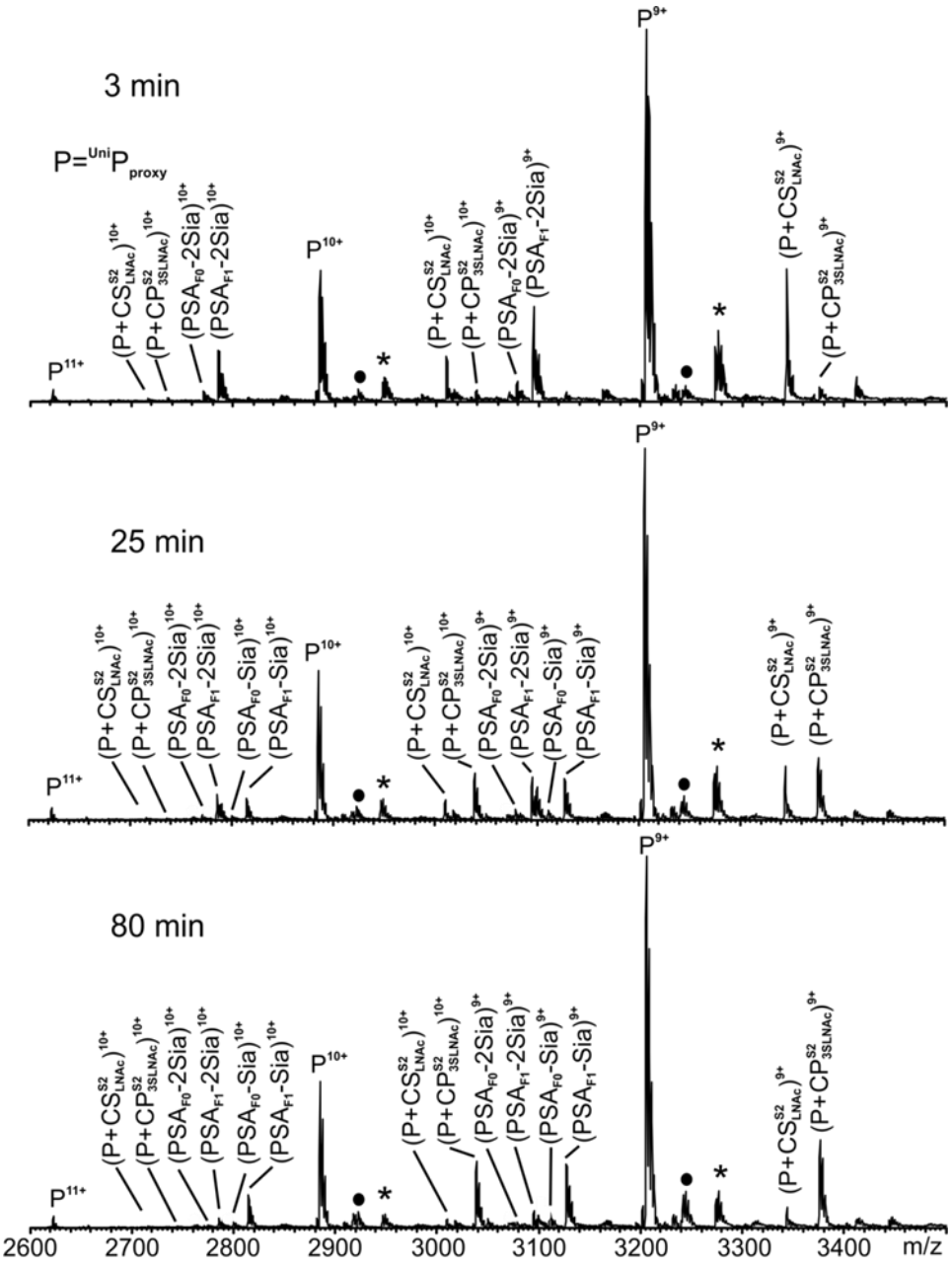

Figure 2.16. Representative ESI mass spectra acquired for an aqueous ammonium acetate solution (200 mM, pH 7 and 25 ºC) of asialo-PSA (5 μM), $^{Uni}P_{proxy}$ (hCA, 5 μM), CMP-Neu5Ac (200 μM), $MnCl_2$ (125 μM) and CS^{S2}_{LNAc} (5 μM) treated with ST3Gal4 at 3, 25 and 80 min. Nonspecific complexes of $^{Uni}P_{proxy}$ with CMP-Neu5Ac and CMP are denoted by * and ●, respectively.

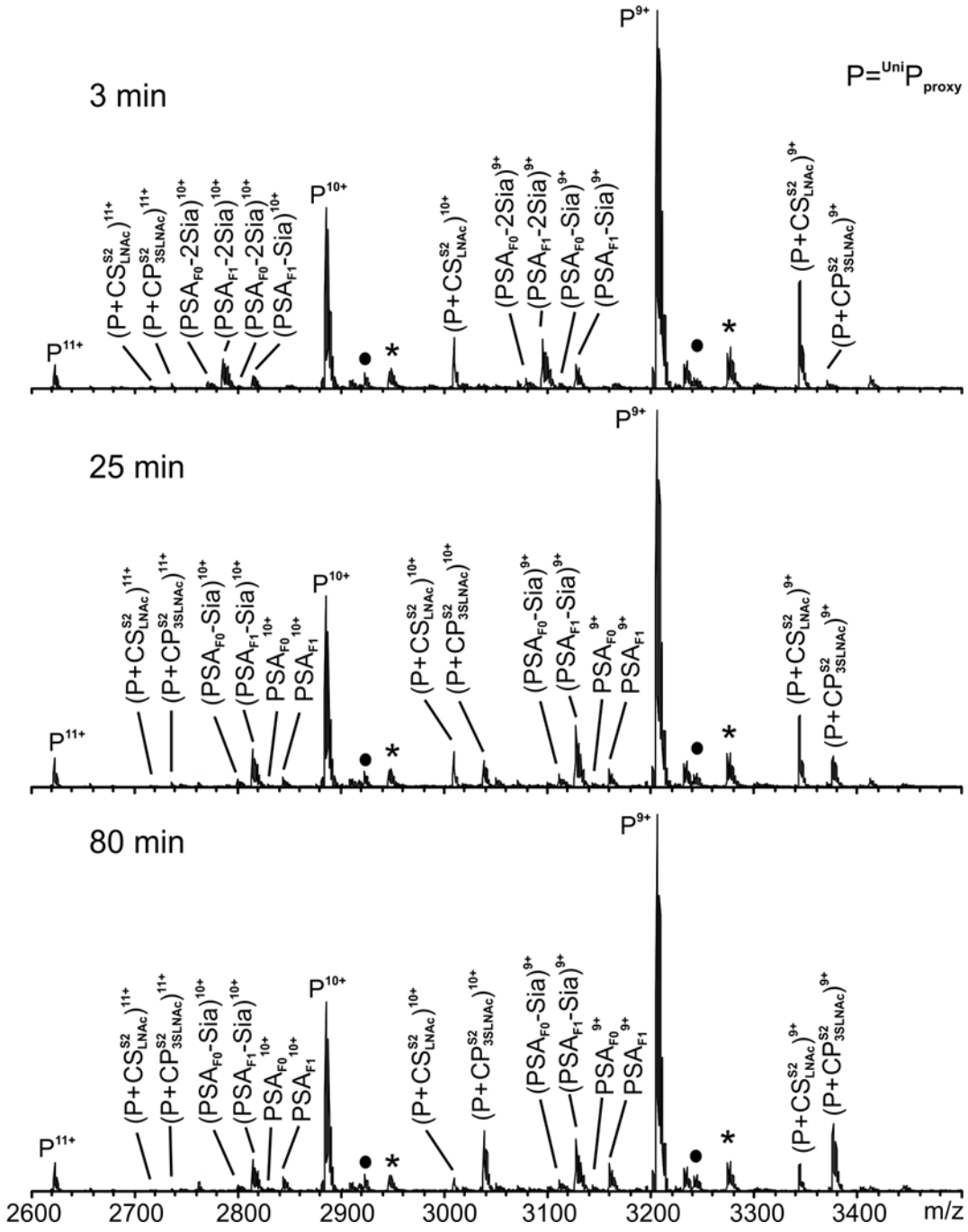

Figure 2.17. Representative ESI mass spectra acquired for an aqueous ammonium acetate solution (200 mM, pH 7 and 25 ºC) of asialo-PSA (5 μM), $^{Uni}P_{proxy}$ (hCA, 5 μM), CMP-Neu5Ac (200 μM) and CS^{S2}_{LNAc} (5 μM) treated with ST6Gal1 at 3, 25 and 80 min. Nonspecific complexes of $^{Uni}P_{proxy}$ with CMP-Neu5Ac and CMP are denoted by * and ●, respectively.

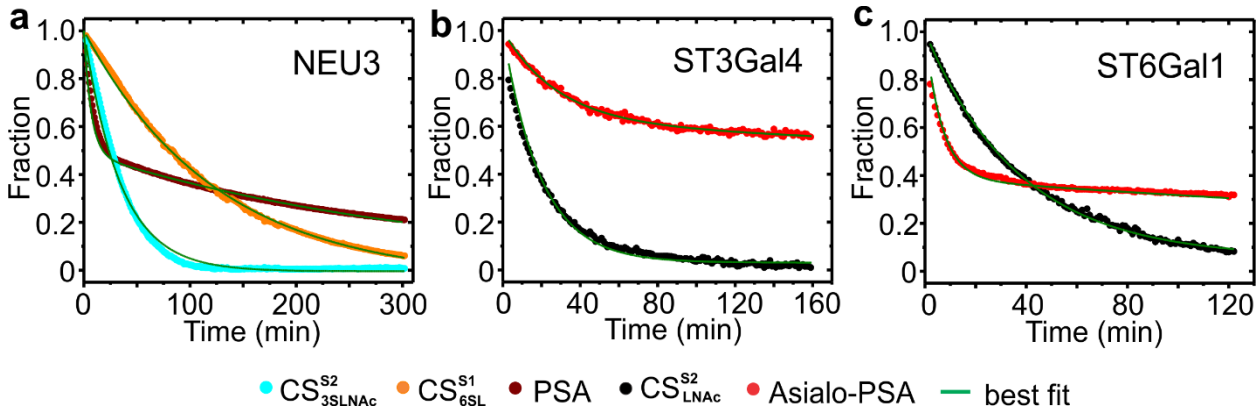

Figure 2.18. Comparison of reactivity of CS and natural glycoconjugates evaluated by CUPRA-ZYME and ESI-MS. (a) Time-dependent fractional concentration of Neu5Ac in the *N*-glycans of PSA measured in an aqueous ammonium acetate solution (200 mM, pH 7 and 25 ºC) of PSA (10 µM), $^{Uni}P_{proxy}$ (hCA, 10 µM), CS^{S1}_{6SL} (20 µM), CS^{S2}_{3SLNAc} (20 µM) and NEU3 (6.25 µg mL^{-1}). (b) Time-dependent fractional concentration of *N*-glycan acceptor substrate in asialo-PSA measured in an aqueous ammonium acetate solution (200 mM, pH 7 and 25 ºC) of asialo-PSA (5 µM), $^{Uni}P_{proxy}$ (hCA, 5 µM), $MnCl_2$ (125 µM), CS^{S2}_{LNAc} (5 µM), CMP-Neu5Ac (200 µM) and ST3Gal4 (200 µg mL^{-1}). (c) Time-dependent fractional concentration of *N*-glycan acceptor substrate in asialo-PSA measured in an aqueous ammonium acetate solution (200 mM, pH 7 and 25 ºC) of asialo-PSA (5 µM), $^{Uni}P_{proxy}$ (hCA, 5 µM), $MnCl_2$ (125 µM), CS^{S2}_{LNAc} (5 µM), CMP-Neu5Ac (200 µM) and ST6Gal1 (42 µg mL^{-1}).

Enzyme	Substrate	k			
NEU3	$\mathbf{CS^{S2}_{3SLNac}}$	0.029±0.001			
	$\mathbf{CS^{S1}_{6SL}}$	0.0080±0.0001			
ST3Gal4 [b]	$\mathbf{CS^{S2}_{LNAc}}$	0.048±0.001			
ST6Gal1	$\mathbf{CS^{S2}_{LNAc}}$	0.024±0.001			
Enzyme	**Substrate**	k_1	f_1	k_2	f_2
NEU3	**PSA**	0.15±0.01	0.51±0.01	0.003±0.0001	0.49±0.01
ST3Gal4 [b]	**asialo-PSA**	0.035±0.001	0.5	0.0006±0.0001	0.5
ST6Gal1	**asialo-PSA**	0.15±0.01	0.5	0.002±0.001	0.5

a. Errors correspond to one standard deviation. b. Solutions contained $MnCl_2$ (125 μM).

Table 2.4. Comparison of kinetics of CUPRA substrates (CS: CS^{S1}_{6SL} CS^{S2}_{3SLNac}, CS^{S2}_{3SLNac}), measured by CUPRA-ZYME, with the biantennary *N*-glycan of the human prostate specific antigen (PSA), measured directly by ESI-MS, for NEU3, ST3Gal4 and ST6Gal1 in aqueous ammonium acetate solutions (200 mM, pH 7 and 25 °C). The rate constant (k) reported for each CS is the best fit of a single exponent decay function (eq 2.2a) to the time-resolved CS concentration. The rate constants k_1 and k_2 reported for PSA, which possesses two Neu5Ac, correspond to the conversion of PSA to mono-sialylated PSA and then asialo-PSA, respectively, by NEU3. The terms f_1 and f_2 represent the fractional abundances of α2,3- and α2,6-linked Neu5Ac, respectively. Rate constants (k_1 and k_2) and fractional abundances (f_1 and f_2) were obtained from the best fit of a double exponential function (eq 2.2b) to the time-resolved data. The k_1 and k_2 reported for asialo-PSA are the rate constants for the transfer of one and two Neu5Ac, respectively, to asialo-PSA, by ST3Gal4 or ST6Gal1. The rate constants ((k_1 and k_2)) were obtained from the best fit of eq 2.2b to the time-resolved data with f_1 and f_2 fixed at 0.5.[a]

2.4 Conclusions

This chapter introduces a powerful MS-based assay for measuring CAZyme activities, monitoring reaction pathways and identifying the formation of intermediates and quantitatively profiling their substrate specificities. Because of the novel manner in which the glycan substrate and corresponding product concentrations are measured, the assay is insensitive to differences in their ESI-MS response factors, regardless of the type of the chemical modification catalyzed by the enzyme. As a result, there is no requirement for calibration curves or the use of internal standards. Currently, due to ion suppression effects and nonspecific association during the ESI process, implementation of the assay is restricted to initial CS concentrations ≤500 μM. However, efforts to extend the accessible concentration range through the use of sub-μm nanoESI emitters are ongoing.[57-59]

Measurements of the hydrolysis kinetics of a CS containing the GM3 oligosaccharide by NEU3 established the reliability of CUPRA-ZYME for measuring kinetic parameters. Application of the assay to a CS composed of the GD3 oligosaccharide, which provided the first direct evidence of endoneuraminidase activity by NEU3, highlighted the advantages of CUPRA-ZYME for studying multistep reactions. The implementation of the assay using human sialyltransferases ST6Gal1 and ST3Gal4 and libraries of CS served to demonstrate the ease with which the substrate specificities of CAZymes can be quantitatively profiled. Finally, the potential of CUPRA-ZYME, when combined with high resolution ESI-MS analysis, to quantify the relative reactivity of CS and natural glycoconjugates was illustrated for the desialylation of PSA (by NEU3) and sialylation of asialo-PSA (by ST6Gal1 and ST3Gal4). Notably, these results showed that, in some cases, the reactivity of the bi-antennary *N*-glycan substrates exhibit significant, kinetic differences compared to the structurally simpler CS tested.

2.5 References

(1) Lombard, V.; Golaconda Ramulu, H.; Drula, E.; Coutinho, P. M.; Henrissat, B. The carbohydrate-active enzymes database (CAZy) in 2013. *Nucleic Acids Res.* **2013**, *42*, D490–D495.

(2) Cantarel, B. L.; Coutinho, P. M.; Rancurel, C.; Bernard, T.; Lombard, V.; Henrissat, B. The carbohydrate-active enzymes database (CAZy): an expert resource for glycogenomics. *Nucleic Acids Res.* **2008**, *37*, D233–D238.

(3) Helbert, W.; Poulet, L.; Drouillard, S.; Mathieu, S.; Loiodice, M.; Couturier, M.; Lombard, V.; Terrapon, N.; Turchetto, J.; Vincentelli, R.; et al. Discovery of novel carbohydrate-active enzymes through the rational exploration of the protein sequences space. *Proc. Natl. Acad. Sci.* **2019**, *116*, 6063 LP – 6068.

(4) Miyagi, T.; Yamaguchi, K. Mammalian sialidases: Physiological and pathological roles in cellular functions. *Glycobiology.* **2012**, *22*, 880–896.

(5) Nijikken, Y.; Tsukada, T.; Igarashi, K.; Samejima, M.; Wakagi, T.; Shoun, H.; Fushinobu, S. Crystal structure of intracellular family 1 β-glucosidase BGL1A from the basidiomycete phanerochaete chrysosporium. *FEBS Lett.* **2007**, *581*, 1514–1520.

(6) Kaoutari, A. El; Armougom, F.; Gordon, J. I.; Raoult, D.; Henrissat, B. The abundance and variety of carbohydrate-active enzymes in the human gut microbiota. *Nat. Rev. Microbiol.* **2013**, *11*, 497.

(7) Zhang, Z.; Wuhrer, M.; Holst, S. Serum sialylation changes in cancer. *Glycoconj. J.* **2018**, *35*, 139–160.

(8) Hou, G.; Liu, G.; Yang, Y.; Li, Y.; Yuan, S.; Zhao, L.; Wu, M.; Liu, L.; Zhou, W. Neuraminidase 1 (NEU1) promotes proliferation and migration as a diagnostic and

prognostic biomarker of hepatocellular carcinoma. *Oncotarget* **2016**, *7*, 64957–64966.

(9) Pinho, S. S.; Reis, C. A. Glycosylation in cancer: mechanisms and clinical implications. *Nat. Rev. Cancer* **2015**, *15*, 540.

(10) Abbott, D. W.; Macauley, M. S.; Vocadlo, D. J.; Boraston, A. B. Streptococcus pneumoniae endohexosaminidase D, structural and mechanistic insight into substrate-assisted catalysis in family 85 glycoside hydrolases. *J. Biol. Chem.* **2009**, *284*, 11676–11689.

(11) Wilson, D. B. Cellulases and biofuels. *Curr. Opin. Biotechnol.* **2009**, *20*, 295–299.

(12) Yuzwa, S. A.; Macauley, M. S.; Heinonen, J. E.; Shan, X.; Dennis, R. J.; He, Y.; Whitworth, G. E.; Stubbs, K. A.; McEachern, E. J.; Davies, G. J.; et al. A potent mechanism-inspired O-GlcNAcase inhibitor that blocks phosphorylation of tau *in vivo*. *Nat. Chem. Biol.* **2008**, *4*, 483-490.

(13) Bardgett, R. D.; Freeman, C.; Ostle, N. J. Microbial contributions to climate change through carbon cycle feedbacks. *Isme J.* **2008**, *2*, 805-814.

(14) Davies, G. J.; Williams, S. J. Carbohydrate-active enzymes: sequences, shapes, contortions and cells. *Biochem. Soc. Trans.* **2016**, *44*, 79 LP – 87.

(15) Li, K. Determination of sialic acids in human serum by reversed-phase liquid chromatography with fluorimetric detection. *J. Chromatogr. B Biomed. Sci. Appl.* **1992**, *579*, 209–213.

(16) Dennis, W.; Gal, U. A Coupled assay for UDP-GlcNAc: Galβl-3GalNAc-R β1,6-N-acetylglucosaminyltransferase(GlcNAc to GalNAc). *Anal. Biochem.* **1992**, *266*, 262–266.

(17) Lowery, R.; Kleman-Leyer, K.; Staeben, M.; Westermeyer, T. Detecting the activity of an screening acceptor substrates, inhibitors, or activators of enzymes catalyzing group transfer reactions to facilitate the development of more selective and therapeutic drugs. US patent

No. 20080233592 (2008).

(18) Kumagai, K., Kojima, H., Okabe, T., and Nagano, T. Development of a highly sensitive, high-throughput assay for glycosyltransferases using enzyme-coupled fluorescence detection. *Anal. Biochem.* **2014**, *447*, 146−155.

(19) Sukovich, D. J., Modavi, C., de Raad, M., Prince, R. N., and Anderson, J. C. DNA-linked enzyme-coupled assay for probing glucosyltransferase specificity. *ACS Synth. Biol.* **2015**, *4*, 833-841.

(20) Sun, H.; Ma, S.; Li, Y.; Qi, H.; Ning, X.; Zheng, J. Electrogenerated chemiluminescence biosensing method for the discrimination of DNA hydroxymethylation and assay of the β-glucosyltransferase activity. *Biosens. Bioelectron.* **2016**, *79*, 92−97.

(21) Pavelka, S. Radiometric enzyme assays: development of methods for extremely sensitive determination of types 1, 2 and 3 iodothyronine deiodinase enzyme activities. *J. Radioanal. Nucl. Chem.* **2010**, *286*, 861–865.

(22) Cleland, W. W. The use of isotope effects to determine enzyme mechanisms. *Arch. Biochem. Biophys.* **2005**, *433*, 2–12.

(23) Liesener, A.; Karst, U. Monitoring enzymatic conversions by mass spectrometry: a critical review. *Anal. Bioanal. Chem.* **2005**, *382*, 1451–1464.

(24) Pi, N.; Armstrong, J. I.; Bertozzi, C. R.; Leary, J. A. Kinetic analysis of NodST sulfotransferase using an electrospray ionization mass spectrometry assay. *Biochemistry* **2002**, *41*, 13283–13288.

(25) Norris, A. J.; Whitelegge, J. P.; Faull, K. F.; Toyokuni, T. Analysis of enzyme kinetics using electrospray ionization mass spectrometry and multiple reaction monitoring: fucosyltransferase V. *Biochemistry* **2001**, *40*, 3774–3779.

(26) Danan, L. M.; Yu, Z.; Hoffhines, A. J.; Moore, K. L.; Leary, J. A. Mass spectrometric kinetic analysis of human tyrosylprotein sulfotransferase-1 and -2. *J. Am. Soc. Mass Spectrom.* **2008**, *19*, 1459–1466.

(27) Fabris, D. Steady-state kinetics of ricin a-chain reaction with the sarcin−ricin loop and with HIV-1 Ψ-RNA hairpins evaluated by direct infusion electrospray ionization mass spectrometry. *J. Am. Chem. Soc.* **2000**, *122*, 8779–8780.

(28) Cheng, S.; Wu, Q.; Xiao, H.; Chen, H. Online monitoring of enzymatic reactions using time-resolved desorption electrospray ionization mass rpectrometry. *Anal. Chem.* **2017**, *89*, 2338–2344.

(29) Sandbhor, M. S.; Soya, N.; Albohy, A.; Zheng, R. B.; Cartmell, J.; Bundle, D. R.; Klassen, J. S.; Cairo, C. W. Substrate recognition of the membrane-associated sialidase NEU3 requires a hydrophobic aglycone. *Biochemistry* **2011**, *50*, 6753–6762.

(30) Hines, H. B.; Brueggemann, E. E.; Hale, M. L. High-performance liquid chromatography–mass selective detection assay for adenine released from a synthetic RNA substrate by ricin A chain. *Anal. Biochem.* **2004**, *330*, 119–122.

(31) Gerber, S. A.; Scott, C. R.; Turecek, F.; Gelb, M. H. Analysis of rates of multiple enzymes in cell lysates by electrospray ionization mass spectrometry. *J. Am. Chem. Soc.* **1999**, *121*, 1102–1103.

(32) Deng, G.; Gu, R.-F.; Marmor, S.; Fisher, S. L.; Jahic, H.; Sanyal, G. Development of an LC–MS based enzyme activity assay for MurC: application to evaluation of inhibitors and kinetic analysis. *J. Pharm. Biomed. Anal.* **2004**, *35*, 817–828.

(33) Ge, X.; Sirich, T. L.; Beyer, M. K.; Desaire, H.; Leary, J. A. A Strategy for the determination of enzyme kinetics using electrospray ionization with an ion trap mass spectrometer. *Anal.*

Chem. **2001**, *73*, 5078–5082.

(34) Kitov, P. I.; Kitova, E. N.; Han, L.; Li, Z.; Jung, J.; Rodrigues, E.; Hunter, C. D.; Cairo, C. W.; Macauley, M. S.; Klassen, J. S. A quantitative, high-throughput method identifies protein–glycan interactions via mass spectrometry. *Commun. Biol.* **2019**, *2*, 268-274.

(35) Moremen, K. W.; Ramiah, A.; Stuart, M.; Steel, J.; Meng, L.; Forouhar, F.; Moniz, H. A.; Gahlay, G.; Gao, Z.; Chapla, D.; et al. Expression system for structural and functional studies of human glycosylation enzymes. *Nat. Chem. Biol.* **2017**, *14*, 156-162.

(36) Kroetsch, A.; Chin, B.; Nguyen, V.; Gao, J.; Park, S. Functional expression of monomeric streptavidin and fusion proteins in escherichia coli: applications in flow cytometry and ELISA. *Appl. Microbiol. Biotechnol.* **2018**, *102*, 10079–10089.

(37) Sun, J.; Kitova, E. N.; Wang, W.; Klassen, J. S. Method for distinguishing specific from nonspecific protein - ligand complexes in nanoelectrospray ionization mass spectrometry. *Anal. Chem.* **2006**, *78*, 3010–3018.

(38) Sun, N.; Soya, N.; Kitova, E. N.; Klassen, J. S. Nonspecific interactions between proteins and charged biomolecules in electrospray. *J. Am. Soc. Mass Spectrom.* **2010**, *21*, 472–481.

(39) Wang, W.; Kitova, E. N.; Klassen, J. S. Nonspecific protein - carbohydrate complexes produced by nanoelectrospray ionization. Factors influencing their formation and stability. *Anal. Chem.* **2005**, *77*, 3060–3071.

(40) Ha, K.-T.; Lee, Y.-C.; Cho, S.-H.; Kim, J.-K.; Kim, C.-H. Molecular characterization of membrane type and ganglioside-specific sialidase (Neu3) expressed in E. coli. *Mol. Cells.* **2004**, *17*, 267–273.

(41) Zanchetti, G.; Colombi, P.; Manzoni, M.; Anastasia, L.; Caimi, L.; Borsani, G.; Venerando, B.; Tettamanti, G.; Preti, A.; Monti, E.; et al. Sialidase NEU3 is a peripheral membrane

protein localized on the cell surface and in endosomal structures. *Biochem. J.* **2007**, *408*, 211–219.

(42) Monti, E.; Bassi, M. T.; Papini, N.; Riboni, M.; Manzoni, M.; Venerando, B.; Croci, G.; Preti, A.; Ballabio, A.; Tettamanti, G.; et al. Identification and expression of NEU3, a novel human sialidase associated to the plasma membrane. *Biochem. J.* **2000**, *349*, 343–351.

(43) Smutova, V.; Albohy, A.; Pan, X.; Korchagina, E.; Miyagi, T.; Bovin, N.; Cairo, C. W.; Pshezhetsky, A. V. Structural basis for substrate specificity of mammalian neuraminidases. *PLoS One* **2014**, *9*, e106320–e106320.

(44) Albohy, A.; Li, M. D.; Zheng, R. B.; Zou, C.; Cairo, C. W. Insight into substrate recognition and catalysis by the human neuraminidase 3 (NEU3) through molecular modeling and site-directed mutagenesis. *Glycobiology.* **2010**, *20*, 1127–1138.

(45) Smith, K. S.; Cosper, N. J.; Stalhandske, C.; Scott, R. A.; Ferry, J. G. Structural and kinetic characterization of an archaeal β-class carbonic anhydrase. *J. Bacteriol.* **2000**, *182*, 6605 – 6613.

(46) Steiner, H.; Jonsson, B.; Lindskog, S. The catalytic mechanism of carbonic anhydrase. *Eur. J. Biochem.* **1975**, *59*, 253–259.

(47) Weinstein, J.; de Souza-e-Silva, U.; Paulson, J. C. Sialylation of glycoprotein oligosaccharides N-linked to asparagine. Enzymatic characterization of a Gal beta 1 to 3(4)GlcNAc alpha 2 to 3 sialyltransferase and a Gal beta 1 to 4GlcNAc alpha 2 to 6 sialyltransferase From Rat Liver. *J. Biol. Chem.* **1982**, *257*, 13845–13853.

(48) Kitagawa, H.; Paulson, J. C. Cloning of a novel alpha 2,3-sialyltransferase that sialylates glycoprotein and glycolipid carbohydrate groups. *J. Biol. Chem.* **1994**, *269*, 1394–1401.

(49) Sasaki, K.; Watanabe, E.; Kawashima, K.; Sekine, S.; Dohi, T.; Oshima, M.; Hanai, N.;

Nishi, T.; Hasegawa, M. Expression cloning of a novel Gal beta (1-3/1-4) GlcNAc alpha 2,3-sialyltransferase using lectin resistance selection. *J. Biol. Chem.* **1993**, *268*, 22782–22787.

(50) Kessel, D.; Chou, T.; Allen, J. Some properties of sialyltransferase in plasma and lymphocytes of patients with chronic lymphocytic leukemia. *Eur. J. Biochem.* **1978**, *82*, 535–541.

(51) Audry, M.; Jeanneau, C.; Imberty, A.; Harduin-Lepers, A.; Delannoy, P.; Breton, C. Current trends in the structure–activity relationships of sialyltransferases. *Glycobiology.* **2010**, *21*, 716–726.

(52) Kono, M.; Ohyama, Y.; Lee, Y.-C.; Hamamoto, T.; Kojima, N.; Tsuji, S. Mouse β-galactoside α2,3-sialyltransferases: comparison of in vitro substrate specificities and tissue specific expression. *Glycobiology.* **1997**, *7*, 469–479.

(53) Shariat, S. F.; Semjonow, A.; Lilja, H.; Savage, C.; Vickers, A. J.; Bjartell, A. Tumor markers in prostate cancer I: blood-based markers. *Acta Oncol. (Madr).* **2011**, *50*, 61–75.

(54) Stamey, T. A.; Yang, N.; Hay, A. R.; McNeal, J. E.; Freiha, F. S.; Redwine, E. Prostate-specific antigen as a serum marker for adenocarcinoma of the prostate. *N. Engl. J. Med.* **1987**, *317*, 909–916.

(55) Okada, T.; Sato, Y.; Kobayashi, N.; Sumida, K.; Satomura, S.; Matsuura, S.; Takasaki, M.; Endo, T. Structural characteristics of the *N*-glycans of two isoforms of prostate-specific antigens purified from human seminal fluid. *Biochim. Biophys. Acta.* **2001**, *1525*, 149–160.

(56) Tabarés, G.; Radcliffe, C. M.; Barrabés, S.; Ramírez, M.; Aleixandre, R. N.; Hoesel, W.; Dwek, R. A.; Rudd, P. M.; Peracaula, R.; de Llorens, R. Different glycan structures in prostate-specific antigen from prostate cancer sera in relation to seminal plasma PSA.

Glycobiology. **2005**, *16*, 132–145.

(57) Susa, A. C.; Xia, Z.; Williams, E. R. Small emitter tips for native mass spectrometry of proteins and protein complexes from nonvolatile buffers that mimic the intracellular environment. *Anal. Chem*. **2017**, *89*, 3116–3122.

(58) Susa, A. C.; Lippens, J. L.; Xia, Z.; Loo, J. A.; Campuzano, I. D. G.; Williams, E. R. Submicrometer emitter ESI tips for native mass spectrometry of membrane proteins in ionic and nonionic detergents. *J. Am. Soc. Mass Spectrom*. **2018**, *29*, 203–206.

(59) Susa, A. C.; Xia, Z.; Williams, E. R. Native mass spectrometry from common buffers with salts that mimic the extracellular environment. *Angew. Chemie Int. Ed*. **2017**, *56*, 7912–7915.

Chapter 3

Quantifying CAZyme Activity with Glycoprotein Substrates using ESI-MS and Center-of-Mass Monitoring (CoMMon)

3.1 Introduction

Carbohydrate-Active enZymes (CAZymes), a large group of enzymes involved in the synthesis, degradation and modification of carbohydrates (glycans), play critical roles in diverse physiological and pathophysiological processes.[1,2] For example, glycosyltransferases (GTs) and glycosyl hydrolases (glycosidases, GHs), which catalyze the synthesis and cleavage of glycosidic bonds, respectively, regulate protein glycosylation, a posttranslational modification that affects protein quality control, cell signaling, and host-pathogen interactions.[3-6] CAZymes are also important to a wide range of biotechnology applications, such as protein glycoengineering, which seeks to control the glycosylation of biotherapeutics, vaccines and diagnostics, as well as in glycomaterials.[7-12] Measurements of CAZyme kinetics provide insight into enzyme activity and substrate specificity. Such information is of fundamental interest and supports diverse applications. However, versatile and robust kinetic assays suitable for natural CAZyme substrates, in particular glycoproteins and glycolipids, are limited. Consequently, the structure-activity relationships of many CAZymes are poorly understood.

CAZyme activity and substrate specificity has traditionally been assessed using radiochemical, spectroscopic (spectrophotometric- and fluorescence-based), and separation

---

† A version of this chapter has been published as: Li, Z.; Kitov, P. I.; Kitova, E. N.; Bui, D. T.; Moremen, K. W.; Wakarchuk, W. W.; Mahal, L. K.; Macauley, M. S.; Klassen, J. S. *Anal. Chem.* **2021**, *93*, 15262–15270.

techniques (e.g. reversed-phase, ion-exchange or thin-layer chromatography).[13-16] For example, radiolabeled CMP-^{14}CNeu5Ac and fluorophore labeled CMP-Neu5Ac-Bodipy have been widely used for the characterization of sialyltransferase (ST) activity.[17,18] Although very sensitive, the radiolabeling technique usually requires a separation step and is limited to special safety certified labs. Spectroscopic techniques, such as fluorescence and luminescence, also offer high sensitivity but are not readily amenable to monitoring multiple substrates simultaneously. Moreover, the introduction of fluorophore (or chromophore) into the substrate can alter, in some cases substantially, CAZyme activity.[19] Separation techniques (e.g. HPLC) coupled to mass spectrometry (MS) detection represent label-free approaches. However, such methods generally require quenching of the reaction and, as such, do not allow for continuous monitoring.[20-21]

Over the past two decades, the use of electrospray ionization mass spectrometry (ESI-MS) to monitor CAZyme (and other classes of enzymes) reactions has grown significantly. The direct ESI-MS approach has the benefit of being label-free, allows for continuous measurements and can simultaneously monitor multiple species (e.g. substrate(s), product(s) and intermediates).[22-26] However, because the ESI-MS response factors for many CAZyme substrates and their corresponding products differ, correlating the measured substrate and product ion abundances with solution concentrations is challenging and generally requires the use of a calibration curve or an internal standard (IS), usually an isotopically-labeled substrate or product.[27-30] Appropriate IS for many CAZyme reactions are not available commercially and are difficult to synthesize; when available for purchase, they tend to be expensive. To address this issue, CUPRA-ZYME method, as described in Chapter 2, was introduced.[31] The assay relies on oligosaccharide substrates labeled with an affinity tag that binds to an appropriate protein receptor called a universal proxy protein, $^{Uni}P_{proxy}$. Because both the substrate and corresponding product bind to the proxy protein, their

concentrations can be determined directly from the relative abundances of the bound $^{Uni}P_{proxy}$ ions measured by ESI-MS, with no requirement for calibration curves or IS. Moreover, the assay is amenable to monitoring simultaneously multiple substrates (provided they have distinct molecular weights (MWs)), thereby allowing the relative reactivity of substrates to be quantified. However, this method requires labeled substrates and is not amenable to native glycoproteins or glycolipids, that can provide important insight into CAZyme substrate specificities.

Despite important advances in direct ESI-MS-based methods for measuring CAZyme reactions involving oligosaccharide substrates, continuous, quantitative monitoring of intact glycoprotein and glycolipid substrates remains problematic. Glycoprotein substrates, in particular, represent a formidable challenge due to their macro- (presence or absence of glycans at a specific glycosylation site) and micro-heterogeneity (different glycan structures at a particular glycosylation site). Glycosylation can occur at multiple sites on the protein, with a range of glycan structures possible at a given site, leading to a complex mixture of structures, many with distinct MWs, which are difficult and, often, impossible to fully resolve, even with the most advanced mass analyzers.[32,33] In this chapter, we describe a simple, versatile and quantitative ESI-MS approach to measure the kinetics of CAZyme reactions involving intact glycoprotein substrates. The assay, referred to as Center-of-Mass (CoM) Monitoring (CoMMon), relies on continuous (real-time) ESI-MS monitoring of the CoM of the ensemble of glycoprotein substrates and their corresponding CAZyme products (Figure 3.1). Importantly, there is no requirement for calibration curves, IS, labelling, or mass spectrum deconvolution. We validated the assay using a GH reaction. We compared reaction progress curves and initial rates for neuraminidase-catalyzed desialylation of a series of mammalian glycoproteins measured with CoMMon and, simultaneously, using an

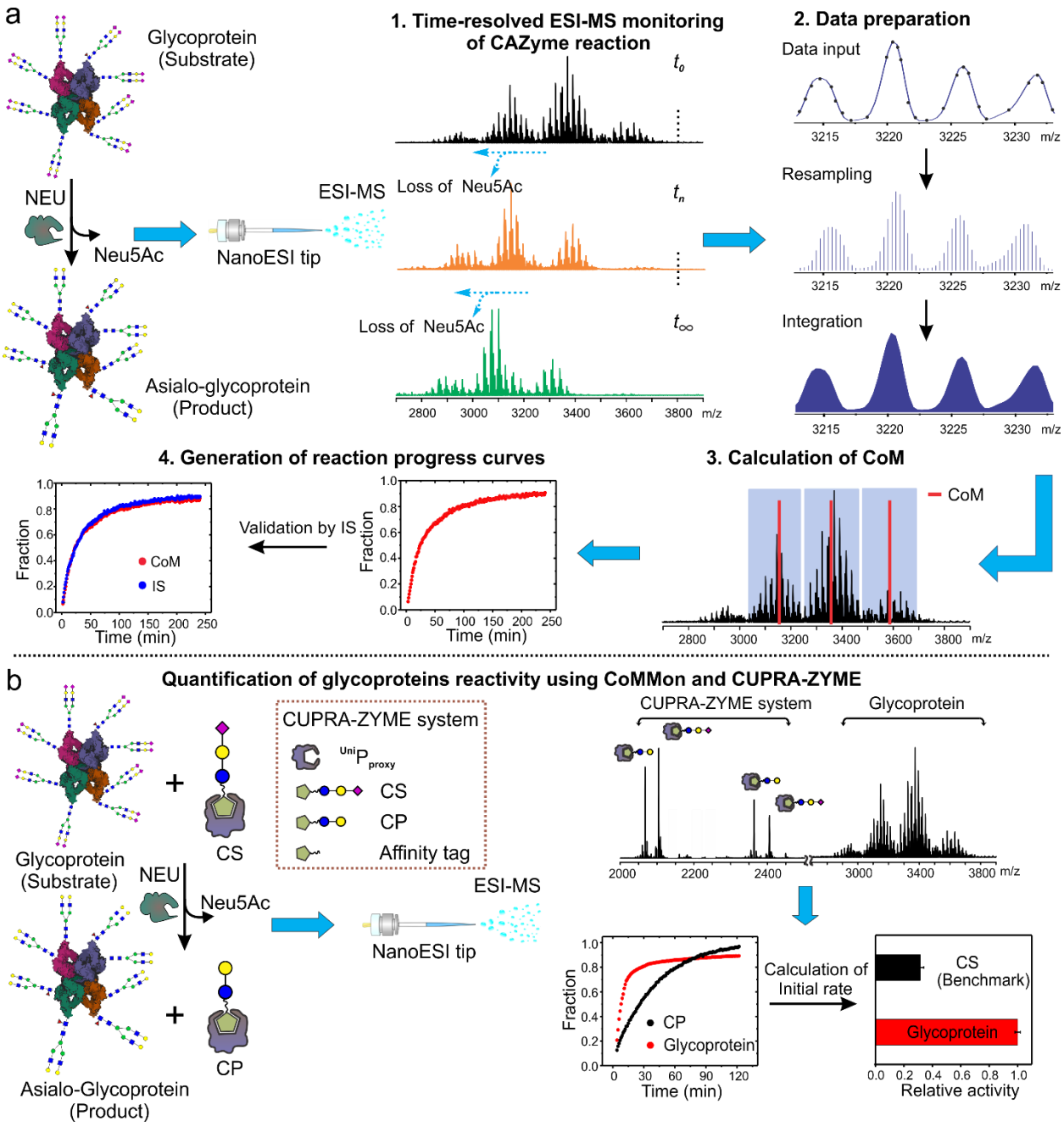

Figure 3.1. (a) CoMMon workflow: 1. Time-resolved ESI-MS monitoring of the CAZyme reaction. 2. Data preparation. 3. Calculation of CoM. 4. Generation of reaction progress curve. (b) Combined CoMMon/CUPRA-ZYME workflow for quantifying the relative reactivity of glycoprotein substrates.

isotopically labeled IS. To illustrate the applicability of CoMMon to GT reactions, we used the assay to measure human ST-catalyzed sialylation of asialoglycoproteins. The feasibility of applying CoMMon to large (MW>500 kDa) and highly heterogeneous glycoprotein substrates was also shown. Finally, we highlight how CoMMon, combined with CUPRA-ZYME, enables the relative reactivity of glycoprotein substrates to be quantitatively established, thereby providing a unique opportunity to reliably study structure-reactivity relationships for CAZyme-catalyzed reactions involving glycoprotein substrates.

3.2 Experimental

3.2.1 Materials

3.2.1.1 Protein and CAZymes

Neuraminidase from *Clostridium perfringens* (NEUC), SAvPhire monomeric streptavidin (mSA, MW 15,650 Da), human carbonic anhydrase (hCA, type 1, MW 28,848 Da), bovine fetuin and bovine asialo-fetuin (BF and asialo-BF from fetal bovine serum, average MW of 47 kDa and 43 kDa, respectively)[34,35] and α1-acid glycoprotein (AGP, a mixture of three (F1, S and A) proteoforms with MWs ~37 kDa, from human plasma)[36] were purchased from Sigma-Aldrich Canada (Oakville, Canada). Human prostate specific antigen (PSA, average MW ~28 kDa, from seminal plasma)[37] was purchased from Lee BioSolutions (Maryland Heights, MO, USA). α1-antitrypsin (α1AT from human plasma, MW ~51 kDa, containing two variant M1 phenotype Val^{213} and M1 phenotype Ala^{213})[38] was purchased from Grifols Therapeutics Inc. (Los Angeles, CA, USA). Human haptoglobin 1-1 (Hp from human plasma, dimer MW ~92 kDa)[39] and human alpha-2-macroglobulin (α2M from human plasma, tetramer MW ~720 kDa,)[40] were purchased from Athens Research&Technology (Athens, GA, USA). A soluble recombinant form of human

sialyltransferases ST6Gal1 (UniProt P15907, amino acid residues 75-406) and ST3Gal4 (UniProt Q11206, amino acid residues 41-333) were expressed in Freestyle 293F cells (Thermo Fisher Scientific) as green fluorescent protein (GFP) fusions in the pGEn2 vector, as previously described.[41]

The asialo-glycoforms of PSA, α1AT, AGP, Hp and tetrameric α2M were prepared by incubating, separately, the glycoproteins with NEUC in 200 mM ammonium acetate (pH 6.7) at room temperature for 48 h. Asialo-PSA was used to produce fully α2-3 or α2-6 sialylated PSA by incubating with CMP-Neu5Ac and either ST3Gal4 or ST6Gal1. Dimeric and monomeric α2M was prepared by incubating tetrameric α2M with DTT (1 mM) for 2 h to cleave the disulfide bonds and dissociate the tetrameric α2M. IAA (10 mM) was then added into the solution and incubated for another 3 h to bind with the free sulfhydryl to prevent the reformation of disulfide bond. Asialo-glycoforms of dimeric and monomeric α2M were prepared using the same procedure described above. All proteins were dialyzed against an aqueous solution of 200 mM ammonium acetate (pH 6.7) using an Amicon 0.5 mL microconcentrator (EMD Millipore, Billerica, MA) with a MW cutoff of 3 kDa and stored at -20 ºC until used.

3.2.1.2 Glycans and reagents

N-acetyl-D-neuraminic acid-1,2,3-$^{13}C_3$ (Neu5Ac-$^{13}C_3$) was purchased from Omicron Biochemicals Inc. (South Bend, IN, USA). Neu5Acα2-3Galβ1-4Glc (3'-sialyllactose, 3SL) and Galβ1-4GlcNAcβ1-3Galβ1-4Glc (LNnT) were purchased from Elicityl SA (Crolles, France). Biotin-PEG4-amine was purchased from BroadPharm (San Diego, USA). Dithiothreitol (DTT), iodoacetamide (IAA), cytidine-5′-monophospho-*N*-acetylneuraminic acid (CMP-Neu5Ac), sodium cyanoborohydride ($NaBH_3$) and 2-aminobenzamide (2-AB) were purchased from Sigma-Aldrich Canada (Oakville, Canada).

3.2.1.3 CUPRA substrates

CUPRA substrates (CS) employing two different affinity tags (sulfonamide or biotin) were used to perform CUPRA-ZYME.[31] Representative structures of the CS (CS^{S}_{3SL}, CS^{B}_{3SL} and CS^{B}_{LNnT}) are shown in Figure 3.2. Human carbonic anhydrase (hCA) and mono-streptavidin (mSA) were used as ${}^{Uni}P_{proxy}$ for the CS containing sulfonamide and biotin affinity tags, respectively. The synthetic methods used to prepare the CS are described elsewhere.[42] Briefly, the free oligosaccharide was mixed with respective primary amine derivative in DMSO and incubated at 50 ºC for between 24 h and 48 h. To this mixture, excess acetic anhydrate was added and incubated at room temperature for 1 h. The mixture was diluted with water and the pH was adjusted to ~10 using NaOH. The solution was then acidified and the CUPRA product was isolated using HPLC on a reverse phase column (C-18). 3SL was conjugated, separately, to the sulfonamide affinity tag and to the biotin affinity tag to give CS^{S}_{3SL} and CS^{B}_{3SL}, respectively (Figure 3.2); LNnT was conjugated to biotin affinity tag to give CS^{B}_{LNnT} (Figure 3.2). hCA (type I) served as ${}^{Uni}P_{proxy}$ for CS^{S}_{3SL}, while mSA was ${}^{Uni}P_{proxy}$ for CS^{B}_{3SL} and CS^{B}_{LNnT}.

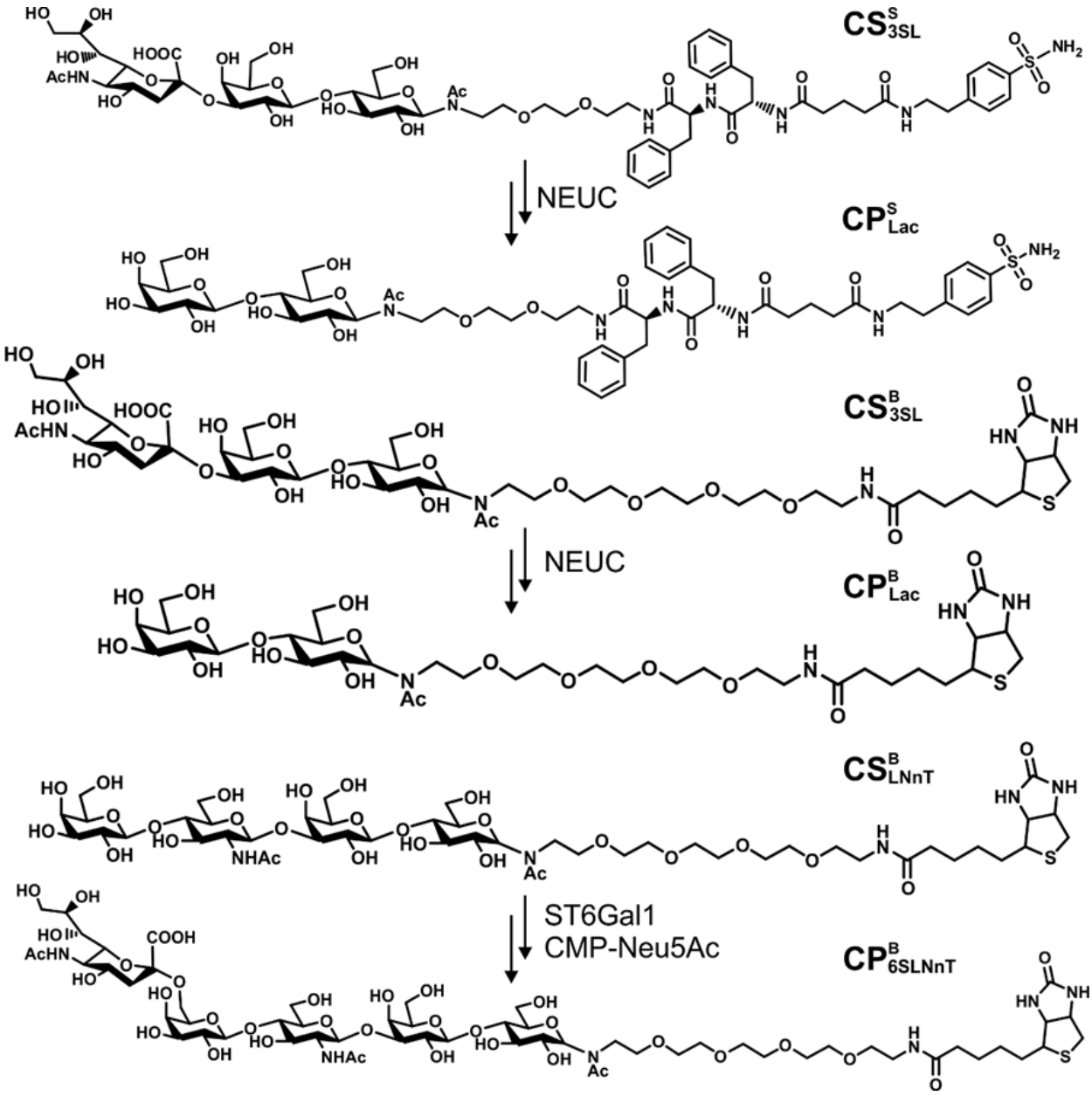

Figure 3.2. Structures of CUPRA substrates (CS) used in the paper and their corresponding CUPRA products (CP). CS^{S} are CUPRA substrates containing a sulfonamide as affinity tag, human carbonic anhydrase (hCA, type I) was employed as corresponding $^{Uni}P_{proxy}$. CS^{B} are CUPRA substrates containing a biotin as affinity tag, monomeric streptavidin (mSA) was employed as corresponding $^{Uni}P_{proxy}$. Details of the synthesis can be found in reference 31.

3.2.2 Mass spectrometry

ESI-MS measurements were carried out in positive ion mode using two instruments, a Q Exactive Orbitrap with Ultra High Mass Range (UHMR Orbitrap) and a Q Exactive Orbitrap (Orbitrap) mass spectrometer (Thermo Fisher Scientific, Bremen, Germany), each equipped with a nanoflow ESI (nanoESI) source. NanoESI tips, with an outer diameter of approximately 2.0 μm, were produced from borosilicate capillaries using a P-1000 micropipette puller (Sutter Instruments, Novato, CA) using the following parameters: heat 520 °C, pull 1, velocity 57, delay 150, pressure 490 and ramp 518. To perform nanoESI, a voltage of ~0.8 kV was applied a platinum wire inserted into the back end of the tip and in contact with the sample solution. The capillary temperature was set at 120 °C. Raw data were processed using the Thermo Xcalibur 2.2 software. Time-resolved mass spectra were averaged over 1 min intervals. CoM values were calculated automatically from the average mass spectra using the SWARM software (https://github.com/pkitov/CUPRA-SWARM) and used to construct reaction progress curves. CoMMon was implemented using a new module (which includes automatic extraction of mass spectra at different time points from the total ion chromatograms recorded using the Orbitrap and UHMR Orbitrap instruments) in the SWARM package. SWARM was originally designed to process mass spectra acquired using mass analyzers for which the intensity of ion signal is independent of charge state (e.g. time-of-flight mass spectrometers). However, for Fourier-transform mass spectrometers (e.g. Orbitrap instruments) the ion intensity is proportional to charge state. Consequently, intensity must be normalized by charge state to obtain ion abundance. This option was added to SWARM. The workflow for CoMMon analysis in SWARM is: collection of the exact mass list for each mass spectrum averaged over a defined period of time (e.g. 1 min); calculation of the weighted average mass

(CoM) within a well-defined mass range for each charge state; the CoM for each charge state is averaged to give the CoM_t value.

All CAZyme reactions were performed in the nanoESI tip and continuously monitored by ESI-MS. To carry out the reactions, aliquots of stock solutions of CAZyme, substrate(s) and IS (where applicable) were mixed with 200 mM aqueous ammonium acetate (pH6.7) in an Eppendorf tube, vortexed and then transferred to the nanoESI tip. ESI mass spectra were collected continuously starting at 3 min reaction time (the minimum time to prepare and load the sample into the tip). All measurements were carried out at pH 6.7 and 25 °C.

With the exception of the experiments performed using the IS, the UHMR Orbitrap was used to monitor the reaction. The resolution was set at 6250 and the automatic gain control (AGC) was 5E5. For experiments including PSA, α1AT, BF and AGP (and their corresponding asialo forms) the *m/z* range was 1500 to 6000, the S-lens RF level was 50, the maximum inject time was 150 ms and each 10 microscans were combined to a single scan. In the case of Hp and α2M samples, the *m/z* range was 2000 to 18000, the S-lens RF level was 200, the maximum inject time was 200 ms, and each 20 microscans were combined to a single scan. The Orbitrap was used for experiments involving IS (which was used to quantify the concentration of released Neu5Ac). For these measurements the *m/z* range was 280 to 5000, the S-lens RF level was 30, the resolution was 17500 and the AGC was 5E5, the maximum inject time was 200 ms and each 10 microscans were combined to a single scan.

3.2.3 Implementation of CoMMon

The CoMMon approach to measuring the progress of CAZyme reactions involving an ensemble (mixture of glycoforms) of glycoprotein substrates is based on changes in the time-dependent CoM

(CoM_t) of the substrates. Specifically, the time-dependent fractional abundance of the substrates (F_t) can be expressed in terms of CoM_t as shown in eq 3.1:

$$F_t = \left|(CoM_0 - CoM_t)\right| / \left|(CoM_0 - CoM_\infty)\right| \tag{3.1}$$

where the CoM_0 and CoM_∞ represent the initial and final values of CoM_t, respectively. The value of CoM_0 is established prior to addition of CAZyme; in principle, CoM_∞ represents the theoretical end point. However, and as discussed in more detail below, in some cases the CAZyme reaction does not proceed to completion on the timescale of the measurements. In such instances CoM_∞ represent the apparent (measured) end point of the reaction.

Calculation of CoM_t. In cases where all MW-distinct (corresponding to unique glycan composition) glycoprotein species are fully resolved in the mass spectrum, the CoM_t of a glycoprotein sample can be calculated from the arithmetic mean of the MWs of the individual species using eq 3.2:

$$CoM_t = \sum_i f_{i,t} MW_{i,t} \tag{3.2}$$

where i corresponds to a specific glycan composition (at reaction time t) with $MW_{i,t}$ and fractional abundance $f_{i,t}$ (which is calculated from the total, charge-state (n) normalized relative abundances (Ab_i) of the corresponding gas-phase ions), eq 3.3:

$$f_{i,t} = \frac{\sum_n Ab_i (MW_{i,t})_n}{\sum_i \sum_n Ab_i (MW_{i,t})_n} \tag{3.3}$$

Uniform ESI-MS response factors for all glycoforms is an implicit assumption made in the calculation of $f_{i,t}$ (and CoM_t). Based on the results of ESI-MS protein-ligand binding measurements, this assumption is reasonable in cases where glycoprotein substrates undergo relatively small changes (≤5%) in MW.[43,44]

Typically, it is not possible to fully resolve all or even most MW-distinct glycoprotein species, making it challenging to accurately calculate Ab_i from ESI mass spectra. This limitation can be overcome by calculating CoM_t from the total signal corresponding to all glycoprotein species (i.e., substrates, intermediates and products). If the charge state distributions of all glycoprotein species are similar, CoM_t can be approximated as the weighted average mass-to-charge ratio (*m/z*) of all detectable glycoprotein signal, eq 3.4:

$$\mathrm{CoM}_t = \frac{A_t}{\sum_x Int_{x,t}} \tag{3.4}$$

where A_t, which is calculated from eq 3.5, represents the *m/z*-weighted signal intensity within the selected *m/z* range; *x* represents the specific *m/z* value, and $Int_{x,t}$ represents the intensity of the signal at position $(m/z)_x$:

$$A_t = \sum_x Int_{x,t}(m/z)_x \tag{3.5}$$

However, as the charge state distributions of glycoproteins often change over the course of the CAZyme reaction, CoM_t is more reliably calculated as the average of CoM_t values for individual glycoprotein charge states ($\mathrm{CoM}_{t,n}$), eq 3.6:

$$\mathrm{CoM}_{t,n} = \frac{A_{t,n}}{\sum_x Int_{x,t,n}} \tag{3.6}$$

where $A_{t,n}$ represents the *m/z*-weighted signal intensity within the *m/z* range corresponding to charge state *n*, eq 3.7:

$$A_{t,n} = \sum_x Int_{x,t,n}(m/z)_{x,n} \tag{3.7}$$

$Int_{x,t,n}$ represents the peak intensity at $(m/z)_{x,n}$ and x represents the specific m/z value, within the range, at charge state n. After determination of $CoM_{t,n}$ for each charge state, the final CoM_t can be found using eq 3.8:

$$\mathrm{CoM}_t = \frac{\sum_n CoM_{t,n}}{h} \tag{3.8}$$

where h is number of total charge state envelops being considered.

A modified version of our previously reported SWARM software was used to extract CoM values from the time-resolved mass spectra.[45] The original SWARM software was designed for the analysis of mass spectra acquired using mass analyzers for which the intensity of ion signal is independent of charge state.[45] In this chapter, we modified SWARM to enable the analysis of mass spectra acquired using mass analyzers for which ion intensity is proportional to its charge state and to automatically calculate CoMt from time-resolved mass spectra. The compiled program and source code for CoMMon software are available on https://github.com/pkitov/CUPRA-SWARM. An overview of the data analysis procedures is given in Figure 3.3.

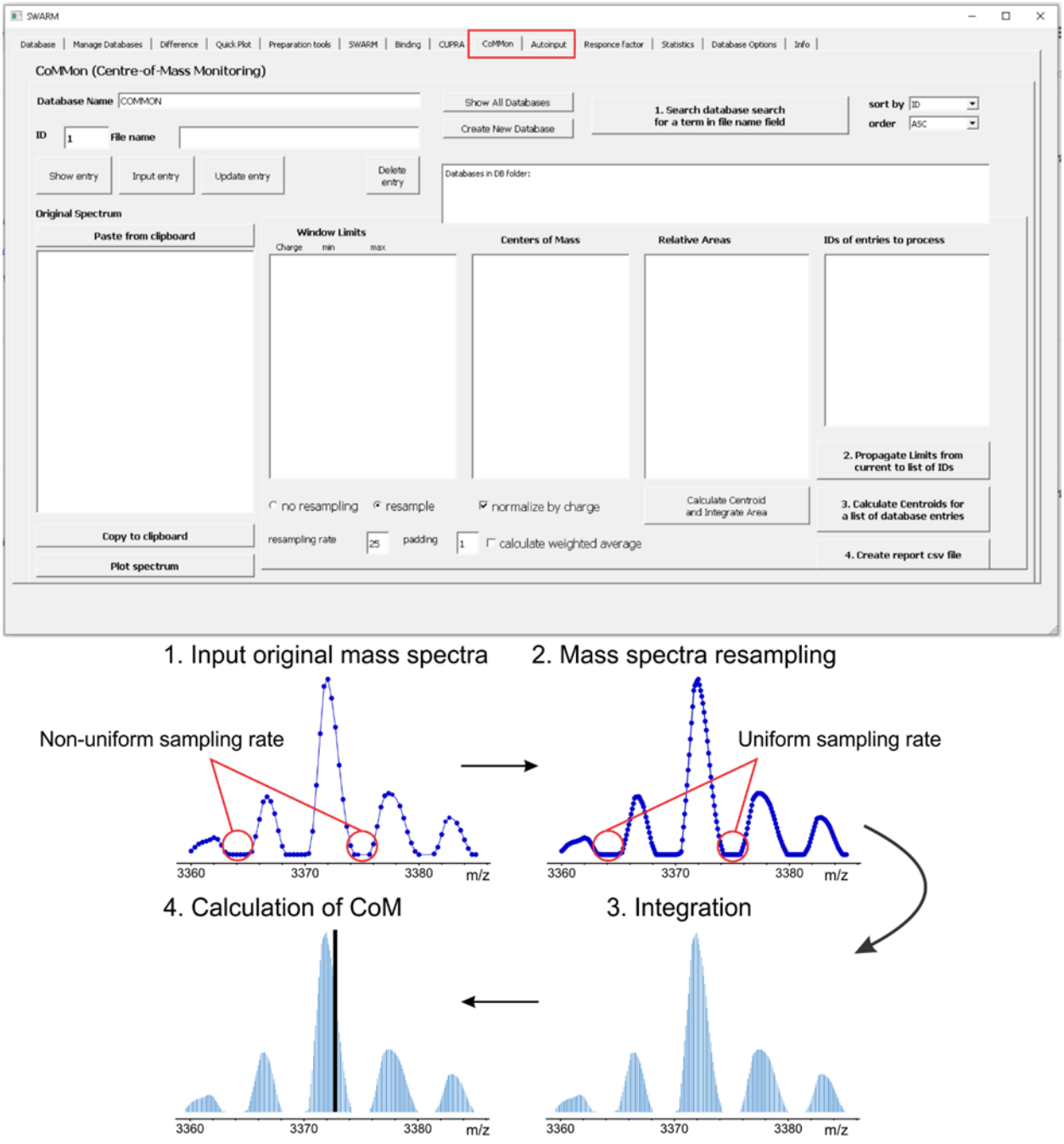

Figure 3.3. SWARM software (CoMMon module) interface and workflow for calculating CoM. Because of the non-uniform MS sampling rate, software resamples each mass spectrum by linear interpolation to produce mass spectra with uniform spacing between each data point.

3.2.4 CUPRA-ZYME

Where indicated, CUPRA-ZYME was performed simultaneously with CoMMon. Briefly, the time-dependent concentrations of the CUPRA substrate (CS) and product (CP) are calculated from the total, charge-state normalized abundances of the gas-phase ions corresponding to $^{Uni}P_{proxy}$ bound non-covalently to CS and CP ($Ab(^{Uni}P_{proxy}+CS)$ and $Ab(^{Uni}P_{proxy}+CP)$, respectively), measured by ESI-MS, and the known initial CS concentration ($[CS]_0$), eqs 3.9a and 3.9b:

$$[CP]=\frac{[CS]_0\, Ab(^{Uni}P_{proxy}+CP)}{Ab(^{Uni}P_{proxy}+CS)+Ab(^{Uni}P_{proxy}+CP)} \tag{3.9a}$$

$$[CS]=\frac{[CS]_0\, Ab(^{Uni}P_{proxy}+CS)}{Ab(^{Uni}P_{proxy}+CS)+Ab(^{Uni}P_{proxy}+CP)} \tag{3.9b}$$

3.2.5 Internal standard approach

Where indicated, CoMMon was implemented in the presence of isotopically labeled Neu5Ac (Neu5Ac-$^{13}C_3$), which served as an IS to quantify the time-dependent concentration of released (by neuraminidase) Neu5Ac. Based on the assumption that Neu5Ac and $^{13}C_3$-Neu5Ac have identical ESI-MS response factors, the time-dependent concentration of Neu5Ac is calculated from the total abundance ratio of Neu5Ac and $^{13}C_3$-Neu5Ac ions and the concentration of Neu5Ac-$^{13}C_3$ ([Neu5Ac-$^{13}C_3$]), eq 3.10:

$$[Neu5Ac]=\frac{[Neu5Ac\text{-}^{13}C_3](Ab(Neu5Ac)+Ab(Neu5Ac^{Na})+Ab(Neu5Ac^{P}))}{Ab(Neu5Ac\text{-}^{13}C_3)+Ab(Neu5Ac\text{-}^{13}C_3{}^{Na})+Ab(Neu5Ac\text{-}^{13}C_3{}^{P})} \tag{3.10}$$

where Ab(Neu5Ac), Ab(Neu5Ac^{Na}) and Ab(Neu5Ac^{P}) are the gas-phase abundances of protonated, sodiated and potassiated Neu5Ac ions, respectively, Ab(Neu5Ac-$^{13}C_3$), and Ab(Neu5Ac-$^{13}C_3{}^{Na}$) and Ab(Neu5Ac-$^{13}C_3{}^{P}$) are the gas-phase abundances of protonated, sodiated and potassiated Neu5Ac-$^{13}C_3$ ions.

3.2.6 Initial rates and relative initial rates

Where reported, the initial rate (v_0) of a given CAZyme substrate was determined from the best linear fit of the initial portion of the reaction progress curve (plot of the fractional abundance of product versus time). Unless otherwise noted, data acquired from 3 min to 6 min were used. These values were also used for the determination of the relative initial rate (v_{rel}) of glycoprotein substrates (GP) through comparison with the v_0 determined, simultaneously, for a CS, eq 3.11:

$$v_{rel} = \frac{v_{0,GP}}{v_{0,CS}} \tag{3.11}$$

where $v_{0,GP}$ and $v_{0,CS}$ is the initial rate of the GP and the CS, respectively.

3.2.7 Glycoprotein glycosylation

Human prostate specific antigen (PSA), which is produced by the prostate epithelial cells, contains a single *N*-glycosylation site (Asn45) occupied predominantly by bi-antennary complex *N*-glycans.[46,47] Human α-1 antitrypsin (α1AT), an acute phase protein, consists of two variants (M1 Val^{213} and M1 Ala^{213}), each with three *N*-glycosylation sites (Asn46, Asn83 and Asn247) occupied predominantly by bi-antennary and tri-antennary complex *N*-glycans.[48] Bovine fetuin (BF) contains three *N*-glycosylation sites (Asn99, Asn156 and Asn176) with bi-antennary and tri-antennary complex *N*-glycans and five possible *O*-glycosylation sites (Ser271, Thr280, Ser282, Ser296 and Ser341), which are predominantly mucin-type core 1 *O*-glycans.[35] Human α1- acid glycoprotein (AGP), an acute-phase protein found in plasma, consists of three proteoforms (F1, S and A), each possessing five *N*-glycosylation sites (Asn15, Asn38, Asn54, Asn75 and As85), predominantly occupied with complex bi-antennary, tri-antennary and minor content of tetra-antennary *N*-glycans.[33] Human haptoglobin 1-1 (Hp), also an acute-phase protein, is composed of a heavy β chain and a light α_1 chain and exists as a tetramer $(\alpha_1\beta)_2$ *in vivo*. It has four *N*-glycosylation sites for each $\alpha_1\beta$ dimer (Asn184, Asn207, Asn211 and Asn241), all located on its β

chain; dominated by bi-antennary, tri-antennary and tetra-antennary *N*-glycans.[49-51] Human plasma α2M, an acute-phase protein, was detected as both a tetramer with MW ~720 kDa and a dimer with MW ~360 kDa (Figure 3.19). α2M contains 8 *N*-glycosylation sites in each monomer subunit (Asn55, Asn70, Asn247, Asn396, Asn410, Asn869, Asn991 and Asn1424); the tetramer possesses 32 glycosylation sites.[52]

3.2.8 Neu5Ac content determination

To determine the average number of Neu5Ac contained in a given glycoprotein sample (N_{Neu5Ac}), the ESI mass spectrum measured for the substrate was deconvoluted using Thermo BioPharma Finder (v3.0) and MWs of the glycoforms determined. Based on the known amino acid sequence, the number of glycosylation sites and glycans composition (Glycoprotein glycosylation information section) and possible combination of HexNAc (N, 203.1925 Da), Hex (H, 162.1406 Da), Fuc (F, 146.1412 Da) and Sia (S, 291.2546 Da), the glycan composition of each glycoform was calculated. Annotation results and relative abundances of the glycoforms are shown below. Based on the number of Neu5Ac in each glycoform and relative abundance of glycoforms, the distribution of the number of Neu5Ac in each glycoprotein sample was calculated and plotted as a heat map (Figure 3.10).

N_{Neu5Ac} was also calculated from the difference between CoM_0 (starting point) and CoM_∞ (end point) after treating with NEUC, eq 3.12:

$$N_{\text{Neu5Ac}} = \frac{\left|\text{CoM}_0 - \text{CoM}_\infty\right|_n n}{291.25} \tag{3.12}$$

where $\left|\text{CoM}_0 - \text{CoM}_\infty\right|_n$ is the absolute difference between starting point and end point CoM for charge state *n*, 291.25 is the contribution of each Neu5Ac residue to the glycoprotein MW. The average Neu5Ac content determined by two procedures is given in Figure 3.5 and for AGP and PSA are consistent with available comparable results.[46,53]

3.2.9 Kinetics analysis

To analyze CAZyme kinetics of the glycoprotein substrates, the progress curves (fractional product abundance) were analyzed using a double exponential growth function, eq 3.13:

$$F_t = f_1(1 - e^{-k_1 t}) + f_2(1 - e^{-k_2 t}) \quad (3.13)$$

where F_t is the fractional product abundance, k_1 and k_2 are the apparent rate constants for the two distinct reactive forms and f_1 and f_2 represent their corresponding fractional abundances.

3.2.10 Analysis of *N*-glycan by HILIC-UHPLC-MS

Analysis of the *N*-glycans present in the glycoprotein substrates was performed by releasing the glycans enzymatically, isolating them as a mixture, labeling with 2-aminobenzamide (2-AB) and analyzing the mixiture by hydrophilic interaction-ultra high performance liquid chromatography (HILIC). Details of the sample preparation, experimental conditions and data analysis are described below.

***N*-glycan extraction.** *N*-glycans were released from the glycoprotein substrates using PNGase F (New England BioLabs, MA, USA) following the vendor's protocol. Briefly, denaturing buffer (0.5 % SDS, 40 mM DTT) was added to 15 µg of the protein followed by 10 min heating at 100 ºC. After cooling down on ice, GlycoBuffer 2 (sodium phosphate, 50 mM), NP-40 and PNGase F were added to the solution. The mixture was then incubated at 37 ºC for 24 h. Protein was separated from the released glycans by centrifuging at 14000 g for 10 min (5 times, 200 µL of MS grade water was added each time) using Amicon Ultra-0.5 mL centrifugal filters (EMD Millipore, Billerica, MA, USA) with 30 kDa MW cut off. The supernatant containing the glycans was collected, lyophilized and stored at -20 ºC until needed.

***N*-glycan labeling.** The extracted *N*-glycans were labeled with 2-aminobenzamide (2-AB) using reported procedures.[54,55] Briefly, the dried *N*-glycans were dissolved in the fluorophores solution (in DMSO:acettic acid 70:30 v/v) containing sodiumcyanoborohydride and 2-AB and incubated

at 65 ºC for 3.5 h. The solution was cooled down to room temperature and purified using the acetone precipitation method.[56] 950 µL of acetone was added to each 50 µL of the glycans solution with fluorophore, vortexed and centrifuged at 18000 g for 10 min. The supernatant was discarded. This process was repeated twice. The pellet was dried under a N_2 stream and reconstituted with 25 µL of acetonitrile-water (75:25 v/v) for HILIC analysis.

HILIC analysis. The 2-AB labeled glycans were analyzed by HILIC on a Thermo Scientific™ Vanquish™ UHPLC system coupled with fluorescent (FLD) detector (Thermo Scientific, Waltham, MA, USA) and ESI-MS (Thermo Q Exactive Orbittrap). Separation was carried out using a packed column (Waters, Glycan BEH Amide, 150x2.1 mm) filled with amide-bonded particles (size of 1.7 µm). Ammonium formate (100 mM, pH 4.5) and acetonitrile were used as mobile phases A and B. The flow rate was 0.2 mL/min with the following gradient: 0-46.5 min, 75-65% B; 46.5-80 min, 65-55% B; 80-104.6 min, 55-50% B. The column compartment temperature was 60ºC during the runs. The injection volume was 4 µL. For the fluorescent detection the excitation and detection wavelengths were at λ_{ex} = 330 and λ_{em} = 420 nm, respectively. The following parameters were used for MS detection: capillary temperature, 275 ºC; probe heater temperature, 250 ºC; sheath gas flow rate, 40 arb; aux gas flowrate,10 arb; spray voltage, 3.5 kV. The analyses were performed in positive acquisition mode with *m/z* range of 250-3000. The maximum injection time was 100 ms, the AGC target was set to 1E6. Mass spectra were acquired at 70000 resolution and each 10 microscans were combined to a single scan. MS spectra were recorded and processed using Xcalibur (Thermo, Version 4.1). Glycan identification was performed manually according to the MS data, the glycan composition were annotated using the GlycoWorkbench software (ver 2.1) and biosynthetic pathways of *N*-glycan.[57] The relative retention time (calculated as Glucose Unit) was used to assign the isomers.[58,59]

3.3 Results and Discussion

3.3.1 Validation of CoMMon using NEUC desialylation of glycoproteins

To test the reliability of CoMMon for monitoring the progress of CAZyme-catalyzed reactions, we first applied the method to measure the kinetics of NEUC-catalyzed cleavage of Neu5Ac from five glycoprotein substrates – prostate specific antigen (PSA), α1-antitrypsin (α1AT), bovine fetuin (BF), α1-acid glycoprotein (AGP), and haptoglobin (Hp). NEUC (NanI subtype secreted by *Clostridium perfringens*) is a non-specific exo-neuraminidase that cleaves α2-3, α2-6, and α2-8-linked Neu5A, albeit with a preference for α2-3-linked Neu5Ac.[60,61] Detailed glycosylation information for the five glycoproteins is described below.

Putative glycan compositions of the detected glycoforms for the five glycoprotein substrates used in here are assigned based on possible combinations of *N*-glycans (PSA, α1AT, AGP and Hp) or *N*- and *O*-glycans (BF), as given in Fig 3.4-3.8 and Table 3.1-3.5. Shown in Figure 3.9 are representative mass spectra acquired for the five glycoproteins, as well as their corresponding asialo-forms. The CoM of a given glycoprotein and its asialo-form represents the starting point (CoM_0) and end point (CoM_∞), respectively, for the NEUC-catalyzed reactionsThe Neu5Ac content of each glycoprotein sample is summarized in Figure 3.10a in the form of heat maps. According to the heat maps, Hp has the highest degree of sialylation (an average of ~19 Neu5Ac); AGP and BF exhibit a similar degree of sialylation (~13), followed by α1AT (~7) and PSA (~2).[46,53] Similar average degrees of sialylation were obtained by considering the differences in the measured CoM_0 and CoM_∞ values (Figures 3.10b and 3.10c).

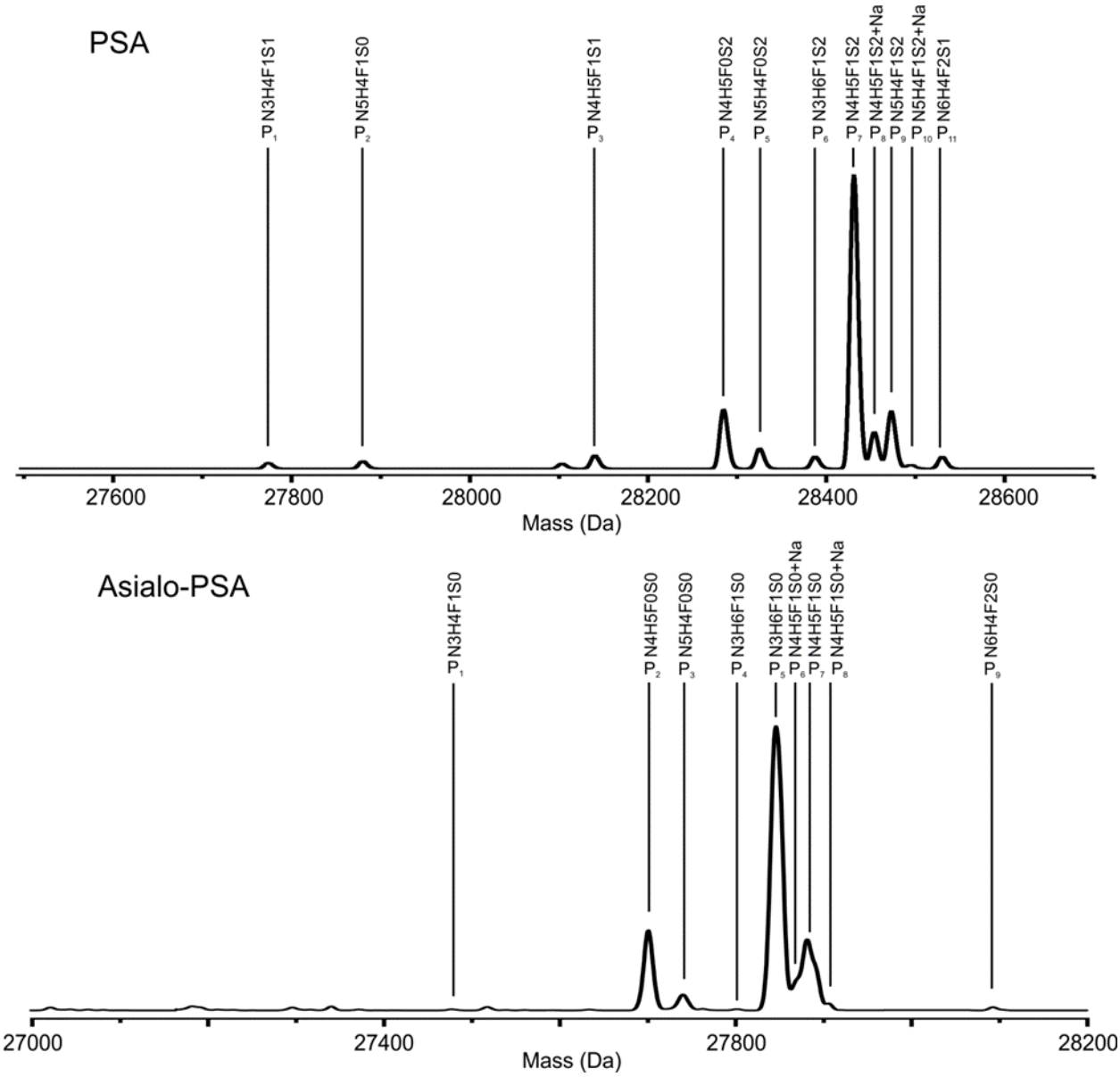

Figure 3.4. Deconvoluted mass spectra of PSA and asialo-PSA and the annotation of glycoforms. Symbols represent different type of the monosaccharides: N (HexNAc, 203.1925 Da), H (Hex, 162.1406 Da), F (Fuc, 146.1412 Da) and S (Sia, 291.2546 Da).

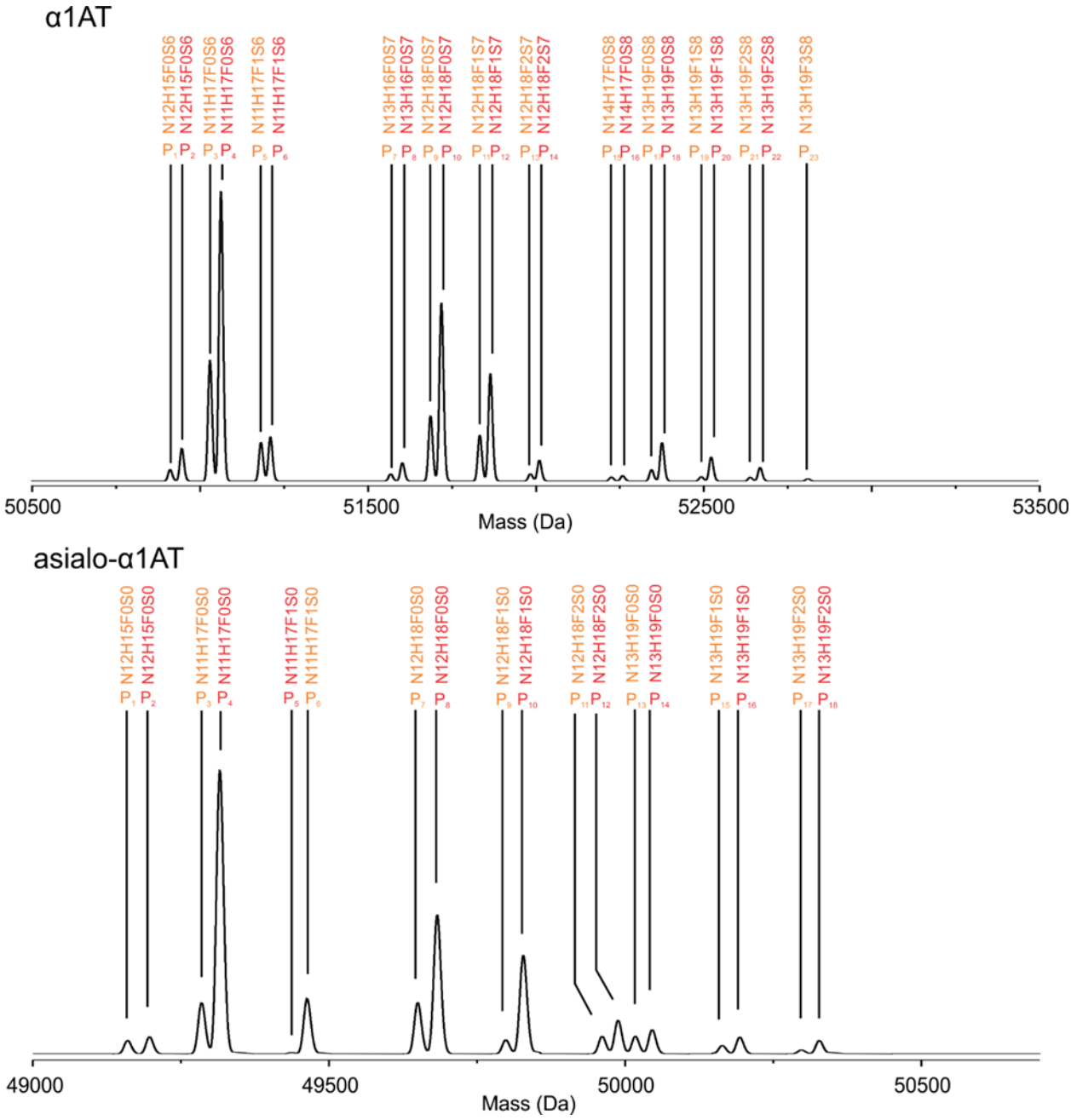

Figure 3.5. Deconvoluted mass spectra of α1AT and asialo-α1AT and the annotation of glycoforms. Annotation shown in different colors represent α1AT variant M1 Ala^{213} (orange) and variant M1 Val^{213} (red).

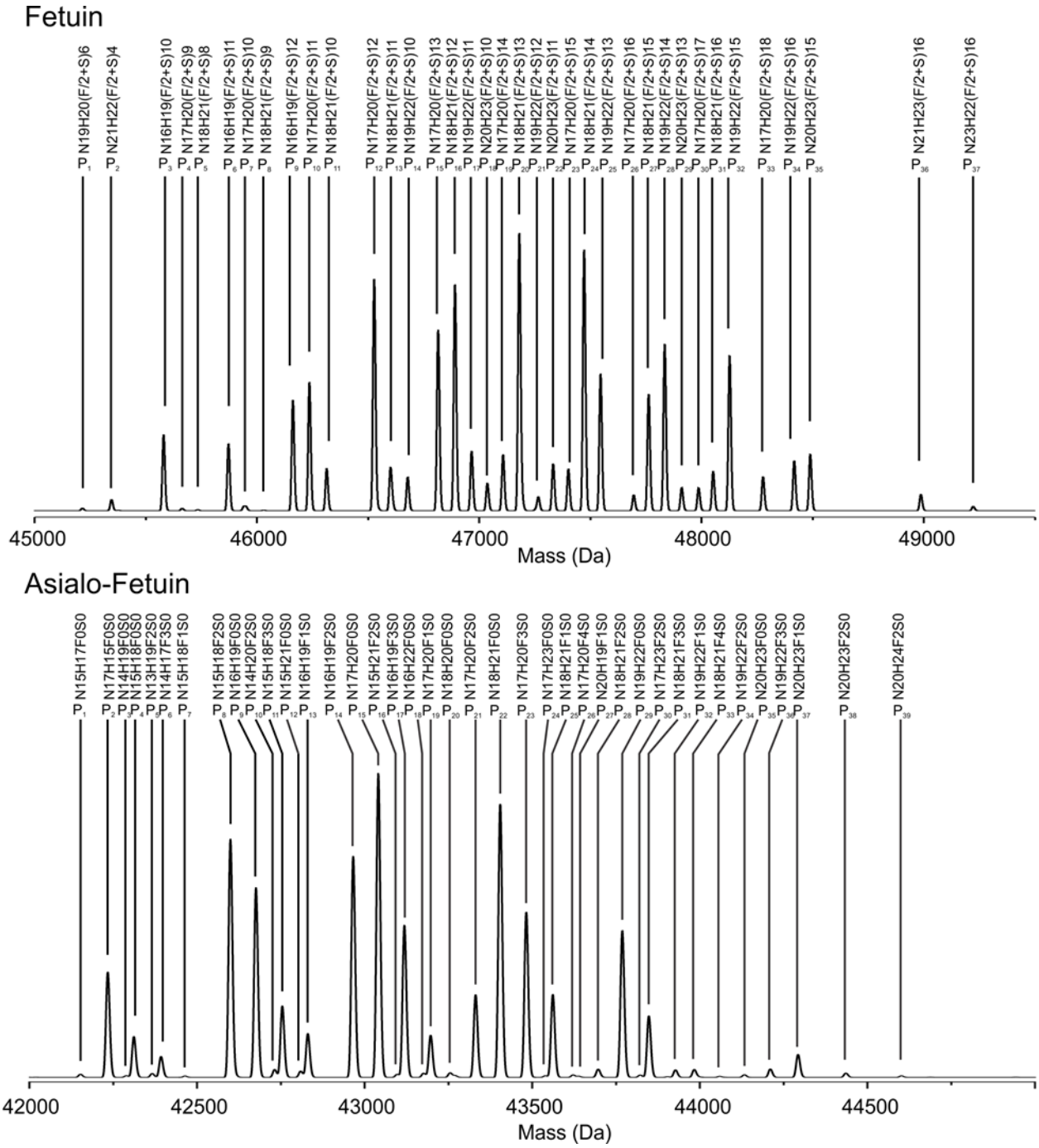

Figure 3.6. Deconvoluted mass spectra of BF and asialo-BF and the annotation of glycoforms.

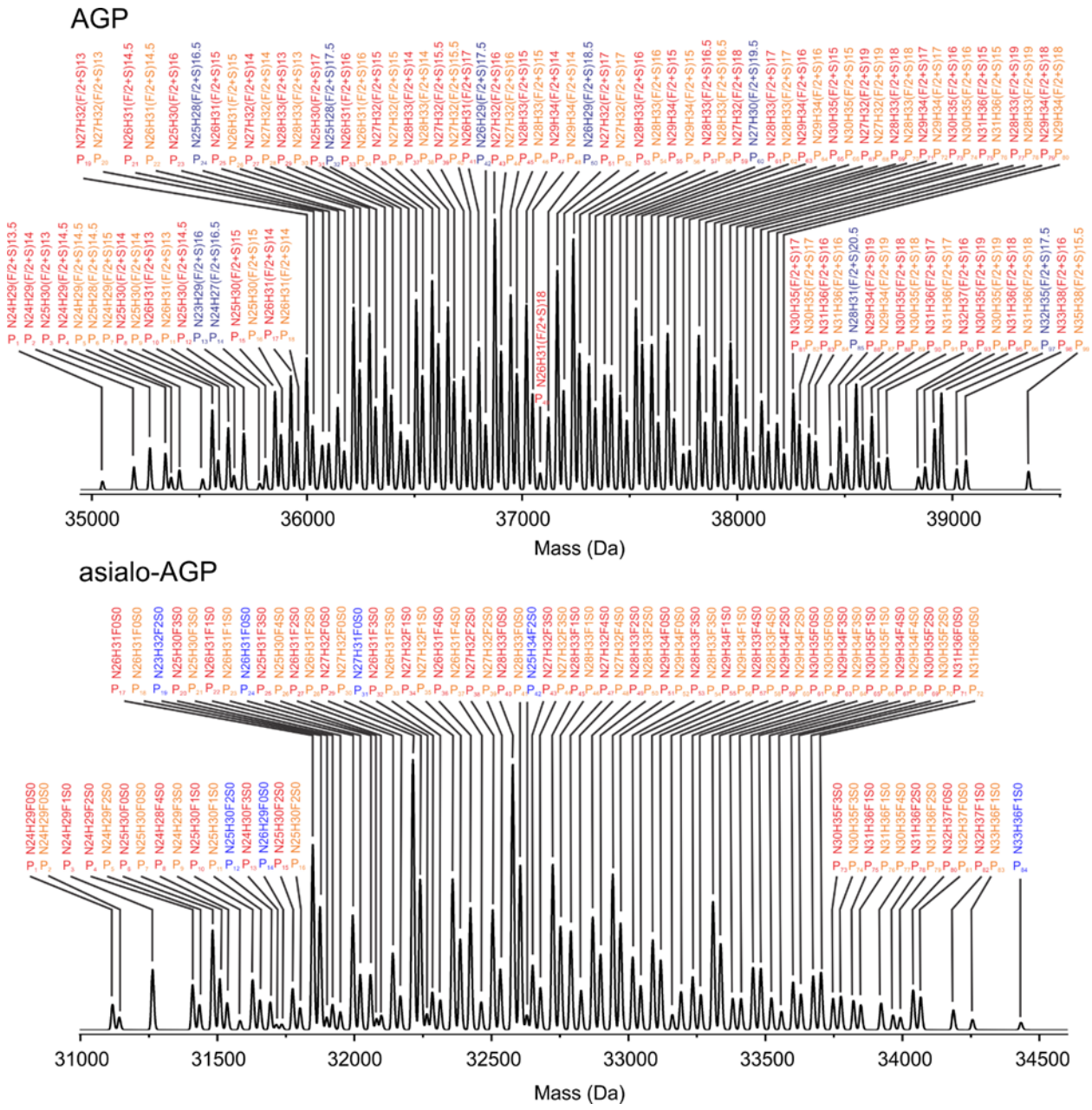

Figure 3.7. Deconvoluted mass spectra of AGP and asialo-AGP and the annotation of glycoforms. Different colors represent AGP F1 variant (red), AGP S variant (orange) and AGP A variant (blue).

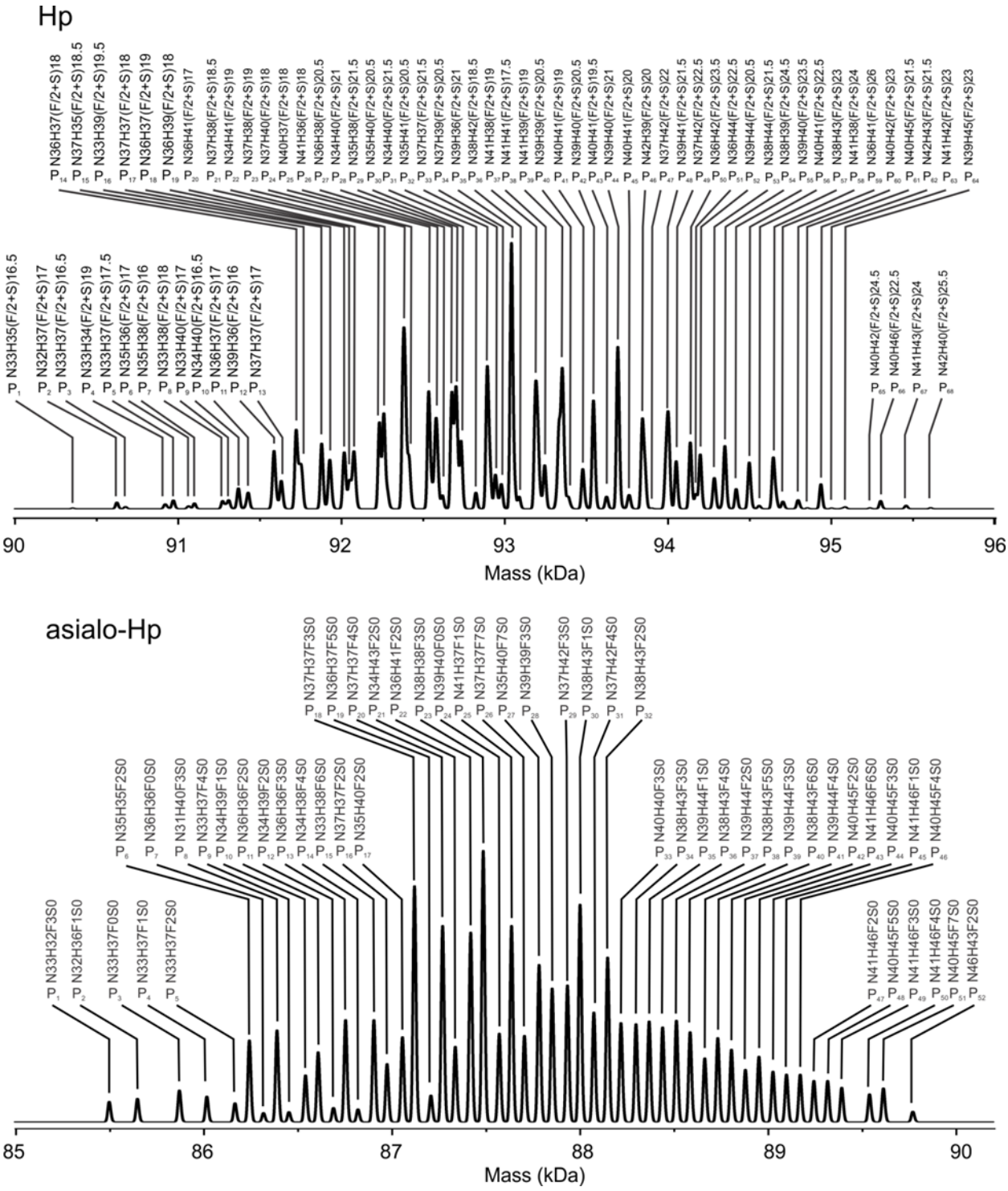

Figure 3.8. Deconvoluted mass spectra of Hp and asialo-Hp and the annotation for glycoforms.

P_x	Measured MW (Da)	Relative abundance (%)	Putative glycan composition N_H_F_S	Calculated MW (Da)
P1	27774.2	1.7	3_4_1_1	27773.4
P2	27887.1	2.4	5_4_1_0	27888.4
P3	28140.2	4.3	4_5_1_1	28138.5
P4	28284.8	20.0	4_5_0_2	28283.5
P5	28325.0	6.5	5_4_0_2	28324.6
P6	28388.0	3.9	3_6_1_2	28388.6
P7	28430.9	100.0	4_5_1_2	28429.6
P8	28472.4	19.5	5_4_1_2	28470.6
P9	28529.5	3.9	6_4_2_1	28528.7

Table 3.1. Putative glycan compositions, measured and theoretical molecular weights (MW) and relative abundances of the PSA glycoforms (P_x) identified by ESI-MS. Compositions are given as N_H_F_S: N (HexNAc, 203.0794 Da), H (Hex, 162.0528 Da), F (Fuc, 146.0579 Da) and S (Sia, 291.0954 Da).

P_x	Measured MW (Da)	Relative abundance (%)	Putative glycan composition N_H_F_S	Calculated MW (Da)
P1	50911.7	4.0	12_15_0_6	50910.1
P2	50940.6	11.2	12_15_0_6	50938.1
P3	51032.4	41.6	11_17_0_6	51033.2
P4	51062.1	100.0	11_17_0_6	51061.3
P5	51179.4	13.4	11_17_1_6	51179.3
P6	51208.7	15.2	11_17_1_6	51207.3
P7	51568.8	2.5	13_16_0_7	51566.3
P8	51595.5	6.2	13_16_0_7	51594.4
P9	51689.1	22.5	12_18_0_7	51689.5
P10	51717.5	61.5	12_18_0_7	51717.5
P11	51835.2	15.8	12_18_1_7	51835.5
P12	51862.2	37.1	12_18_1_7	51863.6
P13	51980.6	2.5	12_18_2_7	51981.6

P14	52010.3	7.2	12_18_2_7	52009.6
P15	52227.5	1.4	14_17_0_8	52222.5
P16	52254.0	1.8	14_17_0_8	52250.6
P17	52345.4	3.9	13_19_0_8	52345.7
P18	52373.4	13.3	13_19_0_8	52373.7
P19	52490.9	1.5	13_19_1_8	52491.7
P20	52523.0	8.3	13_19_1_8	52519.8
P21	52636.8	1.3	13_19_2_8	52637.8
P22	52665.5	4.7	13_19_2_8	52665.8
P23	52813.4	0.8	13_19_3_8	52811.9

Table 3.2. Putative glycan compositions, measured and theoretical molecular weights (MW) and relative abundances of the α1AT glycoforms (P_x) identified by ESI-MS. The M phenotype contains two variants: Ala^{213} (P_x shown in orange) and Val^{213} (P_x shown in red).[38] Compositions are given as N_H_F_S: N (HexNAc, 203.0794 Da), H (Hex, 162.0528 Da), F (Fuc, 146.0579 Da) and S (Sia, 291.0954 Da).

P_x	Measured MW (Da)	Relative abundance (%)	Putative glycan composition N_H_F/2+S	Calculated MW (Da)
P1	45199.9	0.1	19_20_6	45198.6
P2	45347.9	2.8	21_22_4	45346.6
P3	45589.2	27.1	16_19_10	45591.6
P4	45668.1	0.4	17_20_9	45665.7
P5	45738.4	0.04	18_21_8	45739.7
P6	45881.4	23.6	16_19_11	45882.7
P7	45959.2	1.5	17_20_10	45956.8
P8	46031.5	0.02	18_21_9	46030.8
P9	46169.8	39.3	16_19_12	46173.7
P10	46245.9	45.8	17_20_11	46247.9
P11	46325.3	14.9	18_21_10	46321.9
P12	46538.2	82.9	17_20_12	46539.0
P13	46613.1	14.9	18_21_11	46613.0

P14	46687.3	11.8	19_22_10	46687.0
P15	46830.4	64.7	17_20_13	46830.1
P16	46903.2	81.0	18_21_12	46904.1
P17	46981.6	21.0	19_22_11	46978.1
P18	47053.9	9.5	20_23_10	47052.2
P19	47121.3	19.9	17_20_14	47121.2
P20	47195.4	100	18_21_13	47195.2
P21	47271.1	4.9	19_22_12	47269.2
P22	47346.0	16.6	20_23_11	47343.3
P23	47409.3	14.6	17_20_15	47412.3
P24	47485.9	93.6	18_21_14	47486.3
P25	47561.5	48.8	19_22_13	47560.3
P26	47702.9	5.3	17_20_16	47703.4
P27	47778.9	41.7	18_21_15	47777.4
P28	47850.5	59.7	19_22_14	47851.4
P29	47925.1	7.7	20_23_13	47925.5

P30	47992.7	7.7	17_20_17	47994.4
P31	48069.3	13.4	18_21_16	48068.5
P32	48142.8	55.3	19_22_15	48142.5
P33	48282.4	12.1	17_20_18	48285.5
P34	48435.5	17.8	19_22_16	48433.6
P35	48509.4	19.9	20_23_15	48507.7
P36	49003.9	5.4	21_23_16	49001.8
P37	49242.1	1.2	22_23_16	49245.9

Table 3.3. Putative glycan compositions, measured and theoretical molecular weights (MW) and relative abundances of the BF glycoforms (P_x) identified by ESI-MS. Compositions are given as N_H_F_S: N (HexNAc, 203.0794 Da), H (Hex, 162.0528 Da), F (Fuc, 146.0579 Da) and S (Sia, 291.0954 Da).

P_x	Measured MW (Da)	Relative abundance (%)	Putative glycan composition N_H_F/2+S	Calculated MW (Da)
P1	35049.1	3.2	24_29_13.5	35047.7
P2	35195.2	8.5	24_29_14	35193.8
P3	35269.5	15.5	25_30_13	35266.8
P4	35341.5	13.5	24_29_14.5	35338.9
P5	35367.8	4.6	24_29_14.5	35367.0
P6	35406.5	7.3	25_28_14.5	35408.1
P7	35515.5	4.0	24_29_15	35513.1
P8	35560.2	29.5	25_30_14	35559.0
P9	35587.2	11.0	25_30_14	35587.1
P10	35634.2	22.9	26_31_13	35632.0
P11	35660.3	5.3	26_31_13	35661.1
P12	35706.7	21.0	25_30_14.5	35704.2
P13	35780.4	2.4	23_29_16	35782.9

P14	35808.4	9.0	24_27_16.5	35808.2
P15	35851.4	36.3	25_30_15	35849.3
P16	35879.0	20.4	25_30_15	35878.4
P17	35925.0	42.2	26_31_14	35923.3
P18	35953.0	17.8	26_31_14	35952.3
P19	35998.3	48.8	27_32_13	35997.3
P20	36025.9	23.7	27_32_13	36026.3
P21	36070.7	16.5	26_32_14.5	36069.4
P22	36100.6	17.1	26_32_14.5	36098.5
P23	36142.7	30.5	25_30_16	36140.5
P24	36172.9	14.4	25_28_16.5	36174.4
P25	36216.2	67.4	26_31_15	36214.5
P26	36244.4	44.4	26_31_15	36243.6
P27	36290.4	65.2	27_32_14	36288.5
P28	36318.1	30.7	27_32_14	36317.6
P29	36362.9	49.3	28_33_13	36362.5

P30	36391.3	34.9	28_33_13	36391.6
P31	36435.4	21.5	24_30_17	36431.8
P32	36465.9	18.3	25_28_17.5	36465.7
P33	36507.7	70.3	26_31_16	36505.8
P34	36536.2	42.2	26_31_16	36534.9
P35	36581.6	77.3	27_32_15	36579.8
P36	36609.9	54.0	27_32_15	36608.8
P37	36654.7	67.6	28_33_14	36653.8
P38	36682.9	40.1	28_33_14	36682.8
P39	36727.3	41.8	27_32_14.5	36725.9
P40	36756.6	25.9	27_32_14.5	36755.0
P41	36798.5	52.6	26_31_17	36797.0
P42	36829.8	24.1	26_29_17.5	36830.9
P43	36872.6	100.0	27_32_16	36871.0
P44	36901.5	51.2	27_32_16	36900.1

P45	36946.5	72.0	28_33_15	36945.0
P46	36975.1	43.0	28_33_15	36974.1
P47	37019.4	68.3	29_34_14	37020.0
P48	37047.8	35.4	29_34_14	37048.1
P49	37084.2	6.2	26_31_18	37088.3
P50	37122.5	26.9	26_29_18.5	37122.2
P51	37163.9	81.1	27_32_17	37162.3
P52	37193.0	36.7	27_32_17	37191.4
P53	37238.1	92.7	28_33_16	37236.3
P54	37266.7	50.5	28_33_16	37265.3
P55	37310.9	46.6	29_34_15	37310.3
P56	37340.1	30.3	29_34_15	37339.3
P57	37383.6	42.4	28_33_16.5	37382.4
P58	37414.2	42.4	28_33_16.5	37411.5
P59	37455.2	35.0	27_32_18	37453.5
P60	37486.7	25.7	27_32_18.5	37487.4

P61	37529.2	67.2	28_33_17	37527.5
P62	37558.5	53.7	28_33_17	37556.6
P63	37602.6	53.7	29_34_16	37601.5
P64	37632.7	24.9	29_34_16	37630.6
P65	37676.4	57.8	30_35_15	37675.5
P66	37705.3	26.3	30_35_15	37704.6
P67	37749.5	13.3	27_32_19	37744.8
P68	37778.5	14.6	27_32_19	37773.9
P69	37821.0	57.1	28_33_18	37818.8
P70	37850.8	25.0	28_33_18	37847.9
P71	37893.9	46.2	29_34_17	37892.8
P72	37923.6	25.4	29_34_17	37921.8
P73	37968.7	54.4	30_35_16	37966.8
P74	37997.2	38.7	30_35_16	37995.8
P75	38039.6	23.2	31_36_15	38040.7

P76	38072.5	12.6	31_36_15	38069.8
P77	38113.0	32.8	28_33_19	38110.0
P78	38143.9	21.5	28_33_19	38139.1
P79	38184.8	24.6	29_34_18	38184.0
P80	38217.0	13.4	29_34_18	38213.1
P81	38260.3	35.7	30_35_17	38258.0
P82	38288.6	24.3	30_35_17	38287.1
P83	38332.7	20.7	31_36_16	38332.0
P84	38363.9	17.9	31_36_16	38361.1
P85	38435.4	6.1	28_31_16	38435.2
P86	38476.1	23.2	29_34_19	38475.3
P87	38508.0	13.2	29_34_19	38504.4
P88	38552.5	39.1	30_35_18	38549.3
P89	38582.1	16.5	30_35_18	38578.3
P90	38625.1	27.1	31_36_17	38623.3

P91	38656.0	10.1	31_36_17	38652.3
P92	38698.2	11.9	32_37_16	38697.2
P93	38842.8	4.8	30_35_19	38840.5
P94	38873.9	8.5	30_35_19	38869.6
P95	38917.7	22.5	31_36_18	38914.5
P96	38949.4	35.8	31_36_18	38943.6
P97	39020.8	7.7	32_35_17.5	39021.4
P98	39064.1	10.9	33_38_16	39062.5
P99	39354.0	6.8	35_38_15.5	39351.8

Table 3.4. Putative glycan compositions, measured and theoretical molecular weights (MW) and relative abundances of the AGP glycoforms (P_x) identified by ESI-MS. AGP has three variant: F1 variant (Px shown in red), S variant (P_x shown in orange) and A variant (P_x shown in blue). Relative abundances of these three variants are approximately F1: S: A ≈ 70:25:5.[62] Compositions are given as N_H_F_S: N (HexNAc, 203.0794 Da), H (Hex, 162.0528 Da), F (Fuc, 146.0579 Da) and S (Sia, 291.0954 Da).

P_x	Measured MW (Da)	Relative abundance (%)	Putative glycan composition N_H_F/2+S	Calculated MW (Da)
P1	90353.8	0.3	33_35_16.5	90353.0
P2	90623.1	2.5	32_37_17	90620.1
P3	90676.5	0.8	33_37_16.5	90677.1
P4	90920.3	1.8	33_34_17	90920.2
P5	90970.0	3.3	33_37_17.5	90968.2
P6	91065.6	1.1	35_36_17	91066.2
P7	91099.0	2.1	35_38_16	91098.2
P8	91275.1	3.0	33_38_18	91276.3
P9	91308.9	3.4	33_40_17	91308.3
P10	91366.8	7.8	34_40_16.5	91365.3
P11	91429.9	6.2	36_37_17	91431.4
P12	91586.5	21.9	39_36_16	91586.4
P13	91633.2	10.6	37_37_17	91634.4

P14	91722.4	29.8	36_37_18	91722.4
P15	91748.5	17.1	37_35_18.5	91747.5
P16	91877.6	24.6	33_39_19.5	91875.5
P17	97927.2	18.5	37_37_18	91925.5
P18	92015.8	21.3	36_37_19	92014.6
P19	92048.6	11.1	36_39_18	92046.6
P20	92076.5	21.8	36_41_17	92078.5
P21	92232.5	32.6	37_38_18.5	92233.6
P22	92257.5	36.0	34_41_19	92256.6
P23	92381.2	68.3	37_38_19	92379.7
P24	92412.1	20.0	37_40_18	92411.7
P25	92534.3	44.3	40_37_18	92534.8
P26	92576.3	34.3	41_36_18	92575.8
P27	92615.9	5.2	36_38_20.5	92614.8
P28	92676.3	44.1	34_40_21	92677.8
P29	92701.5	46.2	35_38_21.5	92701.8

P30	92733.4	25.7	35_40_20.5	92734.8
P31	92823.0	6.1	34_40_21.5	92822.8
P32	92894.9	53.8	35_41_20.5	92895.8
P33	92944.7	12.9	37_37_21.5	92945.9
P34	92978.4	9.4	37_39_20.5	92977.9
P35	93042.0	100.0	39_36_21	93043.9
P36	93085.9	4.7	38_42_18.5	93084.9
P37	93190.5	48.4	41_38_19	93191.0
P38	93242.2	16.4	41_41_17.5	93240.0
P39	93351.8	53.1	41_39_19	93353.0
P40	93383.0	4.6	39_39_20.5	93384.0
P41	93476.5	15.0	40_41_19	93474.1
P42	93545.4	40.8	39_40_20.5	93546.1
P43	93621.5	4.7	40_41_19.5	93620.1
P44	93691.9	61.0	39_40_21	93692.2

P45	93764.4	5.3	40_41_20	93765.2
P46	93845.2	34.1	42_39_20	93846.2
P47	93899.5	0.3	37_42_22	93901.2
P48	93999.2	36.8	39_41_21.5	93999.2
P49	94049.1	18.0	37_42_22.5	94047.3
P50	94135.8	25.0	36_42_23.5	94135.3
P51	94168.8	5.7	36_44_22.5	94167.3
P52	94194.6	20.5	39_44_20.5	94193.3
P53	94283.1	11.7	38_44_21.5	94281.3
P54	94347.1	23.7	38_39_24.5	94345.3
P55	94417.9	7.5	39_40_23.5	94419.4
P56	94494.1	17.5	40_41_22.5	94492.4
P57	94557.0	1.3	38_43_23	94556.4
P58	94645.4	19.4	41_38_24	94646.5
P59	94702.6	2.8	36_41_26	94700.4
P60	94798.4	3.4	40_42_23	94800.5

P61	94851.7	0.3	40_45_21.5	94849.5
P62	94935.1	9.3	42_43_21.5	94932.6
P63	95001.9	0.3	41_42_23	95002.6
P64	95084.4	0.7	39_45_23	95082.6
P65	95236.6	0.3	40_42_24.5	95237.7
P66	95302.0	3.0	40_46_22.5	95302.7
P67	95457.1	1.3	41_43_24	95455.7
P68	95608.9	0.4	42_40_25.5	95610.8

Table 3.5. Putative glycan compositions, measured and theoretical molecular weights (MWs) and relative abundances of the Hp glycoforms (P_x) identified by ESI-MS.[63] Compositions are given as N_H_F_S: N (HexNAc, 203.0794 Da), H (Hex, 162.0528 Da), F (Fuc, 146.0579 Da) and S (Sia, 291.0954 Da).

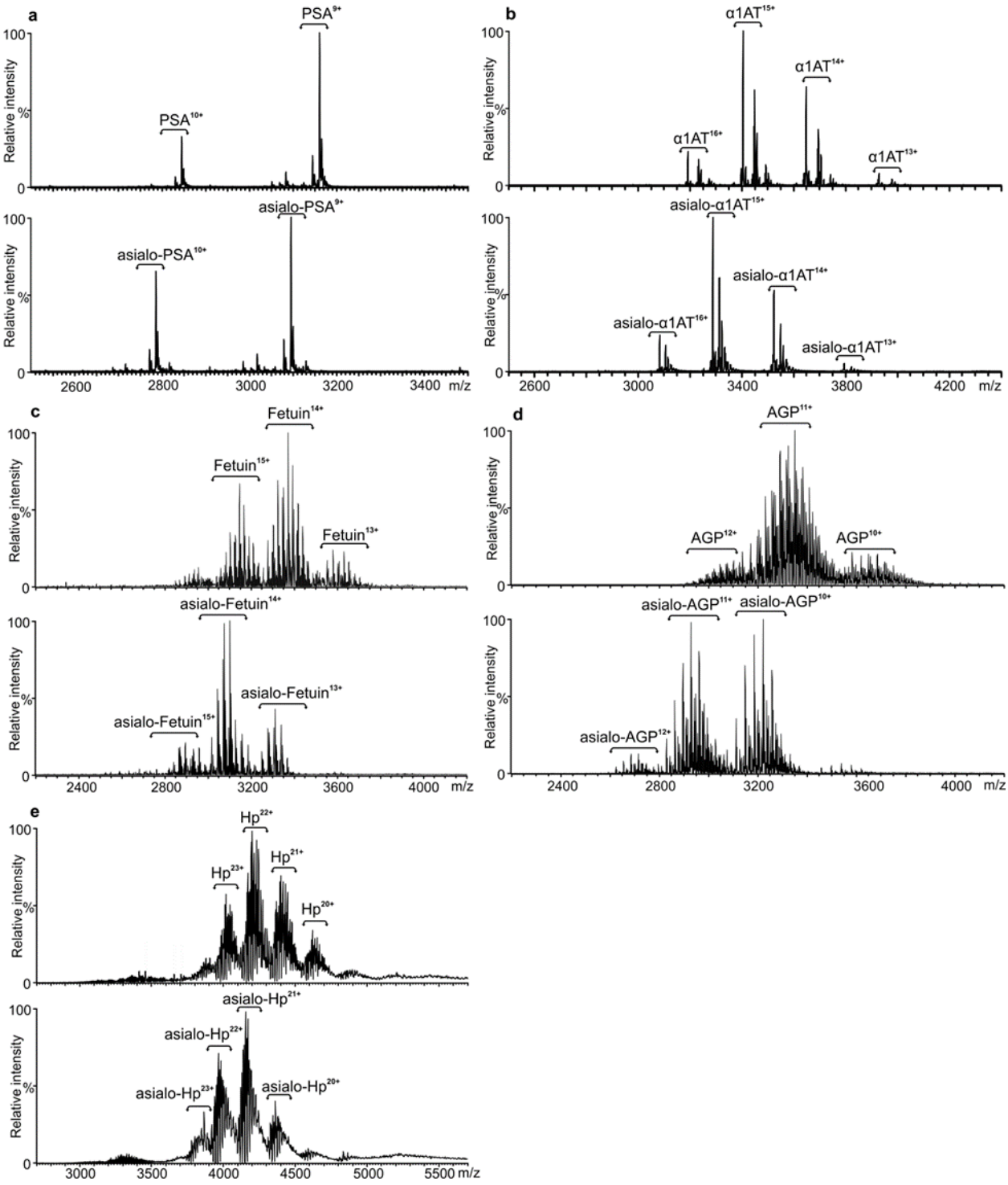

Figure 3.9. Representative ESI mass spectra acquired with the UHMR Orbitrap for aqueous ammonium acetate solutions (200 mM, pH 6.7 and 25 ºC) of (a) 5 μM PSA (top) and 5 μM asialo-PSA (bottom), (b) 5 μM α1AT (top) and 5 μM asialo-α1AT (bottom), (c) 5 μM bovine fetuin (top)

and 5 μM asialo-bovine fetuin (bottom), (d) 5 μM AGP (top) and 5 μM asialo-AGP (bottom), (e) 5 μM Hp (top) and 5 μM asialo-Hp (bottom). The asialo-glycoproteins were prepared by incubating the corresponding glycoproteins with NEUC for 2 days.

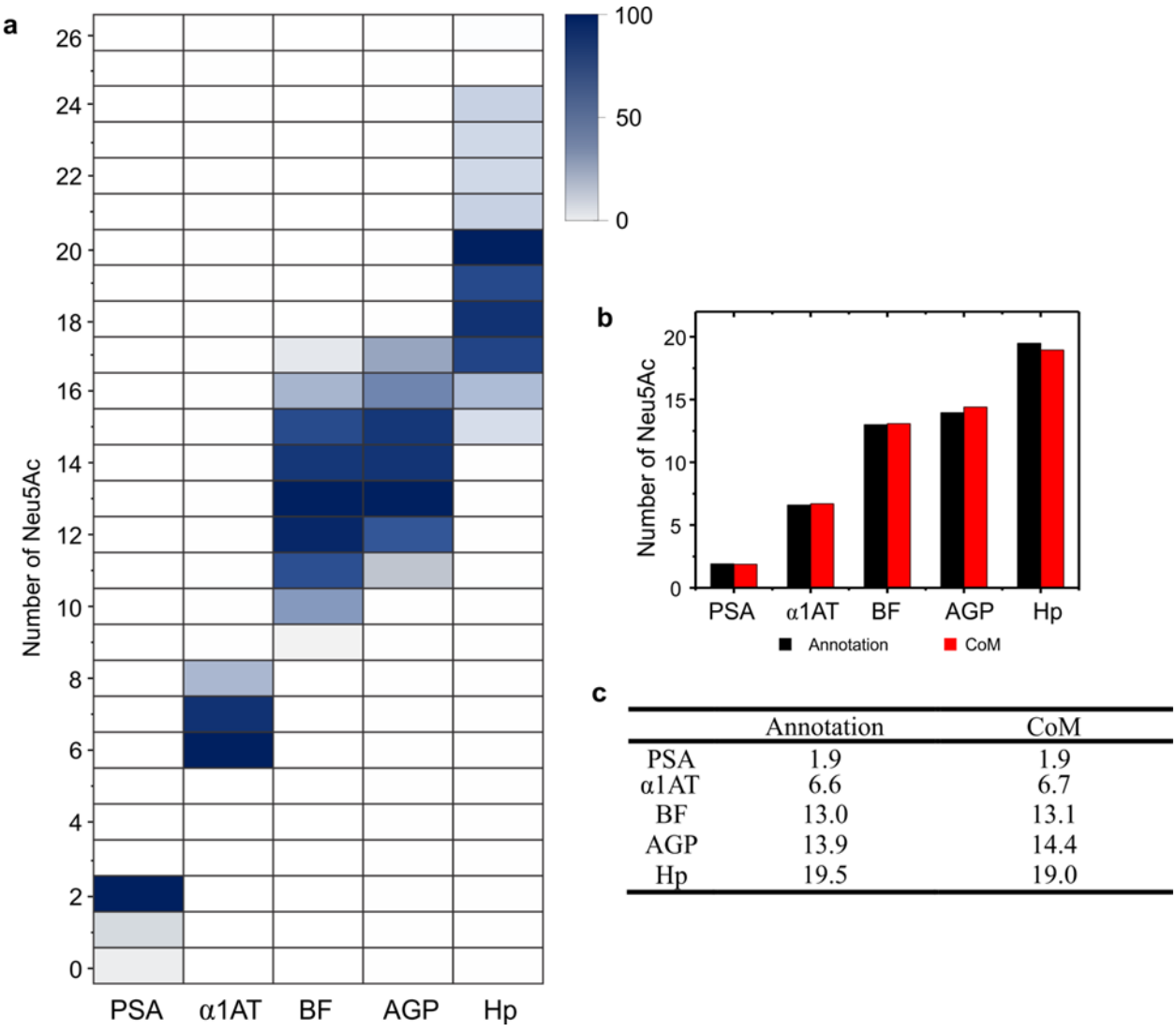

c

	Annotation	CoM
PSA	1.9	1.9
α1AT	6.6	6.7
BF	13.0	13.1
AGP	13.9	14.4
Hp	19.5	19.0

Figure 3.10. (a) Heat map representation of the distribution of the number of Neu5Ac residues in PSA, α1AT, BF, AGP and Hp. (b) Average number of Neu5Ac for each glycoprotein calculated by CoM and MS annotation. (c) Average number of Neu5Ac estimated from CoM and MS annotation.

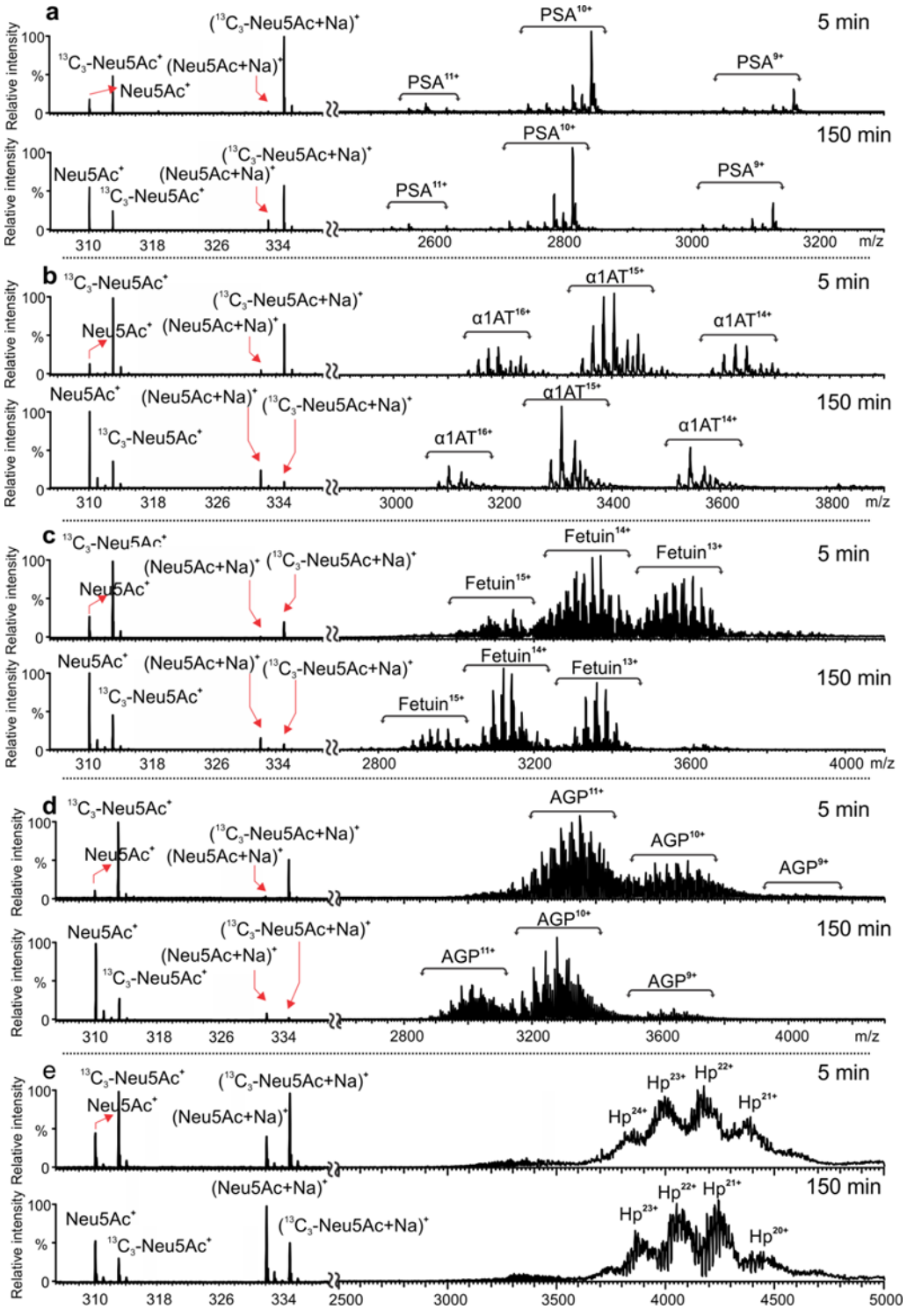

Figure 3.11. NEUC-catalyzed desialylation of glycoprotein substrates and validation by IS ($^{13}C_3$-Neu5Ac). Representative ESI mass spectra acquired with the Orbitrap for aqueous ammonium acetate solutions (200 mM, pH 6.7 and 25 °C) of NEUC (0.14 μM) and: (a) PSA (10 μM) and $^{13}C_3$-

Neu5Ac (10 μM), (b) α1AT (20 μM) and $^{13}C_3$-Neu5Ac (50 μM), (c) BF (15 μM) and $^{13}C_3$-Neu5Ac (50 μM), (d) AGP (15 μM) and $^{13}C_3$-Neu5Ac (50 μM), and (e) Hp (5 μM) and $^{13}C_3$-Neu5Ac (50 μM), measured at 5 min and 150 min reaction times.

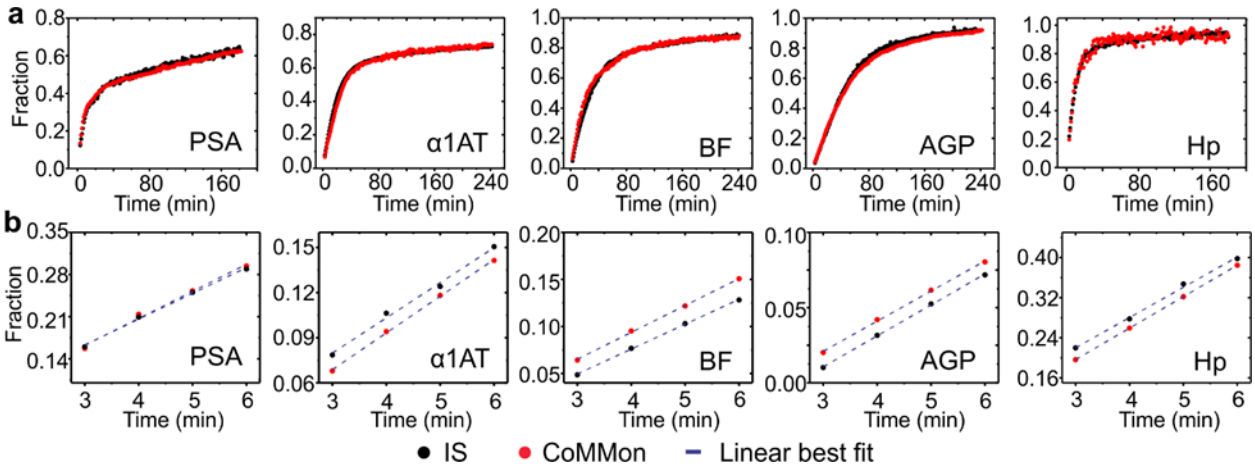

Figure 3.12. Comparison of kinetics of desialylation of glycoprotein substrates by NEUC measured by CoMMon and with an internal standard (IS). (a) Progress curves for PSA, α1AT, BF, AGP and Hp determined by CoMMon (red circles) and using $^{13}C_3$-Neu5Ac as an IS (black circles). Solution conditions are indicated in Figure 3.6. (b) Initial rates determined by linear fitting of progress curves shown in (a) from 3 min to 6 min reaction times.

The NEUC-catalyzed cleavage of Neu5Ac from each of the five glycoprotein substrates was continuously monitored by ESI-MS performed on aqueous ammonium acetate (200 mM, pH 6.7 and 25 ºC) of NEUC and PSA, α1AT, AGP, BF, or Hp at reaction times ranging from 3 min to 240 min (α1AT, BF and AGP) or 180 min (PSA and Hp). A known concentration of $^{13}C_3$-Neu5Ac, which served as an IS to monitor the concentration of Neu5Ac released from the glycoproteins, was added to each solution. Representative ESI mass spectra for each substrate, measured at reaction times of 5 min and 150 min, are shown in Figure 3.12. Over the course of the

reaction, a noticeable shift to lower *m/z* was observed for each glycoprotein, consistent with the loss of Neu5Ac residues. Also shown in Figure 3.12 are signals corresponding to protonated and sodiated ions of Neu5Ac and $^{13}C_3$-Neu5Ac. The relative abundances of the Neu5Ac ions increased with reaction time, consistent with the increasing concentration of free Neu5Ac in solution.

Substrate	Method	Initial rate (slope)[a]	Error (%)	NRMSD%
PSA	IS	0.037±0.002		
	CoMMon	0.035±0.001	4.4%	2.3%
α1AT	IS	0.023±0.001		
	CoMMon	0.023±0.001	3.6%	2.8%
BF	IS	0.028±0.001		
	CoMMon	0.029±0.002	2.5%	2.9%
AGP	IS	0.014±0.001		
	CoMMon	0.014±0.001	2.7%	2.3%
Hp	IS	0.060±0.003		
	CoMMon	0.063±0.001	4.0%	4.6%

a. errors correspond to one standard deviation

Table 3.6. NEUC-catalyzed desialylation of glycoprotein substrates. Initial rates were determined by linear fitting of the reaction progress curves (the first four data points, from 3 min to 6 min,) measured by IS and CoMMon. Errors correspond to one standard deviation. Error (%) was calculated by comparing initial rate found using CoMMon with initial rate found by IS. To determine the similarity of progress curves, the normalized root-mean-square deviation (NRMSD, %) was calculated for progress curves determined by CoMMon and IS.

Progress curves were constructed from the time-resolved ESI mass spectra acquired for the five glycoproteins using CoMMon (Figure 3.12a). Progress curves corresponding to the time-dependent concentration of free Neu5Ac were also calculated using the IS method, which is, arguably, the most reliable approach to measure reaction progress using ESI-MS (Figure 3.12a).

It can be seen that, for all substrates, there is excellent agreement between progress curves measured using CoMMon and with the IS, with a normalized root-mean-square deviation (NRMSD) of <5% (Table 3.6). Moreover, the initial rates obtained from the CoMMon- and IS-derived progress curves (Figure 3.12b) agree within 5% (Table 3.6). Together, these results indicate that CAZyme kinetics data for glycoprotein substrates extracted from time-resolved ESI-MS mass spectra using the CoMMon method are of comparable quality to data obtained using an IS. This new method, therefore, alleviates the requirement for internal standards, which are not always available and can be difficult to synthesize.

3.3.2 Glycoprotein specificity of NEUC

To quantitatively compare the reactivity of the five glycoproteins with NEUC, we simultaneously performed CoMMon and CUPRA-ZYME in aqueous ammonium acetate (200 mM, pH 6.7 and 25 ºC), using CS^{B}_{3SL} as a reference substrate to account for differences in NEUC activity. Shown in Figure 3.13a are representative ESI mass spectra for α1AT. Illustrative ESI mass spectra for the other glycoproteins and the corresponding progress curves are given in Figures 3.14 and 3.15.

Inspection of the normalized progress curves (Figure 3.13b) reveals a number of interesting features. First, all five glycoproteins exhibit higher initial rates than CS^{B}_{3SL} and the trend in relative (to CS^{B}_{3SL}) initial rates relative (Hp > BF > AGP > α1AT > PSA) qualitatively tracks with the average number of Neu5Ac residues present on each glycoprotein (Figures 3.13c, 3.13d and 3.15 and Table 3.7), although BF is an outlier. NEUC is known to have a sialic acid binding module, in addition to a catalytic domain, which recruits substrate.[64] The presence of the binding module likely accounts for the observed dependence of rate on the number of Neu5Ac.[64] The reason for the higher relative initial rate observed for BF (compared to AGP) is not known but may reflect the presence of sialylated *O*-glycans (dominated with 2-3 linked Neu5Ac), which are possibly

more preferred substrates than the sialylated *N*-glycans.[65] Interestingly, the slope of a linear fit of the initial rate data for each glycoprotein substrate versus their corresponding number of Neu5Ac is only ~0.2, suggesting that, generally, the Neu5Ac residues are partially shielded from NEUC. At present, the origin of this shielding effect is not known and requires further investigation. Possibly, it is due to steric effects associated with the local protein environment, which limit accessibility of the Neu5Ac residues to NEUC, *vide infra*.

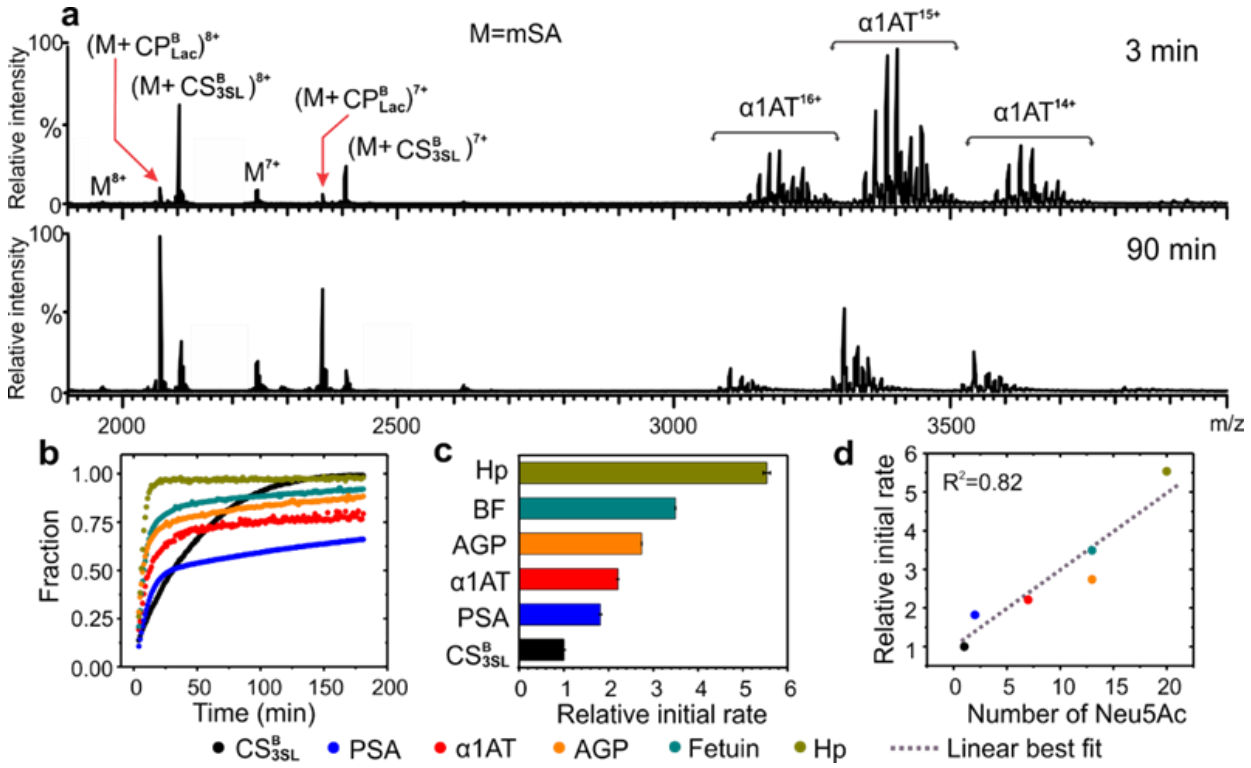

Figure 3.13. Comparison of kinetics of desialylation of CUPRA and glycoprotein substrates by NEUC measured by CUPRA-ZYME and CoMMon. (a) Representative ESI mass spectra, acquired with a UHMR Orbitrap mass spectrometer, for aqueous ammonium acetate (200 mM, pH 6.7 and 25 °C) containing NEUC (0.14 μM), α1AT (5 μM), mSA (5 μM) and CS^{B}_{3SL} (5 μM) measured at 3, 30 and 90 min reaction times. (b) Progress curves for α1AT (solution conditions same as in (a)) and PSA, BF, AGP and Hp (solution conditions given in Figures 3.14-3.15) determined by CoMMon. (c) Relative (to CS^{B}_{3SL}) initial rates determined by linear fitting of progress curves shown in (b) from 3 min to 6 min reaction times. (d) Relationship between Neu5Ac content for each glycoprotein and their relative initial rate.

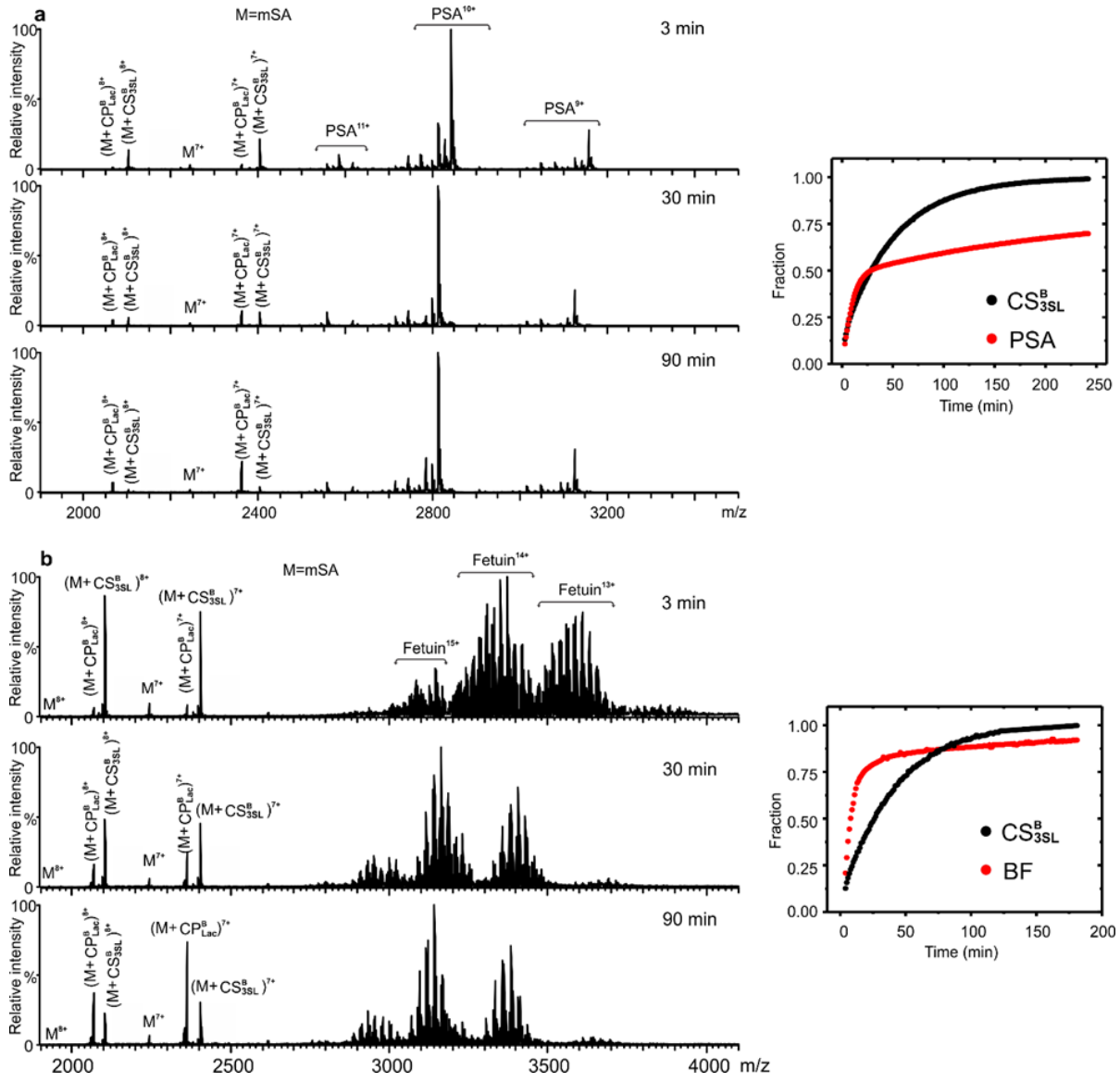

Figure 3.14. (a) Representative mass spectra acquired with the UHMR Orbitrap for aqueous ammonium acetate solutions (200 mM, pH 6.7 and 25 ºC) of NEUC (0.14 µM), PSA (5 µM), mSA (5 µM) and CS^{B}_{3SL} (5 µM) measured at 3 min, 30 min and 90 min. The progress curves measured for CS^{B}_{3SL} (black) and PSA (red) were shown in the right. (b) Representative mass spectra acquired by UHMR Orbitrap for aqueous ammonium acetate solutions (200 mM, pH 6.7 and 25 ºC) of NEUC (0.14 µM), BF (5 µM), mSA (5 µM) and CS^{B}_{3SL} (5 µM) measured at 3 min, 30 min and 90 min. The progress curves for CS^{B}_{3SL} (black) and BF (red) are shown on the right.

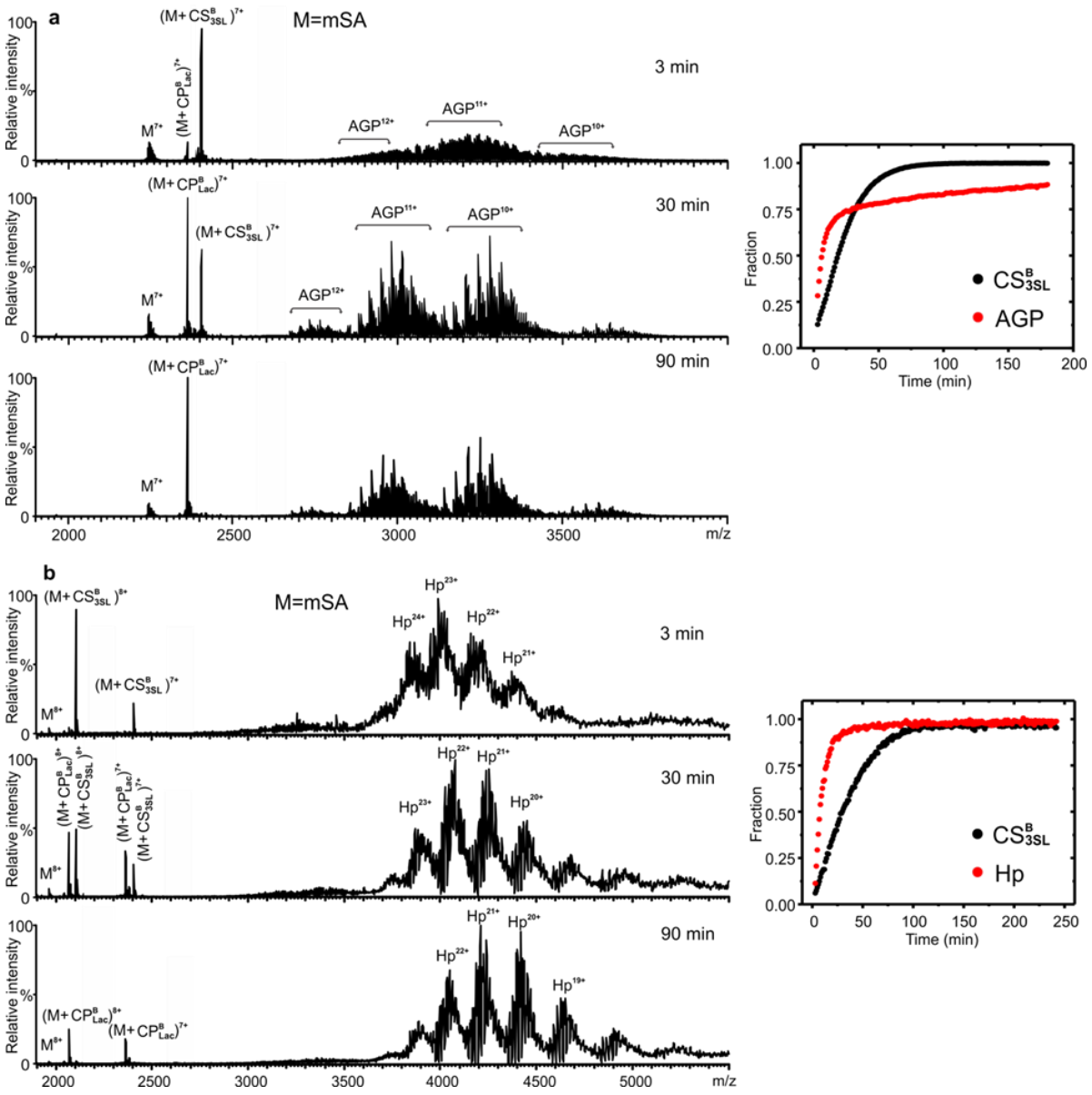

Figure 3.15. (a) Representative mass spectra acquired with the UHMR Orbitrap for aqueous ammonium acetate solutions (200 mM, pH 6.7 and 25 ºC) of NEUC (0.14 µM), AGP (5 µM), mSA (5 µM) and CS^{B}_{3SL} (5 µM) measured at 3 min, 30 min and 90 min. The progress curves for CS^{B}_{3SL} (black) and AGP (red) are shown are shown on the right. (b) Representative mass spectra acquired with the UHMR Orbitrap for aqueous ammonium acetate solutions (200 mM, pH 6.7 and 25 ºC) of NEUC (0.14 µM), Hp (5 µM), mSA (5 µM) and CS^{B}_{3SL} (5 µM) measured at 3 min, 30 min and 90 min. The progress curves for CS^{B}_{3SL} (black) and Hp (red) are shown on the right.

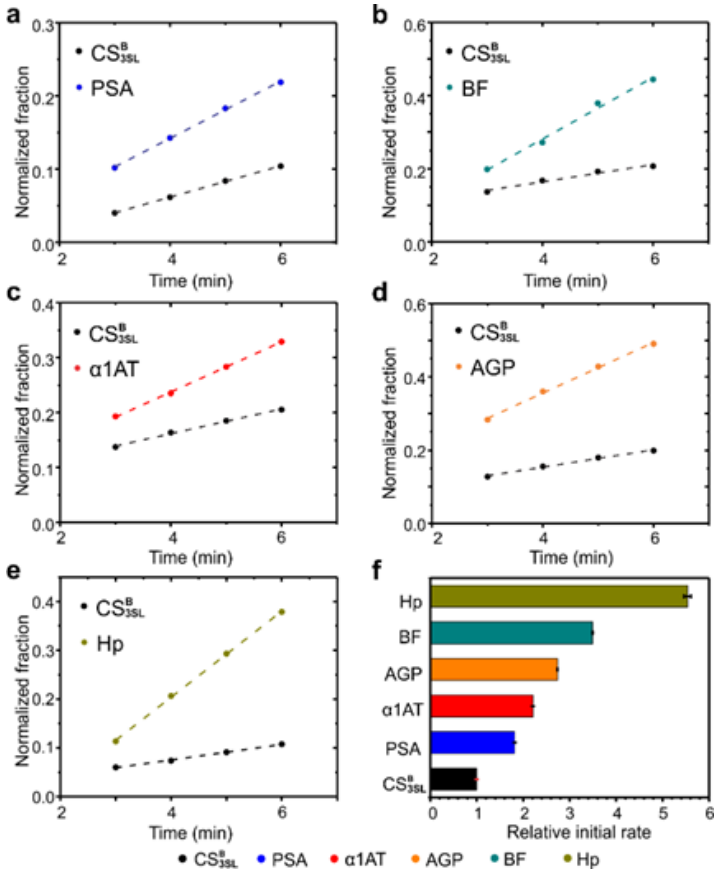

Figure 3.16. (a)-(e) Determination of initial rates by linear fitting for the first four data points (reaction time 3 min to 6 min) and (f) comparison of the normalized (to CS^{B}_{3SL}) relative initial rate values. Fitting results are given in Table 3.7.

Secondly, the overall appearance of the progress curves differs considerably among the five glycoproteins. However, all the substrates exhibit kinetics (Figure 3.17) that are reasonably described by a double exponential function (eq 3.13), albeit with significantly different rate constants (k_1 and k_2) and fractional abundances (f_1 and f_2, Table 3.8). Double exponential kinetics were previously observed for PSA treated with human neuraminidase 3 (NEU3).[31] One possible explanation for the observed kinetics is the different reactivity of α2-3- and α2-6-linked terminal Neu5Ac. However, analogous measurements performed on PSA prepared with all α2-3- or all α2-

6-linked Neu5Ac also revealed double exponential kinetics (Figure 3.18 and Table 3.9). These results rule out Neu5Ac linkage as the origin of this phenomenon and, instead, suggest that the double exponential kinetics observed for PSA arises from the different reactivity of Neu5Ac associated with the α1-3 and α1-6 branches of the biantennary *N*-glycans. It is also possible that such an explanation applies to tri- and tetra-antennary *N*-glycans, wherein the Neu5Ac associated with the α1-3 and α1-6 branches have distinct kinetics. However, it must be stressed that the suggestion that branch specificity is responsible for the double exponential kinetics is speculative and requires follow up investigations (by CoMMon) of additional glycoprotein substrates with known *N*-glycan compositions. It will also be important to test other neuraminidases to establish whether this is a general phenomenon.

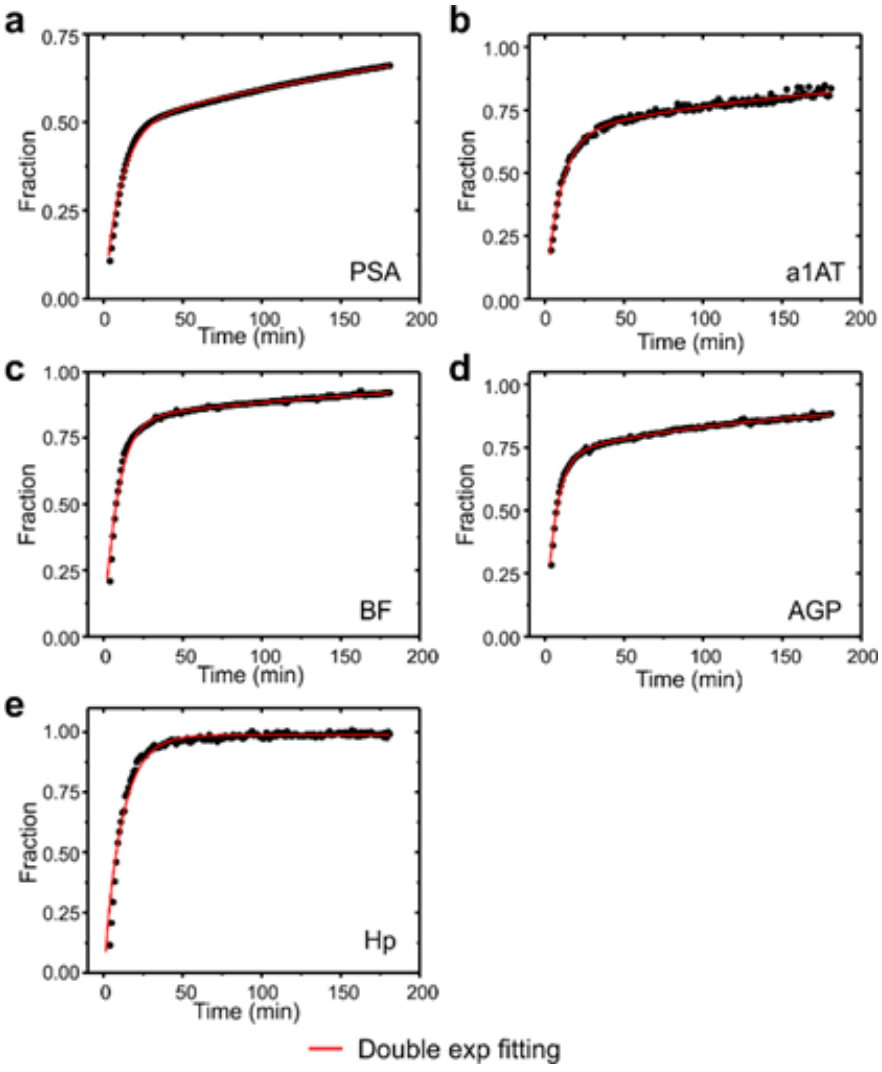

Figure 3.17. Best fits of double exponential function (eq 3.13) to the measured progress curves for NEUC-catalyzed reaction for each of five glycoprotein substrates, (a) PSA, (b) a1AT, (c) BF, (d) AGP and (e) Hp. Fitting results are given in Table 3.8.

Substrate	Initial rate (slope)	Relative initial rate (to CS^{B}_{3SL})
CS^{B}_{3SL}	0.021±0.001	1.00
PSA	0.038±0.010	1.82±0.05
CS^{B}_{3SL}	0.021±0.001	1.00
α1AT	0.046±0.001	2.21±0.03
CS^{B}_{3SL}	0.022±0.002	1.00
BF	0.078±0.005	3.49±0.24
CS^{B}_{3SL}	0.023±0.001	1.00
AGP	0.063±0.004	2.74±0.19
CS^{B}_{3SL}	0.016±0.001	1.00
Hp	0.088±0.001	5.54±0.08

a. Errors correspond to one standard deviation.

Table 3.7. Initial rates and relative initial rates of NEUC-catalyzed desialylation of glycoprotein and CS^{B}_{3SL} substrates. Initial rates were determined by linear fitting of the reaction progress curves (the first four data points, from 3 min to 6 min). Errors correspond to one standard deviation. The normalized relative initial rates correspond to the relative initial rates, normalized to the initial rate measured for CS^{B}_{3SL}.[a]

Substrate	k_1	f_1	k_2	f_2
PSA	0.09±0.01	0.49±0.01	0.002±0.02	0.50±0.02
α1AT	0.10±0.01	0.66±0.01	0.004±0.01	0.29±0.04
BF	0.12±0.01	0.82±0.01	0.004±0.001	0.19±0.01
AGP	0.15±0.01	0.73±0.01	0.007±0.001	0.24±0.01
Hp	0.17±0.01	0.97±0.01	0.002±0.001	0.05±0.01

a. Errors correspond to one standard deviation.

Table 3.8. Kinetics of NEUC-catalyzed desialylation of glycoprotein substrates. Rate constants (k_1 and k_2) and fractional abundances (f_1 and f_2) were obtained from the best fit of a double exponential function (eq 3.13) to the measured progress curves.[a]

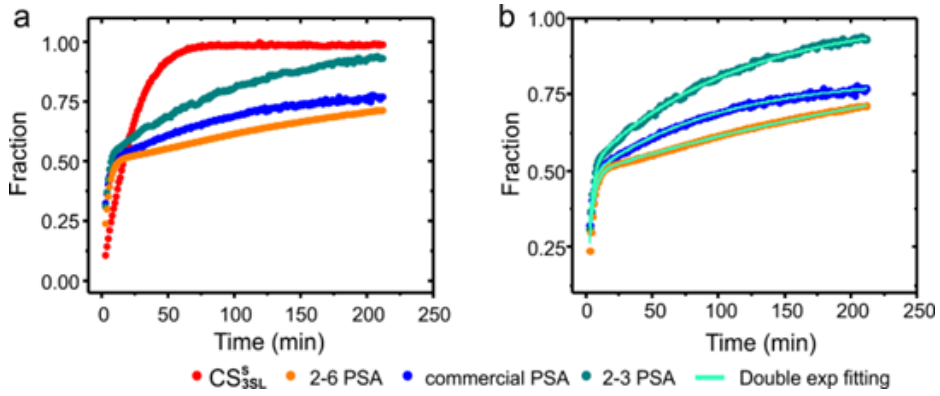

Figure 3.18. (a) NEUC-catalyzed progress curves for 2-3 PSA (contains only α2-3 Neu5Ac), commercial PSA (contains a mixture of α2-3 and α2-6 Neu5Ac) and 2-6 PSA (contains only α2-6 Neu5Ac). CUPRA substrates CS^{S}_{3SL} were used as reference. (b) Best fits of double exponential function (eq 3.13) to the measured progress curves. Fitting results are given in Table 3.9.

Substrate	k_1	f_1	k_2	f_2
2-3 PSA	0.32±0.001	0.51±0.01	0.02±0.01	0.50±0.01
PSA	0.34±0.01	0.48±0.01	0.01±0.01	0.49±0.01
2-6 PSA	0.29±0.01	0.49±0.01	0.003±0.001	0.50±0.02

a. Errors correspond to one standard deviation.

Table 3.9. Kinetics of NEUC-catalyzed desialylation of 2-3 PSA (contains only α2-3 Neu5Ac), commercial PSA (contains both α2-3 and α2-6 Neu5Ac) and 2-6 PSA (contains only α2-6 Neu5Ac). Rate constants (k_1 and k_2) and fractional abundances (f_1 and f_2) were obtained from the best fit of a double exponential function (eq 3.13) to the measured progress curves.[a]

3.3.3 Application of CoMMon to large glycoprotein substrates

To demonstrate the ability of CoMMon to measure CAZyme kinetics for large glycoprotein substrates, for which individual species (glycan compositions) cannot be resolved by ESI-MS, we applied the method to the NEUC-catalyzed desialylation of alpha-2-macroglobulin (α2M). Human

α2M, an acute-phase protein that acts as proteinase inhibitor, exists predominantly as a tetramer (MW ~720 kDa) at neutral pH; each α2M monomer possesses 8 *N*-glycosylation sites consisting predominantly of bi- and tri- antennary complex type *N*-glycans.[66] Representative ESI mass spectra for α2M and asialo-α2M are shown in Figure 3.19; mass spectra acquired at reaction times of 5 and 150 min are shown in Figure 3.20a. Notably, the optimal instrumental parameters required to detect the α2M tetramer were not ideal for the detection of free Neu5Ac and the associated IS ions. As a result, it was not possible (with the current instrumentation) to apply CoMMon to the α2M tetramer and, simultaneously, monitor the free Neu5Ac released. Instead, CUPRA-ZYME, using CS^{S}_{3SL}, was performed together with CoMM on to assess relative reactivity.

Comparison of the resulting progress curves and initial rates for tetrameric α2M and CS^{S}_{3SL} (Figure 3.20c) reveals that, despite possessing approximately 65 reactive Neu5Ac residues (calculated from the difference in CoM_0 and CoM_∞ values), α2M is a slightly poorer substrate than CS^{S}_{3SL}. This finding suggests significant shielding of the Neu5Ac residues in tetrameric α2M, which is qualitatively consistent with the results obtained for the other glycoproteins tested. Indeed, inspection of the available crystal structure of deglycosylated human α2M[67] (PDB: 4ACQ) shows that all but one (N869) of the *N*-glycosylation sites are located in close proximity of subunit-subunit interfaces (Figure 3.21), which could limit their accessibility to NEUC. To test whether the slow relative kinetics of α2M result from protein shielding of the Neu5Ac residues, we reduced the α2M sample by treatment with DTT (to cleave the disulfide bonds) and then incubated with IAA (to bind with the free sulfhydryl to prevent the reformation of disulfide bonds) with the goal of making the *N*-glycans more accessible to NEUC. ESI-MS analysis of the resulting sample revealed the presence of both monomeric and dimeric α2M (Figure 3.22); ESI mass spectra acquired for the corresponding asialo-glycoforms are also shown. Representative ESI mass spectra

of the monomeric and dimeric α2M, measured after 5 min and 150 min treatment with NEUC are shown in Figure 3.20b and corresponding progress curves are shown in Figure 3.20d. Notably, inspection of progress curves reveals that monomeric and dimeric α2M are more reactive than tetrameric α2M, with relative initial rates that are ~3.5 and ~1.6 times higher, respectively. The greater reactivity of the monomer and dimer provides support for the hypothesis of widespread Neu5Ac shielding in tetrameric α2M.

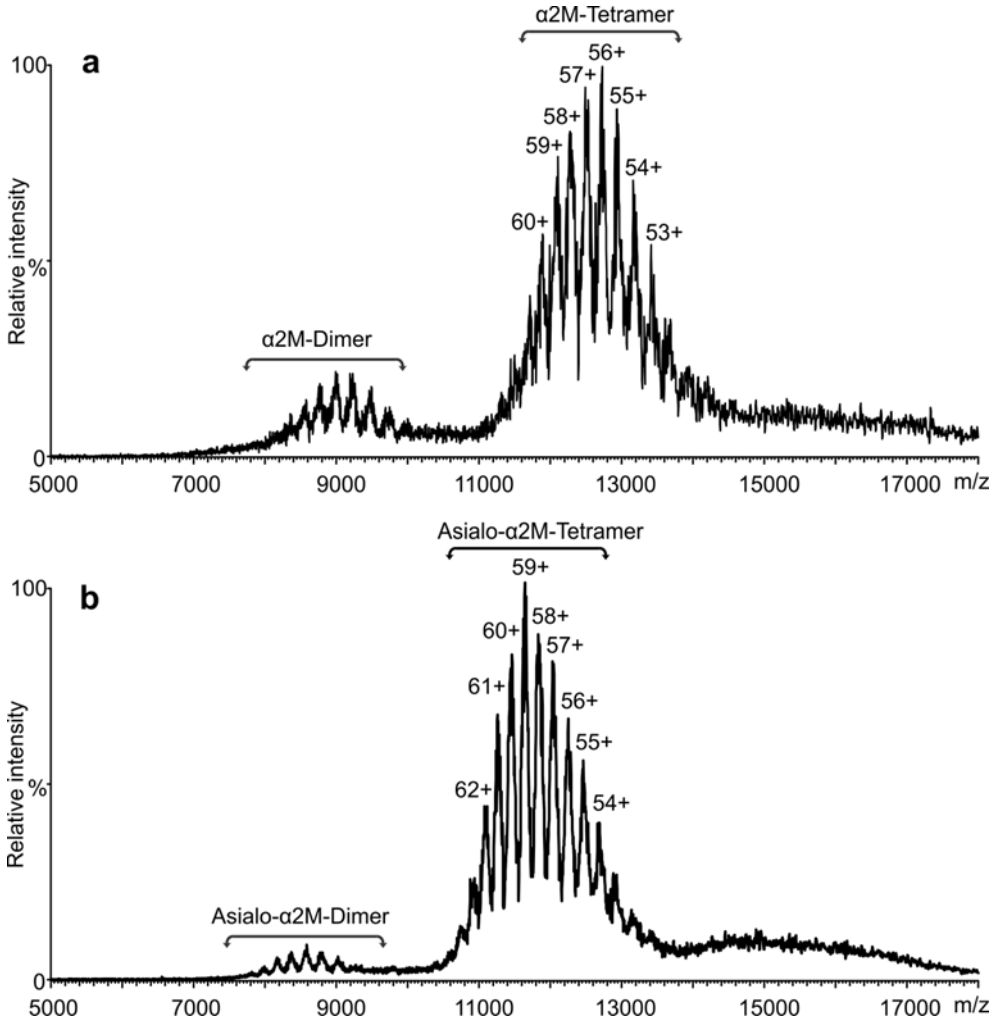

Figure 3.19. Representative ESI mass spectra acquired with the UHMR Orbitrap for aqueous ammonium acetate solutions (200 mM, pH 6.7 and 25 ºC) of (a) 5 μM α2M and (b) 5 μM asialo-α2M (prepared by incubating α2M with NEUC for 2 d).

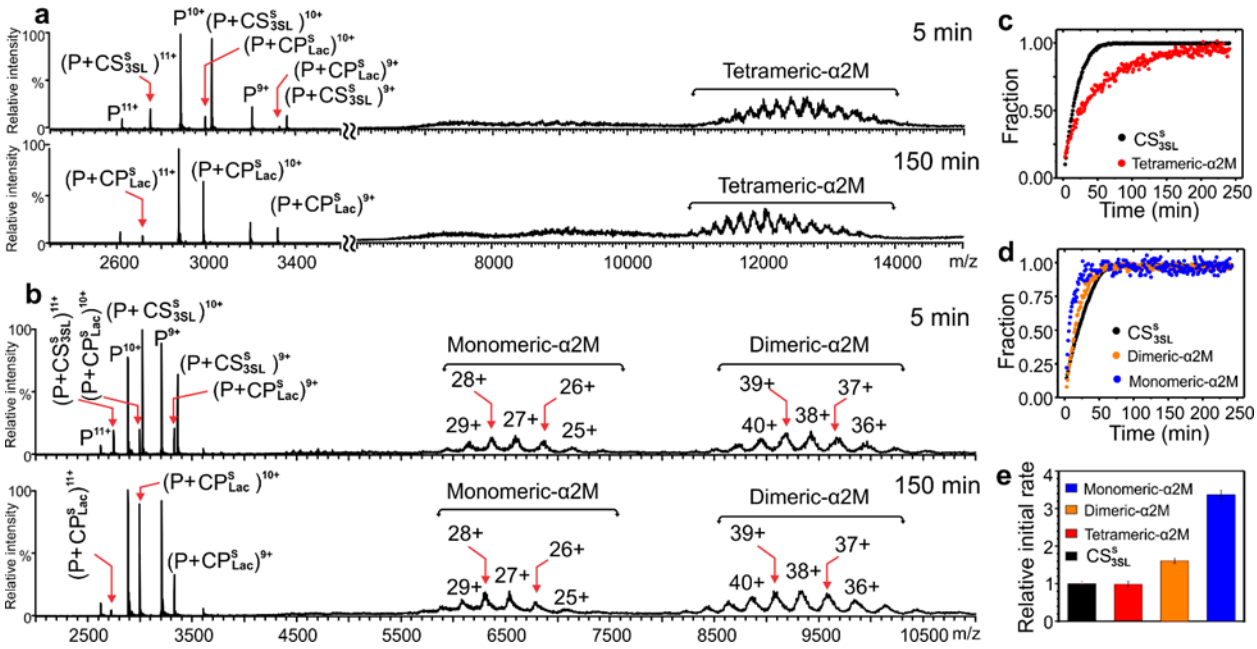

Figure 3.20. Kinetics of desialylation of monomeric, dimeric and tetrameric α2M by NEUC measured by CoMMon. Representative mass spectra, acquired with a UHMR Orbitrap mass spectrometer, for aqueous ammonium acetate (200 mM, pH 6.7 and 25 °C) containing NEUC (0.14 μM), hCA (5 μM), CS^{S}_{3SL} (5 μM) and: (a) tetrameric α2M (5 μM), (b) monomeric and dimeric α2M mixture (10 μM in total), measured at 5 and 150 min reaction times. (c) Progress curves for tetrameric α2M and CS^{S}_{3SL}. (d) Progress curves for monomeric, dimeric α2M and CS^{S}_{3SL}. (e) Relative initial rates (to CS^{B}_{3SL}) of monomeric, dimeric and tetrameric α2M.

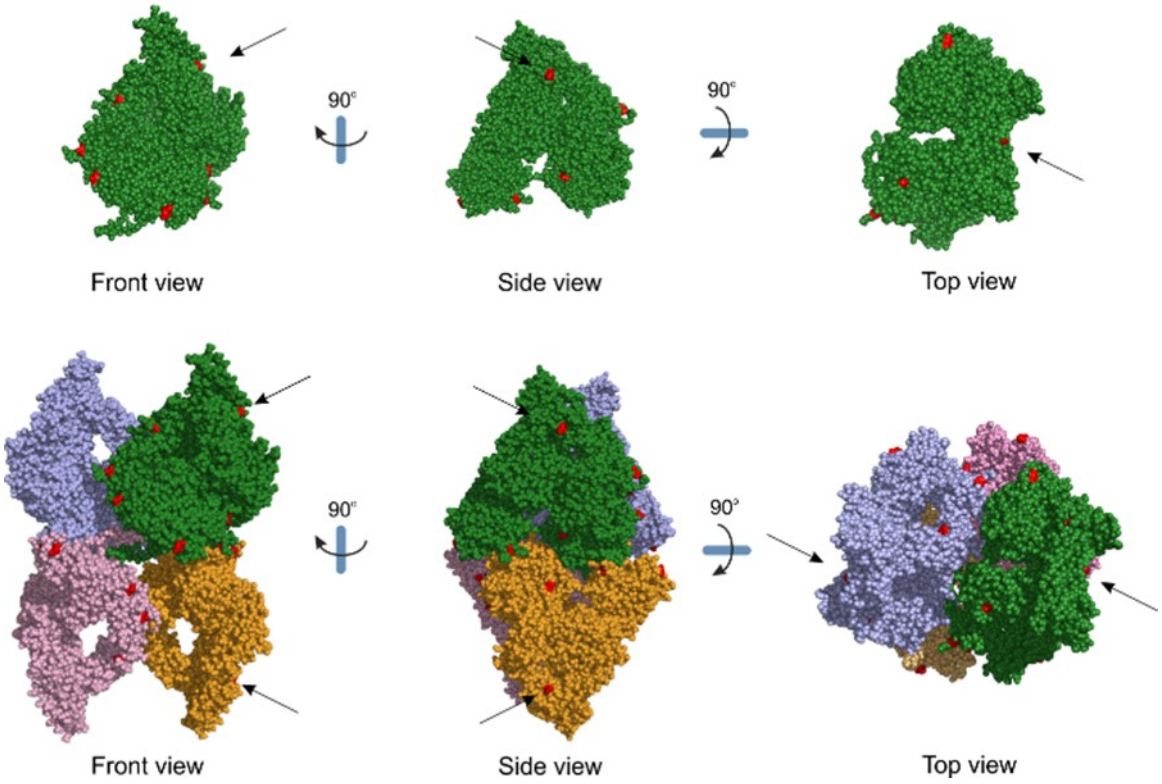

Figure 3.21. Structure of monomeric α2M (top) and tetrameric α2M (bottom) shown in front view (left), side view (middle) and top view (right, PDB: 4ACQ). Monomer subunits are shown in different colors and all glycosylation sites are shown in red. With the exception of N869 (indicated with arrow), all glycosylation sites are close to the subunit-subunit interface.

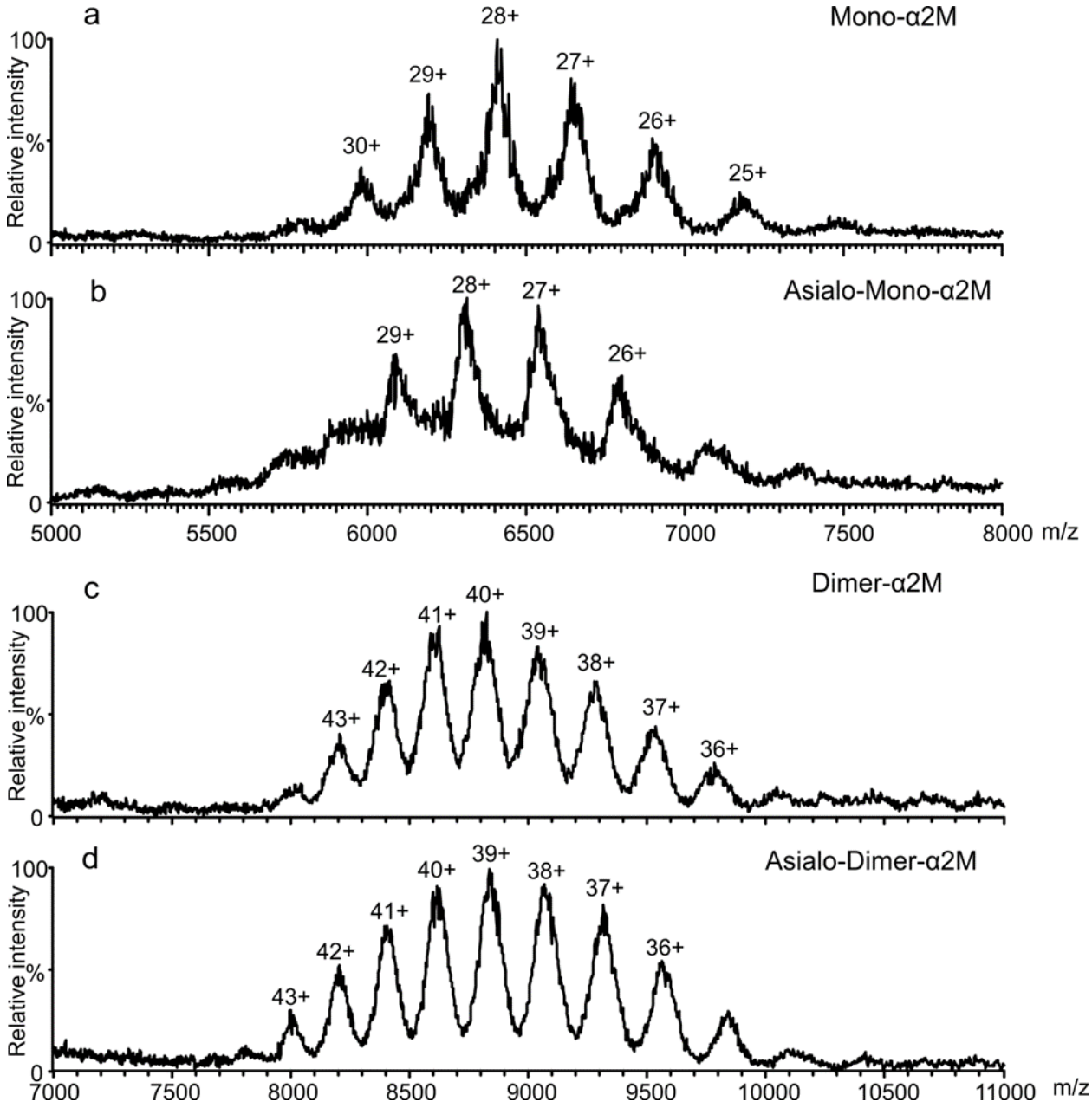

Figure 3.22. Representative ESI mass spectra acquired with the UHMR Orbitrap for aqueous ammonium acetate solutions (200 mM, pH 6.7 and 25 ºC) of (a) 5 µM monomeric α2M, (b) 5 µM asialo-monomeric α2M, (c) 5 µM dimer α2M, (d) 5 µM asialo-dimer α2M (asialo-forms prepared by incubating mono/dimer-α2M mixture with NEUC for 2 d).

3.3.4 Application of CoMMon to ST6Gal1

To demonstrate the applicability of CoMMon for monitoring the kinetics of GT reactions, the transfer Neu5Ac from the CMP-Neu5Ac donor to asialo-PSA, asialo-α1AT, asialo-BF and asialo-AGP by a soluble recombinant form of human ST6Gal1 was investigated. ST6Gal1, one of two human STs responsible for the formation of α2-6 Neu5Ac linkages to Gal, transfers Neu5Ac to Galβ1-4GlcNAc-R acceptors with high specificity.[68] To quantitatively assess the specificity of ST6Gal1 for the four asialo-glycoproteins, CUPRA-ZYME, employing CS^{B}_{LNnT}, was performed simultaneously. Shown in Figure 3.23a are representative ESI mass spectra acquired for sialylation of asialo-α1AT in an aqueous ammonium acetate (200 mM, pH 6.7 and 25 ºC). The corresponding mass spectra for the other three substrates are shown in Figures 3.24-3.25. Normalized (to CS^{B}_{LNnT}) progress curves for each of the asialo-glycoproteins are shown in Figure 3.23b; relative initial rates are plotted in Figure 3.23c and detailed fitting results are shown in Table 3.10.

Inspection of the CoMMon-derived progress curves reveals a number of significant features. First, and in contrast to what was observed for desialylation by NEUC, there is no correlation between initial rate and the number of acceptor sites in the four asialo-glycoproteins (Figure 3.23d). Asialo-BF and asialo-AGP, which have a similar number of *N*-glycan acceptor sites, exhibit relative initial rates ~2.1 and ~1.4 times higher than CS^{B}_{LNnT}, respectively. The higher reactivity agrees with the results of a previous study of human ST6Gal1 using CMP-^{14}CNeu5Ac as donor.[69,70] The higher relative initial rate measured for asialo-PSA (~1.7 times higher than that of CS^{B}_{LNnT}) also agrees with the findings of our previous study.[31] In contrast, the initial rate for asialo-α1AT is ~0.75 times that of CS^{B}_{LNnT}, despite possessing an average of 8 acceptor sites.

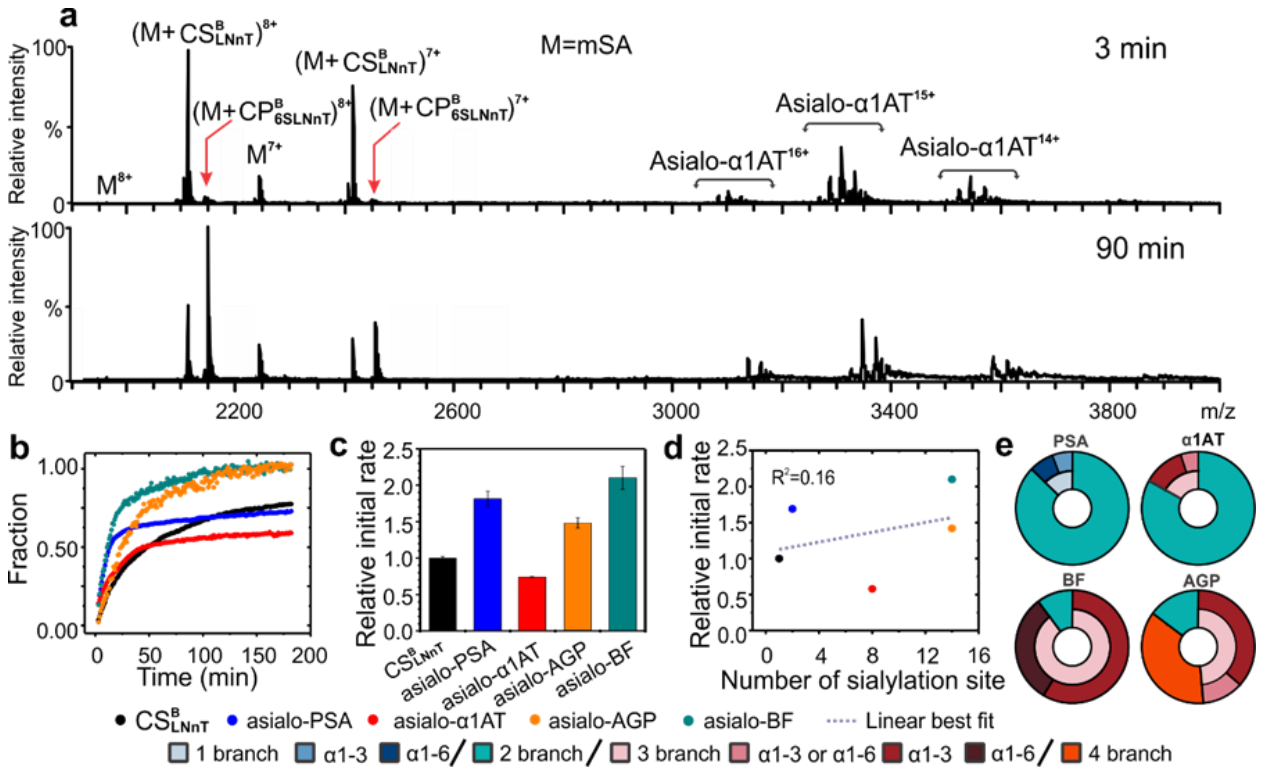

Figure 3.23. (a) Representative ESI mass spectra, acquired with a UHMR Orbitrap mass spectrometer, for aqueous ammonium acetate (200 mM, pH 6.7 and 25 °C) containing ST6Gal1 (nominal concentration 0.27 μM), asialo-α1AT (5 μM), mSA (5 μM) and CS^{B}_{LNnT} (5 μM) measured at 3, 30 and 90 min. (b) Progress curves for asialo-α1AT, asialo-PSA, asialo-BF and asialo-AGP determined by CoMMon. (c) Relative initial rates (to CS^{B}_{LNnT}) determined by linear fitting of progress curves shown in (b) from 3 min to 6 min reaction times. (d) Relationship between sialylation sites for each asialo-glycoprotein and their relative initial rate. (e) *N*-glycan composition of the asialo-glycoprotein: bi-antennary glycans with one Gal on the α1-3 or α1-6 branch (blue); bi-antennary glycans with two Gal, one on each of the α1-3 and α1-6 branches (green); tri-antennary glycans (violet); tetra-antennary glycans (orange).

Substrate	Initial rate (slope)	Relative initial rate (to CS^{B}_{LNnt})
CS^{B}_{LNnT}	0.022±0.001	1.00
asialo-PSA	0.037±0.002	1.69±0.09
CS^{B}_{LNnT}	0.021±0.001	1.00
asialo-α1AT	0.012±0.001	0.58±0.01
CS^{B}_{LNnT}	0.019±0.001	1.00
asialo-BF	0.041±0.001	2.10±0.16
CS^{B}_{LNnT}	0.022±0.001	1.00
asialo-AGP	0.031±0.001	1.42±0.06

a. Errors correspond to one standard deviation.

Table 3.10. Initial rates and relative initial rates of ST6Gal1-catalyzed sialylation of asialo-glycoprotein and CS^{B}_{LNnT} substrates. Initial rates were determined by linear fitting of the reaction progress curves (the first four data points, from 3 min to 6 min). The normalized relative initial rates correspond to the relative initial rates, normalized to the initial rate measured for CS^{B}_{LNnT}.[a]

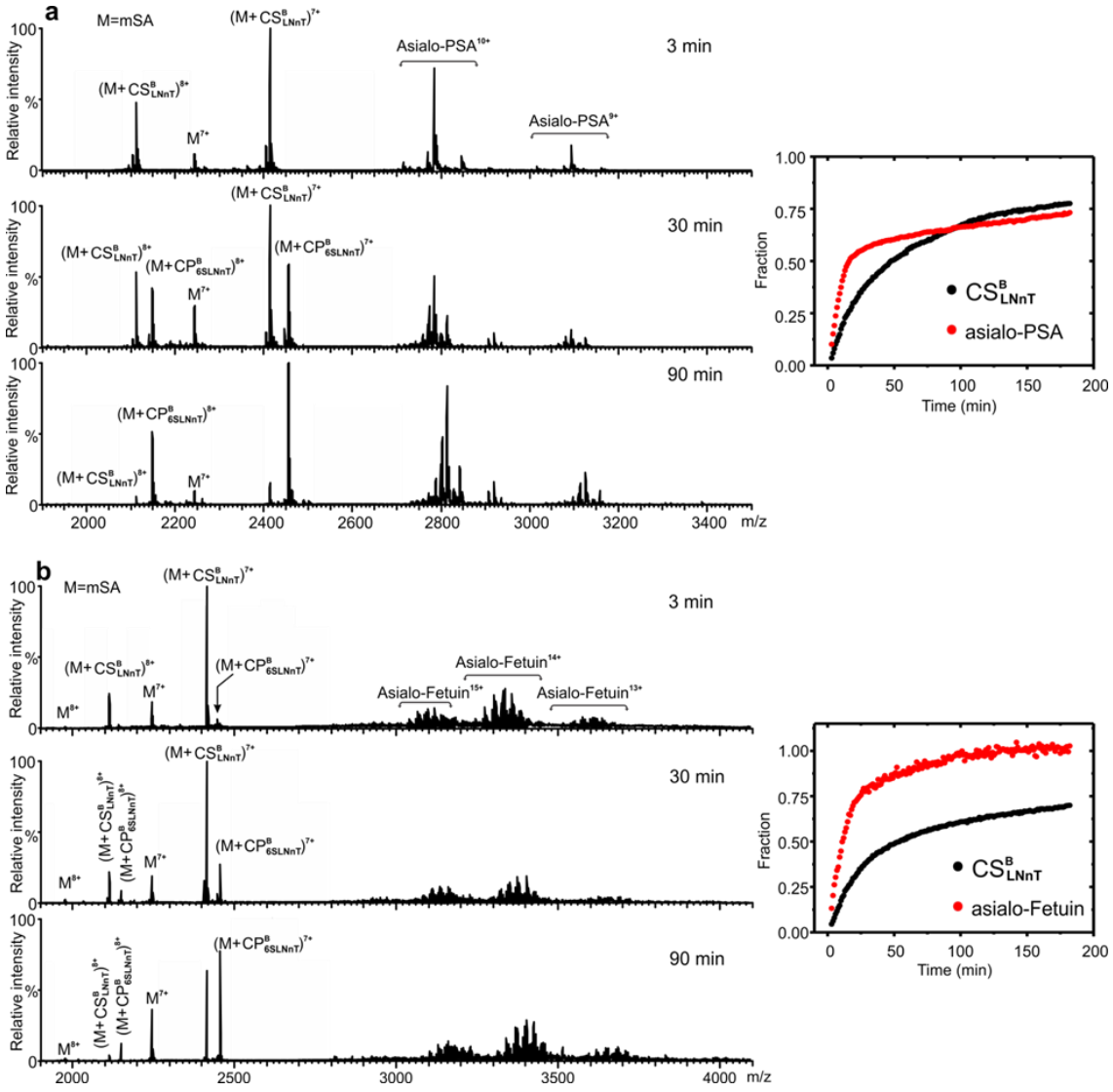

Figure 3.24. (a) Representative mass spectra acquired with the UHMR Orbitrap for aqueous ammonium acetate solutions (200 mM, pH 6.7 and 25 ºC) of ST6Gal1 (0.27 µM), asialo-PSA (5 µM), mSA (5 µM) and CS^{B}_{LNnT} (5 µM) measured at 3 min, 30 min and 90 min. The progress curves for CS^{B}_{LNnT} (black) and asialo-PSA (red) are shown on the right. (b) Representative mass spectra acquired with the UHMR Orbitrap for aqueous ammonium acetate solutions (200 mM, pH 6.7 and 25 ºC) of ST6Gal1 (0.27 µM), asialo-BF (5 µM), mSA (5 µM) and CS^{B}_{LNnT} (5 µM) measured at 3 min, 30 min and 90 min. The progress curves for CS^{B}_{LNnT} (black) and asialo-BF (red) are shown on the right.

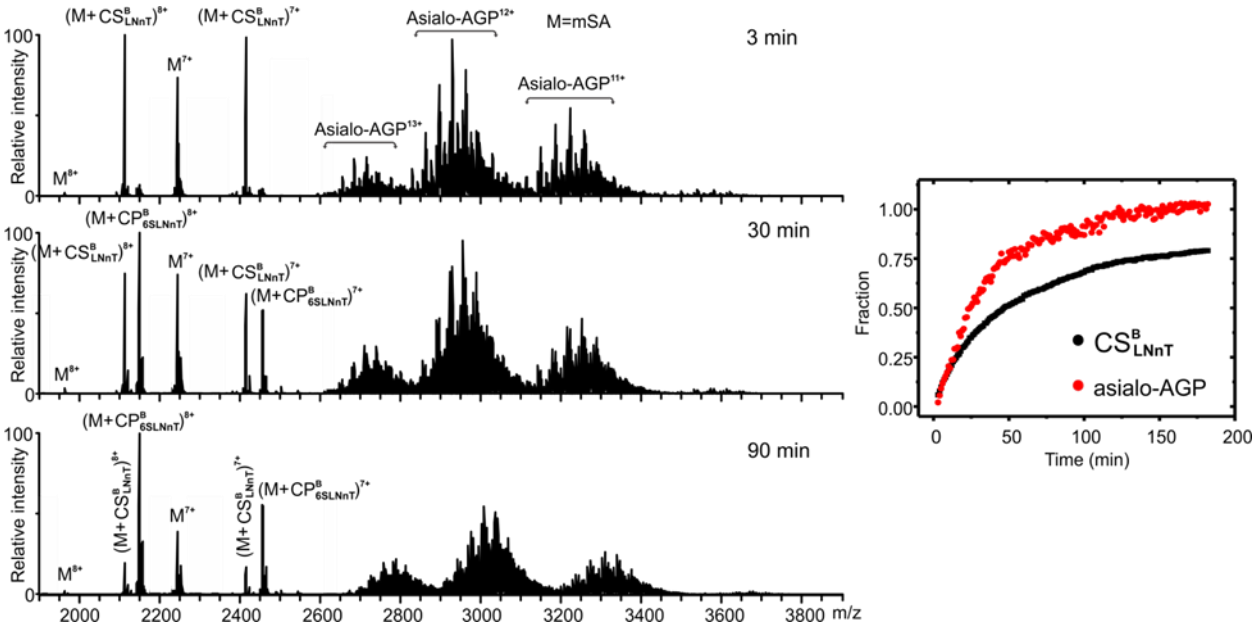

Figure 3.25. Representative mass spectra acquired with the UHMR Orbitrap for aqueous ammonium acetate solutions (200 mM, pH 6.7 and 25 °C) of ST6Gal1 (0.27 μM), asialo-AGP (5 μM), mSA (5 μM) and CS^{B}_{LNnT} (5 μM) measured at 3 min, 30 min and 90 min. The progress curves for CS^{B}_{LNnT} (black) and asialo-AGP (red) are shown on the right.

Secondly, the apparent kinetics for ST6Gal1-catalyzed sialylation of the four glycoproteins are reasonably well described by double exponential functions (Figure 3.26). Although such behavior was previously reported for PSA, it has not been shown to be a general feature of ST6Gal1-catalyzed reactions.[31] Given that the fractional abundances (f_1 and f_2) of the two reactive forms of PSA are similar (~0.5, Table 3.11), the double exponential kinetics can be explained by the different reactivity ($k_1/k_2 \approx 55$, Table 3.11) of Neu5Ac acceptor sites on the bi-antennary *N*-glycan, which is the dominant glycan found on the PSA sample used in this work (Figures 3.23e and 3.27). Indeed, analysis of the released PSA *N*-glycans at early reaction times shows that Neu5Ac is present only on the Gal residue associated with the α1-3 branch (Figure 3.27). Similar

behavior was found for asialo-α1AT, which also contains predominantly (~85%) bi-antennary *N*-glycans (Figure 3.23e). Like with PSA, the fractional abundances are similar (~0.5, Table 3.11) but the rate constants differ significantly ($k_1/k_2 \approx 13$, Table 3.11). Moreover, Neu5Ac is found only on the Gal residue associated with the α1-3 branch of the bi-antennary *N*-glycans at early reaction times (Figure 3.28). This clear preference for the α1-3 branch of bi-antennary *N*-glycans of asialo forms of PSA and α1AT is consistent with observations reported for the sialylation of the Fc fragment of immunoglobulin G by ST6Gal1.[71,72] It is notable, however, that, even though both PSA and α1AT contain predominantly bi-antennary *N*-glycans, asialo-α1AT exhibits much slower reactivity compared with asialo-PSA. These results suggest that, in addition to the inherent differences in the reactivity of α1-3 and α1-6 branches of the bi-antennary *N*-glycans, other factors (perhaps local protein environment) affect ST6Gal1 kinetics.

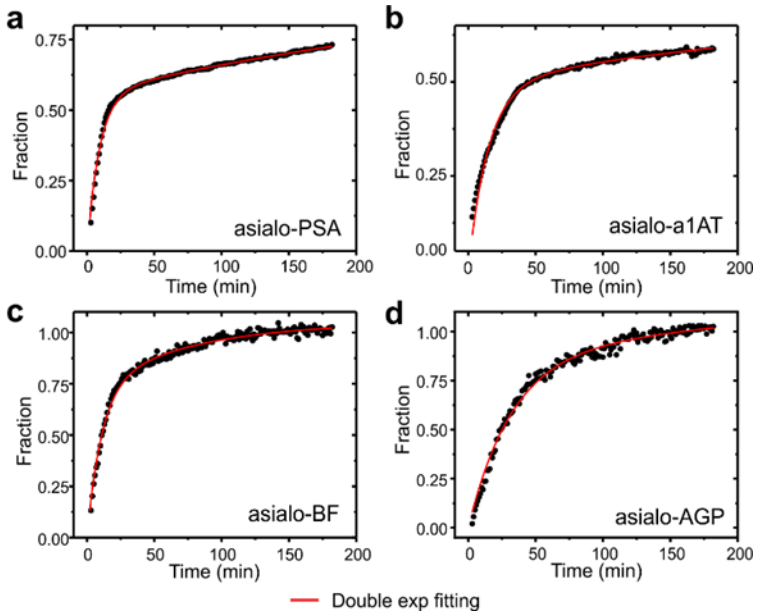

Figure 3.26. Progress curves for ST6Gal1-catalyzed reaction for four asialo-glycoprotein substrates: (a) asialo-PSA, (b) asialo-α1AT, (c) asialo-BF and (d) asialo-AGP. The best fits of double exponential function (eq 3.13) to the progress curves are also shown (in red). Fitting results are given in Table 3.11.

Substrate	k_1	f_1	k_2	f_2
asialo-PSA	0.109±0.002	0.52±0.01	0.0026±0.0003	0.47±0.01
asialo-α1AT	0.084±0.002	0.49±0.02	0.0065±0.001	0.48±0.03
asialo-BF	0.091±0.004	0.72±0.02	0.013±0.002	0.32±0.01
asialo-AGP	0.032±0.003	0.69±0.01	0.0043±0.0001	0.29±0.01

a. Errors correspond to one standard deviation.

Table 3.11. Kinetics of ST6Gal1-catalyzed sialylation of asialo-glycoprotein substrates. Rate constants (k_1 and k_2) and fractional abundances (f_1 and f_2) were obtained from the best fit of a double exponential function (eq 3.13) to the measured progress curves.[a]

The kinetics measured for the other two glycoproteins, asialo-BF (which contains predominantly tri-antennary *N*-glycans, Figures 3.23e and 3.29) and asialo-AGP (tri- and tetra-antennary *N*-glycans, Figures 3.23e and 3.30), exhibit a significantly larger (compared to asialo-PSA and asialo-α1AT) fast component (f_1 ~0.7), suggesting that terminal Gal residues associated with these more branched *N*-glycans are better substrates. An analysis of *N*-glycan released from asialo-AGP and asialo-BF reveals that terminal Gal residues are more abundant on the antennae associated with the α1-3 branch (Galβ1-4GlcNAcβ1-2Manα1-3 or Galβ1-4GlcNAcβ1-4Manα1-3, Table 3.12) than on those on the α1-6 branch. Together, these findings suggest that the antennae associated with α1-3 branch of tri- or tetra-antennary *N*-glycans are better ST6Gal1 substrates than those associated with the α1-6 branch. This conclusion agrees with previous observations made for sialylation of asialo-transferrin and asialo-AGP by bovine ST6Gal1.[73] It is also qualitatively consistent with conclusions drawn from the results of a nuclear magnetic resonance spectroscopy study of ST6Gal1 and glycopeptides possessing tri- and tetra-antennary *N*-glycans, wherein the Galβ1-4GlcNAcβ1-6Manα1-6 branch was found to be a poorer substrate compared to the Galβ1-

4GlcNAcβ1-2Manα1-3, Galβ1-4GlcNAcβ1-4Manα1-3 and Galβ1-4GlcNAcβ1-2Manα1-6 branches.[74]

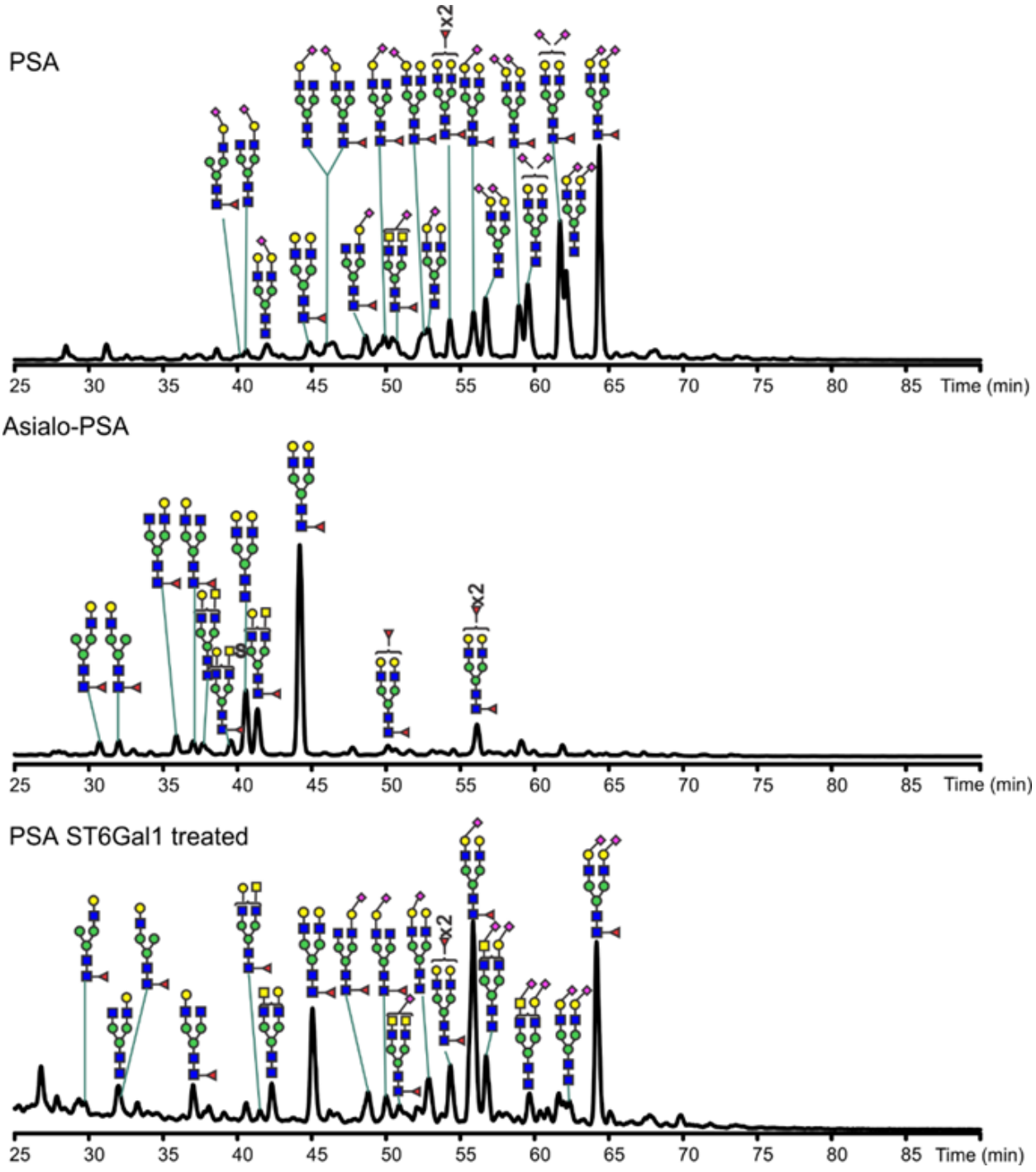

Figure 3.27. *N*-glycan analysis for PSA (top), asialo-PSA (middle) and ST6Gal1-treated PSA (bottom, reaction quenched at ~8 min).

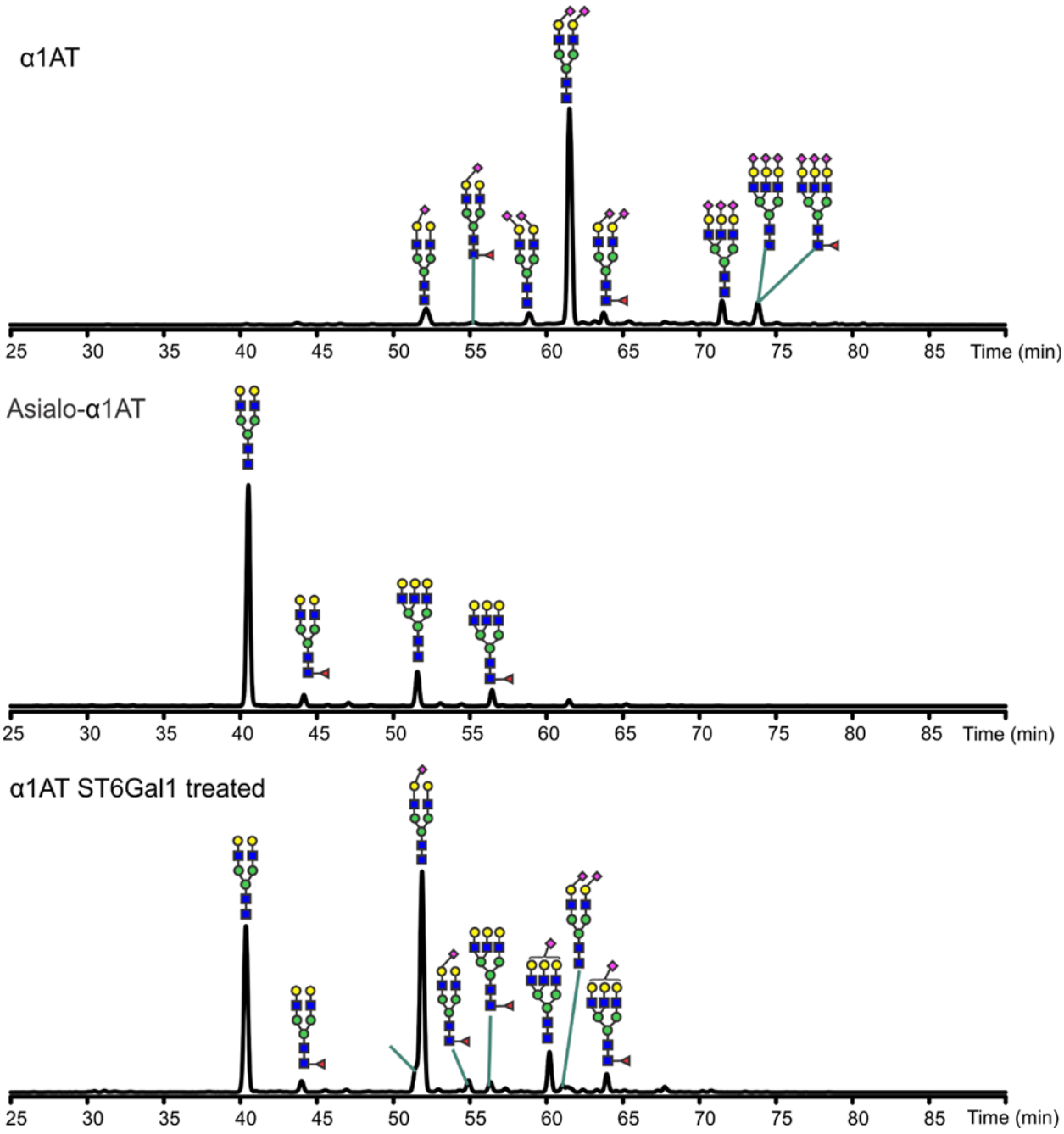

Figure 3.28. *N*-glycan analysis for α1AT (top), asialo-α1AT (middle) and ST6Gal1-treated α1AT (bottom, reaction quenched at ~8 min).

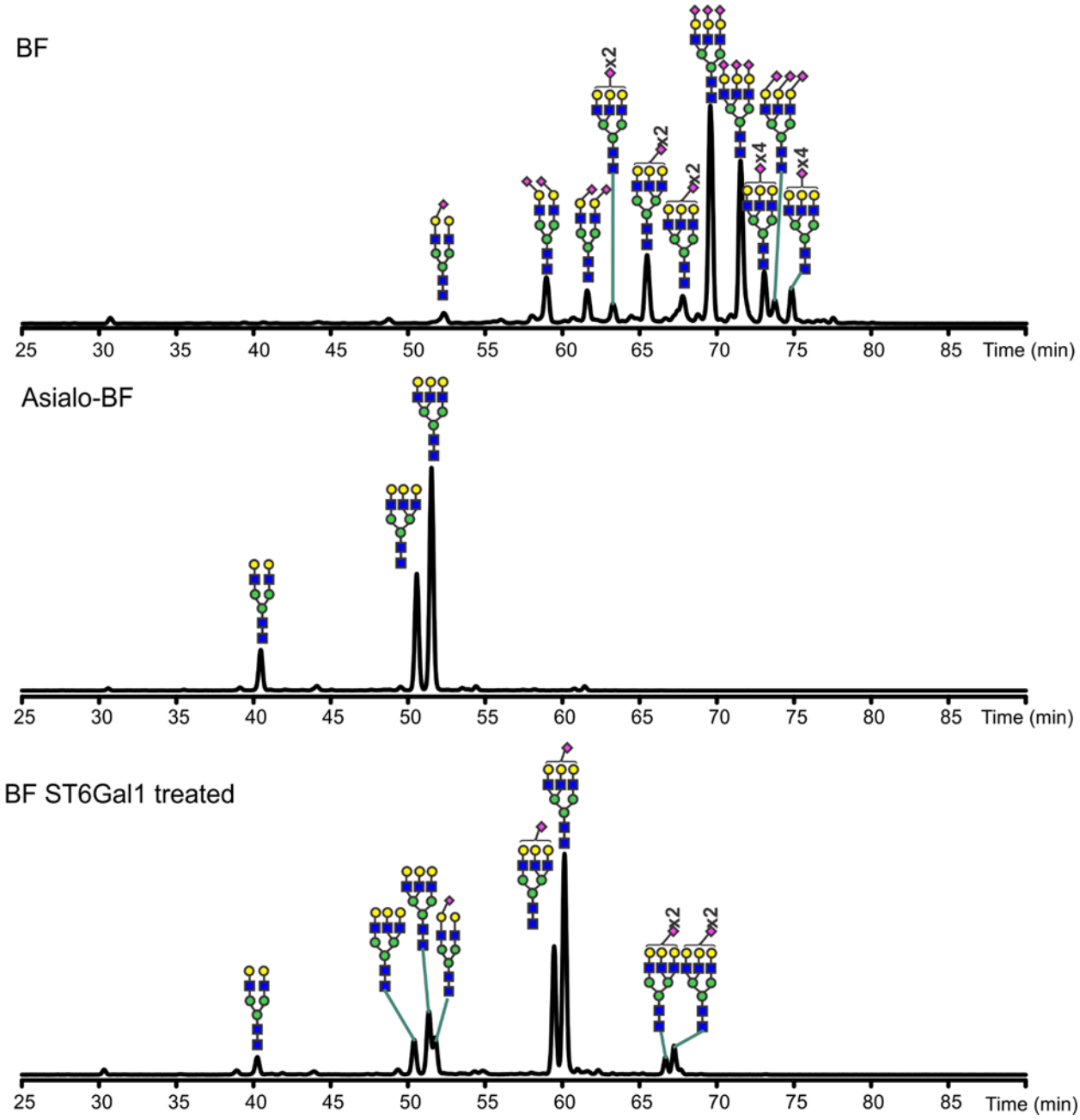

Figure 3.29. *N*-glycan analysis for BF (top), asialo-BF (middle) and ST6Gal1-treated BF (bottom, reaction quenched at ~8 min).

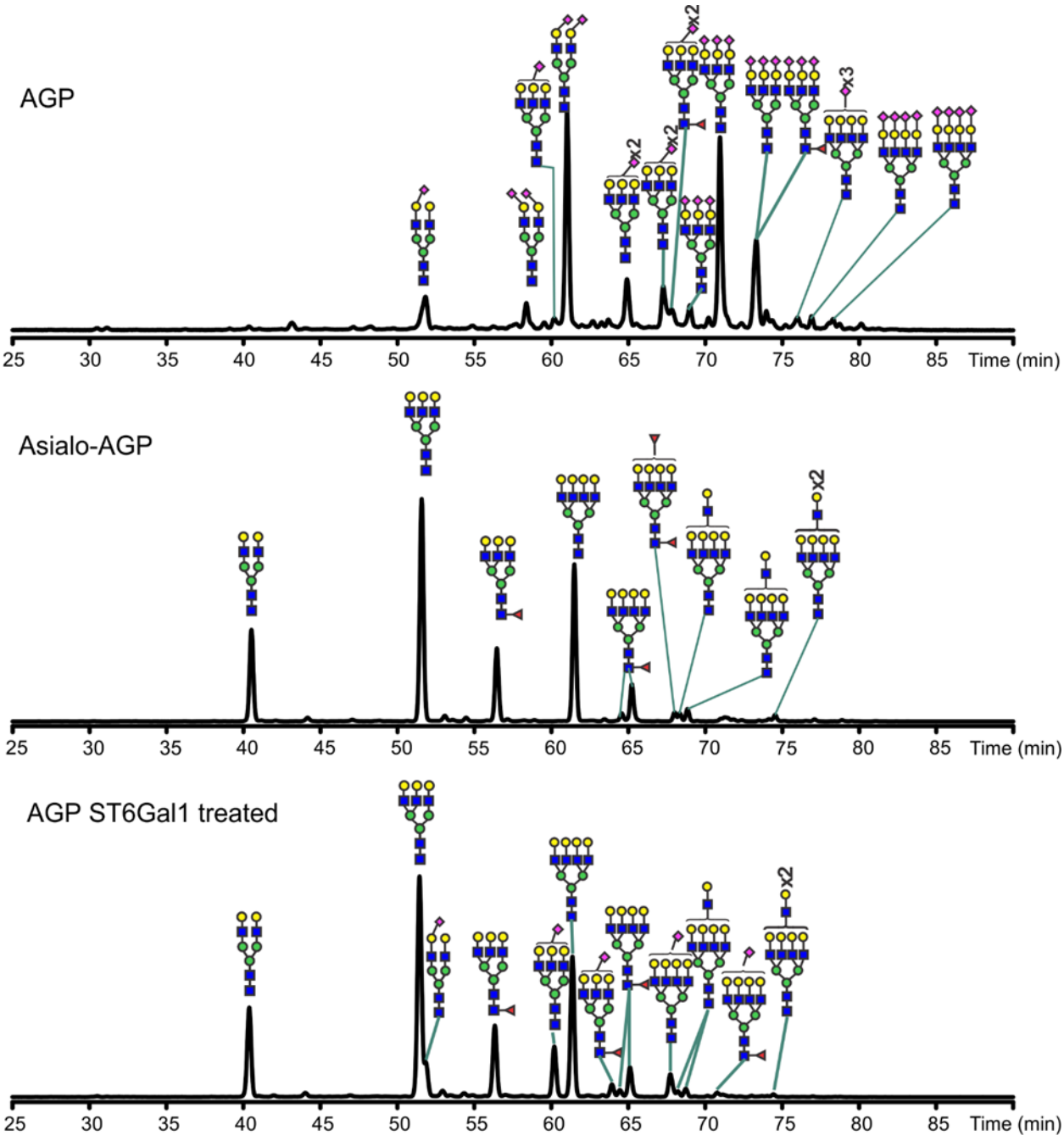

Figure 3.30. *N*-glycan analysis for AGP (top), asialo-AGP (middle) and ST6Gal1-treated AGP (bottom, reaction quenched at ~8 min).

Substrate	Type	Putative structure[a]	Relative abundance
asialo-PSA	1	α1-3 	5.7%
		α1-6 	7.1%
	2	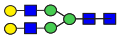	87.2%
asialo-α1AT	2	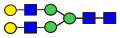	83.1%
		Unknown[b] 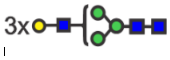	5.0%
	3	α1-3 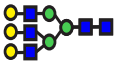	11.9%
		α1-6 	0%
asialo-BF	2	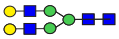	10.3%
	3	α1-3 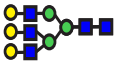	58.5%
		α1-6 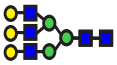	31.2%
asialo-AGP	2	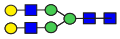	14.9%
		Unknown[b] 	11.9%
	3	α1-3 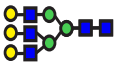	36.7%
		α1-6 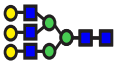	0%
	4	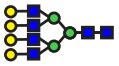	36.8%

a. Glycan fucosylation is not shown.
b. The linkages were not identified.

Table 3.12. Glycan composition of the asialo-glycoproteins analyzed by HILIC-LC/MS. *N*-glycans were classified into four types: Type 1 includes the bi-antennary glycans with one Gal either on α1-3 or α1-6 branch. Type 2 includes bi-antennary glycans with two Gals, one on each branch. Type 3 includes tri-antennary glycans with three Gals, two of them on α1-3 or α1-6 branch. Type 4 includes tetra-antennary glycans with four Gals.

3.4 Conclusions

This chapter introduces CoMMon, a simple, versatile and quantitative ESI-MS method for measuring the kinetics of CAZyme reactions involving heterogeneous, intact glycoprotein substrates. The CoMMon assay relies on continuous monitoring of the CoM of the ensemble of glycoprotein substrates and their corresponding CAZyme products using ESI-MS. The reaction progress curve is generated from the time-dependent changes of CoM. Importantly, there is no requirement for calibration curves, IS, labelling or mass spectrum deconvolution.

To test reliability, the assay was used to monitor the NEUC-catalyzed cleavage of Neu5Ac residues from a series of glycoproteins of varying MWs and degrees of glycosylation. The measured progress curves and initial rates determined with CoMMon are in good agreement (within ≤5%) with results obtained, simultaneously, using an isotopically-labeled IS. Interestingly, all the glycoprotein substrates tested exhibit progress curves that are reasonably well described by double exponential functions. This finding suggests distinct kinetic reactivity for Neu5Ac associated with the underlying α1-3 and the α1-6 branches of the *N*-glycans. Future efforts will be directed towards further testing this hypothesis and assessing whether it is a common feature of neuraminidase-catalyzed reactions.

A powerful feature of CoMMon is that it can be performed simultaneously with CUPRA-ZYME, thereby enabling the relative reactivity of glycoprotein substrates to be quantitatively established. Application of the combined CoMMon/CUPRA-ZYME approach to the NEUC-catalyzed cleavage of Neu5Ac residues from a series of glycoproteins revealed that the initial rates, normalized to that of a common CUPRA substrate, increase with increasing Neu5Ac content, as expected. However, the increase in rate per Neu5Ac residue (~0.2x) suggests that the Neu5Ac residues of the glycoproteins are partially shielded from NEUC. Measurements performed using

other neuraminidases are now needed to establish the extent to which shielding is enzyme dependent.

To illustrate versatility, the combined CoMMon/CUPRA-ZYME approach was used to monitor the kinetics of Neu5Ac transfer to a series of asialo-glycoproteins by human ST6Gal1. Notably, no correlation between relative initial rates and the number of acceptor sites was observed. Moreover, the initial rates of the asialo-glycoproteins are found to be similar to the initial rate measured for the CUPRA substrate (which has a single acceptor site), suggesting that ST6Gal1 has limited accessibility to the *N*-glycan acceptor sites. Similar to what was observed for the NEUC-catalyzed reactions, the progress curves measured for ST6Gal1 are reasonably described by double exponential functions. The results of *N*-glycan analysis showed that ST6Gal1 has a preference for the Galβ1-4GlcNAcβ1-2Manα1-3 branch of bi-antennary *N*-glycans and suggests a preference for the Galβ1-4GlcNAcβ1-2Manα1-3 and Galβ1-4GlcNAcβ1-4Manα1-3 branches of tri- and tetra-antennary *N*-glycans. Efforts to elucidate the relative kinetics of acceptor sites in tri- and tetra-antennary *N*-glycans are ongoing.

Finally, it is important to emphasize that CoMMon is not limited to CAZymes and glycoprotein substrates. The method is general and, in principle, can be applied to many different enzyme classes to monitor reaction kinetics for heterogeneous substrates that are amenable to direct ESI-MS detection. Examples include protein post-translational modifications, such as kinase-catalyzed phosphorylation,[75,76] and enzymatic degradation of polymers and of phospholipids in model membranes.[77,78] Importantly, the CoMMon method removes the need for expensive homogeneous substrates to study kinetics and provides a reliable method suitable for natural substrates, including macromolecules. Furthermore, CoMMon is not restricted to enzyme reactions and can be used to measure the kinetics of chemical reactions involving one or more

heterogeneous reactants, for the relative quantification of proteins and complexes in heterogeneous samples (e.g., determination of drug-to-antibody ratios and cargo loading of viral particles)[79,80] and lipid binding to membrane proteins.[81]

3.5 References

(1) Schmaltz, R. M.; Hanson, S. R.; Wong, C.-H. Enzymes in the synthesis of glycoconjugates. *Chem. Rev.* **2011**, *111*, 4259–4307.

(2) Schwarz, F.; Aebi, M. Mechanisms and principles of *N*-linked protein glycosylation. *Curr. Opin. Struct. Biol.* **2011**, *21*, 576–582.

(3) Varki, A. Biological roles of glycans. *Glycobiology* **2017**, *27*, 3–49.

(4) Arnold, J. N.; Wormald, M. R.; Sim, R. B.; Rudd, P. M.; Dwek, R. A. The impact of glycosylation on the biological function and structure of human immunoglobulins. *Annu. Rev. Immunol.* **2007**, *25*, 21–50.

(5) Ott, C.; Jacobs, K.; Haucke, E.; Navarrete Santos, A.; Grune, T.; Simm, A. Role of advanced glycation end products in cellular signaling. *Redox Biol.* **2014**, *2*, 411–429.

(6) Moremen, K. W.; Tiemeyer, M.; Nairn, A. V. Vertebrate protein glycosylation: diversity, synthesis and function. *Nat. Rev. Mol. Cell Biol.* **2012**, *13*, 448–462.

(7) Kightlinger, W.; Warfel, K. F.; DeLisa, M. P.; Jewett, M. C. Synthetic glycobiology: parts, systems, and applications. *ACS Synth. Biol*. **2020**, *9*, 1534-1562.

(8) Jaroentomeechai, T.; Stark, J. C.; Natarajan, A.; Glasscock, C. J.; Yates, L. E.; Hsu, K. J.; Mrksich, M.; Jewett, M. C.; DeLisa, M. P. Single-pot glycoprotein biosynthesis using a cell-free transcription-translation system enriched with glycosylation machinery. *Nat. Commun*. **2018**, *9*, 2686-2696.

(9) Natarajan, A.; Jaroentomeechai, T.; Cabrera-Sánchez, M.; Mohammed, J. C.; Cox, E. C.; Young, O.; Shajahan, A.; Vilkhovoy, M.; Vadhin, S.; Varner, J. D.; et al. Engineering orthogonal human O-linked glycoprotein biosynthesis in bacteria. *Nat. Chem. Biol*. **2020**, *16*, 1062-1070.

(10) Kightlinger, W.; Duncker, K. E.; Ramesh, A.; Thames, A. H.; Natarajan, A.; Stark, J. C.; Yang, A.; Lin, L.; Mrksich, M.; DeLisa, M. P.; et al. A cell-free biosynthesis platform for modular construction of protein glycosylation pathways. *Nat. Commun.* **2019**, *10*, 5404-5412.

(11) Giddens, J. P.; Lomino, J. V; DiLillo, D. J.; Ravetch, J. V; Wang, L.-X. Site-selective chemoenzymatic glycoengineering of Fab and Fc glycans of a therapeutic antibody. *Proc. Natl. Acad. Sci.* **2018**, *115*, 12023-12027.

(12) Wang, L.-X.; Lomino, J. V. Emerging technologies for making glycan-defined glycoproteins. *ACS Chem. Biol.* **2012**, *7*, 110-122.

(13) Czabany, T.; Schmölzer, K.; Luley-Goedl, C.; Ribitsch, D.; Nidetzky, B. All-in-one assay for β-D-galactoside sialyltransferases: quantification of productive turnover, error hydrolysis, and site selectivity. *Anal. Biochem.* **2015**, *483*, 47-53.

(14) Yu, H.; Chokhawala, H.; Karpel, R.; Yu, H.; Wu, B.; Zhang, J.; Zhang, Y.; Jia, Q.; Chen, X. A multifunctional *Pasteurella multocida* sialyltransferase: a powerful tool for the synthesis of sialoside libraries. *J. Am. Chem. Soc.* **2005**, *127*, 17618-17619.

(15) Gosselin, S.; Alhussaini, M.; Streiff, M. B.; Takabayashi, K.; Palcic, M. M. A continuous spectrophotometric assay for glycosyltransferase. *Anal. Biochem.* **1994**, *220*, 92-97.

(16) Ibatullin, F. M.; Banasiak, A.; Baumann, M. J.; Greffe, L.; Takahashi, J.; Mellerowicz, E. J.; Brumer, H. A real-time fluorogenic assay for the visualization of glycoside hydrolase activity in planta. *Plant Physiol.* **2009**, *151*, 1741-1750.

(17) Weinstein, J.; de Souza-e-Silva, U.; Paulson, J. C. Sialylation of glycoprotein oligosaccharides N-linked to asparagine. Enzymatic characterization of a Galβ1-

3(4)GlcNAc α2-3 sialyltransferase and a Galβ1-4GlcNAc α2-6 sialyltransferase from rat liver. *J. Biol. Chem.* **1982**, *257*, 13845-13853.

(18) Abukar, T.; Rahmani, S.; Thompson, N. K.; Antonescu, C. N.; Wakarchuk, W. W. Development of BODIPY labelled sialic acids as sialyltransferase substrates for direct detection of terminal galactose on N- and O-Linked glycans. *Carbohydr. Res.* **2021**, *500*, 108249.

(19) Sun, C. Q.; Hubl, U.; Hoefakker, P.; Vasudevamurthy, M. K.; Johnson, K. D. A new assay for determining ganglioside sialyltransferase activities lactosylceramide-2,3-sialyltransferase (SAT I) and monosialylganglioside-2,3-sialyltransferase (SAT IV). *PloS One* **2014**, *9*, e94206.

(20) Schmölzer, K.; Ribitsch, D.; Czabany, T.; Luley-Goedl, C.; Kokot, D.; Lyskowski, A.; Zitzenbacher, S.; Schwab, H.; Nidetzky, B. Characterization of a multifunctional α2,3-sialyltransferase from *Pasteurella dagmatis*. *Glycobiology* **2013**, *23*, 1293–1304.

(21) Li, W.; Xiao, A.; Li, Y.; Yu, H.; Chen, X. Chemoenzymatic synthesis of Neu5Ac9NAc-containing α2–3- and α2–6-Linked sialosides and their use for sialidase substrate specificity studies. *Carbohydr. Res.* **2017**, *451*, 51–58.

(22) Norris, A. J.; Whitelegge, J. P.; Faull, K. F.; Toyokuni, T. Analysis of enzyme kinetics using electrospray ionization mass spectrometry and multiple reaction monitoring: fucosyltransferase V. *Biochemistry* **2001**, *40*, 3774–3779.

(23) Sandbhor, M. S.; Soya, N.; Albohy, A.; Zheng, R. B.; Cartmell, J.; Bundle, D. R.; Klassen, J. S.; Cairo, C. W. Substrate recognition of the membrane-associated sialidase NEU3 requires a hydrophobic aglycone. *Biochemistry* **2011**, *50*, 6753–6762.

(24) Nagy, G.; Peng, T.; Pohl, N. L. B. General label-free mass spectrometry-based assay to identify glycosidase substrate competence. *Anal. Chem.* **2016**, *88*, 7183–7190.

(25) Jänis, J.; Pulkkinen, P.; Rouvinen, J.; Vainiotalo, P. Determination of steady-state kinetic parameters for a xylanase-catalyzed hydrolysis of neutral underivatized xylooligosaccharides by mass spectrometry. *Anal. Biochem.* **2007**, *365*, 165–173.

(26) Liesener, A.; Karst, U. Monitoring enzymatic conversions by mass spectrometry: a critical review. *Anal. Bioanal. Chem.* **2005**, *382*, 1451–1464.

(27) Cheng, S.; Wu, Q.; Xiao, H.; Chen, H. Online monitoring of enzymatic reactions using time-resolved desorption electrospray ionization mass spectrometry. *Anal. Chem.* **2017**, *89*, 2338–2344.

(28) Solano, M. I.; Woolfitt, A. R.; Williams, T. L.; Pierce, C. L.; Gubareva, L. V; Mishin, V.; Barr, J. R. Quantification of influenza neuraminidase activity by ultra-high performance liquid chromatography and isotope dilution mass spectrometry. *Anal. Chem.* **2017**, *89*, 3130–3137.

(29) Hines, H. B.; Brueggemann, E. E.; Hale, M. L. High-performance liquid chromatography–mass selective detection assay for adenine released from a synthetic RNA substrate by ricin A chain. *Anal. Biochem.* **2004**, *330*, 119-122.

(30) Gerber, S. A.; Scott, C. R.; Turecek, F.; Gelb, M. H.; August, R. V. Analysis of rates of multiple enzymes in cell lysates by electrospray ionization mass spectrometry. *J. Am. Chem. Soc*. **1999**, *121*, 1102–1103.

(31) Li, Z.; Kitov, P. I.; Kitova, E. N.; Mozenah, F.; Rodrigues, E.; Chapla, D. G.; Moremen, K. W.; Macauley, M. S.; Klassen, J. S. CUPRA-ZYME: an assay for measuring

carbohydrate-active enzyme activities, pathways, and substrate specificities. *Anal. Chem*. **2020**, *92*, 3228–3236.

(32) Struwe, W. B.; Robinson, C. V. Relating glycoprotein structural heterogeneity to function – insights from native mass spectrometry. *Curr. Opin. Struct. Biol.* **2019**, *58*, 241-248.

(33) Wang, Y.; Park, H.; Lin, H.; Kitova, E. N.; Klassen, J. S. Multipronged ESI–MS approach for studying glycan-binding protein interactions with glycoproteins. *Anal. Chem.* **2019**, *91*, 2140–2147.

(34) Katarzyna M., D.; William M., B.; Sarah-Jane, C.; David L., C.; Richard C., F.; Rena M., H.; N. R. S. The complete cDNA and amino acid sequence of bovine fetuin. *J. Biol. Chem.* **1990**, *265*, 4354-4357.

(35) Lin, Y.-H.; Franc, V.; Heck, A. J. R. Similar Albeit Not the Same: In-depth analysis of proteoforms of human serum, bovine serum, and recombinant human fetuin. *J. Proteome Res.* **2018**, *17*, 2861–2869.

(36) Fournier, T.; Medjoubi-N, N.; Porquet, D. Alpha-1-acid glycoprotein. Biochim. Biophys. Acta - Protein Struct. *Mol. Enzymol.* **2000**, *1482*, 157-171.

(37) Guo, S.; Briza, P.; Magdolen, V.; Brandstetter, H.; Goettig, P. Activation and activity of glycosylated KLKs 3, 4 and 11. *Biol. Chem.* **2018**, *399*, 1009–1022.

(38) Brantly, M.; Nukiwa, T.; Crystal, R. G. Molecular basis of alpha-1-antitrypsin deficiency. *Am. J. Med.* **1988**, *84*, 13-31.

(39) Ang, I. L.; Poon, T. C. W.; Lai, P. B. S.; Chan, A. T. C.; Ngai, S.-M.; Hui, A. Y.; Johnson, P. J.; Sung, J. J. Y. Study of serum haptoglobin and its glycoforms in the diagnosis of hepatocellular carcinoma: A glycoproteomic approach. *J. Proteome Res.* **2006**, *5*, 2691–2700.

(40) Sottrup-Jensen, L.; Stepanik, T. M.; Kristensen, T.; Wierzbicki, D. M.; Jones, C. M.; Lønblad, P. B.; Magnusson, S.; Petersen, T. E. Primary structure of human a2-Macroglobulin. *J. Biol. Chem.* **1984**, *259*, 8318-8327.

(41) Moremen, K. W.; Ramiah, A.; Stuart, M.; Steel, J.; Meng, L.; Forouhar, F.; Moniz, H. A.; Gahlay, G.; Gao, Z.; Chapla, D.; et al. Expression system for structural and functional studies of human glycosylation enzymes. *Nat. Chem. Biol.* **2017**, *14*, 156-162.

(42) Kitov, P. I.; Kitova, E. N.; Han, L.; Li, Z.; Jung, J.; Rodrigues, E.; Hunter, C. D.; Cairo, C. W.; Macauley, M. S.; Klassen, J. S. A quantitative, high-throughput method identifies protein–glycan interactions via mass spectrometry. *Commun. Biol.* **2019**, *2*, 268-274.

(43) Wang, W.; Kitova, E. N.; Klassen, J. S. Influence of solution and gas phase processes on protein−carbohydrate binding affinities determined by nanoelectrospray Fourier transform ion cyclotron resonance mass spectrometry. *Anal. Chem.* **2003**, *75*, 4945–4955.

(44) Kitova, E. N.; El-Hawiet, A.; Schnier, P. D.; Klassen, J. S. Reliable determinations of protein – ligand interactions by direct ESI-MS measurements. Are we there yet? *J. Am. Soc. Mass Spectrom.* **2012**, *23*, 431–441.

(45) Kitov, P. I.; Han, L.; Kitova, E. N.; Klassen, J. S. Sliding window adduct removal method (SWARM) for enhanced electrospray ionization mass spectrometry binding data. *J. Am. Soc. Mass Spectrom.* **2019**, *30*, 1446–1454.

(46) Behnken, H. N.; Ruthenbeck, A.; Schulz, J.-M.; Meyer, B. Glycan analysis of prostate specific antigen (PSA) directly from the intact glycoprotein by HR-ESI/TOF-MS. *J. Proteome Res.* **2014**, *13*, 997–1001.

(47) Song, E.; Mayampurath, A.; Yu, C.-Y.; Tang, H.; Mechref, Y. Glycoproteomics: Identifying the glycosylation of prostate specific antigen at normal and high isoelectric points by LC–MS/MS. *J. Proteome Res.* **2014**, *13*, 5570–5580.

(48) McCarthy, C.; Saldova, R.; Wormald, M. R.; Rudd, P. M.; McElvaney, N. G.; Reeves, E. P. The role and importance of glycosylation of acute phase proteins with focus on alpha-1 antitrypsin in acute and chronic inflammatory conditions. *J. Proteome Res.* **2014**, *13*, 3131–3143.

(49) Zhang, S.; Shang, S.; Li, W.; Qin, X.; Liu, Y. Insights on N-glycosylation of human haptoglobin and its association with cancers. *Glycobiology* **2016**, *26*, 684–692.

(50) Zhu, J.; Wu, J.; Yin, H.; Marrero, J.; Lubman, D. M. Mass spectrometric N-glycan analysis of haptoglobin from patient serum samples using a 96-Well plate format. *J. Proteome Res.* **2015**, *14*, 4932–4939.

(51) Lee, S. H.; Jeong, S.; Lee, J.; Yeo, I. S.; Oh, M. J.; Kim, U.; Kim, S.; Kim, S. H.; Park, S. Y.; Kim, J. H.; et al. Glycomic profiling of targeted serum haptoglobin for gastric cancer using nano LC/MS and LC/MS/MS. *Mol. Biosyst.* **2016**, *12*, 3611–3621.

(52) Marrero, A.; Duquerroy, S.; Trapani, S.; Goulas, T.; Guevara, T.; Andersen, G. R.; Navaza, J.; Sottrup-Jensen, L.; Gomis-Rüth, F. X. The Crystal Structure of Human α2-Macroglobulin Reveals a Unique Molecular Cage. *Angew. Chemie Int. Ed.* **2012**, *51*, 3340–3344.

(53) Baerenfaenger, M.; Meyer, B. Intact human alpha-acid glycoprotein analyzed by ESI-QTOF-MS: simultaneous determination of the glycan composition of multiple glycosylation sites. *J. Proteome Res.* **2018**, *17*, 3693–3703.

(54) Bigge, J. C.; Patel, T. P.; Bruce, J. A.; Goulding, P. N.; Charles, S. M.; Parekh, R. B. Nonselective and efficient fluorescent labeling of glycans using 2-Amino benzamide and anthranilic acid. *Anal. Biochem.* **1995**, *230*, 229–238.

(55) Nwosu, C.; Yau, H. K.; Becht, S. Assignment of core versus antenna fucosylation types in protein N-glycosylation via procainamide labeling and tandem mass spectrometry. *Anal. Chem.* **2015**, *87*, 5905–5913.

(56) Zhuo, Y.; Keire, D. A.; Chen, K. Minor N-glycan mapping of monoclonal antibody therapeutics using middle-down NMR spectroscopy. Mol. Pharm. 2021, 18, 441–450.

(57) Stanley, P.; Taniguchi, N.; Aebi, M. N-glycans. In Essentials of Glycobiology. 3rd edition. Cold Spring Harbor Laboratory Press: **2017**.

(58) Walsh, I.; O'Flaherty, R.; Rudd, P. M. Bioinformatics applications to aid high-throughput glycan profiling. *Perspect. Sci*. **2017**, *11*, 31-39.

(59) Naka, R.; Kamoda, S.; Ishizuka, A.; Kinoshita, M.; Kakehi, K. Analysis of total N-glycans in cell membrane fractions of cancer cells using a combination of serotonin affinity chromatography and normal phase chromatography. *J. Proteome Res.* **2006**, *5*, 88–97.

(60) Li, J.; McClane, B. A. The sialidases of Clostridium perfringens type D strain CN3718 differ in their properties and sensitivities to inhibitors. *Appl. Environ. Microbiol.* **2014**, *80*, 1701–1709.

(61) Chiarezza, M.; Lyras, D.; Pidot, S. J.; Flores-Díaz, M.; Awad, M. M.; Kennedy, C. L.; Cordner, L. M.; Phumoonna, T.; Poon, R.; Hughes, M. L.; et al. The NanI and NanJ sialidases of Clostridium perfringens are not essential for virulence. *Infect. Immun.* **2009**, *77*, 4421–4428.

(62) Hervé, F.; Gomas, E.; Duché, J.-C.; Tillement, J.-P. Fractionation of the genetic variants of human α1-acid glycoprotein in the native form by chromatography on an immobilized copper(II) affinity adsorbent: Heterogeneity of the separate variants by isoelectrofocusing and by concanavalin A affinity chromatography. *J. Chromatogr. B Biomed. Sci. Appl.* **1993**, *615*, 47-57.

(63) Sadrzadeh, S. H.; Bozorgmehr, J. Haptoglobin phenotypes in health and disorders. *Pathol. Patterns Rev.* **2004**, *121*, S97-S104.

(64) Ribeiro, J. P.; Pau, W.; Pifferi, C.; Renaudet, O.; Varrot, A.; Mahal, L. K.; Imberty, A. Characterization of a high-affinity sialic acid-specific CBM40 from Clostridium perfringens and engineering of a divalent form. *Biochem. J.* **2016**, *473*, 2109–2118.

(65) Windwarder, M.; Altmann, F. Site-specific analysis of the O-glycosylation of bovine fetuin by electron-transfer dissociation mass spectrometry. *J. Proteomics* **2014**, *108*, 258–268.

(66) Lin, Z.; Lo, A.; Simeone, D. M.; Ruffin, M. T.; Lubman, D. M. An N-glycosylation analysis of human alpha-2-macroglobulin using an integrated approach. *J. Proteomics Bioinform.* **2012**, *5*, 127–134.

(67) Marrero, A.; Duquerroy, S.; Trapani, S.; Goulas, T.; Guevara, T.; Andersen, G. R.; Navaza, J.; Sottrup-Jensen, L.; Gomis-Rüth, F. X. The crystal structure of human α2-macroglobulin reveals a unique molecular cage. *Angew. Chemie - Int. Ed.* **2012**, *51*, 3340–3344.

(68) Kitagawa, H.; Paulson, J. C. Differential expression of five sialyltransferase genes in human tissues. *J. Biol. Chem.* **1994**, *269*, 17872–17878.

(69) Takashima, S.; Tsuji, S.; Tsujimoto, M. Characterization of the second type of human β-galactoside α2,6-sialyltransferase (ST6Gal II), which sialylates Galβ1,4GlcNAc structures

on oligosaccharides preferentially: genomic analysis of human sialyltransferase genes. *J. Biol. Chem.* **2002**, *277*, 45719–45728.

(70) Kitazume, S. ST6 beta-galactoside alpha-2,6-sialyltranferase 1 (ST6GAL1). In handbook of glycosyltransferases and related genes (Taniguchi N, Honke K, Fukuda M, Narimatsu H, Yamaguchi Y, Angata T, Eds.), pp 693–703, Springer, Japan, Tokyo.

(71) Barb, A. W.; Brady, E. K.; Prestegard, J. H. Branch-specific sialylation of IgG-Fc glycans by ST6Gal-I. *Biochemistry* **2009**, *48*, 9705–9707.

(72) Barb, A. W.; Meng, L.; Gao, Z.; Johnson, R. W.; Moremen, K. W.; Prestegard, J. H. NMR characterization of immunoglobulin G Fc glycan motion on enzymatic sialylation. *Biochemistry* **2012**, *51*, 4618–4626.

(73) Paulson, J. C.; Prieels, J. P.; Glasgow, L. R.; Hill, R. L. Sialyl- and fucosyltransferase in the biosynthesis of asparaginyl-linked oligosaccharides in glycoproteins. Mutually exclusive glylcosylation by β-Galactoside α2-6 sialyltransferase and N-acetylglucosaminide α1-3 fucosyltransferase. *J. Biol. Chem.* **1978**, *253*, 5617–5624.

(74) Joziasse, D. H.; Schiphorst, W. E.; Van den Eijnden, D. H.; Van Kuik, J. A.; Van Halbeek, H.; Vliegenthart, J. F. Branch specificity of bovine colostrum CMP-Sialic acid: Galβ 1-4GlcNAc-R α2-6 sialyltransferase. Sialylation of bi-, tri-, and tetraantennary oligosaccharides and glycopeptides of the N-acetyllactosamine type. *J. Biol. Chem.* **1987**, *262*, 2025–2033.

(75) Drepper, F.; Biernat, J.; Kaniyappan, S.; Meyer, H. E.; Mandelkow, E. M.; Warscheid, B.; Mandelkow, E. A combinatorial native MS and LC-MS/MS approach reveals high intrinsic phosphorylation of human Tau but minimal levels of other key modifications. *J. Biol. Chem*. **2020**, *295*, 18213–18225.

(76) Van de Waterbeemd, M.; Lössl, P.; Gautier, V.; Marino, F.; Yamashita, M.; Conti, E.; Scholten, A.; Heck, A. J. R. Simultaneous assessment of kinetic, site-specific, and structural aspects of enzymatic protein phosphorylation. *Angew. Chemie Int. Ed*. **2014**, *53*, 9660–9664.

(77) Mohanan, N.; Montazer, Z.; Sharma, P. K.; Levin, D. B. Microbial and enzymatic degradation of synthetic plastics. *Frontiers in Microbiology*. **2020**, *11*, 2837-2859.

(78) Mumtaz Virk, M.; Reimhult, E. Phospholipase A2-induced degradation and release from lipid-containing polymersomes. *Langmuir* **2018**, *34*, 395–405.

(79) Nagornov, K. O.; Gasilova, N.; Kozhinov, A. N.; Virta, P.; Holm, P.; Menin, L.; Nesatyy, V. J.; Tsybin, Y. O. Drug-to-antibody ratio estimation via proteoform peak integration in the analysis of antibody–oligonucleotide conjugates with Orbitrap fourier transform mass spectrometry. *Anal. Chem*. **2021**, *93*, 12930-12937.

(80) Strasser, L.; Morgan, T. E.; Guapo, F.; Füssl, F.; Forsey, D.; Anderson, I.; Bones, J. A native mass spectrometry-based assay for rapid assessment of the empty:full capsid ratio in adeno-associated virus gene therapy products. *Anal. Chem*. **2021**, *93*, 12817-12821.

(81) Bechara, C.; Robinson, C. V. Different modes of lipid binding to membrane proteins probed by mass spectrometry. *J. Am. Chem. Soc*. **2015**, *137*, 5240–5247.

Chapter 4

Native Mass Spectrometry Quantitation of α2-3- and α2-6-linked N-Acetylneuraminic Acid Content of Prostate Specific Antigen: An Accurate Liquid Biopsy for Clinically Significant Prostate Cancer

4.1 Introduction

Prostate cancer (PCa) is the second most commonly diagnosed cancer in men and the fifth leading cause of cancer deaths in men.[1,2] The serum prostate-specific antigen (PSA) test is the most commonly used test for PCa screening and has greatly reduced PCa-related mortality.[3,4] However, the PSA test is not specific for clinically significant forms of PCa, histologically classified as Gleason Group 2 (GG2/intermediate-risk PCa) and Gleason Groups 3, 4, and 5 (GG3/4/5/high-risk PCa). The serum PSA test has a false positive rate of 35-45% when using a cut-off of ≥4 ng/mL, causing many individuals to undergo a needle biopsy procedure that often yields no evidence of clinically significant PCa.[5-7] More men die from the side effects of a prostate needle biopsy (0.08% mortality) than from low-risk PCa (Gleason Group 1/GG1) (<0.01% mortality), making it the most lethal biopsy procedure in medicine.[8-11] There is an urgent need for more accurate biomarkers that distinguish patients with clinically significant PCa from all other diseases of the prostate, such as low-risk PCa (GG1), prostatitis, and benign prostatic hyperplasia (BPH).

Aberrant protein glycosylation is a feature common of all cancers and altered PSA glycosylation has been observed in PCa.[7,12,13] PSA has a single *N*-glycosylation site (Asn-69), which is occupied primarily by fucosylated or non-fucosylated complex-type disialylated bi-antennary *N*-glycans, comprised of α2-3- or α2-6-linked sialic acid (*N*-acetylneuraminic acid,

Neu5Ac).[7,14,15] There is growing evidence of altered *N*-glycans on PSA secreted by PCa cells, compared to that secreted from normal prostatic epithelium.[16] Differences observed in PCa include increased levels of α2-3-linked Neu5Ac,[17-21] and increases in hybrid, oligomannose, and bi-antennary digalactosylated monosialylated glycans, bisecting and mono-antennary glycans, and multisialylated LacdiNAc.[17-21] These levels appear to increase in a graded fashion with PCa progression.[22,23] Indeed, altered PSA glycosylation is a promising biomarker for distinguishing clinically significant PCa from all other prostatic diseases.[16,24-27] For example, recent studies on the relative content of α2-3-linked Neu5Ac and core fucosylation of serum PSA, independently or together, is specific for GG4 PCa.[13,24-26,28,29] However, it is not clear if α2-3-linked Neu5Ac and core fucosylation is specific for clinically significant PCa, histologically classified as Gleason Group 2-5 (GG2-5) disease. Far more patients are diagnosed with GG2 and GG3 than GG4 disease, risk types that are often confused for low-risk PCa (GG1) by serum PSA and other blood tests (e.g., the Prostate Health Index (PHI) and the four-kallikrein panel (4Kscore)).[30,31]

Typically, PSA glycosylation analysis is performed on released *N*-glycans or glycopeptides using high performance liquid chromatography (HPLC) or capillary electrophoresis (CE) separation, combined with mass spectrometry (MS) detection.[32-34] For example, PSA tryptic glycopeptides can be separated using hydrophilic interaction liquid chromatography (HILIC) or by CE.[32,34,35] Separation of isomeric glycopeptides containing α2-3- and α2-6-linked Neu5Ac, and their relative quantification by HILIC, coupled with multiple reaction monitoring MS, has been demonstrated with identification of the Neu5Ac linkages achieved through non-specific and α2-3-linked Neu5Ac-specific neuraminidases.[32]

While commonly used for PSA glycosylation analysis, the bottom-up LC/CE-MS workflow involves multiple steps, including enzymatic digestion and *N*-glycan/glycopeptide

enrichment.[36] Such bottom-up strategies are labour intensive to implement, suffer from sample loss(es) and, most importantly, are susceptible to contamination by other glycoproteins that co-purify with PSA.[36,37] In contrast, top-down approaches, based on the glycan analysis of intact PSA, avoid these sources of error.[15] For example, lectin-based immunoassays have been used to quantify the α2-3-linked Neu5Ac content of intact PSA for the diagnosis of PCa.[32] Currently, the most sensitive diagnostic tests include detection of α2,3-linked sialic acid in intact PSA using anti-α2-3-linked Neu5Ac antibody or the *Sambucus Nigra* agglutinin (SNA) conjugated to agarose beads, with luminescence as the readout.[24,26] However, antibody- and lectin-based assays underestimate α2-3-linked Neu5Ac content owing to the inability to accurately quantify bi-antennary *N*-glycans possessing all α2-3- Neu5Ac (anti-α2-3-Neu5Ac antibody) or both α2-3- and α2-6-Neu5Ac (SNA). Recently, LC-MS analysis of intact PSA for the determination of glycan composition was demonstrated.[15] This approach does not allow for the α2-3- and α2-6-linked Neu5Ac content of PSA to be quantified, thus is not sufficiently quantitative for clinical practice. This is essential because it is the ratio of the two Neu5Ac linkage states that is hypothesized to discriminate between GG1 disease (low-risk) from GG2-5 disease (intermediate- to high-risk PCa), also known as clinically significant PCa.[25-31,38]

Here, we demonstrate a top-down native MS assay, employing center-of-mass monitoring (CoMMon) and a combination of specific (α2-3-linked) and non-specific (cleaves both α2-3- and α2-6-Neu5Ac) neuraminidases, for the accurate quantification of the relative α2-3-Neu5Ac content of PSA. Because the assay involves direct MS analysis of intact PSA, it is not affected by the presence of other serum glycoproteins that may contaminate the sample. Moreover, the method avoids sample handling steps (enzymatic release of *N*-glycans and addition of a fluorophore) required for HPLC or CE analysis and the limitations of antibody/lectin-based assays. Validation

of the assay was performed using purified PSA from a commercial source, for which the relative α2-3- and α2-6-Neu5Ac content was predetermined and two artificial PSA standards containing either α2-3- or α2-6-Neu5Ac exclusively (23PSA and 26PSA, respectively). To assess the potential of the assay for clinical diagnosis of PCa and disease staging, the percentage of Neu5Ac present as α2-3-Neu5Ac on PSA (%α23PSA) in serum of 102 individuals (41 low-grade, 20 intermediate-grade and 41 high-grade) was measured. Our results demonstrate that %α23PSA of blood serum PSA, which can be precisely measured in a non-invasive manner with our dual neuraminidase native MS/CoMMon assay, discriminates between clinically significant PCa (GG2-5) and low-grade PCa (GG1). This is the first study showing discrimination of lower, but clinically significant PCa (GG2 and above) from GG1 and demonstrates the tremendous potential of PSA glycosylation and native MS/CoMMon to diagnose and monitor disease progression in PCa.

4.2 Experimental

4.2.1 Ethics

Serum samples were collected in Sunnybrook Research Institute with the approval of the Research Ethics Board committee at Sunnybrook Health Sciences Centre (Toronto, ON). The mass spectrometry analysis of purified PSA from patient blood serum samples (a collaboration with Sunnybrook hospital) was approved by the Health Research Ethics Board at the University of Alberta (Pro00122665).

4.2.2 Materials and Methods

4.2.2.1 Protein and CAZymes

Prostate Specific Antigen (PSA, MW 28,430 Da, purified from human seminal plasma) was purchased from LEE Biosolutions (Maryland Heights, MO). Human carbonic anhydrase (hCA,

type I, MW 28,848 Da) and neuraminidase from *Clostridium perfringens* (NanI subtype, denoted as NEUC) were purchased from Sigma-Aldrich Canada (Oakville, Canada). Neuraminidase from *Streptococcus pneumonia* (NanB subtype, denoted as NEUS) was produced following a reported protocol.[39] Asialo-PSA was prepared by incubating PSA with NEUC in 200 mM ammonium acetate (pH 6.7) at room temperature overnight. Asialo-PSA was further used to produce α2-3 or α2-6 disialylated PSA as previously described by incubating with CMP-Neu5Ac and ST3Gal4 or ST6Gal1, respectively.[40] All proteins and enzymes were dialyzed against an aqueous solution of 200 mM ammonium acetate (pH 6.8) using an Amicon 0.5 mL microconcentrator (EMD Millipore, Billerica, MA) with a MW cutoff of 3 kDa and stored at -20 ºC until used. The concentrations of protein and enzyme stock solutions were measured by UV absorption at 280 nm.

4.2.2.2 Glycans and other reagents

Neu5Acα2-6Galβ1-4Glc (6SL) was purchased from Carbosynth (San Diego, CA), Neu5Acα2-3Galβ1-4Glc (3SL) was purchased from Elicityl SA (Crolles, France) and Neu5Acα2-3Galβ1-4GlcNAc-ethylamine (3SLNAc-ethylamine) was synthesized, as described in Chapter 2 and elsewhere.[41] *N*-acetyl-neuraminic acid-1,2,3-$^{13}C_3$ (Neu5Ac-$^{13}C_3$) was purchased from Omicron Biochemicals Inc. (South Bend, IN, USA). Cytidine-5'-monophosphate-*N*-acetylneuraminic acid (CMP-Neu5Ac) were purchased from Sigma-Aldrich Canada (Oakville, Canada). Other reagents and solvents were purchased from common commercial sources.

4.2.3 Competitive Universal Proxy Receptor Assay (CUPRA) substrates

The CUPRA substrates CS_{3SL}, CS_{6SL} and CS_{3SLNAc}, which employ a sulfonamide affinity tag (Figure 4.1), were produced from the oligosaccharides 6SL and 3SLNAc, respectively, as described in Chapter 2 and 3.

4.2.4 Sample collection

Whole blood serum samples from patients were collected into serum-specific vacutainers (BD Biosciences Inc.) and then allowed to clot overnight. After centrifugation at 1000 x g for 15 minutes at room temperature, the serum upper phase supernatant was aliquoted and stored at -80 °C until used.

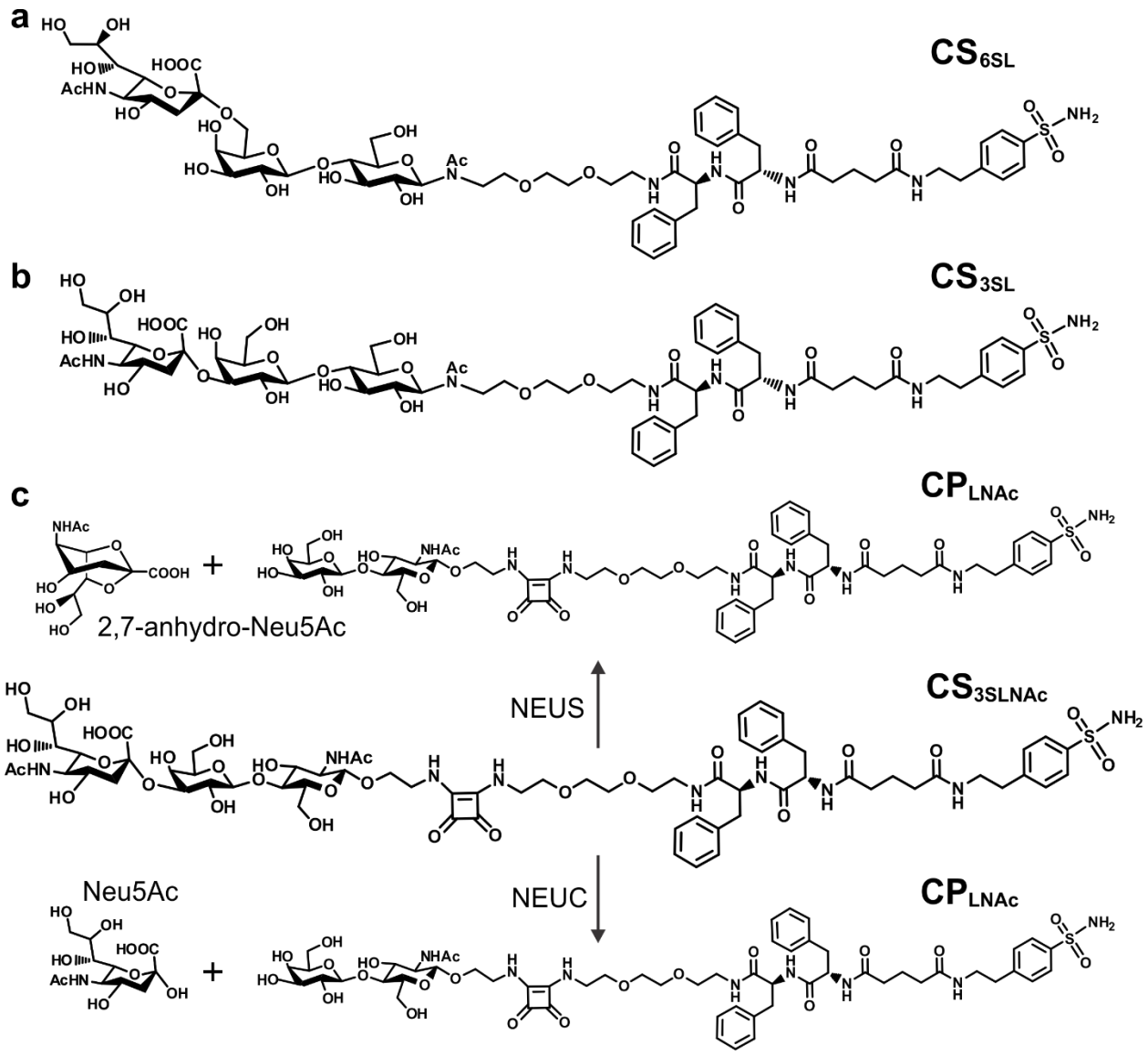

Figure 4.1. Structure of CUPRA substrates (a) CS_{6SL}, (b) CS_{3SL} and (c) and CS_{3SLNAc}. Details of the synthesis can be found in Chapter 2 and elsewhere.[41] Shown in (c) are the hydrolysis products resulting from treatment of CS_{3SLNAc} with NEUS or NEUC.

4.2.5 PSA extraction

The method used to exctract PSA from blood serum is based on standard protocols, but with modifications.[27,42,43] Before extraction, the blood serum sample (~800 μL) was mixed with 5 M

ethanolamine (~250 µL), with a final pH ~10, and incubated at room temperature for 72 h to release any PSA bound to α1-antichymotrypsin.[43] After incubation, the pH was adjusted to ~7.5 and the solution dialyzed into aqueous ammonium acetate (200 mM, pH 6.7) and concentrated to ~200 uL using a 3 kDa MW centrifugal filter. The resulting solution was stored at -20 °C until PSA extraction performed.

As a first step for PSA extraction, 400 µL of Milli-Q water was added to the streptavidin containing cartridge (Streptavidin HP Spintrap, Cytiva, UK) and centrifuged for 1 min at 150 x g 3 times. Then 400 µL of PBS buffer (1X) was added and centrifuged for 1 min at 150 x g 3 times to equilibrate the streptavidin. An aliquot of 100 µL of the biotinylated anti-PSA antibody (PSA monoclonal antibody, Biotin, ThermoFisher Scientific, MA, USA) was mixed with 200 µL of PBS and added to the cartridge. The cartridge was placed on a tube rotator (Barnstead/Thermolyne, IA, USA) for 2 h. Then the cartridge was centrifuged for 1 min at 150 x g and washed with 400 µL of PBS 3 times to remove unbound antibody. 200 µL of PBS and 200 µL of blood serum prepared previously were added to the cartridge and mixed using a tube rotator for 2 h. Then the cartridge was centrifuged for 1 min at 150 x g 3 times with 200 µL Milli-Q water to remove all unbound proteins and chemicals. 150 µL of 0.2 M glycine buffer (pH ~2.5, adjusted with acetic acid) was added to the cartridge and mixed using tube rotator for 30 min to release bound PSA. This step was repeated 3 times and the collected eluent was transferred into a 3 kDa filter, dialyzed and concentrated in aqueous ammonium acetate (pH 6.7, 200 mM) using a centrifuge (30 min at 14000 x g and 5 ºC). Finally, the concentrated PSA solution (20 µL) was used for ESI-MS analysis. To determine the recovery efficiency of the extraction protocol, a known concentration of purified PSA in aqueous ammonium acetate (1.99 µg/mL, concentration measured by BCA protein assay) was subjected to the extraction procedure. A recovery efficiency of 77.8% ± 2.9% (from three

replicates) was determined based on the concentration of extracted PSA determined by BCA protein assay (Figure 4.2).

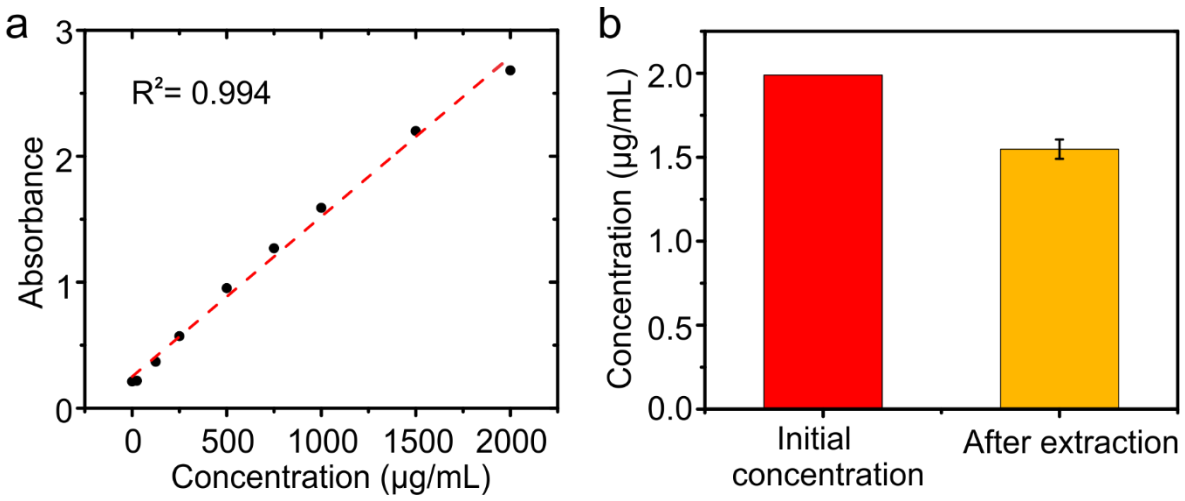

Figure 4.2. Recovery efficiency of PSA extraction (77.8% ± 2.9%) determined by adding purified PSA into 1 mL ammonia acetate (200 mM, pH 6.7, 25 °C) with a final concentration of 1.99 µg/mL (measured by BCA protein assay). Recovery efficiency (from three replicates) was determined based on the concentration of extracted PSA determined by BCA protein assay. (a) Calibration curve obtained by the BCA assay for quantification of PSA. (b) Concentration quantified before (red) and after extraction (orange), errors are one standard deviation from three replicates.

4.2.6 Mass spectrometry

ESI-MS measurements were carried out in positive ion mode using two instruments, a Q Exactive Ultra High Mass Range (UHMR) Hybrid Quadrupole-Orbitrap and a Q Exactive Hybrid Quadrupole-Orbitrap mass spectrometer (Thermo Fisher Scientific, Bremen, Germany), each equipped with a nanoflow ESI (nanoESI) source. The nanoESI tips were produced from

borosilicate capillaries using a P-1000 micropipette puller (Sutter Instruments, Novato, CA). To carry out nanoESI, a platinum wire was inserted into the back end of the tip and in contact with the sample solution, and a voltage of 0.7-0.8 kV was applied. For both instruments, the capillary temperature was set at 120 °C. For analysis of PSA on the UHMR Orbitrap, the *m/z* range was set from 2000 to 6000, the S-lens RF level was set at 100, the maximum inject time was set at 150, each 10 microscans were combined to a single scan. For the IS approach, the *m/z* range was set from 275 to 4000, the S-lens RF level was set at 40, the maximum inject time was set at 200 ms and each 10 microscans were combined to a single scan. Raw data were processed using the Thermo Xcalibur 2.2 software; the SWARM software was used to extract ion intensities, calculate CoM values and construct reaction progress curves (https://github.com/pkitov/CUPRA-SWARM). To carry out the enzyme-catalyzed hydrolysis reactions, aliquots of stock solutions of enzyme, substrate(s) and IS (where applicable) were mixed with 200 mM aqueous ammonium acetate (pH 6.7) in an Eppendorf tube, vortexed and then transferred to the nanoESI tip. ESI mass spectra were collected continuously starting at 3 min reaction time (the minimum time to prepare and load the sample into the tip). All measurements were carried out at pH 6.7 and 25 °C.

4.2.7 Hydrophilic interaction-ultra high performance liquid chromatography (HILIC) analysis of *N*-glycans

PSA *N*-glycans were released enzymatically (PNGase F), isolated as a mixture, labeled with 2-aminobenzamide (2-AB) and analyzed by hydrophilic interaction-ultra high performance liquid chromatography (HILIC) on a Thermo Scientific™ Vanquish™ UHPLC system coupled with fluorescent (Thermo Scientific, Waltham, MA, USA) and ESI-MS detectors (Thermo Q Exactive Orbitrap).

***N*-glycan extraction.** *N*-glycans were released from the standard PSA (before and after treatment of NEUS) using PNGase F (New England BioLabs, MA, USA) following the vendor's protocol. Briefly, denaturing buffer (0.5 % SDS, 40 mM DTT) was added to 15 µg of PSA and the solution was heated for 10 min at 100 ^{o}C. After cooling the PSA solution on ice, GlycoBuffer 2 (sodium phosphate, 50 mM), NP-40 and PNGase F were added to the solution. The mixture was then incubated at 37 ^{o}C for 24 h. Protein was separated from the released glycans by centrifuging at 14000 g for 10 min (5 times, 200 µL of Milli-Q water was added each time) using Amicon Ultra-0.5 mL centrifugal filters (EMD Millipore, Billerica, MA, USA) with 30 kDa MW cut off. The supernatant containing *N*-glycans was collected, lyophilized and stored at -20 ^{o}C until needed.

***N*-glycan labeling.** The extracted *N*-glycans were labeled with 2-AB (Sigma-Aldrich Canada) using standard procedures.[44,45] Briefly, the dried *N*-glycans were dissolved in DMSO:acetic acid (70:30 v/v) solution containing sodium cyanoborohydride (Sigma-Aldrich Canada) and 2-AB and incubated at 65 °C for 3.5 h. The solution was cooled to room temperature and purified using the acetone precipitation method.[46] 950 µL of acetone was added to each 50 µL of glycan solution (with fluorophore), vortexed and centrifuged at 18000 g for 10 min. The supernatant was discarded. This process was repeated twice. The pellet was dried under a N_2 stream and reconstituted with 25 µL of acetonitrile-water (75:25 v/v) for HILIC analysis.

HILIC-UPLC analysis. The 2-AB labeled glycans were analyzed by HILIC on a Thermo Scientific™ Vanquish™ UHPLC system coupled with fluorescent (FLD) detector (Thermo Scientific, Waltham, MA, USA) and ESI-MS (Thermo Q Exactive Orbittrap). Separation was carried out using a packed column (Waters, Glycan BEH Amide, 150x2.1 mm) filled with amide-bonded particles (size of 1.7 µm). Ammonium formate (100 mM, pH 4.5) and acetonitrile were used as mobile phases A and B. The flow rate was 0.2 mL/min with the following gradient: 0-46.5

min, 75-65% B; 46.5-80 min, 65-55% B; 80-104.6 min, 55-50% B. The column compartment temperature was 60ºC during the runs. The injection volume was 4 µL. For the fluorescent detection the excitation and detection wavelengths were at λ_{ex} = 330 and λ_{em} = 420 nm, respectively. The following parameters were used for MS detection: capillary temperature, 275 °C; probe heater temperature, 250 °C; sheath gas flow rate, 40 arb; aux gas flowrate, 10 arb; spray voltage, 3.5 kV. The analyses were performed in positive acquisition mode with *m/z* range of 250-3000. The maximum injection time was 100 ms, the AGC target was set to 1E6. Mass spectra were acquired at resolution of 70000 and each 10 microscans were combined to a single scan. MS spectra were recorded and processed using Xcalibur (Thermo, Version 4.1).

The glycan composition of each peak identified by HILIC analysis was preliminarily assigned according to the MS, MS/MS data with the aid of the Glycoworkbench software and known biosynthetic pathways of *N*-glycans.[47] The structures of separated isomers were then assigned according to the measured retention times (known as Glucose Unit (GU)).[48,49] In addition to the GU, the linkage of the sialic acid were confirmed by treating the glycans with NEUS which specifically cleaves α2-3-linked sialic acid residues. For each glycan in the mixture, the fractional abundance was determined from relative fluorescent signal in the chromatogram.

4.2.8 CUPRA-ZYME

To implement the CUPRA-ZYME assay, the time-dependent concentrations of the CUPRA substrate (CS) and product (CP) were calculated from the total, charge-state normalized abundances of the gas-phase ions corresponding to $^{Uni}P_{proxy}$ bound non-covalently to CS and CP (*Ab*($^{Uni}P_{proxy}$+CS) and *Ab*($^{Uni}P_{proxy}$+CP), respectively), measured by ESI-MS, and the known initial CS concentration ($[CS]_0$), eqs 4.1a and 4.1b:

$$[\mathrm{CP}]_t = \frac{[\mathrm{CS}]_0 \, Ab_t(^{\mathrm{Uni}}\mathrm{P}_{\mathrm{proxy}} + \mathrm{CP})}{Ab_t(^{\mathrm{Uni}}\mathrm{P}_{\mathrm{proxy}} + \mathrm{CS}) + Ab_t(^{\mathrm{Uni}}\mathrm{P}_{\mathrm{proxy}} + \mathrm{CP})} \tag{4.1a}$$

$$[\mathrm{CS}]_t = \frac{[\mathrm{CS}]_0 \, Ab_t(^{\mathrm{Uni}}\mathrm{P}_{\mathrm{proxy}} + \mathrm{CS})}{Ab_t(^{\mathrm{Uni}}\mathrm{P}_{\mathrm{proxy}} + \mathrm{CS}) + Ab_t(^{\mathrm{Uni}}\mathrm{P}_{\mathrm{proxy}} + \mathrm{CP})} \tag{4.1b}$$

Progress curves (fractional abundance of product CP versus time) were constructed from the time resolved ESI mass spectra. The fractional abundance of CP ($f_{\mathrm{CP,t}}$) was calculated fraction determined by eq 4.1c:

$$f_{\mathrm{CP},t} = \frac{[\mathrm{CP}]_t}{[\mathrm{CS}]_t + [\mathrm{CP}]_t} \tag{4.1c}$$

4.2.9 Center-of-Mass Monitoring (CoMMon)

Where indicated, CoMMon was used to process PSA mass spectra to obtain progress curves and calculation of %α23PSA. Complete details of CoMMon and its implementation was discussed in Chapter 3. Briefly, the time-dependent fraction (f_t) of Neu5Ac on PSA during the neuraminidase hydrolysis reaction was calculated by eq 4.2a:

$$f_t = \left| (\mathrm{CoM}_0 - \mathrm{CoM}_t)/(\mathrm{CoM}_0 - \mathrm{CoM}_\infty) \right| \tag{4.2a}$$

where CoM_t is the center-of-mass (CoM) value of PSA at reaction time t; CoM_0 and CoM_∞ represent the initial and final CoM values, respectively. The value of CoM_0 was established prior to addition of neuraminidase; CoM_∞ represents the CoM of asialo-PSA obtained by treatment with NEUC. The CoM_t was determined by eqs 4.2b and 4.2c:

$$\mathrm{CoM}_t = \sum_i f_{i,t} \mathrm{MW}_{i,t} \tag{4.2b}$$

$$f_{i,t} = \frac{\sum_{\mathrm{n}} Ab_i \, (\mathrm{MW}_{i,t})^{\mathrm{n}+}}{\sum_i \sum_{\mathrm{n}} Ab_i \, (\mathrm{MW}_{i,t})^{\mathrm{n}+}} \tag{4.2c}$$

i corresponds to a specific glycan composition (at reaction time *t*) with $MW_{i,t}$ and fractional abundance $f_{i,t}$ (which is calculated from the total, charge-state (n) normalized relative abundances (Ab_i) of the corresponding gas-phase ions.

The fraction of α2-3linked Neu5Ac in PSA (%α23PSA) was calculated by eq 4.2d:

$$\%\alpha23PSA = \left|(CoM_0 - CoMs)/(CoM_0 - CoM_\infty)\right| \quad (4.2d)$$

where CoMs represent the final CoM value of PSA treated by NEUS (to remove all α2-3-linked Neu5Ac) and CoM_∞ represent the final CoM value of asialo-PSA obtained by treatment with NEUC (to remove all Neu5Ac).

4.2.10 Determination of initial rates and relative initial rates

Initial rates (v_0), where reported, were determined from a linear best fit of the reaction progress curve using data acquired from reaction times of 3 min to 6 min. These values were further used for the determination of relative initial rate of PSA through comparison between the initial rate of PSA and CS_{3SLNAc}, eq 4.3:

$$v_{rel} = \frac{v_{0,PSA}}{v_{0,CS}} \quad (4.3)$$

where v_{rel} represent the relative initial rate between the initial rate of both 23PSA and 26PSA (i.e., $v_{0,PSA}$) and a reference CS_{3SLNAc} (i.e., $v_{0,CS}$).

4.2.11 Internal standard (IS) approach

Where indicated, CoMMon was implemented in the presence of isotopically labeled Neu5Ac (Neu5Ac-$^{13}C_3$), which served as an IS to quantify the time-dependent concentration of released (by NEUS) 2,7-anhydro-Neu5Ac. Based on the control experiments performed in the current study, the ESI-MS response factors for 2,7-anhydro-Neu5Ac and $^{13}C_3$-Neu5Ac are indistinguishable, within experimental error. The time-dependent progress curve (fractional concentration of 2,7-

anhydro-Neu5Ac) was cacluated from the abundance ratio of 2,7-anhydro-Neu5Ac and $^{13}C_3$-Neu5Ac:

$$f_{2,7anhydro-Neu5Ac} = \frac{Ab(\text{2,7anhydro-Neu5Ac}) + Ab(\text{2,7anhydro-Neu5Ac}^{Na})}{Ab(\text{Neu5Ac-}^{13}\text{C}_3) + Ab(\text{Neu5Ac-}^{13}\text{C}_3^{Na})} \quad (4.4)$$

where *Ab*(2,7-anhydro-Neu5Ac) and *Ab*(2,7-anhydro-Neu5Ac^{Na}) are the gas-phase abundances of protonated and sodiated 2,7-anhydro-Neu5Ac ions, respectively. *Ab*(Neu5Ac-$^{13}C_3$) and *Ab*(Neu5Ac-$^{13}C_3^{Na}$) are the gas-phase abundances of protonated and sodiated Neu5Ac-$^{13}C_3$ ions.

4.2.12 Quantification of NEUS substrate specificity

The specificity of the NEUS enzyme for PSA *N*-glycans with α2-3- and α2-6-linked Neu5Ac was quantified using the CUPRA-ZYME assay. Details of the assay are described in Chapter 3.[41] The time-dependent Competitive Universal Proxy Receptor Assay (CUPRA) substrate (CS) and product (CP) concentrations were determined from the relative abundances of CS and CP bound to a universal proxy protein ($^{Uni}P_{proxy}$) as measured by ESI-MS.[42] PSA protein samples containing all α2-3- or all α2-6-linked Neu5Ac (denoted as 23PSA and 26PSA, correspondingly) and CUPRA substrates CS_{3SLNAc} and CS_{6SL} were prepared as described in Chapter 2 and elsewhere.[41] Human carbonic anhydrase (HCA, type 1) was used as $^{Uni}P_{proxy}$. Briefly, NEUS enzyme was added to aqueous ammonium acetate solutions (200 mM, pH 6.7 and 25 ºC) of CS_{3SLNAc} (5 μM), CS_{6SL} (5 μM), $^{Uni}P_{proxy}$ (5 μM) and 23PSA protein standard (5 μM) or 26PSA protein standard (5 μM). An aliquot of each solution was injected into a nanoESI tip and mass spectra were continuously acquired (acquisition rate of 1 min^{-1}) for reaction times (*t*) from 3 min (the minimum time needed to load the tip and initiate spray) to 90 min. The reaction progress curves, reported as fraction of substrate converted to product (eqs 4.1a-c), were constructed from the time-dependent mass

spectra, as described in the previous section. Details of the experimental conditions and data analysis procedures are provided as following:

Aqueous ammonium acetate solutions (200 mM, pH 6.7 and 25 ºC) of NEUS (~0.18 μM), CS_{6SL} (5 μM), CS_{3SLNAc} (5 μM), $^{Uni}P_{proxy}$ (hCA, 5 μM) with 23PSA (5 μM, Figure 2a) or 26PSA (5 μM, Figure 2b) were prepared and mass spectra were collected for reaction times from 3 min to 90 min. The resulting data were analyzed using eqs 4.1a-c (for CUPRA substrate) and eqs 4.2a-d (for 23PSA and 26PSA) to construct progress curves. The initial rates for CS and 23PSA/26PSA were determined from best linear fits of progress curves from reaction times of 3 min to 6 min. Relative initial rate (23PSA/CS_{3SLNAc} and 26PSA/CS_{3SLNAc}) were calculated by eq 4.3.

4.2.12 Statistical analysis

The fractional α2-3-linked Neu5Ac content (%α23PSA) of PSA extracted from serum samples from low-risk (GG1), intermediate-risk (GG2), and high-risk (GG3,4,5) PCa patients was calculated using eq 4.2d. The mean %α23PSA and the corresponding 95% confidence interval values were calculated for each group. Receiver operating characteristics (ROC) curves were generated based on %α23PSA for distinguishing between low-risk (GG1) and clinically significant (GG2-5) disease, and then between low-risk and high-risk (GG3-5) disease. Youden's J-index analysis was used to generate the %α23PSA cut-offs for each comparison. Intergroup differences were statistically analyzed by a Student's t-test for normally distributed variables. In all statistical analyses, the significance level was set at $p<0.05$ and assuming no normality distributions.

4.3 Results and Discussion

4.3.1 Validation of CoMMon using NEUC desialylation of glycoproteins

An overview of the workflow for the top-down native MS/CoMMon method for quantifying the α2-3- and α2-6-linked Neu5Ac content of serum PSA, extracted using anti-PSA antibody, is provided in Figure 4.3 (with a recovery rate of 77.8% ± 2.9%, Figure 4.2). The assay is based on changes in the center-of-mass (CoM) of intact PSA (as measured by native MS and CoMMon)[40] upon treatment with a α2-3-linked Neu5Ac specific neuraminidase, followed by a non-specific neuraminidase (which can remove both α2-3- and α2-6- linked Neu5Ac). NEUS enzyme from *Streptococcus pneumonia* (NanB subtype) was used to selectively remove α2-3-linked Neu5Ac;[50,51] while the NEUC enzyme, a neuraminidase from *Clostridium perfringens* (NanI subtype), served as the non-specific neuraminidase to remove all Neu5Ac (both α2-3-linked and α2-6-linked Neu5Ac on the Asn-69 of PSA protein).[50] The fraction of α2-3-linked Neu5Ac (denoted as %α23PSA) was calculated as the ratio of the CoM change upon treatment with NEUC to the CoM change resulting from combined treatment with NEUC and NEUS (eqs 4.2a-d).

The reliability of the assay for quantifying the relative amount of Neu5Ac on PSA that is α2-3-linked and α2-6-linked Neu5Ac depends critically on the specificity of NEUS (the approach requires near absolute specificity for α2-3-linked Neu5Ac) and accurate measurements of change of Neu5Ac content using the native MS/CoMMon approach. We assessed the relative specificity of NEUS for α2-3- and α2-6-linked Neu5Ac on PSA from the initial rates (determined using time-resolved native MS/CoMMon) for the enzyme-catalyzed hydrolysis of 23PSA 26PSA, measured in the presence of CS_{3SLNAc} and CS_{6SL}. The time-dependent concentrations of CS_{3SLNAc} and CS_{6SL} and their corresponding CUPRA products (CP_{LNAc} and CP_{Lac}, respectively) were measured using CUPRA-ZYME. The accuracy of the %α23PSA values measured by the native MS/CoMMon

approach was assessed by comparison with the results of relative Neu5Ac content of PSA obtained using an internal standard (IS) approach and from a bottom-up LC-MS approach, wherein *N*-glycans were released from PSA before or after enzyme treatment (with NEUS or NEUC), labeled with 2-AB and analyzed by HILIC.

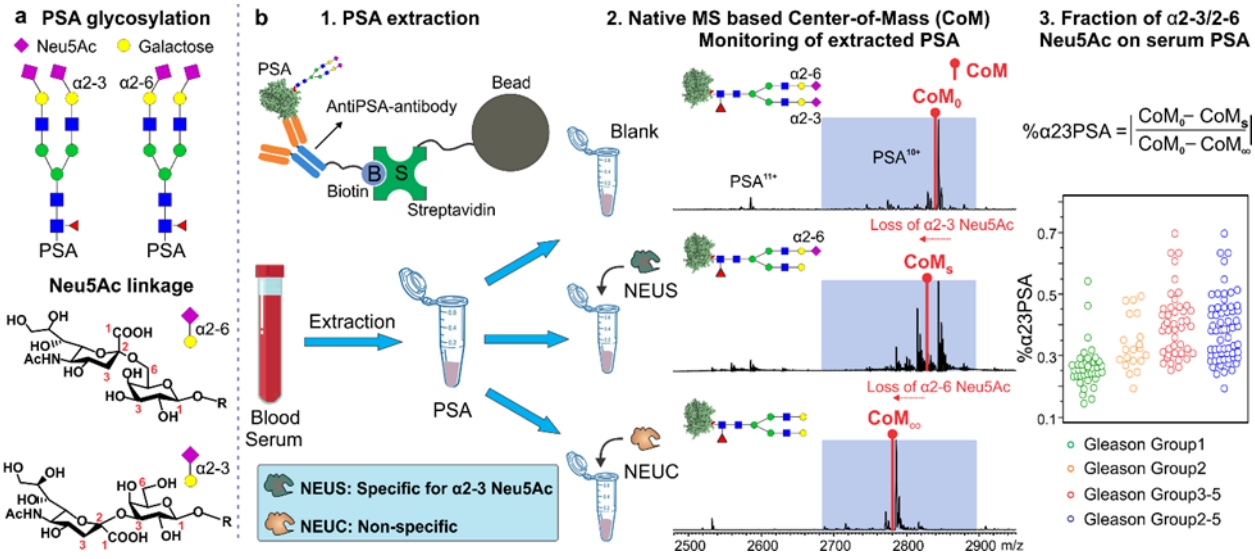

Figure 4.3. (a) Two possible PSA glycoforms corresponding to a biantennary N-glycan with either α2-3- and α2-6-linked Neu5Ac (top) and the chemical structures of α2-3- and α2-6-linked (to galactose) Neu5Ac (bottom). (b) Workflow of the dual neuraminidase-assisted top-down native MS/CoMMon assay: 1. Extraction of PSA from blood serum using an anti-PSA antibody. 2. Mass spectra analysis of extracted PSA, following treatment with NEUS or treatment with NEUC. 3. Quantification of α2-3linked Neu5Ac content (%α23PSA) of extracted PSA (from PCa patient serum) using centre-of-mass (CoM) changes resulting from NEUS/NEUC treatment determined from the mass spectra by CoMMon.

4.3.2 NEUS specificity for α2-3- and α2-6-linked Neu5Ac

Differences in the Neu5Ac linkage specificities of NEUC and NEUS enzymes are key to the performance of our newly developed assay. As shown by our laboratory and others, NEUC catalyzes the hydrolysis of both α2-3- and α2-6-linked Neu5Ac, albeit with a preference for α2-3-linked Neu5Ac.[40,52] In contrast, NEUS is highly specific for glycans with α2-3-linked Neu5Ac.[50,51] However, its relative activity towards α2-6-linked Neu5Ac in PSA has not be definitively established. To determine the relative activity of NEUS for α2-3- and α2-6-linked Neu5Ac CUPRA-ZYME was performed on the 23PSA and 26PSA standards. These measurements were carried out in the presence of the CUPRA substrates CS_{3SLNAc} and CS_{6SL} (Figure 4.1), and using hCA as the $^{Uni}P_{proxy}$. Time-resolved mass spectra were acquired continuously at reaction times (*t*) from 3 min (the minimum time required to load the tip and initiate spray) to 90 min. Shown in Figures 4.4a and 4.4b are the representative ESI mass spectra measured for aqueous ammonium acetate solutions (200 mM, pH 6.7 and 25 ºC) of NEUS, CS_{6SL}, CS_{3SLNAc}, $^{Uni}P_{proxy}$ with 23PSA (Figure 4.4a) or 26PSA (Figure 4.4b).

Substrate (NEUS)	CS_{3SLNAc}	23PSA	CS_{6SL}	26PSA
Initial rate	0.0657	0.0334	0.0002	0.0001
Relative initial rate	1.00	0.5079	0.0031	0.0014
Initial rate	0.0689	0.0349	0.0002	0.0001
Relative initial rate	1.00	0.5065	0.0029	0.0014
Initial rate	0.0701	0.0363	0.0003	0.0001
Relative initial rate	1.00	0.5178	0.0042	0.0014
Average relative initial rate	1.00±0.00	0.510±0.023	0.0034±0.0005	0.0014±0.0002

a. Error corresponds to one standard deviation; measurements performed in triplicates.

Table 4.1. Initial rate and relative initial rate (relative to CS_{3SLNAc}) for the hydrolysis of Neu5Ac from four substrates by NEUS. Initial rate was determined by linear fitting of the first four data points (reaction times 3 min to 6 min).[a]

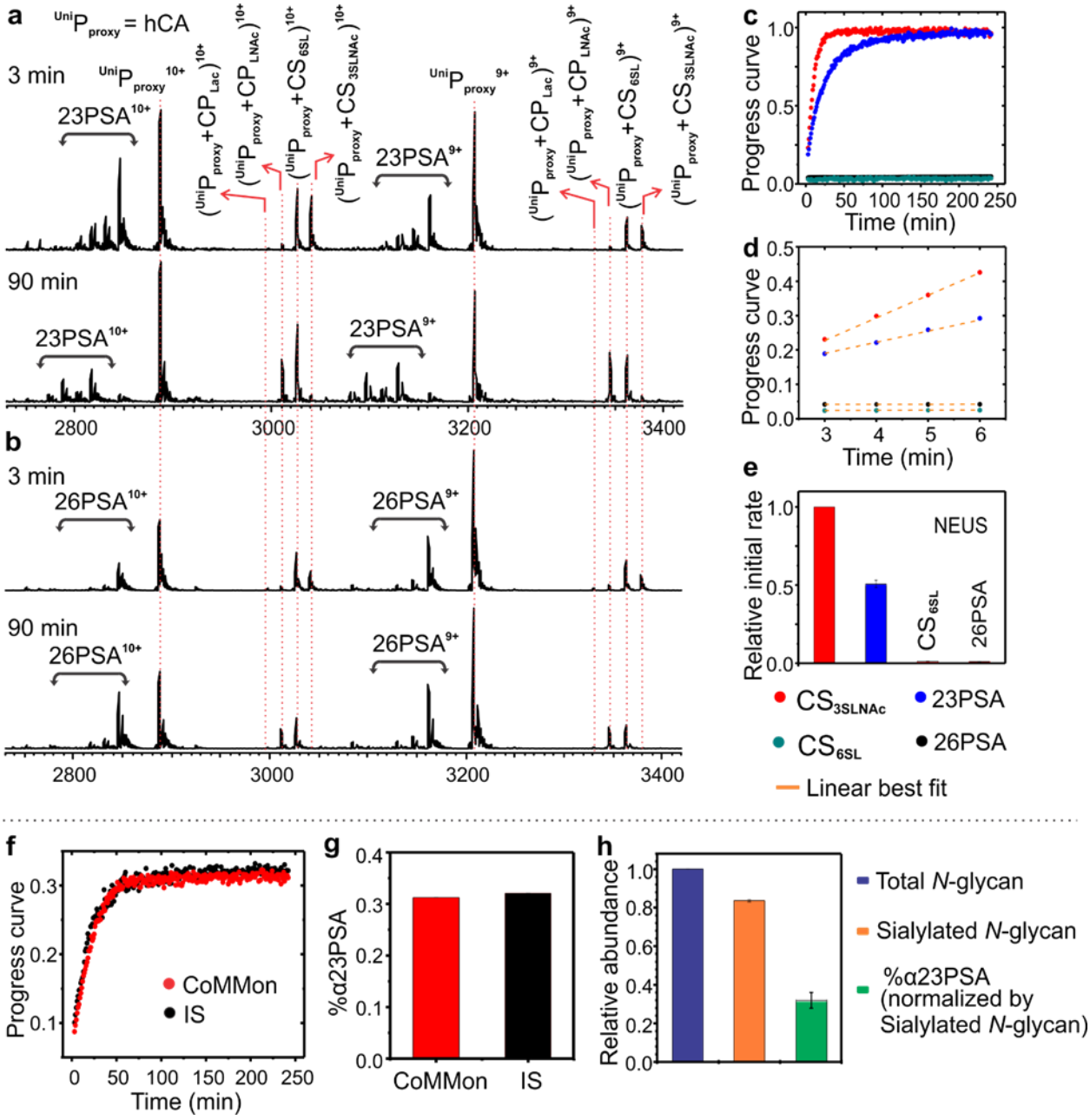

Figure 4.4. Representative mass spectra acquired for aqueous ammonium acetate solutions (200 mM, pH 6.7 and 25 °C) containing NEUS (0.18 μM), hCA (5 μM), CS_{3SLNAc} (5 μM), CS_{6SL} (5 μM), (a) 23PSA (5 μM) and (b) 26PSA (5 μM) at reaction time 3 min and 90 min. (c) Progress curves (fractional abundance of product) for CS_{3SLNAc}, CS_{6SL}, 23PSA and 26PSA. (d) Determination of initial rates by linear fitting of the first 4 data points (from reaction time 3 to 6 min). (e) Relative initial rate (normalized to CS_{3SLNAc}) of CS_{3SLNAc}, CS_{6SL}, 23PSA and 26PSA.

Protonated ions of $^{Uni}P_{proxy}$ bound to CUPRA product CP_{LNAc} and also ions of asialo-PSA can be observed in the mass spectra shown in Figure 2a indicating that NEUS cleaves the α2-3 Neu5Ac from both CS_{3SLNAc} and 23PSA. In contrast, no desialylation products of CS_{6SL} and 26PSA were observed (Figure 4.4b), showing that NEUS has almost no activity towards α2-6 Neu5Ac. (f) Progress curves (fractional abundance of product) for PSA determined by CoMMon (red circles) and using $^{13}C_3$-Neu5Ac as an IS (black circles). (g) Comparison of %α23PSA determined by CoMMon and IS. (h) Relative abundance of all sialylated *N*-glycans and α2-3 Neu5Ac containing *N*-glycans (%α23 PSA) based on HILIC-UPLC results (relative abundance of α2-3 Neu5Ac containing *N*-glycans was normalized to abundance of all sialylated *N*-glycans).

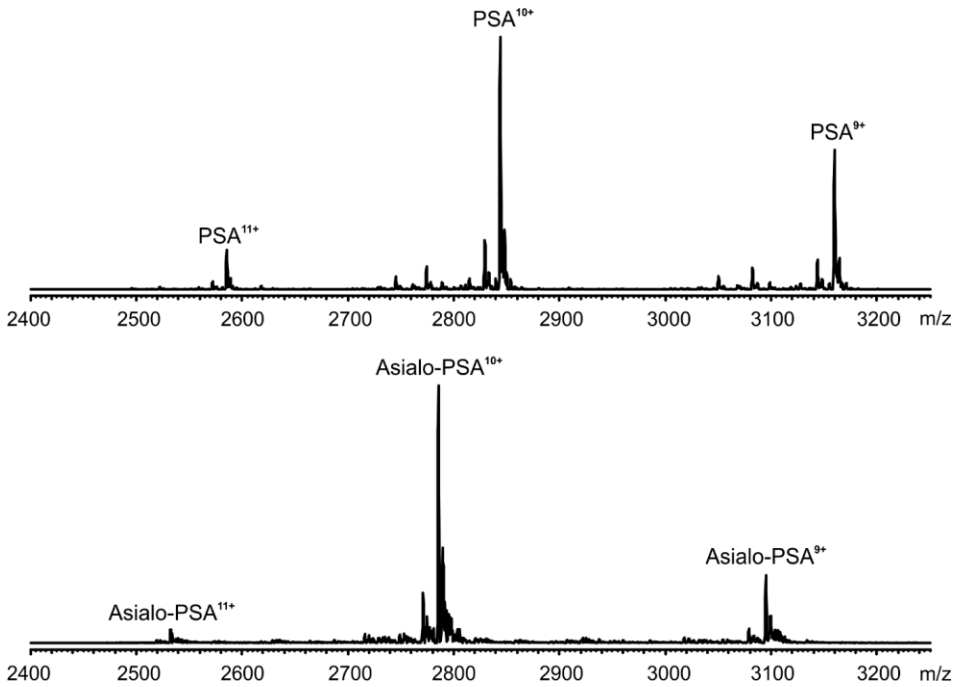

Figure 4.5. Representative ESI mass spectra acquired for an aqueous ammonium acetate solution (200 mM, pH 6.7 and 25 ºC) of PSA (5 μM, top) and asialo-PSA (5 μM, bottom, prepared by incubating PSA with NEUC).

NEUS enzyme specificity for α2-3- and α2-6-linked Neu5Ac *N*-glycans was quantified using the reaction progress curves (Figure 4.4c). For the CS (CS_{3SLNAc} and CS_{6SL}), the progress curves were calculated using eqs 4.1a-c, while for 23PSA and 26PSA, the curves were constructed using the CoMMon method (eqs 4.2a-d), which monitors the time-dependent decrease in PSA *m/z* to the loss of Neu5Ac. The initial and final CoM values (CoM_0 and CoM_∞, respectively) were determined from the mass spectra of PSA and asialo-PSA (Figure 4.5). As expected, only CS_{3SLNAc} and 23PSA underwent hydrolysis in the presence of NEUS. Based on relative (normalized to CS_{3SLNAc}) initial rates (Figure 4.4d, Table 4.1, calculated by eq 4.3), NEUS-catalyzed hydrolysis of CS_{3SLNAc} is 290-fold faster than CS_{6SL}; 23PSA hydrolysis is 360-fold faster than 26PSA (Figure 4.4e). From these results, it is concluded that the use of NEUS to effect complete removal of α2-3-linked Neu5Ac from PSA will result in the fractional (percentage) loss of <0.002 (<0.2%) of the α2-6-linked Neu5Ac, which falls within three standard deviations from the mean value of relative abundance of α2-3 Neu5Ac determined by top-down native MS approach (0.0024, see below).

4.3.3 Fractional content of α2-3-linked Neu5Ac on PSA measured by top-down, bottom up and IS MS methods.

To demonstrate the reliability of the top-down native MS/CoMMon assay for quantifying α2-3 Neu5Ac content in PSA, hydrolysis kinetics measurements were performed on the commercial PSA sample in the presence of $^{13}C_3$-Neu5Ac, which served as an internal standard (IS). Unlike most neuraminidases, NEUS produces the 2,7-anhydro-Neu5Ac product, rather than Neu5Ac, from substrates containing α2-3-linked Neu5Ac (Figure 4.1). However, according to the results of control experiments performed in the current study (Figure 4.6), the ESI-MS response factors of

$^{13}C_3$-Neu5Ac and 2,7-anhydro-Neu5Ac are indistinguishable (within experimental error). Notably, the progress curves for the NEUS-catalyzed hydrolysis of a commercial PSA sample measured by native MS/CoMMon and the IS MS method (eq 4.4) are nearly indistinguishable (Figure 4.4f, representative mass spectra are shown in Figure 4.7a) and reach limiting fractional values of %α23PSA that are in excellent agreement (Figure 4.4g, 0.3164 ± 0.0024 for top-down native MS; 0.3205 ± 0.0012 for IS approach, Table 4.2).

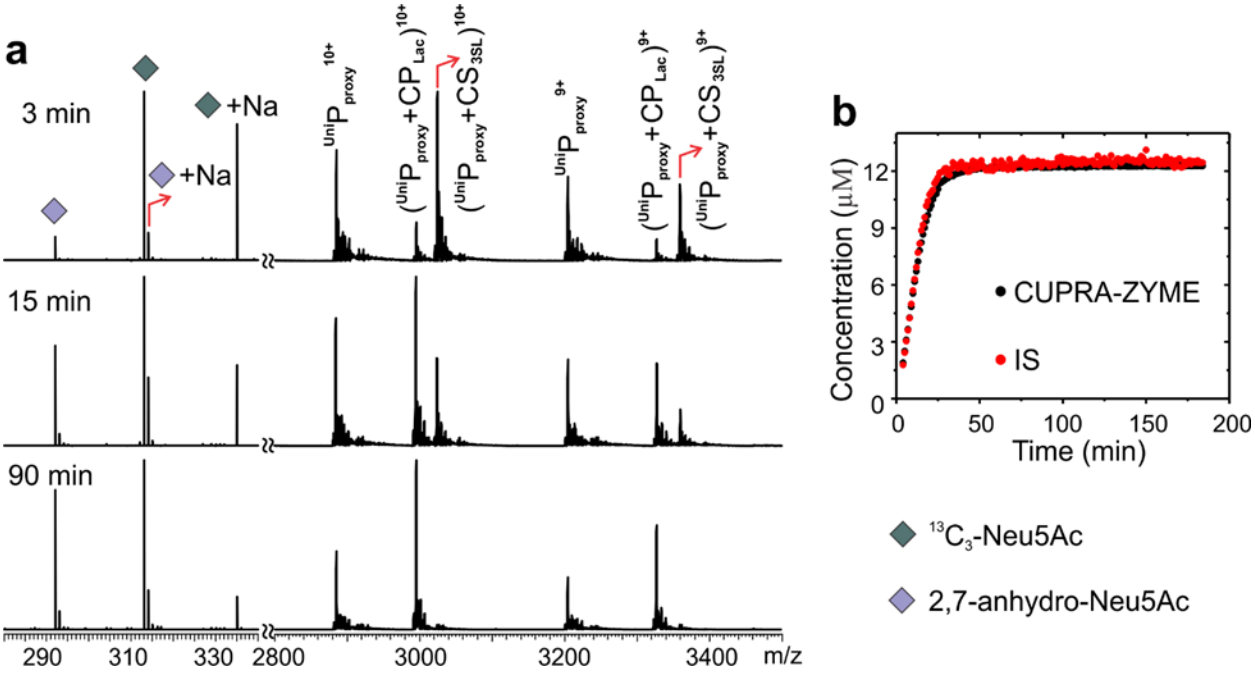

Figure 4.6. (a) Representative ESI mass spectra acquired for an aqueous ammonium acetate solution (200 mM, pH 6.7 and 25 ºC) of NEUS (~0.18 μM), hCA (5 μM, top), CS_{3SL} (12.5 μM) and $^{13}C_3$-Neu5Ac (15 μM) measured at 3 min, 15 min and 90 min. (b) Enzymatic progress of product (CP_{Lac}, which also equals to 2,7-anhydro-Neu5Ac) constructed by CUPRA-ZYME (black circle) and IS (red circle).

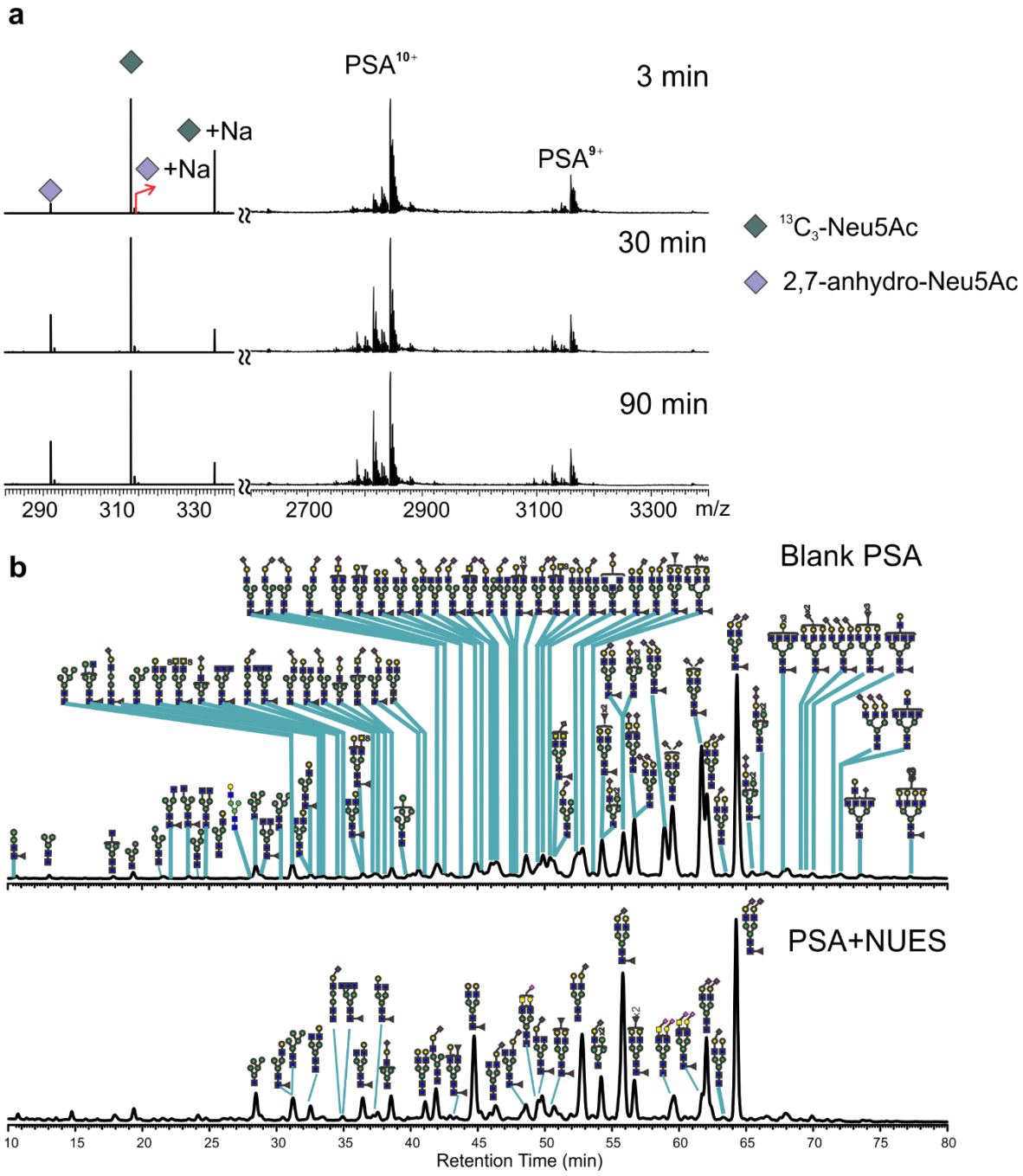

Figure 4.7. (a) Representative mass spectra acquired for aqueous ammonium acetate solutions (200 mM, pH 6.7 and 25 ºC) containing NEUS (0.18 μM), PSA (2 μM) and IS (2.5 μM) at reaction time 3, 30 and 90 min. (b) Analysis of *N*-glycans released from standard PSA before and after treatment with NEUS by HILIC-UPLC coupled with fluorescent and ESI-MS detectors.

Methods	Relative abundance of α2-3 Neu5Ac
top-down native MS/CoMMon	0.3164 ± 0.0008
IS	0.3205 ± 0.0004

a. Error corresponds to one standard deviations; measurements performed in triplicates.

Table 4.2. Relative abundance of α2-3 Neu5Ac (relative to all sialylated *N*-glycans) in commercial PSA sample determined by top-down native MS/CoMMon and IS approaches.[a]

The α2-3-linked Neu5Ac content of the commercial PSA sample was also quantified using a bottom-up LC-MS approach, wherein *N*-glycans released from the PSA sample, before and after treatment with NEUS, were labeled with a fluorophore (2-AB) and analyzed by HILIC-UPLC coupled with fluorescence and ESI-MS detection. LC-MS analysis identified 85 distinct PSA *N*-glycans (Figure 4.7b and Table 4.3), corresponding predominantly to fucosylated bi-antennary desialylated *N*-glycans ((31.37 ± 2.89)%). Tri- and tetra-antennary complex-type *N*-glycans were also present, although at low abundances ((2.90 ± 0.12)% and (0.84 ± 0.21)%, respectively), in agreement with previously published results.[53,54] Of the 85 *N*-glycans, 49 are sialylated, containing from one to three Neu5Ac residues; sialylated *N*-glycans contribute (83.6 ± 0.6)% to total abundance of the detected *N*-glycans. The α2-3 Neu5Ac content of the PSA sample, found from analysis of the *N*-glycans before and after treatment with NEUS, was 0.322 ± 0.120 (Figure 2h and Table 4.4). This value is in excellent agreement with the values obtained by the top-down native MS and IS methods. Together, the results of these analyses demonstrate that our top-down native MS/CoMMon assay is able to accurately quantify the α2-3 Neu5Ac content (%α23PSA) in PSA.

RT (min)	Putative Structure	Relative abundance	Relative abundance	Relative abundance
10.38	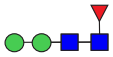	0.04	0.15	0.35
13.04/15.7	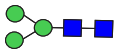	0.28	0.88	0.74
17.83	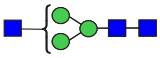	0.15	0.20	0.19
19.31	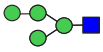	0.45	0.73	0.67
21.58	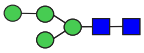	0.22	0.10	0.11
24.11	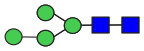	0.08	0.13	0.17
22.13	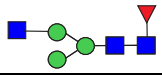	0.03	0.13	0.10
23.45	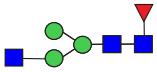	0.22	0.11	0.16
24.73	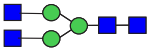	0.14	0.14	0.18
27.26	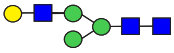	0.08	0.02	0.03
28.1	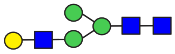	0.08	0.18	0.14
28.46	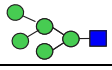	1.14	1.66	1.68
28.8	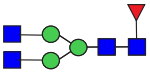	0.28	0.27	0.30
30.43/31.18 33.21	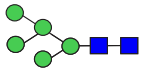	1.16	1.02	1.04
32.55	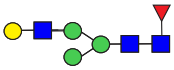	0.17	0.14	0.18
31.18	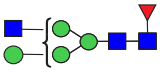	0.24	0.18	0.20
32.55	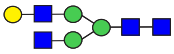	0.17	0.13	0.18
33.49	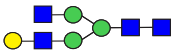	0.12	0.09	0.21
32.13	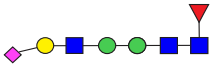	0.07	0.17	0.06
33.21	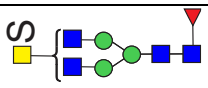	0.06	0.00	0.00
33.49	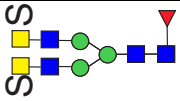	0.05	0.04	0.08
34.73	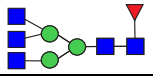	0.04	0.05	0.05

34.98	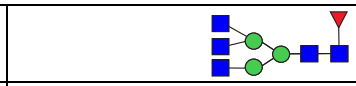	0.03	0.03	0.04
34.73/38.61	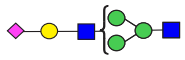	0.80	1.26	1.25
34.98	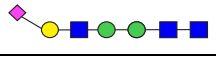	0.17	0.20	0.24
36.45	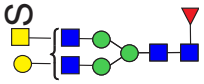	0.07	0.17	0.15
36.45	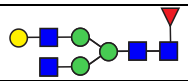	0.32	0.82	0.74
37.44	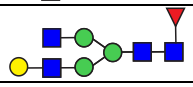	0.26	0.12	0.16
37.33	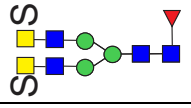	0.45	0.12	0.16
37.15	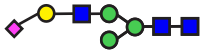	0.03	0.07	0.05
38.18	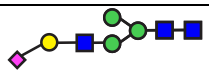	0.09	0.16	0.25
41.06	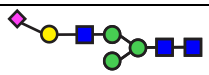	0.02	0.01	0.02
41.98	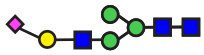	0.43	0.46	0.50
38.61		0.17	0.28	0.27
39.83/41.98		1.03	1.01	1.11
40.6	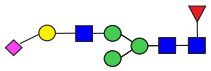	0.88	0.91	0.84
41.98	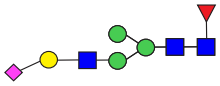	0.11	0.11	0.12
42.52	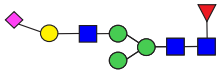	0.02	0.01	0.01
46.03	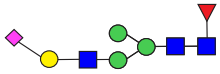	1.09	0.29	0.32
41.06	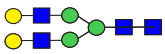	0.11	0.10	0.16
41.98	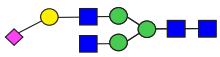	0.51	0.55	0.59
45.27/46.3	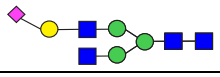	1.34	1.66	2.57
47.79	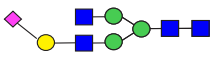	0.01	0.04	0.04
42.52	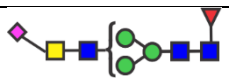	0.26	0.21	0.15

43.86	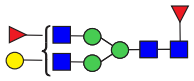	0.02	0.10	0.12
44.87/47.47	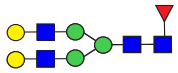	1.31	1.14	2.37
44.87	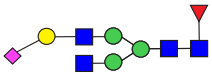	0.62	0.90	1.10
48.63	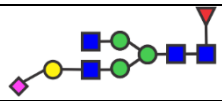	1.70	1.21	1.00
49.88	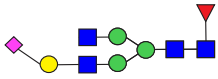	2.21	1.76	1.72
45.25	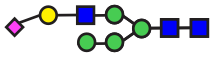	0.03	0.05	0.02
47.47	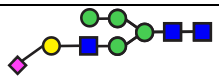	0.01	0.03	0.03
50.7	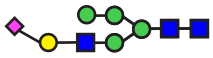	0.19	0.13	0.13
45.68/48.63 49.58	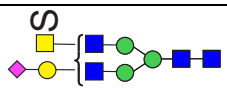	1.16	1.37	0.93
46.41	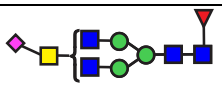	1.00	1.17	0.04
47.79/47.85	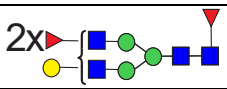	0.05	0.11	0.11
47.85/54.29 56.71	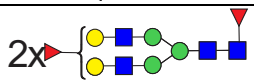	2.95	1.81	1.78
47.85/50.7 51.18/53.61	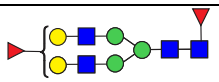	1.22	1.75	1.54
49.3/49.58	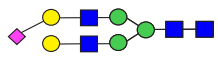	0.81	2.18	1.14
52.84	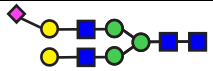	2.32	1.19	1.17
63.52	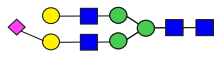	0.12	0.51	0.28
50.43/52.84 53.61	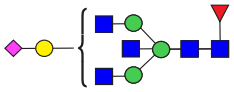	0.73	0.62	0.66
50.43/54.29	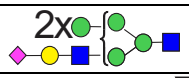	4.80	5.05	5.25
50.7	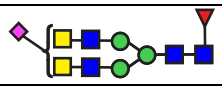	0.17	0.12	0.11
52.36	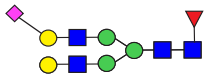	2.83	5.67	5.64
55.89	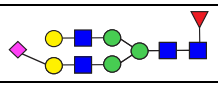	4.30	5.42	4.85

53.61	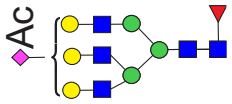	0.12	0.31	0.36
55.89	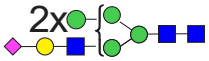	0.34	0.42	0.38
56.71	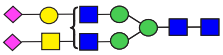	2.40	1.44	1.37
56.71	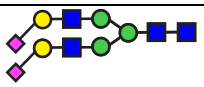	0.90	5.69	6.46
59.54	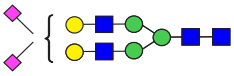	5.98	4.63	4.65
62.13	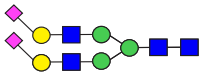	8.04	6.25	6.54
58.95	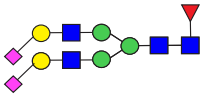	2.88	2.24	2.32
61.72	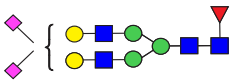	11.16	9.66	9.54
64.36	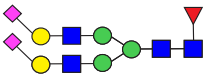	16.67	13.54	13.46
58.95	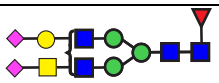	2.60	2.08	2.10
61.72	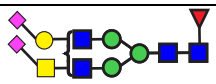	2.15	1.86	1.84
66.26	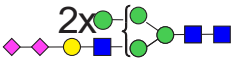	0.20	0.44	0.75
65.51/66.54	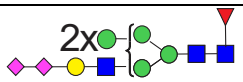	0.84	1.11	1.12
67.85	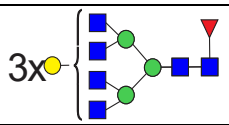	0.45	0.29	0.27
68.1/70.0	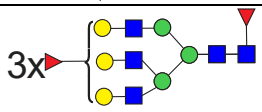	1.57	1.07	1.02
69.09	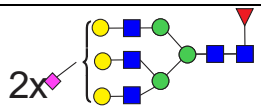	0.08	0.31	0.00
69.5/70.93 72.1/73.68 75.39/75.56	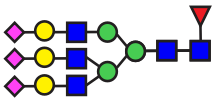	0.44	0.54	0.61
71.28/72.1	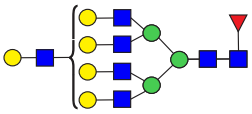	0.19	0.18	0.20
72.1	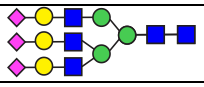	0.10	0.08	0.09

72.1	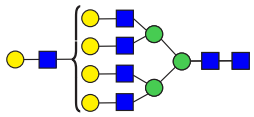	0.10	0.08	0.09
73.68	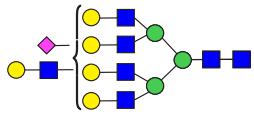	0.20	0.06	0.06
75.39/77.28 79.08	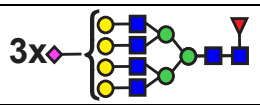	0.16	0.08	0.08
76.08	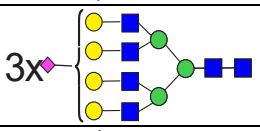	0.02	0.00	0.00
76.08	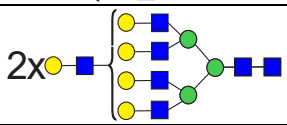	0.02	0.00	0.00

Table 4.3. Assignment of *N*-glycans released from commercial PSA labelled with 2-AB and analyzed by HILIC-UHPLC coupled with fluorescence and ESI-MS detectors. *N*-glycans and their structures are shown in order of increasing retention time (RT). Three replicates of relative abundances were measured.

	Relative abundance
Total *N*-glycans	1
***N*-glycans containing Neu5Ac**	0.8364±0.0063 (relative to Total *N*-glycans)
***N*-glycans Neu5Ac containing α2-3-linked Neu5Ac**	0.3139±0.0401 (relative to *N*-glycans containing Neu5Ac)

a. Error corresponds to one standard deviation; measurements performed in triplicates.

Table 4.4. Relative abundance of PSA *N*-glycans containing Neu5Ac (sialic acid) and *N*-glycans containing α2-3-linked Neu5Ac determined by HILIC-UPLC analysis.[a]

4.3.4 Quantifying %α23PSA of serum PSA for discrimination of low-risk (GG1), intermediate-risk (GG2), and high-risk (GG3/4/5) PCa

Following analytical validation of the top-down native MS method for quantifying the %α23PSA of PSA, the assay was applied to PSA extracted from serum samples obtained from PCa patients representing all risk types; patient cohort clinical information is provided in Table 4.5. Mass spectra of untreated PSA were used for calculation of CoM_0. Then PSA was incubated with NEUS to remove all α2-3 Neu5Ac (Figure 4.7a) to determine CoM at the end point (CoM_S), and with NEUC to remove all Neu5Ac residues from PSA to determine its CoM_∞ value. The fraction of α2-3-linked Neu5Ac in serum PSA (%α23PSA) was calculated using eq 4.2d.

Risk type	N (%)	Gleason Group	Positive Cores		PSA (ng/mL)
			No. Positive Cores	Patients (%)	
Low-risk	41 (40%)	GG1	1-2	16 (40%)	7.68±1.74
			3-4	14 (35%)	6.49±0.81
			≥5	9 (23%)	7.80±0.73
			Not determined	2 (5%)	0.41, 10.50
				Average	6.95±0.79
Intermediate-risk	20 (20%)	GG2	1-2 Cores	4 (25%)	12.71±5.63
			3-4 Cores	7 (35%)	8.29±2.67
			≥5 Cores	9 (45%)	6.24±1.03
				Average	8.25±1.52
High-risk	20 (20%)	GG3	1-2 Cores	2 (10%)	9.81, 14.0
			3-4 Cores	5 (25%)	9.85±3.00
			≥5 Cores	13 (65%)	16.74±4.08[a]
				Average	14.41±2.74
	19 (19%)	GG4	1-4 Cores	2 (11%)	6.0, 13.17
			≥5 Cores	17 (89%)	28.25±8.20
				Average	26.28±7.25
	2 (2%)	GG5	≥5 Cores	2 (100%)	17.3, 87.6
				Average	21.95±4.18

a. A denoted outlier of PSA=1436 ng/mL was removed.

Table 4.5. Patient Clinical Information.

The %α23PSA measured for PSA extracted from serum samples representing GG1-5 PCa patients are shown in Figure 4.7b. The data reveal an upper boundary maximum of 0.317 of α2-3 Neu5Ac (0.256±0.069, 0.233 to 0.278, 95% CI; N=41) in low-risk PCa (GG1) serum samples, consistent with other published data.[27] A significant increase in %α23PSA was found in intermediate-risk (GG2) (0.319±0.088, 0.282 to 0.416, 95% CI; N=20, $p < 0.001$), high-risk (GG3-5) (0.394±0.107, 0.308 to 0.454, 95% CI; N=41, $p < 0.001$) and intermediate plus high-risk (GG2-5) (0.379±0.107, 0.300 to 0.450, 95% CI; N=61, $p < 0.001$) PCa patient serum samples (Figure 4.7b). These results are novel and clinically relevant in that this assay is able to discriminate GG1 (low-risk) disease from GG2 (intermediate-risk) disease, which has not been previously achieved

and is a clinical need. Youden's J-index analysis of the receiver operating characteristic (ROC) curves in Figure 4.7c determined that a %α23PSA cut-off of 0.28 led to test sensitivity and specificity values of 84.9% and 85.0% respectively (Table 4.6) for identifying clinically significant PCa (GG2-5). This resulted in an AUC=0.875±0.038, 0.799 to 0.950, 95% CI for identifying clinically significant PCa (GG2-5, sensitivity and specificity of 85.5% and 84.6% respectively). While not clinically relevant, applying the same cut-off produced an AUC=0.905 when only identifying high-risk PCa (GG3-5). As anticipated, there was moderate sensitivity and specificity for discrimination between intermediate (GG2) and high-risk (GG3-5) PCa with an AUC of 0.681; although having strong discrimination between GG2 and GG3-5 is not clinically relevant.

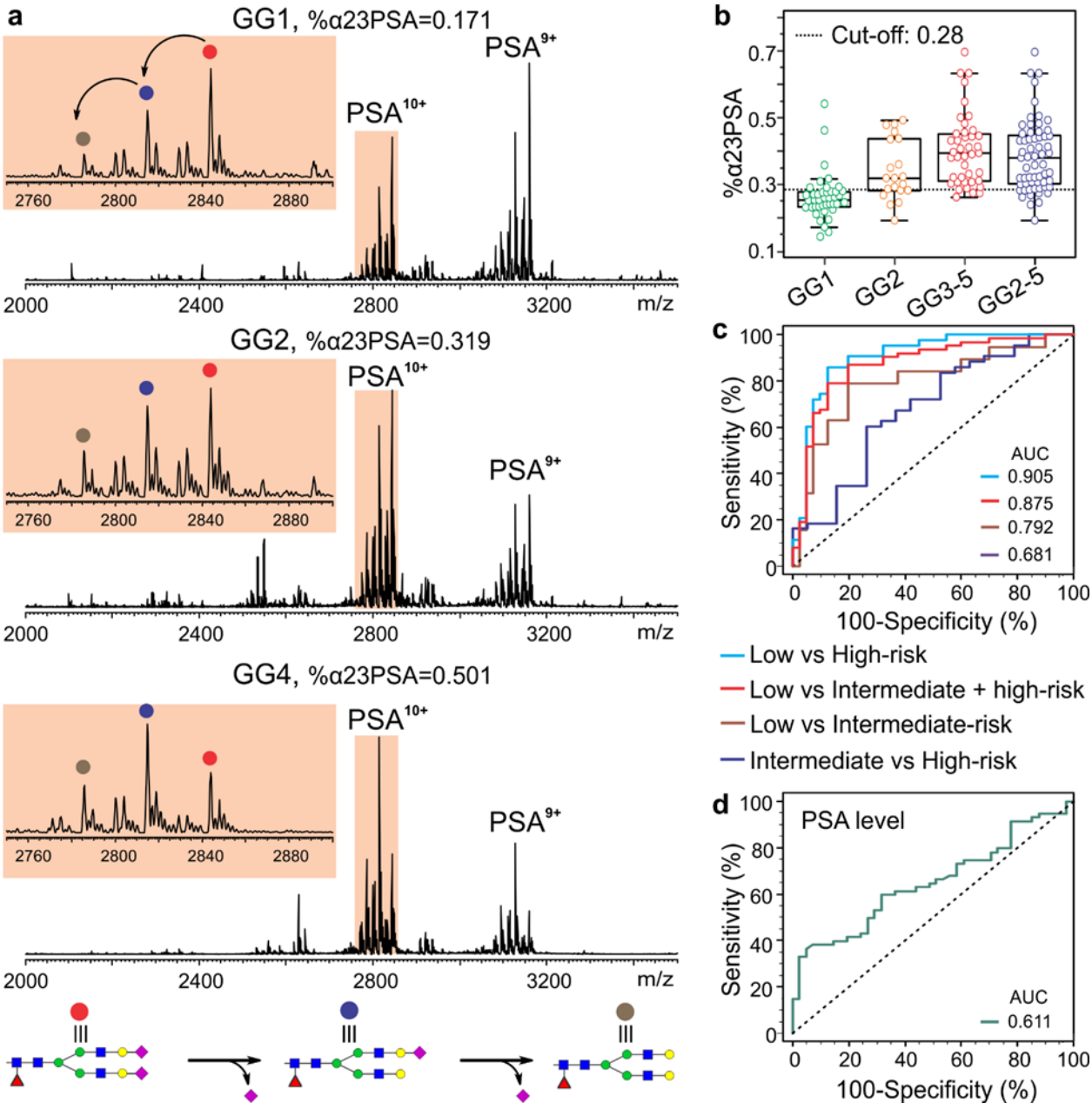

Figure 4.8. (a) Representative mass spectra of serum PSA from GG1, GG2 and GG4 PCa individuals. (b) Fractional abundance of α2-3 Neu5Ac (%α23PSA) of PSA from GG1 (low risk, green dot), GG2 (intermediate risk, orange dot), GG3-5 (high risk, red dot) and GG2-5 (intermediate & high-risk, blue dot) PCa serum samples. Errors represent 95% confidence interval (95% CI). (c) ROC analysis curves of %α23PSA in blood serum PSA for the discrimination of low vs high risk (GG1 vs GG3-5), low vs intermediate risk (GG1 vs GG2), low vs intermediate plus

high risk (GG1 vs GG 2-5), and intermediate vs high risk (GG2 vs GG3-5). Detailed ROC analysis results are shown in Table 4.6. (d) ROC analysis curve of serum PSA levels for the discrimination of low risk vs intermediate plus high risk (GG1 vs GG2-5).

	Sensitivity (%)	Specificity (%)	AUC	Criterion
Low vs High risk (GG1 vs GG3-5)	**86.0**	**87.5**	**0.905**	**0.291**
Low vs Intermediate & High risk (GG1 vs GG2-5)	**85.5**	**84.6**	**0.875**	**0.280**
Low vs Intermediate risk (GG1 vs GG2)	**78.9**	**80.0**	**0.792**	**0.280**
Intermediate vs High risk **(**GG2 vs GG3-5**)**	**60.5**	**73.7**	**0.681**	**0.360**
PSA level	**60.9**	**51.2**	**0.611**	**6.72ng/ml**

Table 4.6. Result of ROC curves for low vs high risk (GG1 vs GG3-5), low vs Intermediate & High risk (GG1 vs GG2-5), low vs intermediate risk (GG1 vs GG2), intermediate vs high risk (GG2 vs GG3-5) and PSA level.

In contrast, serum PSA levels as measured clinically via ELISA did not offer clinical benefit for distinguishing clinically significant PCa from low-risk PCa. As shown in Figure 4.7d, serum PSA led to an AUC = 0.611±0.054 (0.5049 to 0.7160, 95% CI) with a sensitivity of 60.94% and specificity of 51.16% when using a PSA threshold of >6.72 ng/mL. This is consistent with the literature in that serum PSA levels do not distinguish between low-risk and clinically significant PCa. Several other diagnostic biomarkers have been developed to improve the prediction of clinically significant PCa. Some of these include PHI, 4Kscore and the ExoDx IntelliScore.[12,14,55] Recent reviews of these methods concluded that, while all these tests have clinical utility, they do

not add substantially in diagnostic value and are relatively costly to perform.[16,17] For example, the AUCs for each of these tests are 0.652,[30] 0.67,[31] and 0.73,[56] respectively. In contrast, the %α23PSA assay would enable clinical laboratories the power to reduce unnecessary biopsies by 85% if implemented in the diagnostic pathway of localized PCa.

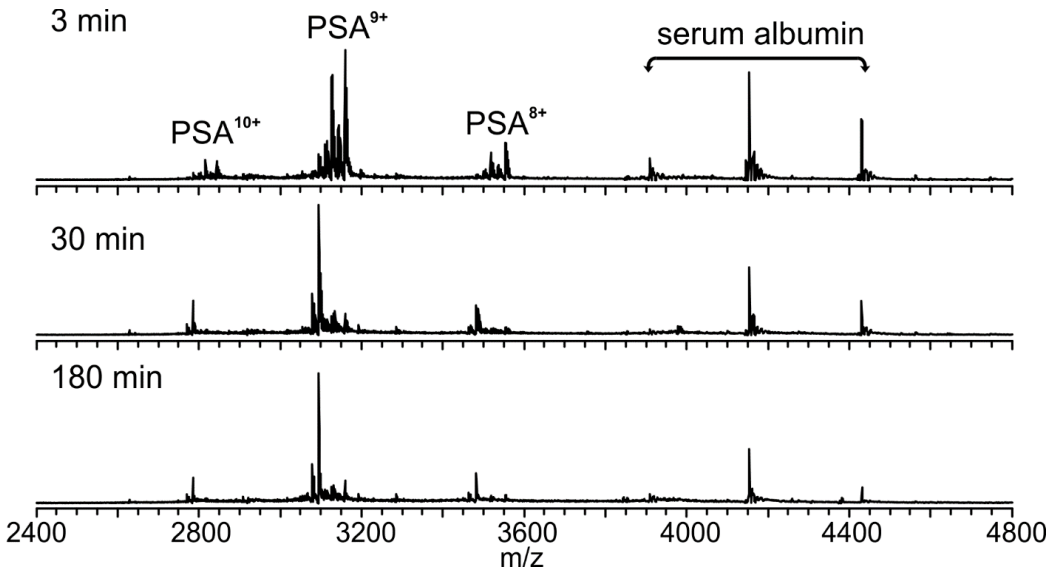

Figure 4.9. Representative ESI mass spectra acquired for an aqueous ammonium acetate solution (200 mM, pH 6.7 and 25 ºC) containing PSA extracted from blood serum incubated with NEUS for 3 min, 30 min and 180 min. Signal corresponding to the most abundant protein in blood serum, serum albumin (35-50 g/L in blood serum), was detected. However, the top-down native MS assay is insensitive to the presence of serum albumin as only PSA signal is considered in the CoMMon analysis.

The unprecedented high sensitivity and specificity for clinically significant PCa made possible by the dual neuraminidase approach combined with top-down native MS/CoMMon analysis has strong clinical implications for improving the diagnostic pathway of PCa. This MS-

based assay can be readily applied to monitor α2-3-Neu5Ac content of extracted PSA for clinical diagnosis of PCa and may help to reduce the need for prostate needle biopsy procedures, a potentially lethal procedure that should be withheld from patients who exclusively harbour low-grade PCa (GG1) disease.

4.4 Conclusions

In summary, a powerful dual neuraminidase-assisted top-down native MS/CoMMon assay for quantification of α2-3- and α2-6-linked Neu5Ac content in blood serum PSA is introduced. We demonstrated that top-down native MS performed using NEUS and NEUC enables the facile quantification of %α23PSA of PSA isolated from serum. Because of near absolute specificity of NEUS towards α2-3-linked Neu5Ac ($k_{2\text{-}3}/k_{2\text{-}6}$ = ~360), native mass spectra of PSA before and after reaction with NEUS, combined with mass spectra after reaction with NEUC, allows for the accurate determination of the relative α2-3- and α2-6-linked Neu5Ac content in PSA. Notably, this top-down native MS approach is independent of co-extracted glycoproteins, rapid (in comparison to bottom-up approach) and can be used reliably for absolute quantification of all α2-3/6-linked Neu5Ac groups in PSA. Additionally, there is no requirement for calibration curves and its related standards. This assay is in contrast to indirect methods, such as ELISA, which rely on an immunoreactive agent to inform the investigator of the level of α2-3/6-linked Neu5Ac groups in PSA. Absolute quantification of α2-3/6-linked Neu5Ac groups in PSA (%α23PSA) is a clear strength of our assay, which led to the discrimination of clinically significant PCa (GG2-5) disease from low-risk PCa. This was previously not achieved with other top-down or bottom-up based approaches.[8,13,27,57]

ELISA and MS methods of quantitating α2-3 Neu5Ac on serum PSA as reported Yoneyama *et al*., relied on a %α23PSA cut-off of ~41.5% and did not find discrimination between low-risk PCa and clinically significant PCa.[24] Their reported AUC of 0.748 was for clinically significant PCa but had a specificity (true negative rate) of 43.4% when using a sensitivity (true positive rate) of 90%. Also Hatano *et al.* reported another ELISA based method to quantify the content of both α2-3 Neu5Ac and α1-6 core fucose to enhance the discrimination, and a AUC of 0.711 was reported for clinically significant PCa with a specificity of 41% and a sensitivity of 90%.[13] In contrast, the dual-neuraminidase native MS approach produced superior performance test characteristics (AUC=0.875, 0.799 to 0.950, 95% CI) with a sensitivity of 85.5% and specificity of 84.6% when using a %α23PSA of 0.28 for clinically significant PCa.

The dual neuraminidase-assisted top-down native MS/CoMMon assay shows significant promise for identifying patients with clinically significant PCa, histologically known as GG2-5 PCa disease. This has important clinical implications for patients on active surveillance. Active surveillance is a therapy option for men with low-risk PCa, wherein radical therapy (prostatectomy, radiation therapy) is deferred until their low-risk tumour (GG1) has evolved or upgraded to an intermediate/high-risk (GG2-5) form. This requires these patients to be biopsied annually or every two years to detect any tumour upgrading (from GG1 to GG2-5). However, we and others have established that active surveillance patients have a 5-year cancer mortality rate <0.01% and only 30% of these patients will ever upgrade.[58,59] This means that they are more likely to die from a needle biopsy than the low-risk cancer itself. A non-invasive means of identifying GG2-5 disease in active surveillance patients is a clinically unmet need in urology in order to minimize unnecessary needle biopsies. The histological grading of tissue biopsies is not infallible either; there exists a 10-20% biopsy sampling error for GG1 PCa when comparing the histologically

assessed needle biopsy tissue against the histologically assessed prostate in its entirety. This sample error is due to the needle missing tumors in the prostate as some of these tumors may reside on the farthest perimeter of the prostate and hence farthest away from the entry points of the 12 needles.[60] Hence, a near perfect correlation of any biomarker to tissue biopsy-dependent diagnosis of clinically significant PCa (GG2-5) is not possible and should be re-evaluated. This intrinsic limitation of the needle biopsy procedure may explain, at least in part, why our specificity and sensitivity test characteristics are 84%-86%.

The use of accurately determined %α23PSA to differentiate patients with PCa from other groups appears promising and, with more extended validation, could serve as a valuable PCa diagnostic tool. Additionally, the dual-neuraminidase native MS/CoMMon approach could serve as a general approach to quantifying the relative α2-3-Neu5Ac content of other glycoproteins related to various diseases and cancers, such as α1-acid glycoprotein (diagnostic marker of lung and laryngeal cancers) and α-fetoprotein (serological marker in the diagnosis of hepatocellular cancer).[61-63]

4.5 References

(1) Siegel, R. L.; Miller, K. D.; Jemal, A. Cancer statistics, 2020. *CA. Cancer J. Clin.* **2020**, *70*, 7–30.

(2) Sung, H.; Ferlay, J.; Siegel, R. L.; Laversanne, M.; Soerjomataram, I.; Jemal, A.; Bray, F. Global cancer statistics 2020: GLOBOCAN estimates of incidence and mortality worldwide for 36 cancers in 185 countries. *CA. Cancer J. Clin.* **2021**, *71*, 209–249.

(3) Schröder, F.H.; Hugosson, J.; Roobol, M.J.; Tammela, T.L.; Ciatto, S.; Nelen, V.; Kwiatkowski, M.; Lujan, M.; Lilja, H.; Zappa, M.; Denis, L.J, Recker, F.; Berenguer, A.; Määttänen, L.; Bangma, C.H.; Aus, G.; Villers, A.; Rebillard, X.; van der Kwast, T.; Blijenberg, B.G.; Moss, S.M.; de Koning, H.J.; Auvinen, A. ERSPC Investigators. Screening and prostate-cancer mortality in a randomized european study. *N. Engl. J. Med.* **2009**, *360*, 1320-1328.

(4) Schröder, F.H.; Hugosson, J.; Roobol, M.J.; Tammela, T.L.; Zappa, M.; Nelen, V.; Kwiatkowski, M.; Lujan, M.; Määttänen, L.; Lilja, H.; Denis, L.J.; Recker, F.; Paez, A.; Bangma, C.H.; Carlsson, S.; Puliti, D.; Villers, A.; Rebillard, X.; Hakama, M.;Stenman, U.H.; Kujala, P.; Taari, K.; Aus, G.; Huber, A.;van der Kwast, T.H.; van Schaik, R.H.; de Koning, H.J.; Moss, S.M.; Auvinen, A. ERSPC Investigators. Screening and prostate cancer mortality: results of the european randomised study of screening for prostate cancer (ERSPC) at 13 years of follow-up. *Lancet.* **2014**, *84*, 2027-2035.

(5) Shoag, J. E.; Nyame, Y. A.; Gulati, R.; Etzioni, R.; Hu, J. C. Reconsidering the trade-offs of prostate cancer screening. *N. Engl. J. Med.* **2020**, *382*, 2465–2468.

(6) Etzioni, R.; Penson, D. F.; Legler, J. M.; di Tommaso, D.; Boer, R.; Gann, P. H.; Feuer, E. J. Overdiagnosis due to prostate-specific antigen screening: Lessons from U.S. prostate

cancer incidence trends. *JNCI J. Natl. Cancer Inst.* **2002**, *94*, 981–990.

(7) Loeb, S.; Bjurlin, M. A.; Nicholson, J.; Tammela, T. L.; Penson, D. F.; Carter, H. B.; Carroll, P.; Etzioni, R. Overdiagnosis and overtreatment of prostate cancer. *Eur. Urol.* **2014**, *65*, 1046–1055.

(8) Brewster, D. H.; Fischbacher, C. M.; Nolan, J.; Nowell, S.; Redpath, D.; Nabi, G. Risk of hospitalization and death following prostate biopsy in Scotland. *Public Health* **2017**, *142*, 102–110.

(9) Jesus, C. M. N. de; Corrêa, L. A.; Padovani, C. R. Complications and risk factors in transrectal ultrasound-guided prostate biopsies. *Sao Paulo Med. J.* **2006**, *124*, 198–202.

(10) Loeb, S.; Vellekoop, A.; Ahmed, H. U.; Catto, J.; Emberton, M.; Nam, R.; Rosario, D. J.; Scattoni, V.; Lotan, Y. Systematic review of complications of prostate biopsy. *Eur. Urol.* **2013**, *64*, 876–892.

(11) Loeb, S.; Carter, H. B.; Berndt, S. I.; Ricker, W.; Schaeffer, E. M. Complications after prostate biopsy: Data from SEER-Medicare. *J. Urol.* **2011**, *186*, 1830–1834.

(12) Saini, S. PSA and beyond: Alternative prostate cancer biomarkers. *Cell. Oncol.* **2016**, *39*, 97–106.

(13) Hatano, K.; Yoneyama, T.; Hatakeyama, S.; Tomiyama, E.; Tsuchiya, M.; Nishimoto, M.;Yoshimura, K.; Miyoshi, E.; Uemura, H.; Ohyama, C.; Nonomura, N.; Fujita, K. Simultaneous analysis of serum α2,3-linked sialylation and core-type fucosylation of prostate-specific antigen for the detection of high-grade prostate cancer. *Br. J. Cancer*. **2022**, *126*, 764-770.

(14) Chang, E. K.; Gadzinski, A. J.; Nyame, Y. A. Blood and urine biomarkers in prostate cancer: Are we ready for reflex testing in men with an elevated prostate-specific antigen? *Asian J.*

Urol. **2021**, *8*, 343–353.

(15) Behnken, H.N.; Ruthenbeck, A.; Schulz, J.M.; Meyer, B. Glycan analysis of prostate specific antigen (PSA) directly from the intact glycoprotein by HR-ESI/TOF-MS. *J Proteome Res*. **2014**, *13*, 997-1001.

(16) Kałuża, A.; Szczykutowicz, J.; Ferens-Sieczkowska, M. Glycosylation: Rising potential for prostate cancer evaluation. *Cancers* **2021**. *13*, 3726- 3728.

(17) Sugár, S.; Tóth, G.; Bugyi, F.; Vékey, K.; Karászi, K.; Drahos, L.; Turiák, L. Alterations in protein expression and site-specific *N*-glycosylation of prostate cancer tissues. *Sci. Rep.* **2021**, *11*, 15886.

(18) Hatakeyama, S.; Yoneyama, T.; Tobisawa, Y.; Ohyama, C. Recent progress and perspectives on prostate cancer biomarkers. *Int. J. Clin. Oncol*. **2017**, *22*, 214-221.

(19) Pihikova, D.; Kasak, P.; Kubanikova, P.; Sokol, R.; Tkac, J. Aberrant sialylation of a prostate-specific antigen: Electrochemical label-free glycoprofiling in prostate cancer serum samples. *Anal. Chim. Acta* **2016**, *934*, 72–79.

(20) Peracaula, R.; Tabarés, G.; Royle, L.; Harvey, D. J.; Dwek, R. A.; Rudd, P. M.; de Llorens, R. Altered glycosylation pattern allows the distinction between prostate-specific antigen (PSA) from normal and tumour origins. *Glycobiology* **2003**, *13*, 457–470.

(21) Ohyama, C.; Hosono, M.; Nitta, K.; Oh-eda, M.; Yoshikawa, K.; Habuchi, T.; Arai, Y.; Fukuda, M. Carbohydrate structure and differential binding of prostate specific antigen to maackia amurensis lectin between prostate cancer and benign prostate hypertrophy. *Glycobiology* **2004**, *14*, 671–679.

(22) Gilgunn, S.; Murphy, K.; Stöckmann, H.; Conroy, P.J.; Murphy, T.B.; Watson, R.W.; O'Kennedy, R.J.; Rudd, P.M.; Saldova, R. Glycosylation in indolent, significant and

aggressive prostate cancer by automated high-throughput *N*-glycan profiling. *Int. J. Mol. Sci*. **2020**, *21*, 9233.

(23) Haga, Y.; Uemura, M.; Baba, S.; Inamura, K.; Takeuchi, K.; Nonomura, N.; Ueda, K. Identification of multisialylated LacdiNAc structures as highly prostate cancer specific glycan signatures on PSA. *Anal. Chem*. **2019**, *91*, 2247-2254.

(24) Yoneyama, T.; Ohyama, C.; Hatakeyama, S.; Narita, S.; Habuchi, T.; Koie, T.; Mori, K.; Hidari, K.I.;Yamaguchi, M.; Suzuki, T.; Tobisawa, Y. Measurement of aberrant glycosylation of prostate specific antigen can improve specificity in early detection of prostate cancer. *Biochem. Biophys. Res. Commun*. **2014**, *448*, 390-396.

(25) Saldova, R.; Fan, Y.; Fitzpatrick, J. M.; Watson, R. W. G.; Rudd, P. M. Core fucosylation and α2-3 sialylation in serum *N*-glycome is significantly increased in prostate cancer comparing to benign prostate hyperplasia. *Glycobiology* **2011**, *21*, 195–205.

(26) Ferrer-Batallé, M.; Llop, E.; Ramírez, M.; Aleixandre, R.N.; Saez, M.; Comet, J.; De Llorens, R.; Peracaula, R. Comparative study of blood-based biomarkers, α2,3-sialic acid PSA and PHI, for high-risk prostate cancer detection. *Int. J. Mol. Sci*. **2017**, *18*, 845.

(27) Llop, E.; Ferrer-Batallé, M.; Barrabés, S.; Guerrero, P. E.; Ramírez, M.; Saldova, R.; Rudd, P. M.; Aleixandre, R. N.; Comet, J.; de Llorens, R.; Peracaula, R. Improvement of prostate cancer diagnosis by detecting PSA glycosylation-specific changes. *Theranostics* **2016**, *6*, 1190–1204.

(28) Gratacós-Mulleras, A.; Duran, A.; Asadi Shehni, A.; Ferrer-Batallé, M.; Ramírez, M.; Comet, J.; de Llorens, R.; Saldova, R.; Llop, E.; Peracaula, R. Characterisation of the main PSA glycoforms in aggressive prostate cancer. *Sci. Rep.* **2020**, *10*, 1–14.

(29) Wang, C.; Höti, N.; Lih, T.M.; Sokoll, L.J.; Zhang, R.; Zhang, Z.; Zhang, H.; Chan, D.W.

Development of a glycoproteomic strategy to detect more aggressive prostate cancer using lectin-immunoassays for serum fucosylated PSA. *Clin. Proteomics*. **2019**, *16*, 13-21.

(30) Haese, A.; Tin, A. L.; Carlsson, S. V; Sjoberg, D. D.; Pehrke, D.; Steuber, T.; Huland, H.; Graefen, M.; Scardino, P. T.; Schlomm, T.; Vickers, J. A.; Lilja, H.; Sauter, G. A pre-specified model based on four Kallikrein markers in blood improves predictions of adverse pathology and biochemical recurrence after radical prostatectomy. *Br. J. Cancer* **2020**, *123*, 604–609.

(31) Wang, W.; Wang, M.; Wang, L.; Adams, T. S.; Tian, Y.; Xu, J. Diagnostic ability of %p2PSA and prostate health index for aggressive prostate cancer: A meta-analysis. *Sci. Rep.* **2014**, *4*, 5012.

(32) van der Burgt, Y.E.M.; Siliakus, K.M.; Cobbaert, C.M.; Ruhaak, L.R. HILIC-MRM-MS for linkage-specific separation of sialylated glycopeptides to quantify prostate-specific antigen proteoforms. *J. Proteome Res*. **2020**, *19*, 2708-2716.

(33) Reider, B.; Jarvas, G.; Krenkova, J.; Guttman, A. Separation based characterization methods for the *N*-glycosylation analysis of prostate-specific antigen. *J. Pharm. Biomed. Anal*. **2021**, *194*, 113797.

(34) Kammeijer, G.S.M.; Jansen, B.C.; Kohler, I.; Heemskerk, A.A.M.; Mayboroda, O.A.; Hensbergen, P.J.; Schappler, J.; Wuhrer, M. Sialic acid linkage differentiation of glycopeptides using capillary electrophorsis - electrospray ionization - mass spectrometry. *Sci. Rep*. **2017**, *7*, 3733.

(35) Kammeijer, G. S. M.; Nouta, J.; de la Rosette, J. J. M. C. H.; de Reijke, T. M.; Wuhrer, M. An in-depth glycosylation assay for urinary prostate-specific antigen. *Anal. Chem.* **2018**, *90*, 4414–4421.

(36) Gabriele, C.; Prestagiacomo, L.E.; Cuda, G.; Gaspari, M. Mass spectrometry-based glycoproteomics and prostate cancer. *Int. J. Mol. Sci*. **2021**, *22*, 5222.

(37) Etxebarria, J.; Reichardt, N. C. Methods for the absolute quantification of *N*-glycan biomarkers. *Biochim. Biophys. Acta* **2016**, *1860*, 1676–1687.

(38) Zhou, X.; Yang, G.; Guan, F. Biological Functions and Analytical Strategies of Sialic Acids in Tumor. *Cells* **2020**, *9*, 273-291.

(39) Rodrigues, E.; Jung, J.; Park, H.; Loo, C.; Soukhtehzari, S.; Kitova, E. N.; Mozaneh, F.; Daskhan, G.; Schmidt, E. N.; Aghanya, V.; Sarkar, S.; Streith, L.; Laurent D St, C.; Nguyen, L.; Julien, J.; West, L, J.; Williams, K, C.; Klassen, J, S.; Macauley, M, S. A Versatile Soluble Siglec Scaffold for Sensitive and Quantitative Detection of Glycan Ligands. *Nat. Commun.* **2020**, *11*, 5091.

(40) Li, Z.; Kitov, P. I.; Kitova, E. N.; Bui, D. T.; Moremen, K. W.; Wakarchuk, W. W.; Mahal, L. K.; Macauley, M. S.; Klassen, J. S. Quantifying carbohydrate-active enzyme activity with glycoprotein substrates using electrospray ionization mass spectrometry and center-of-mass monitoring. *Anal. Chem.* **2021**, *93*, 15262–15270.

(41) Li, Z.; Kitov, P. I.; Han, L.; Kitova, E. N.; Mozenah, F.; Rodrigues, E.; Chapla, D. G.; Moremen, K. W.; Macauley, M. S.; Klassen, J. S. CUPRA-ZYME: An assay for measuring carbohydrate-active enzyme activities, pathways, and substrate specificities. *Anal. Chem.*, **2020**, *92*, 3228-3236.

(42) Klee, E. W.; Bondar, O. P.; Goodmanson, M. K.; Trushin, S. A.; Bergstralh, E. J.; Singh, R. J.; Anderson, N. L.; Klee, G. G. Serum concentrations of prostate-specific antigen measured using immune extraction, trypsin digestion, and tandem mass spectrometry quantification of LSEPAELTDAVK Peptide. *Arch. Pathol. Lab. Med.* **2014**, *138*, 1381–

1386.

(43) Abu-Bakr El-Bayoumy, A. S.; Hessien Keshta, A. T.; Sallam, K. M.; Ebeid, N. H.; Elsheikh, H. M.; Bayoumy, B. E. S. Extraction, purification of prostate-specific antigen (PSA), and establishment of radioimmunoassay system as a diagnostic tool for prostate disorders. *J. Immunoass*. **2018**, *39*, 12-29.

(44) Bigge, J. C.; Patel, T. P.; Bruce, J. A.; Goulding, P. N.; Charles, S. M.; Parekh, R. B. Nonselective and efficient fluorescent labeling of glycans using 2-amino benzamide and anthranilic acid. *Anal. Biochem.* **1995**, *230*, 229–238.

(45) Nwosu, C.; Yau, H. K.; Becht, S. Assignment of core versus antenna fucosylation types in protein *N*-glycosylation via procainamide labeling and tandem mass spectrometry. *Anal. Chem.* **2015**, *87*, 5905–5913.

(46) Zhuo, Y.; Keire, D. A.; Chen, K. Minor *N*-glycan mapping of monoclonal antibody therapeutics using middle-down NMR spectroscopy. *Mol. Pharm.* **2021**, *18*, 441–450.

(47) Stanley, P.; Taniguchi, N.; Aebi, M. N-glycans. In Essentials of Glycobiology. 3rd edition. Cold Spring Harbor Laboratory Press: **2017**.

(48) Walsh, I.; O'Flaherty, R.; Rudd, P. M. Bioinformatics applications to aid high-throughput glycan profiling. *Perspect. Sci.* **2017**, *11*, 31-39.

(49) Naka, R.; Kamoda, S.; Ishizuka, A.; Kinoshita, M.; Kakehi, K. Analysis of total *N*-glycans in cell membrane fractions of cancer cells using a combination of serotonin affinity chromatography and normal phase chromatography. *J. Proteome Res.* **2006**, *5*, 88–97.

(50) Xu, G.; Potter, J. A.; Russell, R. J. M.; Oggioni, M. R.; Andrew, P. W.; Taylor, G. L. Crystal structure of the NanB sialidase from *Streptococcus Pneumoniae*. *J. Mol. Biol.* **2008**, *384*, 436–449.

(51) Gut, H.; King, S. J.; Walsh, M. A. Structural and functional studies of *Streptococcus Pneumoniae* neuraminidase B: An intramolecular trans-sialidase. *FEBS Lett.* **2008**, *582*, 3348–3352.

(52) Newstead, S. L.; Potter, J. A.; Wilson, J. C.; Xu, G.; Chien, C.-H.; Watts, A. G.; Withers, S. G.; Taylor, G. L. The structure of *Clostridium perfringens* NanI sialidase and its catalytic intermediates. *J. Biol. Chem.* **2008**, *283*, 9080–9088.

(53) Ideo, H.; Kondo, J.; Nomura, T.; Nonomura, N.; Inoue, M.; Amano, J. Study of glycosylation of prostate-specific antigen secreted by cancer tissue-originated spheroids reveals new candidates for prostate cancer detection. *Sci. Rep.* **2020**, *10*, 2708-2726.

(54) Song, E.; Mayampurath, A.; Yu, C.-Y.; Tang, H.; Mechref, Y. Glycoproteomics: Identifying the glycosylation of prostate specific antigen at normal and high isoelectric points by LC–MS/MS. *J. Proteome Res.* **2014**, *13*, 5570–5580.

(55) McKiernan, J.; Donovan, M. J.; Margolis, E.; Partin, A.; Carter, B.; Brown, G.; Torkler, P.; Noerholm, M.; Skog, J.; Shore, N.; Andriole, G.; Thompson, I.; Carroll, P. A prospective adaptive utility trial to validate performance of a novel urine exosome gene expression assay to predict high-grade prostate cancer in patients with prostate-specific antigen 2–10 ng/ml at initial biopsy. *Eur. Urol.* **2018**, *74*, 731–738.

(56) McKiernan, J.; Donovan, M. J.; O'Neill, V.; Bentink, S.; Noerholm, M.; Belzer, S.; Skog, J.; Kattan, M. W.; Partin, A.; Andriole, G.; Brown, G.; Wei, J. T.; Thompson Jr, I. M.; Carroll, P. A novel urine exosome gene expression assay to predict high-grade prostate cancer at initial biopsy. *JAMA Oncol.* **2016**, *2*, 882–889.

(57) Yoneyama, T.; Yamamoto, H.; Sutoh Yoneyama, M.; Tobisawa, Y.; Hatakeyama, S.; Narita, T.; Kodama, H.; Momota, M.; Ito, H.; Narita, S.; Tsushima, F.; Mitsuzuka, K.; Yoneyama,

T.; Hashimoto, Y.; Duivenvoorden, W.; Pinthus, J. H.; Kakeda, S.; Ito, A.; Tsuchiya, N.; Habuchi, T.; Ohyama, C. Characteristics of α2,3-Sialyl *N*-glycosylated PSA as a biomarker for clinically significant prostate cancer in men with elevated PSA level. *Prostate* **2021**, *81*, 1411–1427.

(58) Klotz, L.; Zhang, L.; Lam, A.; Nam, R.; Mamedov, A.; Loblaw, A. Clinical results of long-term follow-up of a large, active surveillance cohort with localized prostate cancer. *J. Clin. Oncol.* **2010**, *28*, 126–131.

(59) Klotz, L.; Vesprini, D.; Sethukavalan, P.; Jethava, V.; Zhang, L.; Jain, S.; Yamamoto, T.; Mamedov, A.; Loblaw, A. Long-term follow-up of a large active surveillance cohort of patients with prostate cancer. *J. Clin. Oncol.* **2015**, *33*, 272–277.

(60) Fine, W. S.; Epstein, I. J. A contemporary study correlating prostate needle biopsy and radical prostatectomy gleason score. *J. Urol.* **2008**, *179*, 1335–1339.

(61) Uslu, C.; Taysi, S.; Akcay, F.; Sutbeyaz, M. Y.; Bakan, N. Serum free and bound sialic acid and alpha-1-acid glycoprotein in patients with laryngeal cancer. *Ann. Clin. Lab. Sci.* **2003**, *33*, 156–159.

(62) Gao, Z.; Xu, M.; Yue, S.; Shan, H.; Xia, J.; Jiang, J.; Yang, S. Abnormal sialylation and fucosylation of saliva glycoproteins: Characteristics of lung cancer-specific biomarkers. *Curr. Res. Pharmacol. Drug Discov.* **2022**, *3*, 100079.

(63) Mondal, G.; Chatterjee, U.; Chawla, Y. K.; Chatterjee, B. P. Alterations of glycan branching and differential expression of sialic acid on alpha fetoprotein among hepatitis patients. *Glycoconj. J.* **2011**, *28*, 1–9.

Chapter 5

Conclusions and Future Work

The research described in this thesis focuses on the development of quantitative ESI-MS methods for measuring the kinetics of CAZyme reactions, assessing the enzymatic pathways and evaluating substrate specificities. These methodological advances, as well as insights into substrate specificities of neuraminidases, led to the development of a CAZyme-assisted, top-down ESI-MS assay for prostate cancer diagnosis. Below is a summary of the major advances made in Chapters 2 – 4. Finally, progress made in an ongoing research project is described in the Future Work section.

5.1 Summary of Research Chapters

The research described in Chapter 2, which introduced CUPRA-ZYME, sought to overcome the challenge of non-uniform ESI-MS response factors in CAZyme kinetics measurements. CUPRA-ZYME employs CUPRA substrates (CS), oligosaccharide labeled at the reducing end with an affinity tag that is recognized by a $^{Uni}P_{proxy}$, and direct ESI-MS analysis of the non-covalent complexes of the CS and $^{Uni}P_{proxy}$. When performed in a time-resolved fashion and in the presence of a CAZyme, CUPRA-ZYME allows for time-dependent changes in the concentrations of CS and CP to be measured. Because of the ESI-MS response factor-independent manner in which substrate concentration is measured, CUPRA-ZYME eliminates the need for calibration curves or internal standards, which are generally required with ESI-MS-based enzyme kinetics. Moreover, the concentrations of any products and intermediates that retain the affinity tag can also be quantified, independent of the nature of the chemical modification catalyzed by the CAZyme. The CUPRA-ZYME method was first validated for NEU3-catalyzed reactions.

Application to human sialytransferases (ST6Gal1 and ST3Gal4) and libraries of CS acceptors demonstrated the potential of the assay to profile the substrate specificities of glycosyltransferases rapidly and quantitatively. Kinetic measurements performed simultaneously on CS and glycans present on glycoproteins offered unprecedented insight into influence of the substrate structure and environment in natural glycoconjugates on CAZyme specificity.

The research described in Chapter 3 aimed to extend the use of ESI-MS for measuring CAZyme kinetics to reactions involving glycoprotein substrates. To achive this, a simple, versatile and quantitative method, referred to as Center-of-Mass (CoM) Monitoring (CoMMon), was developed. This assay relies on continuous ESI-MS monitoring of the CoM of the ensemble of glycoprotein substrates and their corresponding CAZyme products. Importantly, there is no requirement for calibration curves, internal standard (IS), labelling, or mass spectrum deconvolution. The assay was validated using neuraminidase-catalyzed reactions. Reaction progress curves were compared to initial rates of desialylation of a series of mammalian glycoproteins measured with CoMMon and, simultaneously, using an isotopically-labeled IS. The assay was applied to measure human ST-catalyzed sialylation of asialoglycoproteins. The feasibility of applying CoMMon to large (MW>500 kDa) and highly heterogeneous glycoprotein substrates was also shown. CoMMon, combined with CUPRA-ZYME, enables the relative reactivity of glycoprotein substrates to be quantitatively established, thereby providing a unique opportunity to reliably study structure-reactivity relationships for CAZyme-catalyzed reactions involving glycoprotein substrates.

In Chapter 4, a robust top-down native mass spectrometry (MS) approach, which exploits CoMMon and insights into the substrate specificities of neuraminidases gained through the work described in Chapters 2 and 3, was developed. The assay employs a combination of specific (for

α2-3-linked Neu5Ac) and nonspecific neuraminidases, for the quantification of α2-3- and α2-6-linked Neu5Ac content of PSA isolated from serum using CoMMon. The method is free of errors associated with lectin-based quantification of *N*-glycans containing both α2-3- and α2-6-linked Neu5Ac and avoids the sample handling steps required for HPLC analysis, which can introduce error. The assay was validated using purified PSA from a commercial source and PSA standards containing all α2-3- or α2-6-linked Neu5Ac. The α2-3 Neu5Ac content of a PSA standard measured with the assay is in excellent agreement with values obtained by HPLC analysis of released *N*-glycans. To illustrate the potential of the assay for clinical diagnosis of PCa and disease staging, the relative α2-3 Neu5Ac content on PSA extracted from serum of low, intermediate and high-risk PCa individuals were determined. The method could be also used for quantification of α2-3 Neu5Ac on other disease related glycoproteins for diagnosis (e.g. α-fetoprotein in hepatocellular carcinoma). In addition, such method combined with other specific CAZyme, is also applicable for quantification of other monosaccharide related disease (e.g. core fucose).

5.2 Future work

The new ESI-MS techniques described in Chapters 2 and 3 for measuring CAZyme kinetics have opened up exciting opportunities for gaining new and fundamental insights into the catalytic mechanisms of CAZymes and for exploiting CAZymes in biomedically-relevant applications. Described below are preliminary data for an ongoing research project aimed at controlled IgG-Fc glycoenginnering is discussed.

5.2.1 Exploiting temperature-dependent substrate specifcities of neuraminidases for glycoengineering monosialylated immunoglobulin Fc domain

The development of monoclonal antibody (mAb, Figure5.1a)-based therapeutics is a rapidly growing area of research and is dominating both the biopharmaceutical market and the number of approved drugs.[1] Successful treatments have been developed for a variety of medical conditions, including certain autoimmune diseases and cancers (e.g. follicular lymphoma, the first cancer treated by drug rituximab approved by FDA).[2-6] Immunoglobulin G (IgG), as one of the most abundant monoclonal antibodies (mAbs) in blood plasma, has attracted significant attention due to its therapeutic potential. An IgG contains four polypeptide chains: two identical heavy chains (H) and two identical light chains (L). The light and heavy chains pair by covalent disulfide bonds and non-covalent association. Like other mAbs, native human IgG antibodies consist of three globular domain structures, two fragment antigen-binding (Fab) region domains that are responsible for the antigen interaction, and a fragment crystallizable (Fc) region domain that could bind with its corresponding Fc acceptor (Figure 5.1b). A conserved *N*-glycosylation site (N297) which is present at the Fc constant heavy chain region 2 (C_H2) domain is dominated by bi-antennary complex *N*-glycans.[7-9] The glycosylation of IgG is known to be highly related to its biological function and can significantly affect its stability, half-life, antibody-dependent cellular cytotoxicity (ADCC) and receptor binding affinity.[10-13] As one of the most common types of glycosylation, IgG-Fc sialylated with α2-6 Neu5Ac has tremendous potential in therapeutic treatment. Recent papers suggest it could dramatically improve IgG anti-inflammatory activity and is already applied in treatment at a high dose (1-2 g/kg) for inflammatory and some autoimmune diseases.[14-16] Therefore, various strategies have been developed for a higher content of α2-6 Neu5Ac sialylated IgG-Fc. However, recent studies showed high content of terminal Neu5Ac on

therapeutic IgG-Fc could also lead to some undesired drawbacks. First, increased terminal sialylation may lead to a reduced ADCC due to a decreased binding affinity with FcyRIIIa.[16,17] In addition, terminal Neu5Ac on the Fc can decrease the binding of antibodies to cell surface antigens, possibly due to the reduction of hinge region flexibility.[17-21] Another disadvantage is the potential destabilization of the IgG-Fc structure, which will lead to an aggregation of IgG-Fc and makes it more susceptible to enzymatic degradation.[22-24] Studies by NMR indicate that the α1-6 arm on *N*-glycan is much less flexable than the α1-3 arm and strongly interacts with the Fc polypeptide surface to help stabilize its structure.[25,26] However, sialylation of IgG on the α1-6 mannose arm may weaken this interaction and destabilize the IgG-Fc structure.[27-29] Therefore, to maintain the anti-inflammatory property, high ADCC and stability, a highly homogenous *N*-glycan structure with specific mono α2-6 Neu5Ac on the α1-3 mannose arm could be a potential alternative for a better therapeutic applicability.

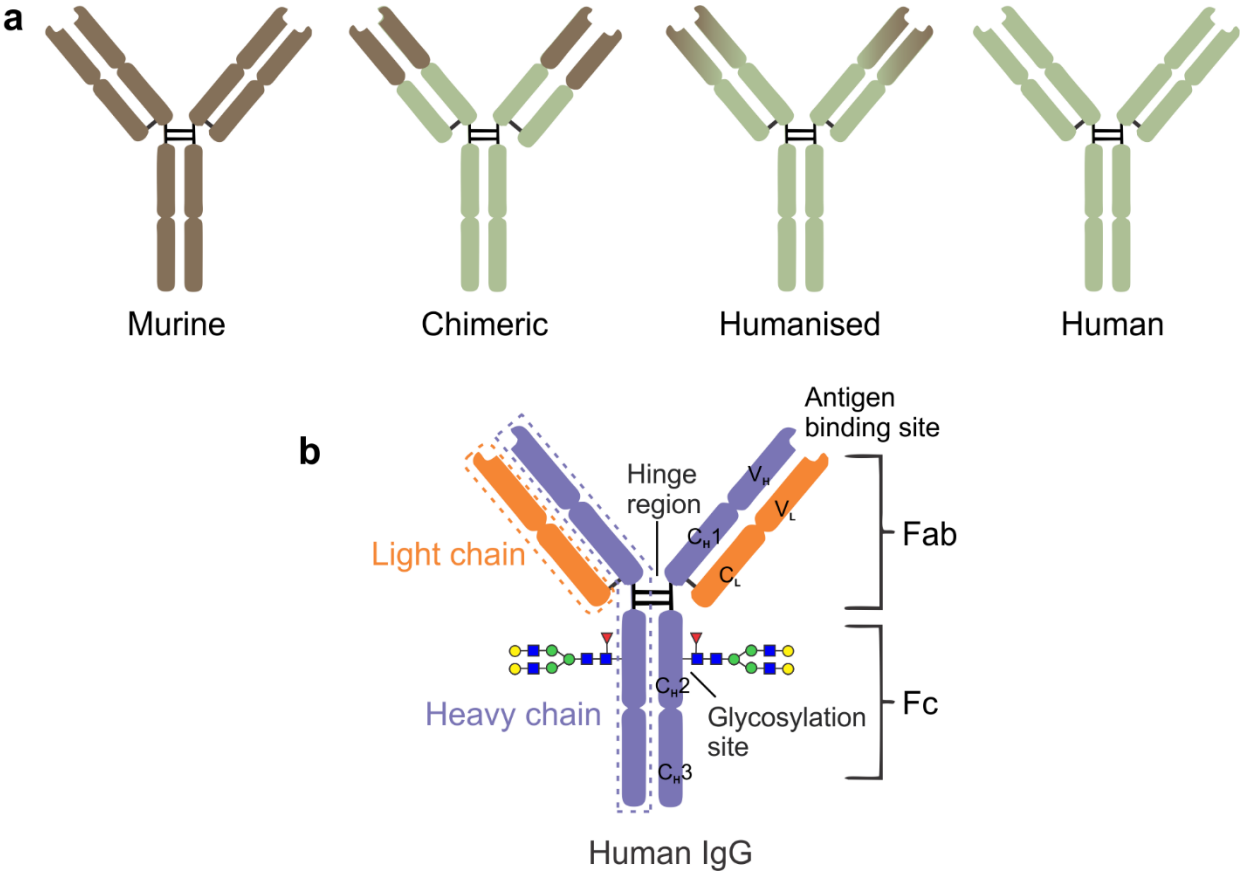

Figure 5.1 (a) Four major types of therapeutic mAbs: murine, chimeric, humanised and human. Non-human part is shown in brown and human part is shown in cyan. (b) Detailed structure of human IgG.

There are several commonly used approaches for remodeling of IgG *N*-glycans. The first is the *in vivo* genetic approach, wherein manipulation of the *N*-glycan biosynthetic pathway is used to control protein glycosylation (i.e., achieve desired *N*-glycan structure). This is widely used to produce and enrich many specific glycoforms such as low fucose or increased galactose. However, due to the restriction of eukaryotic cell lines and complexity of the glycan biosynthetic pathways, only limited glycoforms can be accessed.[30-32] Another approach is *in vitro* chemical glycoengineering, by introducing glycans through organic synthesis; it allows precise and flexible

construction of glycoproteins with desired glycan structure at individual sites. However, difficulty still remains in optimization of synthetic procedures, availability of commercial material and the requirement of complex organic synthesis. Moreover, terminal Neu5Ac is highly labile under organic reaction conditions which limits the use of synthesis.[33-35] Compared with the two approaches described above, enzymatic glycoengineering is more convenient. By treating the glycoprotein with different GHs or GTs, the glycans can be remodeled with high specificity and efficiency.[36] Recently, the use of endoglycosidases and their mutants has attracted attention for the engineering for IgG therapeutics. For example, the endoglycosidase Endo-S can deglycosylate the glycoprotein (with only one GlcNAc at the reducing end left on the glycoprotein). Predefined *N*-glycans can then be transferred by two mutant endoglycosidases (Endo-S-D233A or Endo-S-D233Q).[37,38] However, such method employs a pre-defined *N*-glycan structure as substrate, which still requires enzymatic reactions for its synthesis. Moreover, specificity of the CAZyme has to be well studied prior to its application in enzymatic glycoengineering. Therefore, the demand for more information about specificity of CAZymes is high for the production of diverse well-defined glycans to meet the increasing requirements in therapeutics.

Here, a temperature-dependent screening approach was developed to explore CAZyme specificity that could help in enzymatic glycoginnering of IgG-Fc. By screening the specificity of several bacterial neuraminidases with sialylated CUPRA substrates, NEUC and neuraminidase from *Arthrobacter Ureafaciens* (NEUA, Isozyme S subtype) were found to exhibit significant changes in specificity between α2-3 and α2-6 linked terminal Neu5Ac at different temperatures (Figure 5.2 a-c). Moreover, these two enzymes exhibit temperature-dependent branch specificity. For example, NEUC shows near absolute specificity for Neu5Ac on the α1-6 mannose branch at 50 °C (Figure 5.2 d-g).

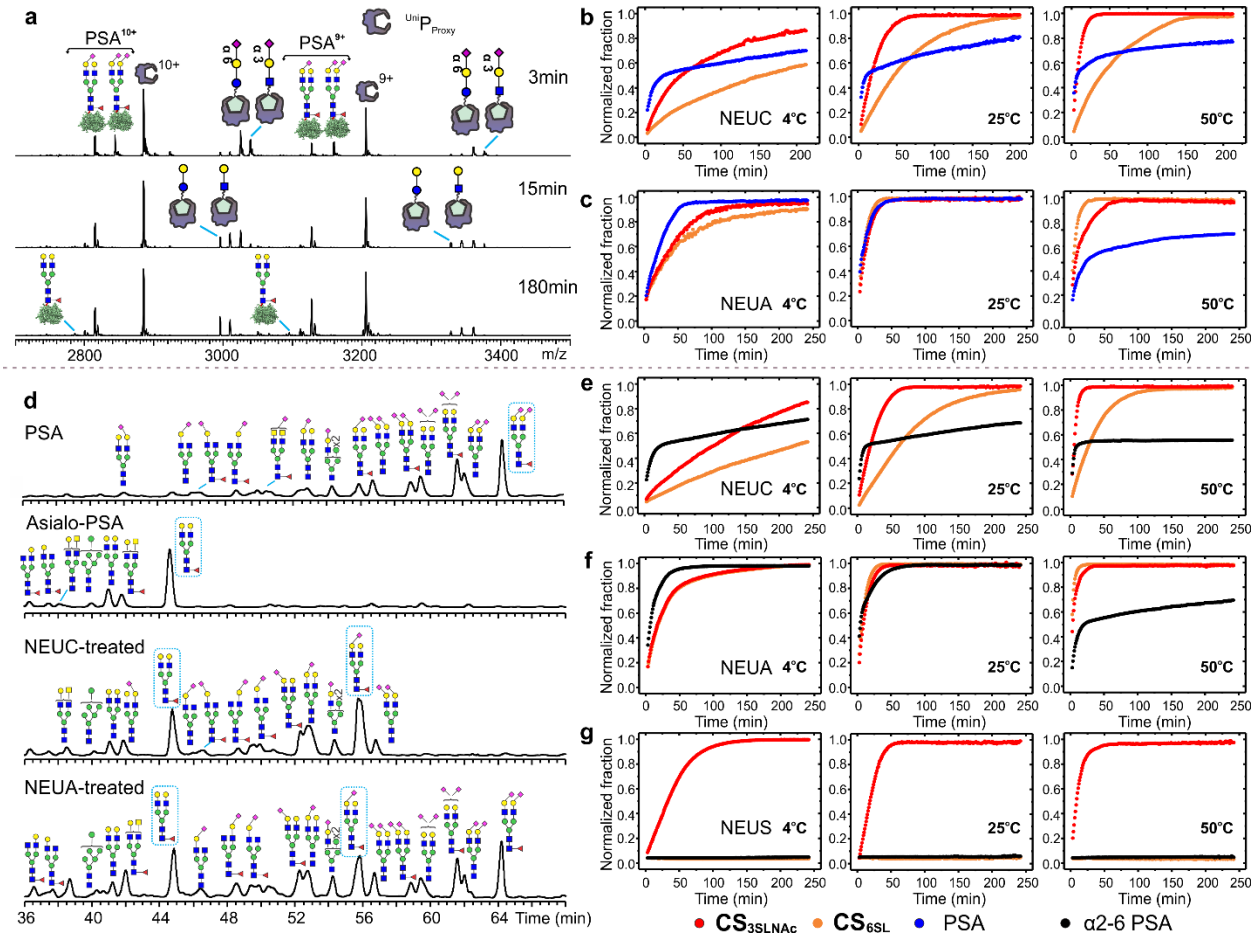

Figure 5.2. (a) Representative ESI mass spectra acquired for aqueous ammonia acetate solution (200 mM, pH 6.7, 25 °C) of NEUC (~0.14 μM), CS_{6SL} (5 μM), CS_{3SLNAc} (5 μM), $^{Uni}P_{proxy}$ (hCA, 10 μM) with PSA (5 μM) measured at 3, 15 and 180 min. Enzyme progress of CS_{6SL}, CS_{3SLNAc} and PSA treated with (b) NEUC and (c) NEUA at 4, 25 and 50 °C. (d) *N*-glycans released from PSA, asialo PSA, NEUC treated PSA and NEUA treated PSA identified by HILIC-UPLC coupled with MS. Enzyme progress of CS_{6SL}, CS_{3SLNAc} and α2-6 PSA treated with (e) NEUC and (f) NEUA at 4, 25 and 50 °C. (g) NEUS, which only cleave terminal α2-3 Neu5Ac, is tested at different temperature as control.

Native IgG-Fc (from a commercial source) contains two conserved glycosylation sites (one for each monomer). Identification of released *N*-glycans by HILIC-UPLC showed that they are predominated by agalactosylated, galactosylated and a small fraction of α2-6 monosialylated bi-antennary *N*-glycans (Figure 5.3a). Deconvolution of the mass spectrum of intact IgG-Fc indicated that it has a MW of ~53 kDa (Figure 5.3a). To be able to remodel IgG-Fc into homogeneous monosialylated glycoprotein, terminal galactose needed to be added to serve as the acceptor for Neu5Ac. So the native IgG-Fc sample was first treated with a human β4-galactosyltransferase-I (β4GalT1) in the presence of Mn^{2+} and excess UDP-Gal. *N*-glycans from galactosylated IgG-Fc were later analyzed by HILIC-UPLC and results (Figure 5.3b) indicate that all the bi-antennary *N*-glycan were fully galactosylated and, therefore, the IgG-Fc sample was ready for the transfer of Neu5Ac. The corresponding deconvoluted mass spectrum of galactosylated IgG-Fc also indicated the successful transfer of Gal leading to an increase in MW from ~53 kDa to ~53.5 kDa. Galactosylated IgG-Fc was then treated with human ST6Gal1 with excess CMP-Neu5Ac. However, complete sialylation of IgG-Fc still was not observed due to the assumed branch specificity and perceived protection shown in our previous chapters and other report.[39] The data shown in Figure 5.3c indicated that majority of bi-antennary *N*-glycans were disialylated (~70%) and a small fraction was monosialylated. The corresponding deconvoluted mass spectrum of sialylated IgG-Fc also indicated an increase of MW from ~53.5 kDa to around ~54.5 kDa. The sialylated IgG-Fc was then treated with NEUC at 50 °C, analysis of released *N*-glycans (Figure 5.3d) indicate that almost all of the disialylated bi-antennary *N*-glycans were converted into α1-3 branch monosialylated bi-antennary *N*-glycan. Corresponding deconvoluted mass spectrum also indicate the loss of Neu5Ac. This result showed the novel branching specificity of NEUC at 50 °C could specificly remove Neu5Ac from α1-3 mannose branch.

Moreover, a homogeneity of ~85% was determined by the HILIC-UPLC data and could be further enhanced to >90% by removing the core fucose.

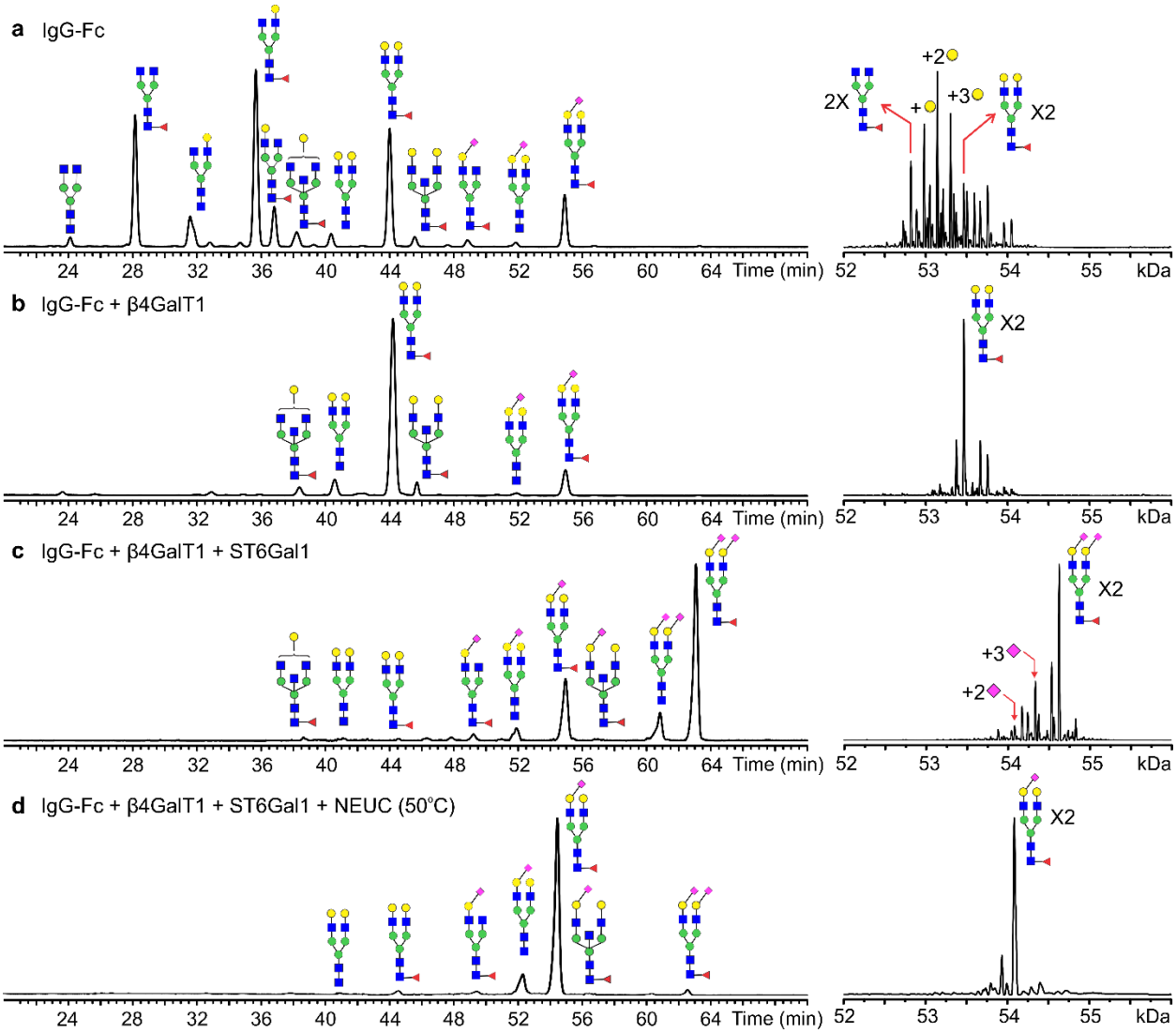

Figure 5.3. Stepwise glycoengineering for monosialylated IgG-Fc. *N*-glycans released from (a) native IgG-Fc, (b) galactosylated IgG-Fc, (c) sialylation of galactosylated IgG-Fc and (d) branch desialylation of sialylated IgG-Fc were analyzed by HILIC-UPLC and mass spectrum.

Follow up study will focus on the quantification of interactions between monosialylated and bisialylated IgG-Fc with different human Fc receptors (e.g. FcγRIII) to further exam if monosialylated IgG-Fc could show similar affinities as bisialylated IgG-Fc.

5.2.2 Top-down ESI-MS for quantification of disease related glycosylation

As described in Chapter 4, a top-down ESI-MS based, enzyme assisted method was developed for diagnosis of prostate cancer by quantification of α2-3 Neu5Ac. The method could be also applied for diagnosis of other diseases which lead to changes in sialylation. For example such as elevated sialylation of α1-acid glycoprotein in breast cancer,[40] increasing sialylation of haptoglobin in lung cancer,[41] increasing sialylation of IgG in malignancy,[42] and decreasing sialylation of IgG in colorectal cancer.[43,44] In addition to the sialylation changes of glycoprotein biomarkers for various cancers, tissue and lipid bound sialic acid levels could also be used for diagnosis of oral pre-cancer and thyroid cancer.[45-47] Moreover, combined with other specific CAZymes, this top-down ESI-MS method could be further applied for diagnosis of disease related with other glycosylations, for example, fucosidase for quantification of core fucose in hepatocellular carcinoma, galactosidase in quantification of galactose in ovarian cancer.[48,49]

5.3 References

(1) Walsh, G. Biopharmaceutical Benchmarks 2018. *Nat. Biotechnol.* **2018**, *36*, 1136–1145.

(2) Pierpont, T. M.; Limper, C. B.; Richards, K. L. Past, present, and future of rituximab-the world's first oncology monoclonal antibody therapy. *Front. Oncol*. **2018**, *8*, 163.

(3) Hirsch, I. B. Insulin analogues. *N. Engl. J. Med*. **2005**, *352*, 174− 183.

(4) Kiss, Z.; Elliott, S.; Jedynasty, K.; Tesar, V.; Szegedi, J. Discovery and basic pharmacology of erythropoiesis-stimulating agents (ESAs), including the hyperglycosylated ESA, darbepoetin alfa: an update of the rationale and clinical impact. *Eur. J. Clin. Pharmacol*. **2010**, *66*, 331−340.

(5) Rustgi, V. K. Albinterferon alfa-2b, a novel fusion protein of human albumin and human interferon alfa-2b, for chronic hepatitis C. *Curr. Med. Res. Opin*. **2009**, *25*, 991−1002.

(6) Kesik-Brodacka, M. Progress in biopharmaceutical development. *Biotechnol. Appl. Biochem*. **2018**, *65*, 306−322.

(7) Mattu, T. S.; Pleass, R. J.; Willis, A. C.; Kilian, M.; Wormald, M. R.; Lellouch, A. C.; Rudd, P. M.; Woof, J. M.; Dwek, R. A. The glycosylation and structure of human serum IgA1, Fab, and Fc regions and the role of *N*-Glycosylation on Fcα receptor interactions. *J. Biol. Chem.* **1998**, *273*, 2260–2272.

(8) Huhn, C.; Selman, M. H. J.; Ruhaak, L. R.; Deelder, A. M.; Wuhrer, M. IgG glycosylation analysis. *Proteomics* **2009**, *9*, 882–913.

(9) Krapp, S.; Mimura, Y.; Jefferis, R.; Huber, R.; Sondermann, P. Structural analysis of human IgG-Fc glycoforms reveals a correlation between glycosylation and structural integrity. *J. Mol. Biol.* **2003**, *325*, 979–989.

(10) Mimura, Y.; Church, S.; Ghirlando, R.; Ashton, P. R.; Dong, S.; Goodall, M.; Lund, J.; Jefferis, R. The influence of glycosylation on the thermal stability and effector function expression of human IgG1-Fc: Properties of a series of truncated glycoforms. *Mol. Immunol.* **2000**, *37*, 697–706.

(11) Borrok, M. J.; Jung, S. T.; Kang, T. H.; Monzingo, A. F.; Georgiou, G. Revisiting the role of glycosylation in the structure of human IgG Fc. *ACS Chem. Biol.* **2012**, *7*, 1596–1602.

(12) Liu, L. Antibody Glycosylation and its impact on the pharmacokinetics and pharmacodynamics of monoclonal antibodies and Fc-fusion proteins. *J. Pharm. Sci.* **2015**, *104*, 1866–1884.

(13) Van Lenten, L.; Ashwell, G. Studies on the chemical and enzymatic modification of glycoproteins: A general method for the tritiation of sialic acid-containing glycoproteins. *J. Biol. Chem.* **1971**, *246*, 1889–1894.

(14) Imbach, P.; d'APUZZO, V.; Hirt, A.; Rossi, E.; Vest, M.; Barandun, S.; Baumgartner, C.; Morell, A.; Schöni, M.; Wagner, H. P. High-dose intravenous gamma-globulin for idiopathic thrombocytopenic purpura in childhood. *Lancet* **1981**, *317*, 1228–1231.

(15) Nimmerjahn, F.; Ravetch, J. V. Anti-inflammatory actions of intravenous immunoglobulin. *Annu. Rev. Immunol.* **2008**, *26*, 513–533.

(16) Kaneko, Y.; Nimmerjahn, F.; Ravetch, J. V. Anti-inflammatory activity of immunoglobulin G resulting from Fc sialylation. *Science.* **2006**, *313*, 670–673.

(17) Scallon, B. J.; Tam, S. H.; McCarthy, S. G.; Cai, A. N.; Raju, T. S. Higher levels of sialylated Fc glycans in immunoglobulin G molecules can adversely impact functionality. *Mol. Immunol.* **2007**, *44*, 1524–1534.

(18) Raju, T. S.; Lang, S. E. Diversity in structure and functions of antibody sialylation in the Fc. *Curr. Opin. Biotechnol.* **2014**, *30*, 147–152.

(19) Naso, M. F.; Tam, S. H.; Scallon, B. J.; Raju, T. S. Engineering host cell lines to reduce terminal sialylation of secreted antibodies. *MAbs* **2010**, *2*, 519–527.

(20) Stadlmann, J.; Pabst, M.; Altmann, F. Analytical and functional aspects of antibody sialylation. *J. Clin. Immunol.* **2010**, *30*, 15–19.

(21) Kapur, R.; Einarsdottir, H. K.; Vidarsson, G. IgG-Effector functions:"The good, the bad and the ugly." *Immunol. Lett.* **2014**, *160*, 139–144.

(22) Chennamsetty, N.; Voynov, V.; Kayser, V.; Helk, B.; Trout, B. L. Design of therapeutic proteins with enhanced stability. *Proc. Natl. Acad. Sci.* **2009**, *106*, 11937–11942.

(23) Chennamsetty, N.; Helk, B.; Voynov, V.; Kayser, V.; Trout, B. L. Aggregation-prone motifs in human immunoglobulin G. *J. Mol. Biol.* **2009**, *391*, 404–413.

(24) Brummitt, R. K.; Nesta, D. P.; Chang, L.; Chase, S. F.; Laue, T. M.; Roberts, C. J. Nonnative aggregation of an IgG1 antibody in acidic conditions: Part 1. Unfolding, colloidal interactions, and formation of high-molecular-weight aggregates. *J. Pharm. Sci.* **2011**, *100*, 2087–2103.

(25) Nagae, M.; Yamaguchi, Y. Function and 3D structure of the *N*-glycans on glycoproteins. *Int. J. Mol. Sci.* **2012**, *13*, 8398–8429.

(26) Kiyoshi, M.; Tsumoto, K.; Ishii-Watabe, A.; Caaveiro, J. M. M. Glycosylation of IgG-Fc: A molecular perspective. *Int. Immunol.* **2017**, *29*, 311–317.

(27) Falck, D.; Jansen, B. C.; Plomp, R.; Reusch, D.; Haberger, M.; Wuhrer, M. Glycoforms of immunoglobulin G based biopharmaceuticals are differentially cleaved by trypsin due to the glycoform influence on higher-order structure. *J. Proteome Res.* **2015**, *14*, 4019–4028.

(28) Fang, J.; Richardson, J.; Du, Z.; Zhang, Z. Effect of Fc-glycan structure on the conformational stability of IgG revealed by Hydrogen/Deuterium exchange and limited proteolysis. *Biochemistry* **2016**, *55*, 860–868.

(29) Zhang, Z.; Shah, B.; Richardson, J. Impact of Fc *N*-glycan sialylation on IgG structure. *MAbs* **2019**, *11*, 1381–1390.

(30) Jefferis, R. Glycosylation as a strategy to improve antibody-based therapeutics. *Nat. Rev. Drug Discov.* **2009**, *8*, 226–234.

(31) Jefferis, R. Glycosylation of recombinant antibody therapeutics. *Biotechnol. Prog.* **2005**, *21*, 11–16.

(32) Yu, X.; Marshall, M. J. E.; Cragg, M. S.; Crispin, M. Improving antibody-based cancer therapeutics through glycan engineering. *BioDrugs* **2017**, *31*, 151–166.

(33) Ma, B.; Guan, X.; Li, Y.; Shang, S.; Li, J.; Tan, Z. Protein glycoengineering: An approach for improving protein properties. *Frontiers in Chemistry*. **2020**, *8*, 622

(34) Wilson, R. M.; Dong, S.; Wang, P.; Danishefsky, S. J. The winding pathway to erythropoietin along the chemistry–biology frontier: A success at last. *Angew. Chemie Int. Ed.* **2013**, *52*, 7646–7665.

(35) Chaffey, P. K.; Guan, X.; Li, Y.; Tan, Z. Using chemical synthesis to study and apply protein glycosylation. *Biochemistry* **2018**, *57*, 413–428.

(36) Hodoniczky, J.; Zheng, Y. Z.; James, D. C. Control of recombinant monoclonal antibody effector functions by Fc *N*-glycan remodeling in Vitro. *Biotechnol. Prog.* **2005**, *21*, 1644–1652.

(37) Huang, W.; Giddens, J.; Fan, S.-Q.; Toonstra, C.; Wang, L.-X. Chemoenzymatic glycoengineering of intact IgG antibodies for gain of functions. *J. Am. Chem. Soc.* **2012**, *134*, 12308–12318.

(38) Giddens, J. P.; Lomino, J. V; DiLillo, D. J.; Ravetch, J. V; Wang, L.-X. Site-selective chemoenzymatic glycoengineering of Fab and Fc glycans of a therapeutic antibody. *Proc. Natl. Acad. Sci.* **2018**, *115*, 12023–12027.

(39) Barb, A. W.; Meng, L.; Gao, Z.; Johnson, R. W.; Moremen, K. W.; Prestegard, J. H. NMR characterization of immunoglobulin G Fc glycan motion on enzymatic sialylation. *Biochemistry* **2012**, *51*, 4618–4626.

(40) Smith, K. D., Behan, J., Matthews-Smith, G., & Magliocco, A. M. Alpha-1-acid glycoprotein (AGP) as a potential biomarker for breast cancer. London, UK: IntechOpen. **2012**, 201-222.

(41) Hoagland IV, L. F., Campa, M. J., Gottlin, E. B., Herndon, J. E., & Patz Jr, E. F.. Haptoglobin and posttranslational glycan-modified derivatives as serum biomarkers for the diagnosis of nonsmall cell lung cancer. *Cancer: Interdisciplinary International Journal of the American Cancer Society.* **2007**, *110*, 2260-2268

(42) Fleming, S. C.; Smith, S.; Knowles, D.; Skillen, A.; Self, C. H. Increased sialylation of oligosaccharides on IgG paraproteins - a potential new tumor marker in multiple myeloma. *J. Clin. Pathol.* **1998**, *51*, 825–830.

(43) Theodoratou, E.; Thaci, K.; Agakov, F.; Timofeeva, M.N.; Stambuk, J.; Pucic-Bakovic, M.; Vuckovic, F.; Orchard, P.; Agakova, A.; Din, F.V.; Brown, E.; Rudd, P.M.; Farrington, S.M.; Dunlop, M.G.; Campbell, H.; Lauc, G. Glycosylation of plasma IgG in colorectal cancer prognosis. *Sci. Rep.* **2016**, *6*, 28098.

(44) Vuckovic, F.; Theodoratou, E.; Thaci, K.; Timofeeva, M.; Vojta, A.; Stambuk, J.; Pucic-Bakovic, M.; Rudd, P.M.; Derek, L.; Servis, D.; Wennerstrom, A.; Farrington, S.M.; Perola, M.; Aulchenko, Y.; Dunlop, M.G.; Campbell, H.; Lauc, G. IgG glycome in colorectal cancer. Clin. *Cancer Res.* **2016**, *22*, 3078–3086.

(45) B. Rajpura, K.; S. Patel, P.; G. Chawda, J.; M. Shah, R. Clinical significance of total and lipid bound sialic acid levels in oral pre-cancerous conditions and oral cancer. *J. Oral Pathol. Med.* **2005**, *34*, 263–267.

(46) Krishnan, K.; Balasundaram, S. Evaluation of total and lipid bound sialic acid in serum in oral leukoplakia. *J Clin of Diagn Res.* **2017**, *11*, 25–27.

(47) Kökoğlu E.; Uslu E.; Uslu I.; Hatemi HH. Serum and tissue total sialic acid as a marker for human thyroid cancer. *Cancer Lett*. **1989**, *46*, 1-5.

(48) Cramer, D. W.; Greenberg, E. R.; Titus-Ernstoff, L.; Liberman, R. F.; Welch, W. R.; Li, E.; Ng, W. G. A Case-Control Study of Galactose Consumption and Metabolism in Relation to Ovarian Cancer1. *Cancer Epidemiol. Biomarkers Prev.* **2000**, *9*, 95–101.

(49) Norton, P. A.; Mehta, A. S. Expression of Genes That Control Core Fucosylation in Hepatocellular Carcinoma: Systematic Review. *World J. Gastroenterol.* **2019**, *25*, 2947–2960.

List of References

Chapter 1

(1) Cummings, J. H.; Stephen, A. M. Carbohydrate terminology and classification. *Eur. J. Clin. Nutr.* **2007**, *61*, S5–S18.

(2) Flynn, R. A.; Pedram, K.; Malaker, S. A.; Batista, P. J.; Smith, B. A. H.; Johnson, A. G.; George, B. M.; Majzoub, K.; Villalta, P. W.; Carette, J. E.; Bertozzi, C. R. Small RNAs are modified with *N*-glycans and displayed on the surface of living cells. *Cell* **2021**, *184*, 3109-3124.

(3) Hart, G. W. Structural and functional diversity of glycoconjugates. *Capill. Electrophor. Carbohydrates* **2003**, 3–24.

(4) Yu, R. K.; Suzuki, Y.; Yanagisawa, M. Membrane glycolipids in stem cells. *FEBS Lett.* **2010**, *584*, 1694–1699.

(5) Simons, K.; Ikonen, E. Functional Rafts in Cell Membranes. *Nature* **1997**, *387*, 569−572.

(6) Dennis, J. W.; Granovsky, M.; Warren, C. E. Protein Glycosylation in Development and Disease. *Bioessays* **1999**, *21*, 412−421.

(7) Hounsell, E. F.; Davies, M. J.; Renouf, D. V. *O*-linked protein glycosylation structure and function. *Glycoconj. J.* **1996**, *13*, 19–26.

(8) Van den Steen, P.; Rudd, P. M.; Dwek, R. A.; Opdenakker, G. Concepts and principles of *O*-linked glycosylation. *Crit. Rev. Biochem. Mol. Biol.* **1998**, *33*, 151–208.

(9) Brockhausen, I. Pathways of *O*-glycan biosynthesis in cancer cells. *Biochim. Biophys. Acta* **1999**, *1473*, 67–95.

(10) Wopereis, S.; Lefeber, D. J.; Morava, E.; Wevers, R. A. Mechanisms in protein *O*-glycan biosynthesis and clinical and molecular aspects of protein *O*-glycan biosynthesis defects: a

review. *Clin. Chem.* **2006**, *52*, 574–600.

(11) Mellquist, J. L.; Kasturi, L.; Spitalnik, S. L.; Shakin-Eshleman, S. H. The amino acid following an Asn-X-Ser/Thr sequon is an important determinant of *N*-linked core glycosylation efficiency. *Biochemistry* **1998**, *37*, 6833–6837.

(12) Imperiali, B.; O'Connor, S. E. Effect of *N*-linked glycosylation on glycopeptide and glycoprotein structure. *Curr. Opin. Chem. Biol.* **1999**, *3*, 643–649.

(13) Ardejani, M. S.; Noodleman, L.; Powers, E. T.; Kelly, J. W. Stereoelectronic effects in stabilizing protein-*N*-glycan interactions revealed by experiment and machine learning. *Nat. Chem.* **2021**, *13*, 480–487.

(14) Varki A. *Essentials of glycobiology*. 3rd edition. Cold Spring Harbor, New York: Cold Spring Harbor Laboratory Press. 2015

(15) Nelson, D. L.; Cox, M. M. *Lehninger Principles of Biochemistry* 5th Ed. **2008**, New York: W.H. Freeman.

(16) Dwek, R. A. Glycobiology: Toward Understanding the Function of Sugars. *Chem. Rev.* **1996**, *96*, 683–720.

(17) Cantarel, B. L.; Coutinho, P. M.; Rancurel, C.; Bernard, T.; Lombard, V.; Henrissat, B. The carbohydrate-active enzymes database (CAZy): an expert resource for glycogenomics. *Nucleic Acids Res.* **2008**, *37*, D233–D238.

(18) Henrissat, B. A classification of glycosyl hydrolases based on amino acid sequence similarities. *Biochem. J.* **1991**, *280*, 309–316.

(19) Davies, G. J.; Gloster, T. M.; Henrissat, B. Recent structural insights into the expanding world of Carbohydrate-Active enzymes. *Curr. Opin. Struct. Biol.* **2005**, *15*, 637–645.

(20) Drula, E.; Garron, M.-L.; Dogan, S.; Lombard, V.; Henrissat, B.; Terrapon, N. The

Carbohydrate-Active enzyme database: functions and literature. *Nucleic Acids Res.* **2022**, *50*, D571–D577.

(21) Chang, A.; Singh, S.; Phillips Jr, G. N.; Thorson, J. S. Glycosyltransferase structural biology and its role in the design of catalysts for glycosylation. *Curr. Opin. Biotechnol.* **2011**, *22*, 800–808.

(22) Taniguchi N, Honke K, Fukuda M, Narimatsu H, Yamaguchi Y, Angata T, Eds. Handbook of glycosyltransferases and related genes. Springer, Japan, Tokyo. **2014**

(23) Zhang, Z.; Wuhrer, M.; Holst, S. Serum sialylation changes in cancer. *Glycoconj. J.* **2018**, *35*, 139–160.

(24) Hou, G.; Liu, G.; Yang, Y.; Li, Y.; Yuan, S.; Zhao, L.; Wu, M.; Liu, L.; Zhou, W. Neuraminidase 1 (NEU1) promotes proliferation and migration as a diagnostic and prognostic biomarker of hepatocellular carcinoma. *Oncotarget* **2016**, *7*, 64957–64966.

(25) Pinho, S. S.; Reis, C. A. Glycosylation in cancer: mechanisms and clinical implications. *Nat. Rev. Cancer* **2015**, *15*, 540.

(26) Helbert, W.; Poulet, L.; Drouillard, S.; Mathieu, S.; Loiodice, M.; Couturier, M.; Lombard, V.; Terrapon, N.; Turchetto, J.; Vincentelli, R.; Henrissat, B. Discovery of novel carbohydrate-active enzymes through the rational exploration of the protein sequences space. *Proc. Natl. Acad. Sci.* **2019**, *116*, 6063 LP – 6068.

(27) Albohy, A.; Li, M. D.; Zheng, R. B.; Zou, C.; Cairo, C. W. Insight into substrate recognition and catalysis by the human neuraminidase 3 (NEU3) through molecular modeling and site-directed mutagenesis. *Glycobiology.* **2010**, *20*, 1127–1138.

(28) Li, J.; McClane, B. A. The sialidases of Clostridium perfringens type D strain CN3718 differ in their properties and sensitivities to inhibitors. *Appl. Environ. Microbiol.* **2014**, *80*, 1701–

1709.

(29) Xu, G.; Potter, J. A.; Russell, R. J. M.; Oggioni, M. R.; Andrew, P. W.; Taylor, G. L. Crystal structure of the NanB sialidase from *Streptococcus Pneumoniae*. *J. Mol. Biol.* **2008**, *384*, 436–449.

(30) Weinstein, J.; de Souza-e-Silva, U.; Paulson, J. C. Sialylation of glycoprotein oligosaccharides N-linked to asparagine. Enzymatic characterization of a Gal beta 1 to 3(4)GlcNAc alpha 2 to 3 sialyltransferase and a Gal beta 1 to 4GlcNAc alpha 2 to 6 sialyltransferase From Rat Liver. *J. Biol. Chem.* **1982**, *257*, 13845–13853.

(31) Kitagawa, H.; Paulson, J. C. Cloning of a novel alpha 2,3-sialyltransferase that sialylates glycoprotein and glycolipid carbohydrate groups. *J. Biol. Chem.* **1994**, *269*, 1394–1401.

(32) Achyuthan, K. E.; Achyuthan, A. M. Comparative enzymology, biochemistry and pathophysiology of human exo-α-sialidases (Neuraminidases). *Comp. Biochem. Physiol. Part B Biochem. Mol. Biol.* **2001**, *129*, 29–64.

(33) Srinivasan B. A guide to the Michaelis–Menten equation: steady state and beyond. *FEBS J.* **2021**.

(34) Wagner, G. K.; Pesnot, T. Glycosyltransferases and Their Assays. *ChemBioChem* **2010**, *11*, 1939–1949.

(35) Li, K. Determination of sialic acids in human serum by reversed-phase liquid chromatography with fluorimetric detection. *J. Chromatogr. B Biomed. Sci. Appl.* **1992**, *579*, 209–213.

(36) Dennis, W.; Gal, U. A Coupled assay for UDP-GlcNAc: Galβl-3GalNAc-R β1,6-N-acetylglucosaminyltransferase(GlcNAc to GalNAc). *Anal. Biochem.* **1992**, *266*, 262–266.

(37) Lowery, R.; Kleman-Leyer, K.; Staeben, M.; Westermeyer, T. Detecting the activity of an

screening acceptor substrates, inhibitors, or activators of enzymes catalyzing group transfer reactions to facilitate the development of more selective and therapeutic drugs. US patent No. 20080233592 (2008).

(38) Kumagai, K., Kojima, H., Okabe, T., and Nagano, T. Development of a highly sensitive, high-throughput assay for glycosyltransferases using enzyme-coupled fluorescence detection. *Anal. Biochem.* **2014**, *447*, 146−155.

(39) Gong, H.; Zhang, B.; Little, G.; Kovar, J.; Chen, H.; Xie, W.; Schutz-Geschwender, A.; Olive, D. M. β-Galactosidase Activity Assay Using Far-Red-Shifted Fluorescent Substrate DDAOG. *Anal. Biochem.* **2009**, *386*, 59–64.

(40) Hunter, C. D.; Porter, E. M.; Cairo, C. W. Human Neuraminidases Have Reduced Activity towards Modified Sialic Acids on Glycoproteins. *Carbohydr. Res.* **2020**, *497*, 108139.

(41) Aharoni, A.; Thieme, K.; Chiu, C. P. C.; Buchini, S.; Lairson, L. L.; Chen, H.; Strynadka, N. C. J.; Wakarchuk, W. W.; Withers, S. G. High-Throughput Screening Methodology for the Directed Evolution of Glycosyltransferases. *Nat. Methods* **2006**, *3*, 609–614.

(42) Helm, J. S.; Hu, Y.; Chen, L.; Gross, B.; Walker, S. Identification of Active-Site Inhibitors of MurG Using a Generalizable, High-Throughput Glycosyltransferase Screen. *J. Am. Chem. Soc.* **2003**, *125*, 11168–11169.

(43) Pavelka, S. Radiometric enzyme assays: development of methods for extremely sensitive determination of types 1, 2 and 3 iodothyronine deiodinase enzyme activities. *J. Radioanal. Nucl. Chem.* **2010**, *286*, 861–865.

(44) Hood, C. M.; Kelly, V. A.; Bird, M. I.; Britten, C. J. Measurement of α(1-3) fucosyltransferase activity using scintillation proximity. *Anal. Biochem.* **1998**, *255*, 8–12.

(45) Miyashiro, M.; Furuya, S.; Sugita, T. A high-throughput screening system for α1–3

fucosyltransferase-VII inhibitor utilizing scintillation proximity assay. *Anal. Biochem.* **2005**, *338*, 168–170.

(46) Ahsen, O. von; Voigtmann, U.; Klotz, M.; Nifantiev, N.; Schottelius, A.; Ernst, A.; Müller-Tiemann, B.; Parczyk, K. A miniaturized high-throughput screening assay for fucosyltransferase VII. *Anal. Biochem.* **2008**, *372*, 96–105.

(47) von Ahsen, O.; Voigtmann, U.; Klotz, M.; Nifantiev, N.; Schottelius, A.; Ernst, A.; Müller-Tiemann, B.; Parczyk, K. A miniaturized high-throughput screening assay for fucosyltransferase VII. *Anal. Biochem.* **2008**, *372*, 96–105.

(48) Brokx, R. D.; Revers, L.; Zhang, Q.; Yang, S.; Mal, T. K.; Ikura, M.; Gariépy, J. Nuclear magnetic resonance-based dissection of a glycosyltransferase specificity for the mucin MUC1 tandem repeat. Biochemistry **2003**, *42*, 13817–13825.

(49) Exnowitz, F.; Meyer, B.; Hackl, T. NMR for direct determination of Km and Vmax of enzyme reactions based on the lambert W function-analysis of progress curves. *Biochim. Biophys. Acta (BBA)-Proteins Proteomics* **2012**, *1824*, 443–449.

(50) Sukovich, D. J., Modavi, C., de Raad, M., Prince, R. N., and Anderson, J. C. DNA-linked enzyme-coupled assay for probing glucosyltransferase specificity. *ACS Synth. Biol.* **2015**, *4*, 833-841.

(51) Sun, H.; Ma, S.; Li, Y.; Qi, H.; Ning, X.; Zheng, J. Electrogenerated chemiluminescence biosensing method for the discrimination of DNA hydroxymethylation and assay of the β-glucosyltransferase activity. *Biosens. Bioelectron.* **2016**, *79*, 92−97.

(52) Liuni, P.; Wilson, D. J. Understanding and optimizing electrospray ionization techniques for proteomic analysis. *Expert Rev. Proteomics* **2011**, *8*, 197–209.

(53) Tang, L.; Kebarle, P. From ions in solution to ions in the gas phase - the mechanism of

electrospray mass spectrometry. *Anal. Chem*. **1993**, *65*, 972A-986A.

(54) Gross, J. H. *Mass Spectrometry*; Springer International Publishing: Cham, **2017**; Vol. 56.

(55) Rayleigh, Lord. XX. On the equilibrium of liquid conducting masses charged with electricity. *London, Edinburgh, Dublin Philos. Mag. J. Sci.* **1882**, *14*, 184–186.

(56) Karas, M.; Bahr, U.; Dülcks, T. Nano-Electrospray ionization mass spectrometry: addressing analytical problems beyond routine. *Fresenius. J. Anal. Chem.* **2000**, *366*, 669–676.

(57) Morad, M. R.; Rajabi, A.; Razavi, M.; Sereshkeh, S. R. P. A very stable high throughput taylor cone-jet in electrohydrodynamics. *Sci. Rep.* **2016**, *6*, 38509.

(58) Iribarne, J. V. On the evaporation of small ions from charged droplets. *J. Chem. Phys.* **1976**, *64*, 2287-2294.

(59) Konermann, L.; Ahadi, E.; Rodriguez, A. D.; Vahidi, S. Unraveling the mechanism of electrospray ionization. *Anal. Chem.* **2013**, *85*, 2–9.

(60) Kaltashov, I. A.; Mohimen, A. Estimates of protein surface areas in solution by electrospray ionization mass spectrometry. *Anal. Chem.* **2005**, *77*, 5370

(61) McAllister, R. G.; Metwally, H.; Sun, Y.; Konermann, L. Release of native-like gaseous proteins from electrospray droplets via the charged residue mechanism: insights from molecular dynamics simulations. *J. Am. Chem. Soc.* **2015**, *137*, 12667–12676.

(62) Metwally, H.; Duez, Q.; Konermann, L. Chain ejection model for electrospray ionization of unfolded proteins: evidence from atomistic simulations and ion mobility spectrometry. *Anal. Chem.* **2018**, *90*, 10069–10077.

(63) March, R. E.; Todd, J. F. J. Radio frequency quadrupole technology: evolution and contributions to mass spectrometry. *Int. J. Mass Spectrom.* **2015**, *377*, 316–328.

(64) Miller, P. E.; Denton, M. B. The quadrupole mass filter: basic operating concepts. *J. Chem. Educ.* **1986**, *63*, 617.

(65) Kero, F. A.; Pedder, R. E.; Yost, R. A. Quadrupole mass analyzers: theoretical and practical considerations. In *Encyclopedia of Genetics, Genomics, Proteomics and Bioinformatics*; **2009**.

(66) Pringle, S. D.; Giles, K.; Wildgoose, J. L.; Williams, J. P.; Slade, S. E.; Thalassinos, K.; Bateman, R. H.; Bowers, M. T.; Scrivens, J. H. An investigation of the mobility separation of some peptide and protein ions using a new hybrid quadrupole/travelling wave IMS/oa-ToF instrument. *Int. J. Mass Spectrom.* **2007***, 261*, 1.

(67) Giles, K.; Pringle, S. D.; Worthington, K. R.; Little, D.; Wildgoose, J. L.; Bateman, R. H. Applications of a travelling wave-based radio-frequency-only stacked ring ion guide. *Rapid Commun. Mass Spectrom.* **2004***, 18*, 2401–2414.

(68) Karasek, F. W. Plasma chromatography. *Anal. Chem.* **1974***, 46*, 710A.

(69) McCullough, B. J.; Kalapothakis, J.; Eastwood, H.; Kemper, P.; MacMillan, D.; Taylor, K.; Dorin, J.; Barran, P. E. *Anal. Chem.* **2008**, *80*, 6336.

(70) Sergio, A.; Manel, A.; Marcelo, B. Development of an ion mobility quadrupole time of flight mass spectrometer. *Anal. Chim. Acta.* **2011***, 703*, 114.

(71) Cohen, M. J.; Karasek, F. W. Plasma chromatography™-a new dimension for gas chromatography and mass spectrometry. *J. Chromatogr. Sci.* **1970***, 8*, 330.

(72) Buryakov, I. A.; Krylov, E. V.; Nazarov, E. G.; Rasulev, U. K. A new method of separation of multi-atomic ions by mobility at atmospheric pressure using a high-frequency amplitude-asymmetric strong electric field. *Int. J. Mass Spectrom. Ion Processes.* **1993***, 128*, 143.

(73) Shvartsburg, A. A.; Smith, R. D. Fundamentals of traveling wave ion mobility spectrometry.

Anal. Chem. **2008**, *80*, 9689.

(74) Wildgoose, J.; McKenna, T.; Hughes, C.; Giles, K.; Pringle, S.; Campuzano, I.; Langridge, J.; Bateman, R. H. Using a novel travelling wave ion mobility device coupled with a time-of-flight mass spectrometer for the analysis of intact proteins. *Mol. Cell. Proteomics.* **2006**, *5*, S14.

(75) Ruotolo, B. T.; Benesch, J. L. P.; Sandercock, A. M.; Hyung, S.-J.; Robinson, C. V. Ion mobility–mass spectrometry analysis of large protein complexes. *Nat. Protocols.* **2008**, *3*, 1139.

(76) Giles, K.; Williams, J. P.; Campuzano, I. Enhancements in travelling wave ion mobility resolution. *Rapid Commun. Mass Spectrom.* **2011**, *25*, 1559.

(77) Guilhaus, M. Special feature: Tutorial. Principles and instrumentation in time-of-flight mass spectrometry. Physical and instrumental concepts. *J. Mass Spectrom.* **1995**, *30*, 1519–1532.

(78) Zubarev, R. A.; Makarov, A. Orbitrap mass spectrometry. *Anal. Chem.* **2013**, *85*, 5288–5296.

(79) Perry, R. H.; Cooks, R. G.; Noll, R. J. Orbitrap mass spectrometry: instrumentation, ion motion and applications. *Mass Spectrom. Rev.* **2008**, *27*, 661–699.

(80) Makarov, A. Electrostatic Axially Harmonic Orbital Trapping: A high-performance technique of mass analysis. *Anal. Chem.* **2000**, *72*, 1156–1162.

(81) Liesener, A.; Karst, U. Monitoring enzymatic conversions by mass spectrometry: a critical review. *Anal. Bioanal. Chem.* **2005**, *382*, 1451–1464.

(82) Pi, N.; Armstrong, J. I.; Bertozzi, C. R.; Leary, J. A. Kinetic analysis of NodST sulfotransferase using an electrospray ionization mass spectrometry assay. *Biochemistry* **2002**, *41*, 13283–13288.

(83) Norris, A. J.; Whitelegge, J. P.; Faull, K. F.; Toyokuni, T. Analysis of enzyme kinetics using

electrospray ionization mass spectrometry and multiple reaction monitoring: fucosyltransferase V. *Biochemistry* **2001**, *40*, 3774–3779.

(84) Danan, L. M.; Yu, Z.; Hoffhines, A. J.; Moore, K. L.; Leary, J. A. Mass spectrometric kinetic analysis of human tyrosylprotein sulfotransferase-1 and -2. *J. Am. Soc. Mass Spectrom.* **2008**, *19*, 1459–1466.

(85) Fabris, D. Steady-state kinetics of ricin a-chain reaction with the sarcin−ricin loop and with HIV-1 Ψ-RNA hairpins evaluated by direct infusion electrospray ionization mass spectrometry. *J. Am. Chem. Soc.* **2000**, *122*, 8779–8780.

(86) Cheng, S.; Wu, Q.; Xiao, H.; Chen, H. Online monitoring of enzymatic reactions using time-resolved desorption electrospray ionization mass rpectrometry. *Anal. Chem.* **2017**, *89*, 2338–2344.

(87) Sandbhor, M. S.; Soya, N.; Albohy, A.; Zheng, R. B.; Cartmell, J.; Bundle, D. R.; Klassen, J. S.; Cairo, C. W. Substrate recognition of the membrane-associated sialidase NEU3 requires a hydrophobic aglycone. *Biochemistry* **2011**, *50*, 6753–6762.

(88) Hines, H. B.; Brueggemann, E. E.; Hale, M. L. High-performance liquid chromatography–mass selective detection assay for adenine released from a synthetic RNA substrate by ricin A chain. *Anal. Biochem.* **2004**, *330*, 119–122.

(89) Gerber, S. A.; Scott, C. R.; Turecek, F.; Gelb, M. H. Analysis of rates of multiple enzymes in cell lysates by electrospray ionization mass spectrometry. *J. Am. Chem. Soc.* **1999**, *121*, 1102–1103.

(90) Deng, G.; Gu, R.-F.; Marmor, S.; Fisher, S. L.; Jahic, H.; Sanyal, G. Development of an LC–MS based enzyme activity assay for MurC: application to evaluation of inhibitors and kinetic analysis. *J. Pharm. Biomed. Anal.* **2004**, *35*, 817–828.

(91) Ge, X.; Sirich, T. L.; Beyer, M. K.; Desaire, H.; Leary, J. A. A Strategy for the determination of enzyme kinetics using electrospray ionization with an ion trap mass spectrometer. *Anal. Chem.* **2001**, *73*, 5078–5082.

(92) Gabelica, V.; Galic, N.; Rosu, F.; Houssier, C.; De Pauw, E. Influence of response factors on determining equilibrium association constants of non-covalent complexes by electrospray ionization mass spectrometry. *J. Mass Spectrom.* **2003**, *38*, 491–501.

(93) Golubović, J.; Birkemeyer, C.; Protić, A.; Otašević, B.; Zečević, M. Structure–Response Relationship in Electrospray Ionization-Mass Spectrometry of Sartans by Artificial Neural Networks. *J. Chromatogr. A* **2016**, *1438*, 123–132.

(94) Huffman, B. A.; Poltash, M. L.; Hughey, C. A. Effect of Polar Protic and Polar Aprotic Solvents on Negative-Ion Electrospray Ionization and Chromatographic Separation of Small Acidic Molecules. *Anal. Chem.* **2012**, *84*, 9942–9950.

(95) Henriksen, T.; Juhler, R. K.; Svensmark, B.; Cech, N. B. The Relative Influences of Acidity and Polarity on Responsiveness of Small Organic Molecules to Analysis with Negative Ion Electrospray Ionization Mass Spectrometry (ESI-MS). *J. Am. Soc. Mass Spectrom.* **2005**, *16*, 446–455.

(96) Liigand, P.; Liigand, J.; Kaupmees, K.; Kruve, A. 30 Years of Research on ESI/MS Response: Trends, Contradictions and Applications. *Anal. Chim. Acta* **2021**, *1152*, 238117.

(97) Stokvis, E.; Rosing, H.; Beijnen, J. H. Stable Isotopically Labeled Internal Standards in Quantitative Bioanalysis Using Liquid Chromatography/Mass Spectrometry: Necessity or Not? *Rapid Commun. Mass Spectrom.* **2005**, *19*, 401–407.

(98) Wang, S.; Cyronak, M.; Yang, E. Does a Stable Isotopically Labeled Internal Standard Always Correct Analyte Response?: A Matrix Effect Study on a LC/MS/MS Method for the

Determination of Carvedilol Enantiomers in Human Plasma. *J. Pharm. Biomed. Anal.* **2007**, *43*, 701–707.

(99) Kitova, E. N.; El-Hawiet, A.; Schnier, P. D.; Klassen, J. S. Reliable determinations of protein–ligand interactions by direct ESI-MS measurements. Are we there yet? *J. Am. Soc. Mass Spectrom.* **2012**, *23*, 431–441.

(100) Marshall, A. G.; Hendrickson, C. L.; Jackson, G. S. Fourier transform ion cyclotron resonance mass spectrometry: a primer. *Mass Spectrom. Rev.* **1998**, *17*, 1–35.

(101) Wang, W.; Kitova, E. N.; Klassen, J. S. Influence of solution and gas phase processes on protein-carbohydrate binding affinities determined by nanoelectrospray fourier transform ion cyclotron resonance mass spectrometry. *Anal. Chem.* **2003**, *75*, 4945–4955.

(102) Hossain, B. M.; Konermann, L. Pulsed hydrogen/deuterium exchange MS/MS for studying the relationship between noncovalent protein complexes in solution and in the gas phase after electrospray ionization. *Anal. Chem.* **2006**, *78*, 1613–1619.

(103) Wang, W.; Kitova, E. N.; Klassen, J. S. Nonspecific protein-carbohydrate complexes produced by nanoelectrospray ionization. Factors influencing their formation and stability. *Anal. Chem.* **2005**, *77*, 3060–3071.

(104) Sun, J.; Kitova, E. N.; Wang, W.; Klassen, J. S. Method for distinguishing specific from nonspecific protein-ligand complexes in nanoelectrospray ionization mass spectrometry. *Anal. Chem.* **2006**, *78*, 3010–3018.

(105) Sun, N.; Soya, N.; Kitova, E. N.; Klassen, J. S. Nonspecific interactions between proteins and charged biomolecules in electrospray ionization mass spectrometry. *J. Am. Soc. Mass Spectrom.* **2010**, *21*, 472–481.

(106) Sun, J.; Kitova, E. N.; Sun, N.; Klassen, J. S. Method for identifying nonspecific protein-

protein interactions in nanoelectrospray ionization mass spectrometry. *Anal. Chem.* **2007**, *79*, 9301–9311.

(107) Daubenfeld, T.; Bouin, A. P.; van der Rest, G. A Deconvolution method for the separation of specific versus nonspecific interactions in noncovalent protein-ligand complexes analyzed by ESI-FT-ICR mass spectrometry. *J. Am. Soc. Mass Spectrom.* **2006**, *17*, 1239–1248.

(108) Shimon, L.; Sharon, M.; Horovitz, A. A method for removing effects of nonspecific binding on the distribution of binding stoichiometries: application to mass spectroscopy data. *Biophys. J.* **2010**, *99*, 1645–1649.

(109) Sun, N.; Sun, J.; Kitova, E. N.; Klassen, J. S. Identifying nonspecific ligand binding in electrospray ionization mass spectrometry using the reporter molecule method. *J. Am. Soc. Mass Spectrom.* **2009**, *20*, 1242–1250.

(110 Kitova, E. N.; Soya, N.; Klassen, J. S. Identifying specific small-molecule interactions using electrospray ionization mass spectrometry. *Anal. Chem.* **2011**, *83*, 5160–5167.

(111) Deng, L.; Sun, N.; Kitova, E. N.; Klassen, J. S. Direct quantification of protein-metal ion affinities by electrospray ionization mass spectrometry. *Anal. Chem.* **2010**, *82*, 2170–2174.

(112) Van Berkel, G. J.; Asano, K. G.; Schnier, P. D. Electrochemical Processes in a Wire-in-a-Capillary Bulk-Loaded, Nano-Electrospray Emitter. *J. Am. Soc. Mass Spectrom*. **2001**, *12*, 853–862.

(113) Báez Bolivar, E. G.; Bui, D. T.; Kitova, E. N.; Han, L.; Zheng, R. B.; Luber, E. J.; Sayed, S. Y.; Mahal, L. K.; Klassen, J. S. Submicron Emitters Enable Reliable Quantification of Weak Protein–Glycan Interactions by ESI-MS. *Anal. Chem*. **2021**, *93*, 4231–4239.

Chapter 2

(1) Lombard, V.; Golaconda Ramulu, H.; Drula, E.; Coutinho, P. M.; Henrissat, B. The carbohydrate-active enzymes database (CAZy) in 2013. *Nucleic Acids Res.* **2013**, *42*, D490–D495.

(2) Cantarel, B. L.; Coutinho, P. M.; Rancurel, C.; Bernard, T.; Lombard, V.; Henrissat, B. The carbohydrate-active enzymes database (CAZy): an expert resource for glycogenomics. *Nucleic Acids Res.* **2008**, *37*, D233–D238.

(3) Helbert, W.; Poulet, L.; Drouillard, S.; Mathieu, S.; Loiodice, M.; Couturier, M.; Lombard, V.; Terrapon, N.; Turchetto, J.; Vincentelli, R.; et al. Discovery of novel carbohydrate-active enzymes through the rational exploration of the protein sequences space. *Proc. Natl. Acad. Sci.* **2019**, *116*, 6063 LP – 6068.

(4) Miyagi, T.; Yamaguchi, K. Mammalian sialidases: Physiological and pathological roles in cellular functions. *Glycobiology.* **2012**, *22*, 880–896.

(5) Nijikken, Y.; Tsukada, T.; Igarashi, K.; Samejima, M.; Wakagi, T.; Shoun, H.; Fushinobu, S. Crystal structure of intracellular family 1 β-glucosidase BGL1A from the basidiomycete phanerochaete chrysosporium. *FEBS Lett.* **2007**, *581*, 1514–1520.

(6) Kaoutari, A. El; Armougom, F.; Gordon, J. I.; Raoult, D.; Henrissat, B. The abundance and variety of carbohydrate-active enzymes in the human gut microbiota. *Nat. Rev. Microbiol.* **2013**, *11*, 497.

(7) Zhang, Z.; Wuhrer, M.; Holst, S. Serum sialylation changes in cancer. *Glycoconj. J.* **2018**, *35*, 139–160.

(8) Hou, G.; Liu, G.; Yang, Y.; Li, Y.; Yuan, S.; Zhao, L.; Wu, M.; Liu, L.; Zhou, W. Neuraminidase 1 (NEU1) promotes proliferation and migration as a diagnostic and

prognostic biomarker of hepatocellular carcinoma. *Oncotarget* **2016**, *7*, 64957–64966.

(9) Pinho, S. S.; Reis, C. A. Glycosylation in cancer: mechanisms and clinical implications. *Nat. Rev. Cancer* **2015**, *15*, 540.

(10) Abbott, D. W.; Macauley, M. S.; Vocadlo, D. J.; Boraston, A. B. Streptococcus pneumoniae endohexosaminidase D, structural and mechanistic insight into substrate-assisted catalysis in family 85 glycoside hydrolases. *J. Biol. Chem.* **2009**, *284*, 11676–11689.

(11) Wilson, D. B. Cellulases and biofuels. *Curr. Opin. Biotechnol.* **2009**, *20*, 295–299.

(12) Yuzwa, S. A.; Macauley, M. S.; Heinonen, J. E.; Shan, X.; Dennis, R. J.; He, Y.; Whitworth, G. E.; Stubbs, K. A.; McEachern, E. J.; Davies, G. J.; et al. A potent mechanism-inspired O-GlcNAcase inhibitor that blocks phosphorylation of tau *in vivo*. *Nat. Chem. Biol.* **2008**, *4*, 483-490.

(13) Bardgett, R. D.; Freeman, C.; Ostle, N. J. Microbial contributions to climate change through carbon cycle feedbacks. *Isme J.* **2008**, *2*, 805-814.

(14) Davies, G. J.; Williams, S. J. Carbohydrate-active enzymes: sequences, shapes, contortions and cells. *Biochem. Soc. Trans.* **2016**, *44*, 79 LP – 87.

(15) Li, K. Determination of sialic acids in human serum by reversed-phase liquid chromatography with fluorimetric detection. *J. Chromatogr. B Biomed. Sci. Appl.* **1992**, *579*, 209–213.

(16) Dennis, W.; Gal, U. A Coupled assay for UDP-GlcNAc: Galβl-3GalNAc-R β1,6-N-acetylglucosaminyltransferase(GlcNAc to GalNAc). *Anal. Biochem.* **1992**, *266*, 262–266.

(17) Lowery, R.; Kleman-Leyer, K.; Staeben, M.; Westermeyer, T. Detecting the activity of an screening acceptor substrates, inhibitors, or activators of enzymes catalyzing group transfer reactions to facilitate the development of more selective and therapeutic drugs. US patent

No. 20080233592 (2008).

(18) Kumagai, K., Kojima, H., Okabe, T., and Nagano, T. Development of a highly sensitive, high-throughput assay for glycosyltransferases using enzyme-coupled fluorescence detection. *Anal. Biochem.* **2014**, *447*, 146−155.

(19) Sukovich, D. J., Modavi, C., de Raad, M., Prince, R. N., and Anderson, J. C. DNA-linked enzyme-coupled assay for probing glucosyltransferase specificity. *ACS Synth. Biol.* **2015**, *4*, 833-841.

(20) Sun, H.; Ma, S.; Li, Y.; Qi, H.; Ning, X.; Zheng, J. Electrogenerated chemiluminescence biosensing method for the discrimination of DNA hydroxymethylation and assay of the β-glucosyltransferase activity. *Biosens. Bioelectron.* **2016**, *79*, 92−97.

(21) Pavelka, S. Radiometric enzyme assays: development of methods for extremely sensitive determination of types 1, 2 and 3 iodothyronine deiodinase enzyme activities. *J. Radioanal. Nucl. Chem.* **2010**, *286*, 861–865.

(22) Cleland, W. W. The use of isotope effects to determine enzyme mechanisms. *Arch. Biochem. Biophys.* **2005**, *433*, 2–12.

(23) Liesener, A.; Karst, U. Monitoring enzymatic conversions by mass spectrometry: a critical review. *Anal. Bioanal. Chem.* **2005**, *382*, 1451–1464.

(24) Pi, N.; Armstrong, J. I.; Bertozzi, C. R.; Leary, J. A. Kinetic analysis of NodST sulfotransferase using an electrospray ionization mass spectrometry assay. *Biochemistry* **2002**, *41*, 13283–13288.

(25) Norris, A. J.; Whitelegge, J. P.; Faull, K. F.; Toyokuni, T. Analysis of enzyme kinetics using electrospray ionization mass spectrometry and multiple reaction monitoring: fucosyltransferase V. *Biochemistry* **2001**, *40*, 3774–3779.

(26) Danan, L. M.; Yu, Z.; Hoffhines, A. J.; Moore, K. L.; Leary, J. A. Mass spectrometric kinetic analysis of human tyrosylprotein sulfotransferase-1 and -2. *J. Am. Soc. Mass Spectrom.* **2008**, *19*, 1459–1466.

(27) Fabris, D. Steady-state kinetics of ricin a-chain reaction with the sarcin−ricin loop and with HIV-1 Ψ-RNA hairpins evaluated by direct infusion electrospray ionization mass spectrometry. *J. Am. Chem. Soc.* **2000**, *122*, 8779–8780.

(28) Cheng, S.; Wu, Q.; Xiao, H.; Chen, H. Online monitoring of enzymatic reactions using time-resolved desorption electrospray ionization mass rpectrometry. *Anal. Chem.* **2017**, *89*, 2338–2344.

(29) Sandbhor, M. S.; Soya, N.; Albohy, A.; Zheng, R. B.; Cartmell, J.; Bundle, D. R.; Klassen, J. S.; Cairo, C. W. Substrate recognition of the membrane-associated sialidase NEU3 requires a hydrophobic aglycone. *Biochemistry* **2011**, *50*, 6753–6762.

(30) Hines, H. B.; Brueggemann, E. E.; Hale, M. L. High-performance liquid chromatography–mass selective detection assay for adenine released from a synthetic RNA substrate by ricin A chain. *Anal. Biochem.* **2004**, *330*, 119–122.

(31) Gerber, S. A.; Scott, C. R.; Turecek, F.; Gelb, M. H. Analysis of rates of multiple enzymes in cell lysates by electrospray ionization mass spectrometry. *J. Am. Chem. Soc.* **1999**, *121*, 1102–1103.

(32) Deng, G.; Gu, R.-F.; Marmor, S.; Fisher, S. L.; Jahic, H.; Sanyal, G. Development of an LC–MS based enzyme activity assay for MurC: application to evaluation of inhibitors and kinetic analysis. *J. Pharm. Biomed. Anal.* **2004**, *35*, 817–828.

(33) Ge, X.; Sirich, T. L.; Beyer, M. K.; Desaire, H.; Leary, J. A. A Strategy for the determination of enzyme kinetics using electrospray ionization with an ion trap mass spectrometer. *Anal.*

Chem. **2001**, *73*, 5078–5082.

(34) Kitov, P. I.; Kitova, E. N.; Han, L.; Li, Z.; Jung, J.; Rodrigues, E.; Hunter, C. D.; Cairo, C. W.; Macauley, M. S.; Klassen, J. S. A quantitative, high-throughput method identifies protein–glycan interactions via mass spectrometry. *Commun. Biol.* **2019**, *2*, 268-274.

(35) Moremen, K. W.; Ramiah, A.; Stuart, M.; Steel, J.; Meng, L.; Forouhar, F.; Moniz, H. A.; Gahlay, G.; Gao, Z.; Chapla, D.; et al. Expression system for structural and functional studies of human glycosylation enzymes. *Nat. Chem. Biol.* **2017**, *14*, 156-162.

(36) Kroetsch, A.; Chin, B.; Nguyen, V.; Gao, J.; Park, S. Functional expression of monomeric streptavidin and fusion proteins in escherichia coli: applications in flow cytometry and ELISA. *Appl. Microbiol. Biotechnol.* **2018**, *102*, 10079–10089.

(37) Sun, J.; Kitova, E. N.; Wang, W.; Klassen, J. S. Method for distinguishing specific from nonspecific protein - ligand complexes in nanoelectrospray ionization mass spectrometry. *Anal. Chem.* **2006**, *78*, 3010–3018.

(38) Sun, N.; Soya, N.; Kitova, E. N.; Klassen, J. S. Nonspecific interactions between proteins and charged biomolecules in electrospray. *J. Am. Soc. Mass Spectrom.* **2010**, *21*, 472–481.

(39) Wang, W.; Kitova, E. N.; Klassen, J. S. Nonspecific protein - carbohydrate complexes produced by nanoelectrospray ionization. Factors influencing their formation and stability. *Anal. Chem.* **2005**, *77*, 3060–3071.

(40) Ha, K.-T.; Lee, Y.-C.; Cho, S.-H.; Kim, J.-K.; Kim, C.-H. Molecular characterization of membrane type and ganglioside-specific sialidase (Neu3) expressed in E. coli. *Mol. Cells.* **2004**, *17*, 267–273.

(41) Zanchetti, G.; Colombi, P.; Manzoni, M.; Anastasia, L.; Caimi, L.; Borsani, G.; Venerando, B.; Tettamanti, G.; Preti, A.; Monti, E.; et al. Sialidase NEU3 is a peripheral membrane

protein localized on the cell surface and in endosomal structures. *Biochem. J.* **2007**, *408*, 211–219.

(42) Monti, E.; Bassi, M. T.; Papini, N.; Riboni, M.; Manzoni, M.; Venerando, B.; Croci, G.; Preti, A.; Ballabio, A.; Tettamanti, G.; et al. Identification and expression of NEU3, a novel human sialidase associated to the plasma membrane. *Biochem. J.* **2000**, *349*, 343–351.

(43) Smutova, V.; Albohy, A.; Pan, X.; Korchagina, E.; Miyagi, T.; Bovin, N.; Cairo, C. W.; Pshezhetsky, A. V. Structural basis for substrate specificity of mammalian neuraminidases. *PLoS One* **2014**, *9*, e106320–e106320.

(44) Albohy, A.; Li, M. D.; Zheng, R. B.; Zou, C.; Cairo, C. W. Insight into substrate recognition and catalysis by the human neuraminidase 3 (NEU3) through molecular modeling and site-directed mutagenesis. *Glycobiology.* **2010**, *20*, 1127–1138.

(45) Smith, K. S.; Cosper, N. J.; Stalhandske, C.; Scott, R. A.; Ferry, J. G. Structural and kinetic characterization of an archaeal β-class carbonic anhydrase. *J. Bacteriol.* **2000**, *182*, 6605 – 6613.

(46) Steiner, H.; Jonsson, B.; Lindskog, S. The catalytic mechanism of carbonic anhydrase. *Eur. J. Biochem.* **1975**, *59*, 253–259.

(47) Weinstein, J.; de Souza-e-Silva, U.; Paulson, J. C. Sialylation of glycoprotein oligosaccharides N-linked to asparagine. Enzymatic characterization of a Gal beta 1 to 3(4)GlcNAc alpha 2 to 3 sialyltransferase and a Gal beta 1 to 4GlcNAc alpha 2 to 6 sialyltransferase From Rat Liver. *J. Biol. Chem.* **1982**, *257*, 13845–13853.

(48) Kitagawa, H.; Paulson, J. C. Cloning of a novel alpha 2,3-sialyltransferase that sialylates glycoprotein and glycolipid carbohydrate groups. *J. Biol. Chem.* **1994**, *269*, 1394–1401.

(49) Sasaki, K.; Watanabe, E.; Kawashima, K.; Sekine, S.; Dohi, T.; Oshima, M.; Hanai, N.;

Nishi, T.; Hasegawa, M. Expression cloning of a novel Gal beta (1-3/1-4) GlcNAc alpha 2,3-sialyltransferase using lectin resistance selection. *J. Biol. Chem.* **1993**, *268*, 22782–22787.

(50) Kessel, D.; Chou, T.; Allen, J. Some properties of sialyltransferase in plasma and lymphocytes of patients with chronic lymphocytic leukemia. *Eur. J. Biochem.* **1978**, *82*, 535–541.

(51) Audry, M.; Jeanneau, C.; Imberty, A.; Harduin-Lepers, A.; Delannoy, P.; Breton, C. Current trends in the structure–activity relationships of sialyltransferases. *Glycobiology.* **2010**, *21*, 716–726.

(52) Kono, M.; Ohyama, Y.; Lee, Y.-C.; Hamamoto, T.; Kojima, N.; Tsuji, S. Mouse β-galactoside α2,3-sialyltransferases: comparison of in vitro substrate specificities and tissue specific expression. *Glycobiology.* **1997**, *7*, 469–479.

(53) Shariat, S. F.; Semjonow, A.; Lilja, H.; Savage, C.; Vickers, A. J.; Bjartell, A. Tumor markers in prostate cancer I: blood-based markers. *Acta Oncol. (Madr).* **2011**, *50*, 61–75.

(54) Stamey, T. A.; Yang, N.; Hay, A. R.; McNeal, J. E.; Freiha, F. S.; Redwine, E. Prostate-specific antigen as a serum marker for adenocarcinoma of the prostate. *N. Engl. J. Med.* **1987**, *317*, 909–916.

(55) Okada, T.; Sato, Y.; Kobayashi, N.; Sumida, K.; Satomura, S.; Matsuura, S.; Takasaki, M.; Endo, T. Structural characteristics of the *N*-glycans of two isoforms of prostate-specific antigens purified from human seminal fluid. *Biochim. Biophys. Acta.* **2001**, *1525*, 149–160.

(56) Tabarés, G.; Radcliffe, C. M.; Barrabés, S.; Ramírez, M.; Aleixandre, R. N.; Hoesel, W.; Dwek, R. A.; Rudd, P. M.; Peracaula, R.; de Llorens, R. Different glycan structures in prostate-specific antigen from prostate cancer sera in relation to seminal plasma PSA.

Glycobiology. **2005**, *16*, 132–145.

(57) Susa, A. C.; Xia, Z.; Williams, E. R. Small emitter tips for native mass spectrometry of proteins and protein complexes from nonvolatile buffers that mimic the intracellular environment. *Anal. Chem*. **2017**, *89*, 3116–3122.

(58) Susa, A. C.; Lippens, J. L.; Xia, Z.; Loo, J. A.; Campuzano, I. D. G.; Williams, E. R. Submicrometer emitter ESI tips for native mass spectrometry of membrane proteins in ionic and nonionic detergents. *J. Am. Soc. Mass Spectrom*. **2018**, *29*, 203–206.

(59) Susa, A. C.; Xia, Z.; Williams, E. R. Native mass spectrometry from common buffers with salts that mimic the extracellular environment. *Angew. Chemie Int. Ed*. **2017**, *56*, 7912–7915.

Chapter 3

(1) Schmaltz, R. M.; Hanson, S. R.; Wong, C.-H. Enzymes in the synthesis of glycoconjugates. *Chem. Rev.* **2011**, *111*, 4259–4307.

(2) Schwarz, F.; Aebi, M. Mechanisms and principles of *N*-linked protein glycosylation. *Curr. Opin. Struct. Biol.* **2011**, *21*, 576–582.

(3) Varki, A. Biological roles of glycans. *Glycobiology* **2017**, *27*, 3–49.

(4) Arnold, J. N.; Wormald, M. R.; Sim, R. B.; Rudd, P. M.; Dwek, R. A. The impact of glycosylation on the biological function and structure of human immunoglobulins. *Annu. Rev. Immunol.* **2007**, *25*, 21–50.

(5) Ott, C.; Jacobs, K.; Haucke, E.; Navarrete Santos, A.; Grune, T.; Simm, A. Role of advanced glycation end products in cellular signaling. *Redox Biol.* **2014**, *2*, 411–429.

(6) Moremen, K. W.; Tiemeyer, M.; Nairn, A. V. Vertebrate protein glycosylation: diversity, synthesis and function. *Nat. Rev. Mol. Cell Biol.* **2012**, *13*, 448–462.

(7) Kightlinger, W.; Warfel, K. F.; DeLisa, M. P.; Jewett, M. C. Synthetic glycobiology: parts, systems, and applications. *ACS Synth. Biol*. **2020**, *9*, 1534-1562.

(8) Jaroentomeechai, T.; Stark, J. C.; Natarajan, A.; Glasscock, C. J.; Yates, L. E.; Hsu, K. J.; Mrksich, M.; Jewett, M. C.; DeLisa, M. P. Single-pot glycoprotein biosynthesis using a cell-free transcription-translation system enriched with glycosylation machinery. *Nat. Commun*. **2018**, *9*, 2686-2696.

(9) Natarajan, A.; Jaroentomeechai, T.; Cabrera-Sánchez, M.; Mohammed, J. C.; Cox, E. C.; Young, O.; Shajahan, A.; Vilkhovoy, M.; Vadhin, S.; Varner, J. D.; et al. Engineering orthogonal human O-linked glycoprotein biosynthesis in bacteria. *Nat. Chem. Biol*. **2020**, *16*, 1062-1070.

(10) Kightlinger, W.; Duncker, K. E.; Ramesh, A.; Thames, A. H.; Natarajan, A.; Stark, J. C.; Yang, A.; Lin, L.; Mrksich, M.; DeLisa, M. P.; et al. A cell-free biosynthesis platform for modular construction of protein glycosylation pathways. *Nat. Commun.* **2019**, *10*, 5404-5412.

(11) Giddens, J. P.; Lomino, J. V; DiLillo, D. J.; Ravetch, J. V; Wang, L.-X. Site-selective chemoenzymatic glycoengineering of Fab and Fc glycans of a therapeutic antibody. *Proc. Natl. Acad. Sci.* **2018**, *115*, 12023-12027.

(12) Wang, L.-X.; Lomino, J. V. Emerging technologies for making glycan-defined glycoproteins. *ACS Chem. Biol.* **2012**, *7*, 110-122.

(13) Czabany, T.; Schmölzer, K.; Luley-Goedl, C.; Ribitsch, D.; Nidetzky, B. All-in-one assay for β-D-galactoside sialyltransferases: quantification of productive turnover, error hydrolysis, and site selectivity. *Anal. Biochem.* **2015**, *483*, 47-53.

(14) Yu, H.; Chokhawala, H.; Karpel, R.; Yu, H.; Wu, B.; Zhang, J.; Zhang, Y.; Jia, Q.; Chen, X. A multifunctional *Pasteurella multocida* sialyltransferase: a powerful tool for the synthesis of sialoside libraries. *J. Am. Chem. Soc.* **2005**, *127*, 17618-17619.

(15) Gosselin, S.; Alhussaini, M.; Streiff, M. B.; Takabayashi, K.; Palcic, M. M. A continuous spectrophotometric assay for glycosyltransferase. *Anal. Biochem.* **1994**, *220*, 92-97.

(16) Ibatullin, F. M.; Banasiak, A.; Baumann, M. J.; Greffe, L.; Takahashi, J.; Mellerowicz, E. J.; Brumer, H. A real-time fluorogenic assay for the visualization of glycoside hydrolase activity in planta. *Plant Physiol.* **2009**, *151*, 1741-1750.

(17) Weinstein, J.; de Souza-e-Silva, U.; Paulson, J. C. Sialylation of glycoprotein oligosaccharides N-linked to asparagine. Enzymatic characterization of a Galβ1-3(4)GlcNAc α2-3 sialyltransferase and a Galβ1-4GlcNAc α2-6 sialyltransferase from rat liver. *J. Biol. Chem.* **1982**, *257*, 13845-13853.

(18) Abukar, T.; Rahmani, S.; Thompson, N. K.; Antonescu, C. N.; Wakarchuk, W. W. Development of BODIPY labelled sialic acids as sialyltransferase substrates for direct detection of terminal galactose on N- and O-Linked glycans. *Carbohydr. Res.* **2021**, *500*, 108249.

(19) Sun, C. Q.; Hubl, U.; Hoefakker, P.; Vasudevamurthy, M. K.; Johnson, K. D. A new assay for determining ganglioside sialyltransferase activities lactosylceramide-2,3-sialyltransferase (SAT I) and monosialylganglioside-2,3-sialyltransferase (SAT IV). *PloS One* **2014**, *9*, e94206.

(20) Schmölzer, K.; Ribitsch, D.; Czabany, T.; Luley-Goedl, C.; Kokot, D.; Lyskowski, A.; Zitzenbacher, S.; Schwab, H.; Nidetzky, B. Characterization of a multifunctional α2,3-sialyltransferase from *Pasteurella dagmatis*. *Glycobiology* **2013**, *23*, 1293–1304.

(21) Li, W.; Xiao, A.; Li, Y.; Yu, H.; Chen, X. Chemoenzymatic synthesis of Neu5Ac9NAc-containing α2–3- and α2–6-Linked sialosides and their use for sialidase substrate specificity studies. *Carbohydr. Res.* **2017**, *451*, 51–58.

(22) Norris, A. J.; Whitelegge, J. P.; Faull, K. F.; Toyokuni, T. Analysis of enzyme kinetics using electrospray ionization mass spectrometry and multiple reaction monitoring: fucosyltransferase V. *Biochemistry* **2001**, *40*, 3774–3779.

(23) Sandbhor, M. S.; Soya, N.; Albohy, A.; Zheng, R. B.; Cartmell, J.; Bundle, D. R.; Klassen, J. S.; Cairo, C. W. Substrate recognition of the membrane-associated sialidase NEU3 requires a hydrophobic aglycone. *Biochemistry* **2011**, *50*, 6753–6762.

(24) Nagy, G.; Peng, T.; Pohl, N. L. B. General label-free mass spectrometry-based assay to identify glycosidase substrate competence. *Anal. Chem.* **2016**, *88*, 7183–7190.

(25) Jänis, J.; Pulkkinen, P.; Rouvinen, J.; Vainiotalo, P. Determination of steady-state kinetic parameters for a xylanase-catalyzed hydrolysis of neutral underivatized xylooligosaccharides by mass spectrometry. *Anal. Biochem.* **2007**, *365*, 165–173.

(26) Liesener, A.; Karst, U. Monitoring enzymatic conversions by mass spectrometry: a critical review. *Anal. Bioanal. Chem.* **2005**, *382*, 1451–1464.

(27) Cheng, S.; Wu, Q.; Xiao, H.; Chen, H. Online monitoring of enzymatic reactions using time-resolved desorption electrospray ionization mass spectrometry. *Anal. Chem.* **2017**, *89*, 2338–2344.

(28) Solano, M. I.; Woolfitt, A. R.; Williams, T. L.; Pierce, C. L.; Gubareva, L. V; Mishin, V.; Barr, J. R. Quantification of influenza neuraminidase activity by ultra-high performance liquid chromatography and isotope dilution mass spectrometry. *Anal. Chem.* **2017**, *89*, 3130–3137.

(29) Hines, H. B.; Brueggemann, E. E.; Hale, M. L. High-performance liquid chromatography–mass selective detection assay for adenine released from a synthetic RNA substrate by ricin A chain. *Anal. Biochem.* **2004**, *330*, 119-122.

(30) Gerber, S. A.; Scott, C. R.; Turecek, F.; Gelb, M. H.; August, R. V. Analysis of rates of multiple enzymes in cell lysates by electrospray ionization mass spectrometry. *J. Am. Chem. Soc*. **1999**, *121*, 1102–1103.

(31) Li, Z.; Kitov, P. I.; Kitova, E. N.; Mozenah, F.; Rodrigues, E.; Chapla, D. G.; Moremen, K. W.; Macauley, M. S.; Klassen, J. S. CUPRA-ZYME: an assay for measuring carbohydrate-active enzyme activities, pathways, and substrate specificities. *Anal. Chem*. **2020**, *92*, 3228–3236.

(32) Struwe, W. B.; Robinson, C. V. Relating glycoprotein structural heterogeneity to function – insights from native mass spectrometry. *Curr. Opin. Struct. Biol.* **2019**, *58*, 241-248.

(33) Wang, Y.; Park, H.; Lin, H.; Kitova, E. N.; Klassen, J. S. Multipronged ESI–MS approach for studying glycan-binding protein interactions with glycoproteins. *Anal. Chem.* **2019**, *91*, 2140–2147.

(34) Katarzyna M., D.; William M., B.; Sarah-Jane, C.; David L., C.; Richard C., F.; Rena M., H.; N. R. S. The complete cDNA and amino acid sequence of bovine fetuin. *J. Biol. Chem.* **1990**, *265*, 4354-4357.

(35) Lin, Y.-H.; Franc, V.; Heck, A. J. R. Similar Albeit Not the Same: In-depth analysis of proteoforms of human serum, bovine serum, and recombinant human fetuin. *J. Proteome Res.* **2018**, *17*, 2861–2869.

(36) Fournier, T.; Medjoubi-N, N.; Porquet, D. Alpha-1-acid glycoprotein. Biochim. Biophys. Acta - Protein Struct. *Mol. Enzymol.* **2000**, *1482*, 157-171.

(37) Guo, S.; Briza, P.; Magdolen, V.; Brandstetter, H.; Goettig, P. Activation and activity of glycosylated KLKs 3, 4 and 11. *Biol. Chem.* **2018**, *399*, 1009–1022.

(38) Brantly, M.; Nukiwa, T.; Crystal, R. G. Molecular basis of alpha-1-antitrypsin deficiency. *Am. J. Med.* **1988**, *84*, 13-31.

(39) Ang, I. L.; Poon, T. C. W.; Lai, P. B. S.; Chan, A. T. C.; Ngai, S.-M.; Hui, A. Y.; Johnson, P. J.; Sung, J. J. Y. Study of serum haptoglobin and its glycoforms in the diagnosis of hepatocellular carcinoma: A glycoproteomic approach. *J. Proteome Res.* **2006**, *5*, 2691–2700.

(40) Sottrup-Jensen, L.; Stepanik, T. M.; Kristensen, T.; Wierzbicki, D. M.; Jones, C. M.; Lønblad, P. B.; Magnusson, S.; Petersen, T. E. Primary structure of human a2-Macroglobulin. *J. Biol. Chem.* **1984**, *259*, 8318-8327.

(41) Moremen, K. W.; Ramiah, A.; Stuart, M.; Steel, J.; Meng, L.; Forouhar, F.; Moniz, H. A.; Gahlay, G.; Gao, Z.; Chapla, D.; et al. Expression system for structural and functional studies of human glycosylation enzymes. *Nat. Chem. Biol.* **2017**, *14*, 156-162.

(42) Kitov, P. I.; Kitova, E. N.; Han, L.; Li, Z.; Jung, J.; Rodrigues, E.; Hunter, C. D.; Cairo, C. W.; Macauley, M. S.; Klassen, J. S. A quantitative, high-throughput method identifies protein–glycan interactions via mass spectrometry. *Commun. Biol.* **2019**, *2*, 268-274.

(43) Wang, W.; Kitova, E. N.; Klassen, J. S. Influence of solution and gas phase processes on protein−carbohydrate binding affinities determined by nanoelectrospray Fourier transform ion cyclotron resonance mass spectrometry. *Anal. Chem.* **2003**, *75*, 4945–4955.

(44) Kitova, E. N.; El-Hawiet, A.; Schnier, P. D.; Klassen, J. S. Reliable determinations of protein – ligand interactions by direct ESI-MS measurements. Are we there yet? *J. Am. Soc. Mass Spectrom.* **2012**, *23*, 431–441.

(45) Kitov, P. I.; Han, L.; Kitova, E. N.; Klassen, J. S. Sliding window adduct removal method (SWARM) for enhanced electrospray ionization mass spectrometry binding data. *J. Am. Soc. Mass Spectrom.* **2019**, *30*, 1446–1454.

(46) Behnken, H. N.; Ruthenbeck, A.; Schulz, J.-M.; Meyer, B. Glycan analysis of prostate specific antigen (PSA) directly from the intact glycoprotein by HR-ESI/TOF-MS. *J. Proteome Res.* **2014**, *13*, 997–1001.

(47) Song, E.; Mayampurath, A.; Yu, C.-Y.; Tang, H.; Mechref, Y. Glycoproteomics: Identifying the glycosylation of prostate specific antigen at normal and high isoelectric points by LC–MS/MS. *J. Proteome Res.* **2014**, *13*, 5570–5580.

(48) McCarthy, C.; Saldova, R.; Wormald, M. R.; Rudd, P. M.; McElvaney, N. G.; Reeves, E. P. The role and importance of glycosylation of acute phase proteins with focus on alpha-1 antitrypsin in acute and chronic inflammatory conditions. *J. Proteome Res.* **2014**, *13*, 3131–3143.

(49) Zhang, S.; Shang, S.; Li, W.; Qin, X.; Liu, Y. Insights on N-glycosylation of human haptoglobin and its association with cancers. *Glycobiology* **2016**, *26*, 684–692.

(50) Zhu, J.; Wu, J.; Yin, H.; Marrero, J.; Lubman, D. M. Mass spectrometric N-glycan analysis of haptoglobin from patient serum samples using a 96-Well plate format. *J. Proteome Res.* **2015**, *14*, 4932–4939.

(51) Lee, S. H.; Jeong, S.; Lee, J.; Yeo, I. S.; Oh, M. J.; Kim, U.; Kim, S.; Kim, S. H.; Park, S. Y.; Kim, J. H.; et al. Glycomic profiling of targeted serum haptoglobin for gastric cancer using nano LC/MS and LC/MS/MS. *Mol. Biosyst.* **2016**, *12*, 3611–3621.

(52) Marrero, A.; Duquerroy, S.; Trapani, S.; Goulas, T.; Guevara, T.; Andersen, G. R.; Navaza, J.; Sottrup-Jensen, L.; Gomis-Rüth, F. X. The Crystal Structure of Human α2-Macroglobulin Reveals a Unique Molecular Cage. *Angew. Chemie Int. Ed.* **2012**, *51*, 3340–3344.

(53) Baerenfaenger, M.; Meyer, B. Intact human alpha-acid glycoprotein analyzed by ESI-QTOF-MS: simultaneous determination of the glycan composition of multiple glycosylation sites. *J. Proteome Res.* **2018**, *17*, 3693–3703.

(54) Bigge, J. C.; Patel, T. P.; Bruce, J. A.; Goulding, P. N.; Charles, S. M.; Parekh, R. B. Nonselective and efficient fluorescent labeling of glycans using 2-Amino benzamide and anthranilic acid. *Anal. Biochem.* **1995**, *230*, 229–238.

(55) Nwosu, C.; Yau, H. K.; Becht, S. Assignment of core versus antenna fucosylation types in protein N-glycosylation via procainamide labeling and tandem mass spectrometry. *Anal. Chem.* **2015**, *87*, 5905–5913.

(56) Zhuo, Y.; Keire, D. A.; Chen, K. Minor N-glycan mapping of monoclonal antibody therapeutics using middle-down NMR spectroscopy. Mol. Pharm. 2021, 18, 441–450.

(57) Stanley, P.; Taniguchi, N.; Aebi, M. N-glycans. In Essentials of Glycobiology. 3rd edition. Cold Spring Harbor Laboratory Press: **2017**.

(58) Walsh, I.; O'Flaherty, R.; Rudd, P. M. Bioinformatics applications to aid high-throughput glycan profiling. *Perspect. Sci*. **2017**, *11*, 31-39.

(59) Naka, R.; Kamoda, S.; Ishizuka, A.; Kinoshita, M.; Kakehi, K. Analysis of total N-glycans in cell membrane fractions of cancer cells using a combination of serotonin affinity chromatography and normal phase chromatography. *J. Proteome Res.* **2006**, *5*, 88–97.

(60) Li, J.; McClane, B. A. The sialidases of Clostridium perfringens type D strain CN3718 differ in their properties and sensitivities to inhibitors. *Appl. Environ. Microbiol.* **2014**, *80*, 1701–1709.

(61) Chiarezza, M.; Lyras, D.; Pidot, S. J.; Flores-Díaz, M.; Awad, M. M.; Kennedy, C. L.; Cordner, L. M.; Phumoonna, T.; Poon, R.; Hughes, M. L.; et al. The NanI and NanJ sialidases of Clostridium perfringens are not essential for virulence. *Infect. Immun.* **2009**, *77*, 4421–4428.

(62) Hervé, F.; Gomas, E.; Duché, J.-C.; Tillement, J.-P. Fractionation of the genetic variants of human α1-acid glycoprotein in the native form by chromatography on an immobilized copper(II) affinity adsorbent: Heterogeneity of the separate variants by isoelectrofocusing and by concanavalin A affinity chromatography. *J. Chromatogr. B Biomed. Sci. Appl.* **1993**, *615*, 47-57.

(63) Sadrzadeh, S. H.; Bozorgmehr, J. Haptoglobin phenotypes in health and disorders. *Pathol. Patterns Rev.* **2004**, *121*, S97-S104.

(64) Ribeiro, J. P.; Pau, W.; Pifferi, C.; Renaudet, O.; Varrot, A.; Mahal, L. K.; Imberty, A. Characterization of a high-affinity sialic acid-specific CBM40 from Clostridium perfringens and engineering of a divalent form. *Biochem. J.* **2016**, *473*, 2109–2118.

(65) Windwarder, M.; Altmann, F. Site-specific analysis of the O-glycosylation of bovine fetuin by electron-transfer dissociation mass spectrometry. *J. Proteomics* **2014**, *108*, 258–268.

(66) Lin, Z.; Lo, A.; Simeone, D. M.; Ruffin, M. T.; Lubman, D. M. An N-glycosylation analysis of human alpha-2-macroglobulin using an integrated approach. *J. Proteomics Bioinform.* **2012**, *5*, 127–134.

(67) Marrero, A.; Duquerroy, S.; Trapani, S.; Goulas, T.; Guevara, T.; Andersen, G. R.; Navaza, J.; Sottrup-Jensen, L.; Gomis-Rüth, F. X. The crystal structure of human α2-macroglobulin reveals a unique molecular cage. *Angew. Chemie - Int. Ed.* **2012**, *51*, 3340–3344.

(68) Kitagawa, H.; Paulson, J. C. Differential expression of five sialyltransferase genes in human tissues. *J. Biol. Chem.* **1994**, *269*, 17872–17878.

(69) Takashima, S.; Tsuji, S.; Tsujimoto, M. Characterization of the second type of human β-galactoside α2,6-sialyltransferase (ST6Gal II), which sialylates Galβ1,4GlcNAc structures on oligosaccharides preferentially: genomic analysis of human sialyltransferase genes. *J. Biol. Chem.* **2002**, *277*, 45719–45728.

(70) Kitazume, S. ST6 beta-galactoside alpha-2,6-sialyltranferase 1 (ST6GAL1). In handbook of glycosyltransferases and related genes (Taniguchi N, Honke K, Fukuda M, Narimatsu H, Yamaguchi Y, Angata T, Eds.), pp 693–703, Springer, Japan, Tokyo.

(71) Barb, A. W.; Brady, E. K.; Prestegard, J. H. Branch-specific sialylation of IgG-Fc glycans by ST6Gal-I. *Biochemistry* **2009**, *48*, 9705–9707.

(72) Barb, A. W.; Meng, L.; Gao, Z.; Johnson, R. W.; Moremen, K. W.; Prestegard, J. H. NMR characterization of immunoglobulin G Fc glycan motion on enzymatic sialylation. *Biochemistry* **2012**, *51*, 4618–4626.

(73) Paulson, J. C.; Prieels, J. P.; Glasgow, L. R.; Hill, R. L. Sialyl- and fucosyltransferase in the biosynthesis of asparaginyl-linked oligosaccharides in glycoproteins. Mutually exclusive glylcosylation by β-Galactoside α2-6 sialyltransferase and N-acetylglucosaminide α1-3 fucosyltransferase. *J. Biol. Chem.* **1978**, *253*, 5617–5624.

(74) Joziasse, D. H.; Schiphorst, W. E.; Van den Eijnden, D. H.; Van Kuik, J. A.; Van Halbeek, H.; Vliegenthart, J. F. Branch specificity of bovine colostrum CMP-Sialic acid: Galβ 1-4GlcNAc-R α2-6 sialyltransferase. Sialylation of bi-, tri-, and tetraantennary oligosaccharides and glycopeptides of the N-acetyllactosamine type. *J. Biol. Chem.* **1987**, *262*, 2025–2033.

(75) Drepper, F.; Biernat, J.; Kaniyappan, S.; Meyer, H. E.; Mandelkow, E. M.; Warscheid, B.; Mandelkow, E. A combinatorial native MS and LC-MS/MS approach reveals high intrinsic phosphorylation of human Tau but minimal levels of other key modifications. *J. Biol. Chem*. **2020**, *295*, 18213–18225.

(76) Van de Waterbeemd, M.; Lössl, P.; Gautier, V.; Marino, F.; Yamashita, M.; Conti, E.; Scholten, A.; Heck, A. J. R. Simultaneous assessment of kinetic, site-specific, and structural aspects of enzymatic protein phosphorylation. *Angew. Chemie Int. Ed*. **2014**, *53*, 9660–9664.

(77) Mohanan, N.; Montazer, Z.; Sharma, P. K.; Levin, D. B. Microbial and enzymatic degradation of synthetic plastics. *Frontiers in Microbiology*. **2020**, *11*, 2837-2859.

(78) Mumtaz Virk, M.; Reimhult, E. Phospholipase A2-induced degradation and release from lipid-containing polymersomes. *Langmuir* **2018**, *34*, 395–405.

(79) Nagornov, K. O.; Gasilova, N.; Kozhinov, A. N.; Virta, P.; Holm, P.; Menin, L.; Nesatyy, V. J.; Tsybin, Y. O. Drug-to-antibody ratio estimation via proteoform peak integration in

the analysis of antibody–oligonucleotide conjugates with Orbitrap fourier transform mass spectrometry. *Anal. Chem*. **2021**, *93*, 12930-12937.

(80) Strasser, L.; Morgan, T. E.; Guapo, F.; Füssl, F.; Forsey, D.; Anderson, I.; Bones, J. A native mass spectrometry-based assay for rapid assessment of the empty:full capsid ratio in adeno-associated virus gene therapy products. *Anal. Chem*. **2021**, *93*, 12817-12821.

(81) Bechara, C.; Robinson, C. V. Different modes of lipid binding to membrane proteins probed by mass spectrometry. *J. Am. Chem. Soc*. **2015**, *137*, 5240–5247.

Chapter 4

(1) Siegel, R. L.; Miller, K. D.; Jemal, A. Cancer statistics, 2020. *CA. Cancer J. Clin.* **2020**, *70*, 7–30.

(2) Sung, H.; Ferlay, J.; Siegel, R. L.; Laversanne, M.; Soerjomataram, I.; Jemal, A.; Bray, F. Global cancer statistics 2020: GLOBOCAN estimates of incidence and mortality worldwide for 36 cancers in 185 countries. *CA. Cancer J. Clin.* **2021**, *71*, 209–249.

(3) Schröder, F.H.; Hugosson, J.; Roobol, M.J.; Tammela, T.L.; Ciatto, S.; Nelen, V.; Kwiatkowski, M.; Lujan, M.; Lilja, H.; Zappa, M.; Denis, L.J, Recker, F.; Berenguer, A.; Määttänen, L.; Bangma, C.H.; Aus, G.; Villers, A.; Rebillard, X.; van der Kwast, T.; Blijenberg, B.G.; Moss, S.M.; de Koning, H.J.; Auvinen, A. ERSPC Investigators. Screening and prostate-cancer mortality in a randomized european study. *N. Engl. J. Med.* **2009**, *360*, 1320-1328.

(4) Schröder, F.H.; Hugosson, J.; Roobol, M.J.; Tammela, T.L.; Zappa, M.; Nelen, V.; Kwiatkowski, M.; Lujan, M.; Määttänen, L.; Lilja, H.; Denis, L.J.; Recker, F.; Paez, A.; Bangma, C.H.; Carlsson, S.; Puliti, D.; Villers, A.; Rebillard, X.; Hakama, M.;Stenman,

U.H.; Kujala, P.; Taari, K.; Aus, G.; Huber, A.;van der Kwast, T.H.; van Schaik, R.H.; de Koning, H.J.; Moss, S.M.; Auvinen, A. ERSPC Investigators. Screening and prostate cancer mortality: results of the european randomised study of screening for prostate cancer (ERSPC) at 13 years of follow-up. *Lancet.* **2014**, *84*, 2027-2035.

(5) Shoag, J. E.; Nyame, Y. A.; Gulati, R.; Etzioni, R.; Hu, J. C. Reconsidering the trade-offs of prostate cancer screening. *N. Engl. J. Med.* **2020**, *382*, 2465–2468.

(6) Etzioni, R.; Penson, D. F.; Legler, J. M.; di Tommaso, D.; Boer, R.; Gann, P. H.; Feuer, E. J. Overdiagnosis due to prostate-specific antigen screening: Lessons from U.S. prostate cancer incidence trends. *JNCI J. Natl. Cancer Inst.* **2002**, *94*, 981–990.

(7) Loeb, S.; Bjurlin, M. A.; Nicholson, J.; Tammela, T. L.; Penson, D. F.; Carter, H. B.; Carroll, P.; Etzioni, R. Overdiagnosis and overtreatment of prostate cancer. *Eur. Urol.* **2014**, *65*, 1046–1055.

(8) Brewster, D. H.; Fischbacher, C. M.; Nolan, J.; Nowell, S.; Redpath, D.; Nabi, G. Risk of hospitalization and death following prostate biopsy in Scotland. *Public Health* **2017**, *142*, 102–110.

(9) Jesus, C. M. N. de; Corrêa, L. A.; Padovani, C. R. Complications and risk factors in transrectal ultrasound-guided prostate biopsies. *Sao Paulo Med. J.* **2006**, *124*, 198–202.

(10) Loeb, S.; Vellekoop, A.; Ahmed, H. U.; Catto, J.; Emberton, M.; Nam, R.; Rosario, D. J.; Scattoni, V.; Lotan, Y. Systematic review of complications of prostate biopsy. *Eur. Urol.* **2013**, *64*, 876–892.

(11) Loeb, S.; Carter, H. B.; Berndt, S. I.; Ricker, W.; Schaeffer, E. M. Complications after prostate biopsy: Data from SEER-Medicare. *J. Urol.* **2011**, *186*, 1830–1834.

(12) Saini, S. PSA and beyond: Alternative prostate cancer biomarkers. *Cell. Oncol.* **2016**, *39*,

97–106.

(13) Hatano, K.; Yoneyama, T.; Hatakeyama, S.; Tomiyama, E.; Tsuchiya, M.; Nishimoto, M.;Yoshimura, K.; Miyoshi, E.; Uemura, H.; Ohyama, C.; Nonomura, N.; Fujita, K. Simultaneous analysis of serum α2,3-linked sialylation and core-type fucosylation of prostate-specific antigen for the detection of high-grade prostate cancer. *Br. J. Cancer*. **2022**, *126*, 764-770.

(14) Chang, E. K.; Gadzinski, A. J.; Nyame, Y. A. Blood and urine biomarkers in prostate cancer: Are we ready for reflex testing in men with an elevated prostate-specific antigen? *Asian J. Urol.* **2021**, *8*, 343–353.

(15) Behnken, H.N.; Ruthenbeck, A.; Schulz, J.M.; Meyer, B. Glycan analysis of prostate specific antigen (PSA) directly from the intact glycoprotein by HR-ESI/TOF-MS. *J Proteome Res*. **2014**, *13*, 997-1001.

(16) Kałuża, A.; Szczykutowicz, J.; Ferens-Sieczkowska, M. Glycosylation: Rising potential for prostate cancer evaluation. *Cancers* **2021**. *13*, 3726- 3728.

(17) Sugár, S.; Tóth, G.; Bugyi, F.; Vékey, K.; Karászi, K.; Drahos, L.; Turiák, L. Alterations in protein expression and site-specific *N*-glycosylation of prostate cancer tissues. *Sci. Rep.* **2021**, *11*, 15886.

(18) Hatakeyama, S.; Yoneyama, T.; Tobisawa, Y.; Ohyama, C. Recent progress and perspectives on prostate cancer biomarkers. *Int. J. Clin. Oncol*. **2017**, *22*, 214-221.

(19) Pihikova, D.; Kasak, P.; Kubanikova, P.; Sokol, R.; Tkac, J. Aberrant sialylation of a prostate-specific antigen: Electrochemical label-free glycoprofiling in prostate cancer serum samples. *Anal. Chim. Acta* **2016**, *934*, 72–79.

(20) Peracaula, R.; Tabarés, G.; Royle, L.; Harvey, D. J.; Dwek, R. A.; Rudd, P. M.; de Llorens,

R. Altered glycosylation pattern allows the distinction between prostate-specific antigen (PSA) from normal and tumour origins. *Glycobiology* **2003**, *13*, 457–470.

(21) Ohyama, C.; Hosono, M.; Nitta, K.; Oh-eda, M.; Yoshikawa, K.; Habuchi, T.; Arai, Y.; Fukuda, M. Carbohydrate structure and differential binding of prostate specific antigen to maackia amurensis lectin between prostate cancer and benign prostate hypertrophy. *Glycobiology* **2004**, *14*, 671–679.

(22) Gilgunn, S.; Murphy, K.; Stöckmann, H.; Conroy, P.J.; Murphy, T.B.; Watson, R.W.; O'Kennedy, R.J.; Rudd, P.M.; Saldova, R. Glycosylation in indolent, significant and aggressive prostate cancer by automated high-throughput *N*-glycan profiling. *Int. J. Mol. Sci*. **2020**, *21*, 9233.

(23) Haga, Y.; Uemura, M.; Baba, S.; Inamura, K.; Takeuchi, K.; Nonomura, N.; Ueda, K. Identification of multisialylated LacdiNAc structures as highly prostate cancer specific glycan signatures on PSA. *Anal. Chem*. **2019**, *91*, 2247-2254.

(24) Yoneyama, T.; Ohyama, C.; Hatakeyama, S.; Narita, S.; Habuchi, T.; Koie, T.; Mori, K.; Hidari, K.I.;Yamaguchi, M.; Suzuki, T.; Tobisawa, Y. Measurement of aberrant glycosylation of prostate specific antigen can improve specificity in early detection of prostate cancer. *Biochem. Biophys. Res. Commun*. **2014**, *448*, 390-396.

(25) Saldova, R.; Fan, Y.; Fitzpatrick, J. M.; Watson, R. W. G.; Rudd, P. M. Core fucosylation and α2-3 sialylation in serum *N*-glycome is significantly increased in prostate cancer comparing to benign prostate hyperplasia. *Glycobiology* **2011**, *21*, 195–205.

(26) Ferrer-Batallé, M.; Llop, E.; Ramírez, M.; Aleixandre, R.N.; Saez, M.; Comet, J.; De Llorens, R.; Peracaula, R. Comparative study of blood-based biomarkers, α2,3-sialic acid PSA and PHI, for high-risk prostate cancer detection. *Int. J. Mol. Sci*. **2017**, *18*, 845.

(27) Llop, E.; Ferrer-Batallé, M.; Barrabés, S.; Guerrero, P. E.; Ramírez, M.; Saldova, R.; Rudd, P. M.; Aleixandre, R. N.; Comet, J.; de Llorens, R.; Peracaula, R. Improvement of prostate cancer diagnosis by detecting PSA glycosylation-specific changes. *Theranostics* **2016**, *6*, 1190–1204.

(28) Gratacós-Mulleras, A.; Duran, A.; Asadi Shehni, A.; Ferrer-Batallé, M.; Ramírez, M.; Comet, J.; de Llorens, R.; Saldova, R.; Llop, E.; Peracaula, R. Characterisation of the main PSA glycoforms in aggressive prostate cancer. *Sci. Rep.* **2020**, *10*, 1–14.

(29) Wang, C.; Höti, N.; Lih, T.M.; Sokoll, L.J.; Zhang, R.; Zhang, Z.; Zhang, H.; Chan, D.W. Development of a glycoproteomic strategy to detect more aggressive prostate cancer using lectin-immunoassays for serum fucosylated PSA. *Clin. Proteomics*. **2019**, *16*, 13-21.

(30) Haese, A.; Tin, A. L.; Carlsson, S. V; Sjoberg, D. D.; Pehrke, D.; Steuber, T.; Huland, H.; Graefen, M.; Scardino, P. T.; Schlomm, T.; Vickers, J. A.; Lilja, H.; Sauter, G. A pre-specified model based on four Kallikrein markers in blood improves predictions of adverse pathology and biochemical recurrence after radical prostatectomy. *Br. J. Cancer* **2020**, *123*, 604–609.

(31) Wang, W.; Wang, M.; Wang, L.; Adams, T. S.; Tian, Y.; Xu, J. Diagnostic ability of %p2PSA and prostate health index for aggressive prostate cancer: A meta-analysis. *Sci. Rep.* **2014**, *4*, 5012.

(32) van der Burgt, Y.E.M.; Siliakus, K.M.; Cobbaert, C.M.; Ruhaak, L.R. HILIC-MRM-MS for linkage-specific separation of sialylated glycopeptides to quantify prostate-specific antigen proteoforms. *J. Proteome Res*. **2020**, *19*, 2708-2716.

(33) Reider, B.; Jarvas, G.; Krenkova, J.; Guttman, A. Separation based characterization methods for the *N*-glycosylation analysis of prostate-specific antigen. *J. Pharm. Biomed.*

Anal. **2021**, *194*, 113797.

(34) Kammeijer, G.S.M.; Jansen, B.C.; Kohler, I.; Heemskerk, A.A.M.; Mayboroda, O.A.; Hensbergen, P.J.; Schappler, J.; Wuhrer, M. Sialic acid linkage differentiation of glycopeptides using capillary electrophorsis - electrospray ionization - mass spectrometry. *Sci. Rep*. **2017**, *7*, 3733.

(35) Kammeijer, G. S. M.; Nouta, J.; de la Rosette, J. J. M. C. H.; de Reijke, T. M.; Wuhrer, M. An in-depth glycosylation assay for urinary prostate-specific antigen. *Anal. Chem.* **2018**, *90*, 4414–4421.

(36) Gabriele, C.; Prestagiacomo, L.E.; Cuda, G.; Gaspari, M. Mass spectrometry-based glycoproteomics and prostate cancer. *Int. J. Mol. Sci*. **2021**, *22*, 5222.

(37) Etxebarria, J.; Reichardt, N. C. Methods for the absolute quantification of *N*-glycan biomarkers. *Biochim. Biophys. Acta* **2016**, *1860*, 1676–1687.

(38) Zhou, X.; Yang, G.; Guan, F. Biological Functions and Analytical Strategies of Sialic Acids in Tumor. *Cells* **2020**, *9*, 273-291.

(39) Rodrigues, E.; Jung, J.; Park, H.; Loo, C.; Soukhtehzari, S.; Kitova, E. N.; Mozaneh, F.; Daskhan, G.; Schmidt, E. N.; Aghanya, V.; Sarkar, S.; Streith, L.; Laurent D St, C.; Nguyen, L.; Julien, J.; West, L, J.; Williams, K, C.; Klassen, J, S.; Macauley, M, S. A Versatile Soluble Siglec Scaffold for Sensitive and Quantitative Detection of Glycan Ligands. *Nat. Commun.* **2020**, *11*, 5091.

(40) Li, Z.; Kitov, P. I.; Kitova, E. N.; Bui, D. T.; Moremen, K. W.; Wakarchuk, W. W.; Mahal, L. K.; Macauley, M. S.; Klassen, J. S. Quantifying carbohydrate-active enzyme activity with glycoprotein substrates using electrospray ionization mass spectrometry and center-of-mass monitoring. *Anal. Chem.* **2021**, *93*, 15262–15270.

(41) Li, Z.; Kitov, P. I.; Han, L.; Kitova, E. N.; Mozenah, F.; Rodrigues, E.; Chapla, D. G.; Moremen, K. W.; Macauley, M. S.; Klassen, J. S. CUPRA-ZYME: An assay for measuring carbohydrate-active enzyme activities, pathways, and substrate specificities. *Anal. Chem.*, **2020**, *92*, 3228-3236.

(42) Klee, E. W.; Bondar, O. P.; Goodmanson, M. K.; Trushin, S. A.; Bergstralh, E. J.; Singh, R. J.; Anderson, N. L.; Klee, G. G. Serum concentrations of prostate-specific antigen measured using immune extraction, trypsin digestion, and tandem mass spectrometry quantification of LSEPAELTDAVK Peptide. *Arch. Pathol. Lab. Med.* **2014**, *138*, 1381–1386.

(43) Abu-Bakr El-Bayoumy, A. S.; Hessien Keshta, A. T.; Sallam, K. M.; Ebeid, N. H.; Elsheikh, H. M.; Bayoumy, B. E. S. Extraction, purification of prostate-specific antigen (PSA), and establishment of radioimmunoassay system as a diagnostic tool for prostate disorders. *J. Immunoass*. **2018**, *39*, 12-29.

(44) Bigge, J. C.; Patel, T. P.; Bruce, J. A.; Goulding, P. N.; Charles, S. M.; Parekh, R. B. Nonselective and efficient fluorescent labeling of glycans using 2-amino benzamide and anthranilic acid. *Anal. Biochem.* **1995**, *230*, 229–238.

(45) Nwosu, C.; Yau, H. K.; Becht, S. Assignment of core versus antenna fucosylation types in protein *N*-glycosylation via procainamide labeling and tandem mass spectrometry. *Anal. Chem.* **2015**, *87*, 5905–5913.

(46) Zhuo, Y.; Keire, D. A.; Chen, K. Minor *N*-glycan mapping of monoclonal antibody therapeutics using middle-down NMR spectroscopy. *Mol. Pharm.* **2021**, *18*, 441–450.

(47) Stanley, P.; Taniguchi, N.; Aebi, M. N-glycans. In Essentials of Glycobiology. 3rd edition. Cold Spring Harbor Laboratory Press: **2017**.

(48) Walsh, I.; O'Flaherty, R.; Rudd, P. M. Bioinformatics applications to aid high-throughput glycan profiling. *Perspect. Sci.* **2017**, *11*, 31-39.

(49) Naka, R.; Kamoda, S.; Ishizuka, A.; Kinoshita, M.; Kakehi, K. Analysis of total *N*-glycans in cell membrane fractions of cancer cells using a combination of serotonin affinity chromatography and normal phase chromatography. *J. Proteome Res.* **2006**, *5*, 88–97.

(50) Xu, G.; Potter, J. A.; Russell, R. J. M.; Oggioni, M. R.; Andrew, P. W.; Taylor, G. L. Crystal structure of the NanB sialidase from *Streptococcus Pneumoniae*. *J. Mol. Biol.* **2008**, *384*, 436–449.

(51) Gut, H.; King, S. J.; Walsh, M. A. Structural and functional studies of *Streptococcus Pneumoniae* neuraminidase B: An intramolecular trans-sialidase. *FEBS Lett.* **2008**, *582*, 3348–3352.

(52) Newstead, S. L.; Potter, J. A.; Wilson, J. C.; Xu, G.; Chien, C.-H.; Watts, A. G.; Withers, S. G.; Taylor, G. L. The structure of *Clostridium perfringens* NanI sialidase and its catalytic intermediates. *J. Biol. Chem.* **2008**, *283*, 9080–9088.

(53) Ideo, H.; Kondo, J.; Nomura, T.; Nonomura, N.; Inoue, M.; Amano, J. Study of glycosylation of prostate-specific antigen secreted by cancer tissue-originated spheroids reveals new candidates for prostate cancer detection. *Sci. Rep.* **2020**, *10*, 2708-2726.

(54) Song, E.; Mayampurath, A.; Yu, C.-Y.; Tang, H.; Mechref, Y. Glycoproteomics: Identifying the glycosylation of prostate specific antigen at normal and high isoelectric points by LC–MS/MS. *J. Proteome Res.* **2014**, *13*, 5570–5580.

(55) McKiernan, J.; Donovan, M. J.; Margolis, E.; Partin, A.; Carter, B.; Brown, G.; Torkler, P.; Noerholm, M.; Skog, J.; Shore, N.; Andriole, G.; Thompson, I.; Carroll, P. A prospective adaptive utility trial to validate performance of a novel urine exosome gene expression

assay to predict high-grade prostate cancer in patients with prostate-specific antigen 2–10 ng/ml at initial biopsy. *Eur. Urol.* **2018**, *74*, 731–738.

(56) McKiernan, J.; Donovan, M. J.; O'Neill, V.; Bentink, S.; Noerholm, M.; Belzer, S.; Skog, J.; Kattan, M. W.; Partin, A.; Andriole, G.; Brown, G.; Wei, J. T.; Thompson Jr, I. M.; Carroll, P. A novel urine exosome gene expression assay to predict high-grade prostate cancer at initial biopsy. *JAMA Oncol.* **2016**, *2*, 882–889.

(57) Yoneyama, T.; Yamamoto, H.; Sutoh Yoneyama, M.; Tobisawa, Y.; Hatakeyama, S.; Narita, T.; Kodama, H.; Momota, M.; Ito, H.; Narita, S.; Tsushima, F.; Mitsuzuka, K.; Yoneyama, T.; Hashimoto, Y.; Duivenvoorden, W.; Pinthus, J. H.; Kakeda, S.; Ito, A.; Tsuchiya, N.; Habuchi, T.; Ohyama, C. Characteristics of α2,3-Sialyl *N*-glycosylated PSA as a biomarker for clinically significant prostate cancer in men with elevated PSA level. *Prostate* **2021**, *81*, 1411–1427.

(58) Klotz, L.; Zhang, L.; Lam, A.; Nam, R.; Mamedov, A.; Loblaw, A. Clinical results of long-term follow-up of a large, active surveillance cohort with localized prostate cancer. *J. Clin. Oncol.* **2010**, *28*, 126–131.

(59) Klotz, L.; Vesprini, D.; Sethukavalan, P.; Jethava, V.; Zhang, L.; Jain, S.; Yamamoto, T.; Mamedov, A.; Loblaw, A. Long-term follow-up of a large active surveillance cohort of patients with prostate cancer. *J. Clin. Oncol.* **2015**, *33*, 272–277.

(60) Fine, W. S.; Epstein, I. J. A contemporary study correlating prostate needle biopsy and radical prostatectomy gleason score. *J. Urol.* **2008**, *179*, 1335–1339.

(61) Uslu, C.; Taysi, S.; Akcay, F.; Sutbeyaz, M. Y.; Bakan, N. Serum free and bound sialic acid and alpha-1-acid glycoprotein in patients with laryngeal cancer. *Ann. Clin. Lab. Sci.* **2003**, *33*, 156–159.

(62) Gao, Z.; Xu, M.; Yue, S.; Shan, H.; Xia, J.; Jiang, J.; Yang, S. Abnormal sialylation and fucosylation of saliva glycoproteins: Characteristics of lung cancer-specific biomarkers. *Curr. Res. Pharmacol. Drug Discov.* **2022**, *3*, 100079.

(63) Mondal, G.; Chatterjee, U.; Chawla, Y. K.; Chatterjee, B. P. Alterations of glycan branching and differential expression of sialic acid on alpha fetoprotein among hepatitis patients. *Glycoconj. J.* **2011**, *28*, 1–9.

Chapter 5

(1) Walsh, G. Biopharmaceutical Benchmarks 2018. *Nat. Biotechnol.* **2018**, *36*, 1136–1145.

(2) Pierpont, T. M.; Limper, C. B.; Richards, K. L. Past, present, and future of rituximab-the world's first oncology monoclonal antibody therapy. *Front. Oncol*. **2018**, *8*, 163.

(3) Hirsch, I. B. Insulin analogues. *N. Engl. J. Med*. **2005**, *352*, 174− 183.

(4) Kiss, Z.; Elliott, S.; Jedynasty, K.; Tesar, V.; Szegedi, J. Discovery and basic pharmacology of erythropoiesis-stimulating agents (ESAs), including the hyperglycosylated ESA, darbepoetin alfa: an update of the rationale and clinical impact. *Eur. J. Clin. Pharmacol*. **2010**, *66*, 331−340.

(5) Rustgi, V. K. Albinterferon alfa-2b, a novel fusion protein of human albumin and human interferon alfa-2b, for chronic hepatitis C. *Curr. Med. Res. Opin*. **2009**, *25*, 991−1002.

(6) Kesik-Brodacka, M. Progress in biopharmaceutical development. *Biotechnol. Appl. Biochem*. **2018**, *65*, 306−322.

(7) Mattu, T. S.; Pleass, R. J.; Willis, A. C.; Kilian, M.; Wormald, M. R.; Lellouch, A. C.; Rudd, P. M.; Woof, J. M.; Dwek, R. A. The glycosylation and structure of human serum IgA1,

Fab, and Fc regions and the role of *N*-Glycosylation on Fcα receptor interactions. *J. Biol. Chem.* **1998**, *273*, 2260–2272.

(8) Huhn, C.; Selman, M. H. J.; Ruhaak, L. R.; Deelder, A. M.; Wuhrer, M. IgG glycosylation analysis. *Proteomics* **2009**, *9*, 882–913.

(9) Krapp, S.; Mimura, Y.; Jefferis, R.; Huber, R.; Sondermann, P. Structural analysis of human IgG-Fc glycoforms reveals a correlation between glycosylation and structural integrity. *J. Mol. Biol.* **2003**, *325*, 979–989.

(10) Mimura, Y.; Church, S.; Ghirlando, R.; Ashton, P. R.; Dong, S.; Goodall, M.; Lund, J.; Jefferis, R. The influence of glycosylation on the thermal stability and effector function expression of human IgG1-Fc: Properties of a series of truncated glycoforms. *Mol. Immunol.* **2000**, *37*, 697–706.

(11) Borrok, M. J.; Jung, S. T.; Kang, T. H.; Monzingo, A. F.; Georgiou, G. Revisiting the role of glycosylation in the structure of human IgG Fc. *ACS Chem. Biol.* **2012**, *7*, 1596–1602.

(12) Liu, L. Antibody Glycosylation and its impact on the pharmacokinetics and pharmacodynamics of monoclonal antibodies and Fc-fusion proteins. *J. Pharm. Sci.* **2015**, *104*, 1866–1884.

(13) Van Lenten, L.; Ashwell, G. Studies on the chemical and enzymatic modification of glycoproteins: A general method for the tritiation of sialic acid-containing glycoproteins. *J. Biol. Chem.* **1971**, *246*, 1889–1894.

(14) Imbach, P.; d'APUZZO, V.; Hirt, A.; Rossi, E.; Vest, M.; Barandun, S.; Baumgartner, C.; Morell, A.; Schöni, M.; Wagner, H. P. High-dose intravenous gamma-globulin for idiopathic thrombocytopenic purpura in childhood. *Lancet* **1981**, *317*, 1228–1231.

(15) Nimmerjahn, F.; Ravetch, J. V. Anti-inflammatory actions of intravenous immunoglobulin. *Annu. Rev. Immunol.* **2008**, *26*, 513–533.

(16) Kaneko, Y.; Nimmerjahn, F.; Ravetch, J. V. Anti-inflammatory activity of immunoglobulin G resulting from Fc sialylation. *Science.* **2006**, *313*, 670–673.

(17) Scallon, B. J.; Tam, S. H.; McCarthy, S. G.; Cai, A. N.; Raju, T. S. Higher levels of sialylated Fc glycans in immunoglobulin G molecules can adversely impact functionality. *Mol. Immunol.* **2007**, *44*, 1524–1534.

(18) Raju, T. S.; Lang, S. E. Diversity in structure and functions of antibody sialylation in the Fc. *Curr. Opin. Biotechnol.* **2014**, *30*, 147–152.

(19) Naso, M. F.; Tam, S. H.; Scallon, B. J.; Raju, T. S. Engineering host cell lines to reduce terminal sialylation of secreted antibodies. *MAbs* **2010**, *2*, 519–527.

(20) Stadlmann, J.; Pabst, M.; Altmann, F. Analytical and functional aspects of antibody sialylation. *J. Clin. Immunol.* **2010**, *30*, 15–19.

(21) Kapur, R.; Einarsdottir, H. K.; Vidarsson, G. IgG-Effector functions:"The good, the bad and the ugly." *Immunol. Lett.* **2014**, *160*, 139–144.

(22) Chennamsetty, N.; Voynov, V.; Kayser, V.; Helk, B.; Trout, B. L. Design of therapeutic proteins with enhanced stability. *Proc. Natl. Acad. Sci.* **2009**, *106*, 11937–11942.

(23) Chennamsetty, N.; Helk, B.; Voynov, V.; Kayser, V.; Trout, B. L. Aggregation-prone motifs in human immunoglobulin G. *J. Mol. Biol.* **2009**, *391*, 404–413.

(24) Brummitt, R. K.; Nesta, D. P.; Chang, L.; Chase, S. F.; Laue, T. M.; Roberts, C. J. Nonnative aggregation of an IgG1 antibody in acidic conditions: Part 1. Unfolding, colloidal interactions, and formation of high-molecular-weight aggregates. *J. Pharm. Sci.* **2011**, *100*, 2087–2103.

(25) Nagae, M.; Yamaguchi, Y. Function and 3D structure of the *N*-glycans on glycoproteins. *Int. J. Mol. Sci.* **2012**, *13*, 8398–8429.

(26) Kiyoshi, M.; Tsumoto, K.; Ishii-Watabe, A.; Caaveiro, J. M. M. Glycosylation of IgG-Fc: A molecular perspective. *Int. Immunol.* **2017**, *29*, 311–317.

(27) Falck, D.; Jansen, B. C.; Plomp, R.; Reusch, D.; Haberger, M.; Wuhrer, M. Glycoforms of immunoglobulin G based biopharmaceuticals are differentially cleaved by trypsin due to the glycoform influence on higher-order structure. *J. Proteome Res.* **2015**, *14*, 4019–4028.

(28) Fang, J.; Richardson, J.; Du, Z.; Zhang, Z. Effect of Fc-glycan structure on the conformational stability of IgG revealed by Hydrogen/Deuterium exchange and limited proteolysis. *Biochemistry* **2016**, *55*, 860–868.

(29) Zhang, Z.; Shah, B.; Richardson, J. Impact of Fc *N*-glycan sialylation on IgG structure. *MAbs* **2019**, *11*, 1381–1390.

(30) Jefferis, R. Glycosylation as a strategy to improve antibody-based therapeutics. *Nat. Rev. Drug Discov.* **2009**, *8*, 226–234.

(31) Jefferis, R. Glycosylation of recombinant antibody therapeutics. *Biotechnol. Prog.* **2005**, *21*, 11–16.

(32) Yu, X.; Marshall, M. J. E.; Cragg, M. S.; Crispin, M. Improving antibody-based cancer therapeutics through glycan engineering. *BioDrugs* **2017**, *31*, 151–166.

(33) Ma, B.; Guan, X.; Li, Y.; Shang, S.; Li, J.; Tan, Z. Protein glycoengineering: An approach for improving protein properties. *Frontiers in Chemistry*. **2020**, *8*, 622

(34) Wilson, R. M.; Dong, S.; Wang, P.; Danishefsky, S. J. The winding pathway to erythropoietin along the chemistry–biology frontier: A success at last. *Angew. Chemie Int. Ed.* **2013**, *52*, 7646–7665.

(35) Chaffey, P. K.; Guan, X.; Li, Y.; Tan, Z. Using chemical synthesis to study and apply protein glycosylation. *Biochemistry* **2018**, *57*, 413–428.

(36) Hodoniczky, J.; Zheng, Y. Z.; James, D. C. Control of recombinant monoclonal antibody effector functions by Fc *N*-glycan remodeling in Vitro. *Biotechnol. Prog.* **2005**, *21*, 1644–1652.

(37) Huang, W.; Giddens, J.; Fan, S.-Q.; Toonstra, C.; Wang, L.-X. Chemoenzymatic glycoengineering of intact IgG antibodies for gain of functions. *J. Am. Chem. Soc.* **2012**, *134*, 12308–12318.

(38) Giddens, J. P.; Lomino, J. V; DiLillo, D. J.; Ravetch, J. V; Wang, L.-X. Site-selective chemoenzymatic glycoengineering of Fab and Fc glycans of a therapeutic antibody. *Proc. Natl. Acad. Sci.* **2018**, *115*, 12023–12027.

(39) Barb, A. W.; Meng, L.; Gao, Z.; Johnson, R. W.; Moremen, K. W.; Prestegard, J. H. NMR characterization of immunoglobulin G Fc glycan motion on enzymatic sialylation. *Biochemistry* **2012**, *51*, 4618–4626.

(40) Smith, K. D., Behan, J., Matthews-Smith, G., & Magliocco, A. M. Alpha-1-acid glycoprotein (AGP) as a potential biomarker for breast cancer. London, UK: IntechOpen. **2012**, 201-222.

(41) Hoagland IV, L. F., Campa, M. J., Gottlin, E. B., Herndon, J. E., & Patz Jr, E. F.. Haptoglobin and posttranslational glycan‐modified derivatives as serum biomarkers for the diagnosis of nonsmall cell lung cancer. *Cancer: Interdisciplinary International Journal of the American Cancer Society.* **2007**, *110*, 2260-2268

(42) Fleming, S. C.; Smith, S.; Knowles, D.; Skillen, A.; Self, C. H. Increased sialylation of oligosaccharides on IgG paraproteins - a potential new tumor marker in multiple myeloma. *J. Clin. Pathol.* **1998**, *51*, 825–830.

(43) Theodoratou, E.; Thaci, K.; Agakov, F.; Timofeeva, M.N.; Stambuk, J.; Pucic-Bakovic, M.; Vuckovic, F.; Orchard, P.; Agakova, A.; Din, F.V.; Brown, E.; Rudd, P.M.; Farrington, S.M.; Dunlop, M.G.; Campbell, H.; Lauc, G. Glycosylation of plasma IgG in colorectal cancer prognosis. *Sci. Rep.* **2016**, *6*, 28098.

(44) Vuckovic, F.; Theodoratou, E.; Thaci, K.; Timofeeva, M.; Vojta, A.; Stambuk, J.; Pucic-Bakovic, M.; Rudd, P.M.; Derek, L.; Servis, D.; Wennerstrom, A.; Farrington, S.M.; Perola, M.; Aulchenko, Y.; Dunlop, M.G.; Campbell, H.; Lauc, G. IgG glycome in colorectal cancer. Clin. *Cancer Res.* **2016**, *22*, 3078–3086.

(45) B. Rajpura, K.; S. Patel, P.; G. Chawda, J.; M. Shah, R. Clinical significance of total and lipid bound sialic acid levels in oral pre-cancerous conditions and oral cancer. *J. Oral Pathol. Med.* **2005**, *34*, 263–267.

(46) Krishnan, K.; Balasundaram, S. Evaluation of total and lipid bound sialic acid in serum in oral leukoplakia. *J Clin of Diagn Res.* **2017**, *11*, 25–27.

(47) Kökoğlu E.; Uslu E.; Uslu I.; Hatemi HH. Serum and tissue total sialic acid as a marker for human thyroid cancer. *Cancer Lett*. **1989**, *46*, 1-5.

(48) Cramer, D. W.; Greenberg, E. R.; Titus-Ernstoff, L.; Liberman, R. F.; Welch, W. R.; Li, E.; Ng, W. G. A Case-Control Study of Galactose Consumption and Metabolism in Relation to Ovarian Cancer1. *Cancer Epidemiol. Biomarkers Prev.* **2000**, *9*, 95–101.

(49) Norton, P. A.; Mehta, A. S. Expression of Genes That Control Core Fucosylation in Hepatocellular Carcinoma: Systematic Review. *World J. Gastroenterol.* **2019**, *25*, 2947–2960.